Cape Peninsula University of Technology

Design and analysis of multifunctional composite structures for nano-satellites

by

Jeffrey Ball - 211207128

Supervisor

Prof. Graeme Oliver

Co-supervisor

Mr Michael Petersen

Date Completed: 30/10/2017

Full thesis submitted in partial/full fulfilment of the requirements for Master's thesis in Mechanical Engineering

MEng in Mechanical Engineering

Plagiarism Declaration

Cape Peninsula University of Technology

The work attached is my own, original work, i.e. free of plagiarism. All sources used in this work have been referenced, using the Harvard method of in-text and end-of-text referencing.

Jeffrey Ball (211207128)

Signed:..... Date: .....

Abstract

The aim of this thesis is to investigate the applications of multifunctional composite (MFC) technology to nano-satellite structures and to produce a working concept design, which can be implemented on future Cube-Satellites (CubeSats). MFC technologies can be used to optimise the performance of the satellite structure in terms of mass, volume and the protection it provides. The optimisation of the structure will allow further room for other sub-systems to be expanded and greater payload allowance. An extensive literature view of existing applications of MFC materials has been conducted, along with the analysis of a MFC CubeSat structural design accounting for the environmental conditions in space and well-known design practices used in the space industry. Numerical analysis data has been supported by empirical analysis that was done where possible on the concept material and structure. The findings indicate that the MFC technology shows an improvement over the conventional aluminium structures that are currently being used. Improvements in rigidity, mass and internal volume were observed. Additional functions that the MFC structure offers include electrical circuitry and connections through the material itself, as well as an increase electromagnetic shielding capability through the use of carbon-fibre composite materials. Empirical data collected on the MFC samples also show good support for the numerical analysis results. The main conclusion to be drawn from this work is that multifunctional composite materials can indeed be used for nano-satellite structures and in the same light, can be tailor-made to the specific mission requirements of the satellite. The technology is in its infancy still and has vast room for improvement and technological development beyond this work and well into the future. Further improvements and additional functions can be added through the inclusion of various other materials.

Keywords: Multifunctional composite technology, nano-satellites, CubeSats, space engineering, space structure design.

Acknowledgements

I wish to thank:

- Professor Graeme Oliver, Supervisor.
- Mr Michael Petersen, Co-supervisor.
- Professor Robert van Zyl, Director at F'SATI.
- Dr Norman G. Fitz-Coy, Research Chair at F'SATI.
- Ben Dixon, Master's Electrical Engineer at F'SATI.
- PLMCC and F'SATI centres for providing the space and the equipment needed to conduct this research.

The financial assistance of the National Research Foundation towards this research is acknowledged, through the F'SATI program. Opinions expressed in this thesis and the conclusions arrived at, are those of the author, and are not necessarily to be attributed to the National Research Foundation.

Dedication

I would like to dedicate this research work to my family who has been truly inspirational and provided the most grounding support and love throughout my entire life. My family has been right there with me every step of the way, through all the great times but also and most importantly through the most difficult times of my life too. Without the support of my parents, I would never have achieved what I have done so far in my life and I owe them every bit of my lifes achievements. No matter where I am in the world or whatever happens in life, I will always know that they are there for me and I will always be there for them. Thank you for being the best mother and father anyone could ever wish for.

Contents

List of Tables

List of Figures

Abbreviations

ADS Antenna Deployment System

ASTM American Society for Testing and Materials

CCM Composite Cylinder Model

CLT Classical Laminate Theory

CNC Computer Numerical Control

CNT Carbon Nanotube

CPUT Cape Peninsula University of Technology

CVCM Collected Volatile Condensable Material

EMC Electro-Magnetic Compatibility

EMI Electromagnetic Interference

ESD Electrostatic Discharge

FEA Finite Element Analysis

FOS Factor Of Safety

FPC Flexible Printed Circuit

F'SATI French South African Institute of Technology

FSDT First-order Shear Deformation Theory

IROM Inverse Rule of Mixtures

LEO Lower Earth Orbit

MFC Multifunctional Composite

NEMA National Electrical Manufacturers Association

PAN Polyacrylonitrile

PCB Printed Circuit Board

PFA Progressive Failure Analysis

PMC Polymer Matrix Composite

PMM periodic micro-structure model

P-POD Poly Picosatellite Orbital Deployer

PSA Pressure-Sensitive Adhesives

ROM Rule of Mixtures

RTM Resin Transfer Moulding

RUC Repetitive Unit Cell

RVE Repetitive Volume Element

SPP Stress Partitioning Parameter

SRB Solid Rocket Booster

SSB Single Sided Board

TML Total Mass Loss

UD Uni-Directional

UV Ultraviolet

Chapter 1

Introduction

1.1 Background

For as long as there has been the need to build tools, parts and equipment, man has been seeking ever better materials for which to construct these array of items from. The influence of materials to mankind has, in fact, been so important that great historical periods have even been named after materials (Barbero, 2010). In the last several decades the use of composite materials has broadened dramatically. Many industries have exploited the unique properties that can be obtained with composite materials and proceeded to use these materials to create improved parts and components. Aerospace, automotive, marine and civil industries, to name a few, are among the greatest users of such composite materials.

To this day, there is no universally accepted definition of a composite material; however, a good description denotes something that consists of two or more different materials, and which are bonded together into one single structure (Harper, 2002). Composite materials consist of two main material types, namely reinforcing and matrix materials. Reinforcement materials are the structural and load-bearing components of the composite, while the matrix material is the binding material which provides a protective layer for the reinforcement material.

It is important to differentiate composite materials from other monolithic (unreinforced) solid materials, such as steel or alloys. Composite materials such as wood, bamboo, bone etc. are also found in nature and are prime examples of natural forms of composite materials (Harper, 2002). Man-made or artificial composite materials have a great advantage, as it allows for the creation of combinations of a wide variety of reinforcement and binding (matrix) materials. The properties of these composites can be customised for specific applications or design intents. Artificial composite materials are, however, not a new invention and date back many years to when bricks, made from straw-reinforced mud, were used in biblical times (Harper, 2002).

Across the various industries, references to composite materials are generally associated with 'high performance' composite materials that are constructed from a com-

bination of plastics/polymers, fibres, ceramics and metals. The four main material categories used as reinforcement and matrix materials are polymers, carbon, ceramics and metals.

The aerospace industry is one of the leading industries in the use and development of composite materials. The wide range of customisable material properties that composite materials provide is a priceless advantage in this field. One of the greatest advantages of composite materials is its ability to produce outstanding strength to weight ratios.

Other important developments have altered the material thermal conductivity to either high or low (Harper, 2002). Examples of such advances are combinations of multiple types of composite reinforcement materials (also called hybrid composite materials), which allow for variations in the materials' impact resistance, and electrical permeability. Both the mechanical and physical properties of composite materials can be tailor-made to suit specific applications and perform multiple tasks that would be impossible for general monolithic materials to achieve. Thus by incorporating or embedding various other materials or components into the composite materials, they can perform not only a structural function but that of electrical conductivity, impact and/or radiation shielding and thermal conductivity simultaneously. These types of materials are generally labelled as 'multifunctional composite materials'.

The aerospace industry in particular continues to push the technological and engineering boundaries which include the composite materials' field, among many others. Various programs and projects have been developed over the years to avail this aerospace technology to smaller-budget companies and institutions. The aim of this increased accessibility is to open research into these technologies across all levels and keep it from being contained only within high-budget organisations or companies, such as NASA, Boeing, Lockheed Martin, etc. One of the more recent and successful projects to create new opportunities in space and deep-space exploration, is the creation of the CubeSat program.

The CubeSat program that was devised from an idea of Bob Twiggs of Stanford University, started in the late 1990s, in an attempt to create a pod that would be able to launch even the smallest satellite possible, while still having a practical purpose as well (Helvajian and Janson, 2008). The primary focus of the program was to allow graduate students the opportunity to design, build, test and operate spacecraft at an affordable cost. The launch-pod would eventually have a pusher-plate design with a spring-loaded door that could also house the smallest practical satellite of a 100 mm cube (Helvajian and Janson, 2008). The weight limit of such a cube is 1.33kg, setting a standard for various constructors who wanted to build a CubeSat for this specific launch-pod.

CubeSats are launched simultaneously in a group at a time, and by implication the cost of the launch-vehicle setup can thus be divided amongst the various universities and companies that are launching satellites. The CubeSat program has now become exceedingly successful with more than 40 universities launching CubeSats from June 2003 to the present day (CubeSAT.org, 2015).

The CubeSat program opens up opportunities for graduate engineers to improve new technologies that can be used as efficiently as possible. In any satellite, there is barely room for redundant, heavy or overweight parts and/or components. Thus, the ultimate goal of the design behind a CubeSat is to produce a 100 mm cube satellite, packing as much functionality and components within the satellite and still weighing below the limit of 1.33kg.

Figures 1.1 and 1.2 respectively are two examples of different structures currently used for CubeSats. The two main commercially available CubeSat structures currently are the ISIS and Pumpkin Structures, both of which are made from aluminium. Some larger universities and organisations manufacture their own structures to suit their specific design requirements.

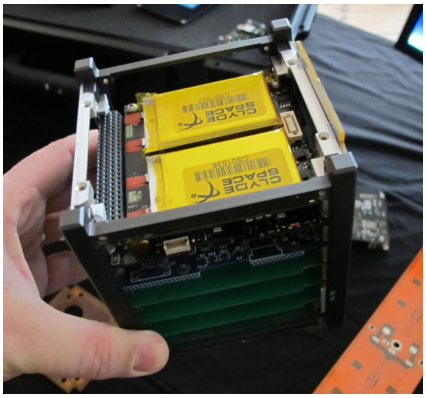

Figure 1.1: ISIS 1-Unit CubeSat structure.
(Wikimedia-Commons, 2011)

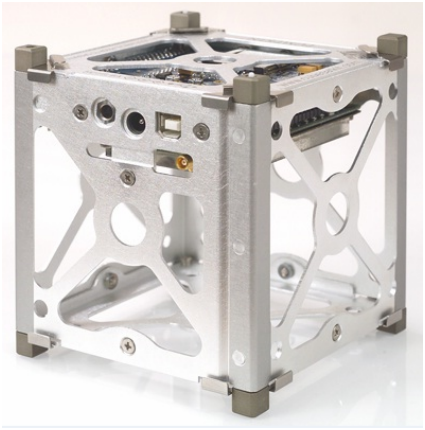

Figure 1.2: Pumpkin 1-Unit CubeSat structure.
(Pumpkin-Inc, 2013)

1.2 Research Focus

It is thus evident from the previous section that any improvement to the efficiency of any satellite component will have great functional benefits for the overall unit. Key areas that can be refined is the design of the structure of the satellite and a revision of the functionality of the structure as a whole.

Recent research and development into composite material use in satellites have revealed the satellite structure as a perfect area for its use. The structure of most nano-satellites that are commercially available and used in their construction are at this stage still primarily aluminium based. Due to composite materials' ability to have customisable material properties, it is possible then to replace the aluminium structure with a composite structure that has properties incorporated into it in order to improve the functionality of the structure of the satellite. Along with the design of the material properties of the composite, other materials or components can be embedded into the composite material. This material is referred to as "multifunctional composites" due to its ability to have more than one main function.

Recent research confirms the use of multifunctional composites as a substance to ameliorate the overall efficiency of the nano-satellite structure. In the research done by (D̋iPalma et al., 2004), FPC's were manufactured into a composite panel with no effect on the structural integrity of the panel with the addition of the FPC layer. Likewise, research performed by (S̋eong Jang et al., 2010) illustrates that positioning thermal materials in designed locations, areas of the composite can be used as extended heat sinks and allows for the possibility of electronic components to be embedded into the composite by allowing thermal cooling if required.
In conditions of energy harvesting from thin-film silicon photovoltaic solar cells, experimental research in the article done by (K̋. Jason Maung et al., 2010) concludes that after subjecting a sample to low strain tensile cyclic loading and to the manufacturing process conditions, no significant signs of performance deterioration were recorded within the solar cells which were bonded to the surface of a load-bearing composite component.
Electronics, in general, are sensitive to exposure to EMI. As composite materials have a fibre and matrix component in their construction, (Gibson, 2010) has reviewed research papers for indications about the use of intrinsically conducted polymer-based (ICP) matrixes. The same study also investigate ways in which conductive material fibres, such as carbon-fibre, can be applied in order to shield electronics against EMI.

The above research shows that multifunctional composites provide certain functions and capabilities, embedding components such as circuit tracks, thermally conductive or insulating materials, EMI shielding materials, and solar panels into a composite material.
Looking at the original aluminium frame structure, the primary design intent of this structure is to provide support and physical protection to the internal components and electronics. With the aluminium structure, protective cover panels and solar panels (with required PCB backing still attached) would have been added to the aluminium "skeleton" frame. Designing a nano-satellite structure based on a multifunctional composite material opens up the opportunity to consolidate many separate structural components into just a few components that perform more than one main function.

As an example, the outer panels of the satellite can have the strength to support the components inside, thus eliminating the need of a separate skeleton frame, but at the same time, the panels can also potentially have the solar cells, electronic circuits, EMI and thermal shielding embedded into the same structure. Thus, one component now effectively delivers the same functions that three separate structures had previously performed. This creates a reduction in overall-weight and increases the available space for components inside the satellite.

1.3 Overall Research Aim and Individual Research Objectives

The overall aim of this research is to design and analyse a multifunctional structure for use on a nano-satellite. However, in order to design a structure for nano-satellites

and effectively analyse its performance, it is critical to first explore the barriers that constrain the nano-satellite design and review the standards to which the structure has to conform to. An investigation into the properties, material composition and manufacture of multifunctional composites also needs to be conducted in order to create a greater understanding of multifunctional composites before any effective design work can be done with the material.

In turn, two main research vehicles will be exploited to facilitate this study: an in-depth literature review and analysis of empirical and numerical data models.
Specifically, within the context of higher education, the key objects are to:

- Explore current technology, developments and implementations of multifunctional composite materials and their applications in nano-satellites;
- Critically evaluate a representative numerical data model of a multifunctional composite sample created in a Finite Element Analysis (FEA) software package, using known material values of individual layer materials;
- Produce physical multifunctional composite samples and collect data from material tests for comparison to the numerical data models; and
- Formulate concept design/s and test a multifunction structure manufactured for use in CubeSats that complies with the current standards.

The first objective is critically important, as it provides a foundation for the research that has already been completed in multifunctional composites and will highlight areas that need to be examined through a further review of literature relating to the subject and/or material testing to find the required data.

A critical evaluation of a numerical data model created in an FEA software package based on the information and methods previously found in the results emanating from the first objective, constitutes the second objective.

The third objective consequently necessitates the investigation and setup of testing method/s on test samples produced to match those that were created for the FEA in the previous objective. As such, the recorded data obtained during the testing of the samples can be directly compared to the data recorded from the earlier FEA simulations. This is a crucial phase, as it will establish the relation between the computer-simulated model of multifunctional composites and the physical results of the material testing.

Finally, the fourth objective would demand the production of a concept design of a nano-satellite structure using multifunctional composites. By initially establishing the relationship between the data found in the literature review, FEA simulations and the physical testing, the eventual goal is to provide clearer data and predictive patterns of the potential behaviour of the concept design within the FEA simulations. Adjustments and optimisation of the concept design can then be executed during the simulation phase, thus reducing the number of structures required to be manufactured physically before a functional structure is manufactured to specification.

1.4 Value of this Research

This study will contribute to development in the field of multifunctional composites, specifically for use as a nano-satellite structure. A critical review of the applications and manners in which multifunctional composites can be used to improve nano-satellite structures will be obtained through the literature review.

Secondly, the manufacture and testing of multifunctional samples will allow empirical data to be collected and compared to numerical data produced by FEA computer models of the samples. This comparison between physical samples and those created by the use of FEA software will grant future designs and material predictions greater accuracy during the numerical computer analysis phase of the design, since a meaningful relationship between theory and practice will be established. This comparative data will not be sufficiently detailed to create final designs, but can be employed for the initial FEA-based designs. This process will, however, reduce the number of prototype models required for production during the research and development phase of the material or parts thereof.

The other key objective of this research is to develop a conceptual multifunctional structure for use in a CubeSat project currently underway at the F'SATI division based at CPUT. Developing a structure from composite-based material allows for greater weight reduction and space optimisation within the satellite system as a whole. It is well recognised in the aerospace industry that the critical component/material parameters are weight, strength and space (volume). A conceptual multifunctional composite CubeSat-structure allows for future development possibilities within the division to generate a production model of the composite structure as a commercial commodity, which could address the current niche in the CubeSat structures market.

This study will not only provide valuable data to future engineers developing structures for use in small satellites, but also for the development of a conceptual structure for current CubeSat project. This could result in vast commercial feasibility if a production model can be developed.

1.5 Outline Structure

The outline structure of this thesis is briefly described under each of the chapter headings that follow:

Chapter 1 - Introduction:
This introductory chapter provides the reader with background information on multifunctional composites and an overview of the potential material functional improvements that are currently under investigation. A background into the focus of the research of nanosatellites, specifically CubeSats, is provided. The application, justification and value of this research for use in nano-satellites structures are discussed. The overall aim and research objectives are also identified and explained in this chapter.

Chapter 2 - Theory Literature Review:
The literature review covers all the theoretical background required to gain an in-depth understanding of the fundamental engineering principles that are applied in this research. The review is extensive and covers most of the theory directly and indirectly related to the research to ensure that the review is sufficiently holistic for a range of engineers, regardless of discipline, to comprehend the theories and implicated practical work presented here. Composite material mechanics is the primary focus of the theory review; however, other sections related to electrical engineering PCB design have also been featured briefly to allow for connections to this field to be made by the reader. Fundamental understandings of spacecraft design, deliberations and theories have also been included as foundation of the research topic. Areas of systems engineering practices have been included, particularly the verification and validation of data and design work of spacecraft components. The testing standards required in this study have also been covered.

Chapter 3 - Numerical and Empirical Data:
The aim of this chapter is to present the data collected from both the numerical simulated use of engineering software and programs, as well as the physical test data collected from verification tests for material strength and structural vibration response. The primary engineering software used to execute the simulations was ABAQUS FEA, along with a progressive failure analysis (PFA) plugin tool created by Autodesk.

Chapter 4 - Discussion and Conclusion:
While the contents of this chapter are fairly self-explanatory, the primary purpose of this chapter has been to examine and discuss the collated data. The examinations and discussions also cover the comparisons of the various numerical and empirical data-sets. Based on these discussions and examinations, concluding statements are connected to the primary objectives of the research set out in Chapter 1.

Chapter 5 - Recommendations:
Following Chapter 4, Chapter 5 summarises various changes and alterations that could be implemented should a research budget allow for it. Over and above research budget issues, various recommendations for concerns discovered during the research, are deliberated in terms of future research work in this area of materials and spacecraft development.

Chapter 2

Theory Literature Review

2.1 Introduction

This literature review will examine the main developments, design methods, applications and manufacturing methods currently being researched in the field of multifunctional composites. The review of literature will stay within the field of nano-satellite applications and will address objectives 1 and partly objective 2 as set out in subsection 1.3. The literature review will provide the intended theory foundation for the overall objectives. Recapping the first objective:

1. Explore further into current the technology, developments and implementations of multifunctional composite materials and their applications in nano-satellites.

By exploring and evaluating relevant areas of literature, a significant contribution will be made to this research. The current developments in the field of multifunctional composite design and manufacture will assist to establish a firm foundation from where to conduct further meaningful practical design and physical material testing for the application in nano-satellite structures. This review of literature is set to cover the main topics of current design methods/philosophies, material data/material properties, existing analytical methods, the comparison of multifunctional composite design and manufacture to that of conventional composite manufacturing techniques.

Importantly, the research will provide quality insight into the predicted outcomes of the material and component performance. This will later be backed up and adjusted where applicable for use in nano-satellite structures. The literature review will additionally provide information about the areas of multifunctional composites which need more scrutiny in the practical material testing; alternatively, it will also highlight areas which lack sufficient data for the design application in nano-satellite structures.

The major purposes of this section is to gain a critical understanding of key issues; to inform the reader in these areas; and to attain a clear focus. It is the express ambition of the researcher to find justification for future empirical and numerical research in the field of multifunctional composites.

The first detailed topic of this section is to concentrate on the aspect of systems engineering. It is vital that the reader becomes acquainted with the practices and methodologies of systems engineering, as it will be used as the foundation for the development of the CubeSat structure covered in the methodology section.

2.2 CubeSats

2.2.1 CubeSat Overview

CubeSats represent a class of satellite classified in the nano-satellite range. The size of CubeSats has been standardised into cube units (also referred to as "U"), where each cube unit is approximately 100x100x110 mm and with a limited weight of 1.33 kg (Loff, 2015).

Various units are available and the range includes 1U to 12U in size. The CubeSats are deployed from launch-pods mounted in axillary payload areas in a launch vehicle. Funders of the primary payload cover most of the cost of the launch vehicle. This secondary payload system to launch a satellite reduces the cost to a fraction of what it would cost to have a dedicated launch vehicle. Thus, the standardisation of the CubeSat size allows any research centre located anywhere in the world to build a CubeSat and have it launched.

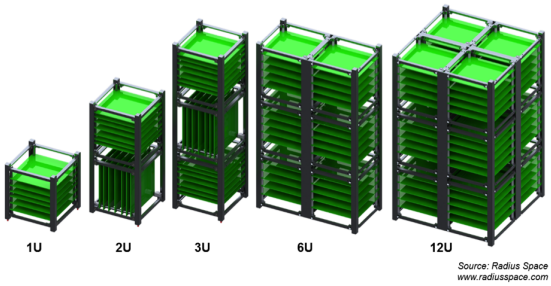

Figure 2.1: CubeSat standard unit sizes that are available.
(Radius-Space, 2015)

The primary purpose of the CubeSat program is to avail global space to universities and research centres to allow them to conduct space-related research. With the developments in technology, most sensors or equipment required to conduct a specific measurement or test in space will fit onto one of an available standard CubeSat-sized chassis.

Examples of space research include the measurement of the earths magnetic field, solar radiation-monitoring, earth imaging etc. One recent idea that has been considered by a university for further testing is the use of laser communication between the satellite and earth. Currently, most satellites still use a form on RF (radio frequency) antenna to provide communications to the satellite. Another issue that is currently under investigation is the development of a satellite with an on-board infrared-camera system that manages a tracking system for ground-based fires on earth.

Due to the restricted size profile of the satellites, it is challenging to have multiple main-payload systems; generally, each satellite has a dedicated purpose, designed around one primary piece of equipment or sensor.

Every CubeSat, however, does have the standard satellite requirements, inter alia a housing, solar panels to provide power, deployment systems and internal electronics. These systems are required by most satellites in one way or another. Generally speaking, each system is separate, individually added to the satellite and then linked together, once assembled. The following subsection discusses the CubeSats structural requirements in more detail.

2.2.2 Structural Requirements of CubeSats

CubeSat chassis have to be built to a standard size and properties specification, due to the fact that the satellites are launched from a holding pod, called Poly Picosatellite Orbital Deployer (P-POD) (Cal-Poly-SLO, Rev. 13).

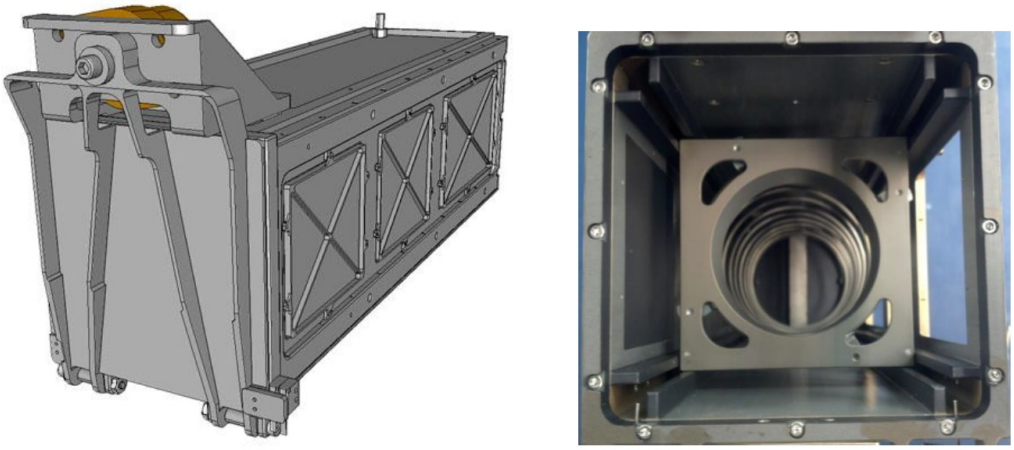

Figure 2.2: P-POD diagram and image.
(Cal-Poly-SLO, Rev. 13)

Figure 2.2 illustrates the rails that are located on the corner vertices of the satellite and which constitute the interface between the CubeSat and the P-POD. A spring-loaded platform at the base of the P-POD pushes out the contained CubeSats along the anodised aluminium rails, once the P-POD door has been released to open.

2.2.2.1 General Requirments

Based on the interfacing requirements of the P-PODS and those of the spacecraft for the operation in space, a list of general CubeSat requirements have been drawn up in the document by (Cal-Poly-SLO, Rev. 13) and consist of the following:

- All parts need to remain attached to the CubeSats during launch.
- No pyrotechnics are allowed.
- CubeSat hazardous materials shall conform to AFSPCMAN 91-710, Volume 3.

- CubeSat materials must satisfy the following out-gassing criteria to prevent contamination of other spacecraft during integration, testing and launch; A Total Mass Loss (TML) $\leq$ 1.0% and a Collected Volatile Condensable Material (CVCM) $\leq$ 0.1%.

The list presented above highlights the important requirements applicable to this specific research effort.

2.2.2.2 Mechanical Requirments

The applicable mechanical requirements for CubeSats as also listed in (Cal-Poly-SLO, Rev. 13) are:

- CubeSat configuration and physical dimensions shall be per the appropriate section, listed in Appendix A.2 and A.3.
- No components on the green and yellow shaded sides shall exceed 6.5 mm normal to the surface.
- When completing a CubeSat Acceptance Checklist (CAC), protrusions will be measured from the plane of the rails.
- Deployables must be contained by the CubeSat.
- Rails must have a minimum width of 8.5 mm.
- Rails must have a surface roughness of less than 1.6 μm.
- Rail edges must be rounded to at least a 1 mm radius.
- The ends of the rails must have at least a 6.5 mm x 6.5 mm contact area.
- A minimum of 75% of the rail must be in contact with the P-POD.
- Maximum mass of the 1U CubeSat shall be 1.33 kg.
- Maximum mass of the 3U CubeSat shall be 4 kg.
- The centre of gravity of the CubeSat must be located within 20 mm from its geometric centre in the X and Y directions.
- The centre of gravity in the Z direction must be within 20 mm of its geometric centre for a 1U CubeSat.
- The centre of gravity in the Z direction must be within 70 mm of its geometric centre for a 3U CubeSat.
- Materials other than the aluminium used for the rails and CubeSat structure must submit a DAR and adhere to the waiver process.

- The rails and stand-off, which contact the P-POD and adjacent CubeSats must be hard anodised aluminium to prevent cold welding within the P-POD.
- 1U CubeSats must use separation springs to ensure proper separation takes place (Refer to Appendix A.1).
- Separation springs are not required on 3U satellites.

2.2.3 Current CubeSat Structures Available

Now that the standard CubeSat specifications are known, an investigation into the current CubeSat structures that are commercially available on the market can be undertaken. In the CubeSat community that has developed at CPUT, two main suppliers are referenced: ISIS and Clyde Space. ISIS (Innovative Solutions In Space) is a company based in the Netherlands at the Delft University of Technology. ISIS develops their own set of structures and the performance characteristics can be seen in Appendix A.4.
The company, ClydeSpace, is based in the United Kingdom. They also produce CubeSat structures and supply CPUT with most of their required CubeSat parts. At the time of writing this thesis, A.5 illustrated the basic specifications available for ClydeSpaces 3U CubeSat structure via the on-line store, which provides the mass of the skeleton structure (390g) as a key parameter of the overall design of the CubeSat.

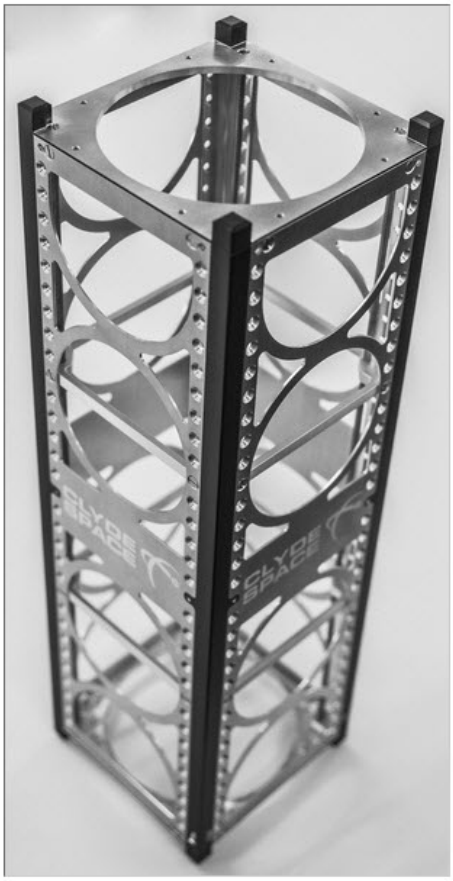

Figure 2.3: Clyde Space 3U Structure. (Clyde-Space, 2016)

The third category of CubeSat structures is produced by Pumpkin Inc. and their type of structure can be seen in Figure 1.2. CAD models of the Pumpkin Inc. structures are publicly available on their website.

All the above-mentioned manufacturers produce the complete CubeSat structure from aluminium, with the ability to attach the solar panels and the accompanying PCB to the exterior surface of the satellite. The visual designs may vary between manufacturers; however, they all conform to the standardised size specifications as initially specified.

All the manufacturers structures have been flight-tested, and in most cases flight-proven by now as well. The advantages of using aluminium as the primary material is twofold: the cost is relatively cheap and it is easier to machine and handle when compared to a composite. The second advantage is the fact that it is listed by NASA as a TML-approved material. Only specified configurations of composite materials, due to the wide range of varieties, have been listed as approved by NASA.

2.2.4 Developments in Composite CubeSat Structures

Up till now, there has been a lively interest in the CubeSat community in the development of a composite-based CubeSat structure. A CubeSat project (NUTS) is based at the Norwegian University of Science and Technology. Reportedly, research and development of a carbon-fibre structure have been under development since 2011. Although there are not many details available on their website at the time of writing, some information was available regarding the structure.

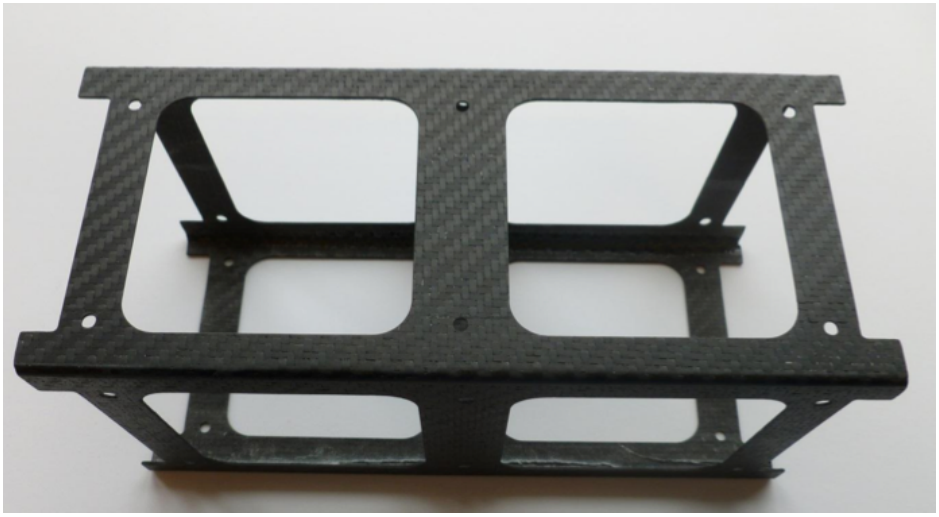

Figure 2.4: NUTS first carbon fibre design.
(Haland, 2013a)

The team reportedly refined and optimised the carbon fibre design from the original one shown in Figure 2.4. Figure 2.5 below shows the updated design and the addition of the aluminium rails. The side panels are still produced from carbon-fibre; however, the design was changed to include the aluminium rails, as the previous full carbon-fibre structure could not comply with the correct tolerance specification required for the interfacing with the P-POD. Additionally, the CubeSat standards state that the interfacing of the P-POD rails to the CubeSat must comply with a specific aluminium surface roughness. The grade of aluminium used in the new design is 7075, which is also the specified grade in the CubeSat standards.

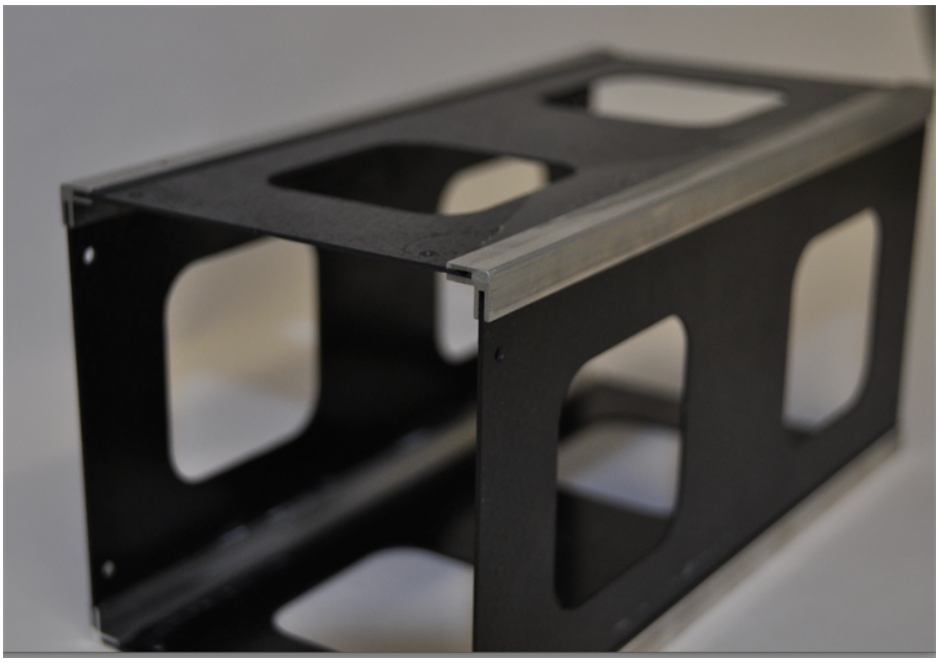

Figure 2.5: NUTS second carbon fibre design.
(Haland, 2013a)

The carbon-fibre reinforcement used on the CubeSat was a high-grade prepreg material. The carbon-fibre was donated to the NUTS project by an aeronautics company. The higher quality carbon-fibre will perform better at the outgassing test; nonetheless this does not necessarily imply that it will pass the required standard qualification of less than 1%.

Machining of the carbon-fibre panels was executed on a PCB CNC milling machine. According to (Haland, 2013b) report, the PCB CNC machine provided a sufficiently accurate finish and tolerance to allow for a successful assembly of the prototype structure.

2.2.4.1 Developments in multifunctional composite applications in spacecraft

The primary focus of this research is the application of secondary functions using MFC structures, incorporating non-structural functions such as electrical conductivity (microcircuitry), thermal conductivity and dissipation, energy harvesting, EMI shielding and radiation shielding. The structural functions of the composites are to be developed according to a proven composite specification that is flight-tested for use in space. This will provide a good structural base in order to experiment and develop the non-structural functions incorporated into the composite. The current research presented below relates to the topic of multifunctional composites field. Each of the research-relevant fields being conducted in this thesis is expanded on in the multifunctional materials subsection later on.

2.2.4.1.1 Electrical conductivity (microcircuitry) Research has been conducted into the positioning of flexible printer circuits by embedding wiring harnesses (FPC) between composite layers in the structural panel. Physical samples have shown that there was no damage to the FCPs under the required curing conditions for a broad range of composites and prepreg composites, and they remained perfectly functional (D̋iPalma et al., 2004). The structural integrity of the panel was not affected by the addition of the FPC layer (D̋iPalma et al., 2004). A possible drawback of the FPC could be the limitation of the current rating of the conducting tracks and ease of manufacturing of the FPC. FPCs are currently available and used in the electronic systems, generally as a method of flexible connection between PCBs.
The compatibility with surface-mounted electronic components utilized in conducting tracks between composite laminates would drastically interfere with the surface-mounted electronic geometry of the composite fabric, which constitutes a weakness.

2.2.4.1.2 Thermal conductivity and dissipation The same method that is utilized to embed the FPCs into composite panels is also used to embed thermal insulating or thermal conducting material. By positioning the thermal materials in planned locations, areas of the composite can be employed as extended heat sinks. It additionally allows for the possibility of electronic components being embedded into the composite by tolerating thermal cooling (S̋eong Jang et al., 2010). The opposite can be achieved as well, by locating thermal insulators in the areas that are too cold. The ability to position and control the thermal insulation of the composite panels allows for a "tailored" (S̋eong Jang et al., 2010) thermal environment for internal electronics. Various materials have been employed as thermal conductors and insulators; amongst these are thermal pyrolytic graphite (TPG) and K13D2U high thermal conductivity fibre (D̋iPalma et al., 2004).
Nevertheless, in this research the thermal focus will be on the applied materials which encompass the composite panel, including a dedicated layer for electrical connections. The configuration of these materials will be evaluated and the possibility to add dedicated thermal material can be investigated in another more detailed research study, which can augment this particular thesis. Once again, this study aims to establish an initial workable structure from which further research and refinement of the concepts can be undertaken with reference to pertinent aspects of the structural characteristics.

2.2.4.1.3 Energy harvesting Multifunctional composites allow for the possibility of incorporating photovoltaic solar cells into or onto the surface of a structural composite component. This will open up the ability for the composite to harvest solar energy as one of its functions. For this application, experiments have been conducted using thin-film silicon photovoltaic solar cells (Ḱ. Jason Maung et al., 2010). The experimental research in this particular study confirms that low-strain tensile cyclic loading, as well as the manufacturing process conditions, do not reveal any significant signs of performance deterioration when the thin film solar cells are bonded to the surface of a load-bearing composite component. The method of co-curing construction has been applied during the fabrication of these test specimens. The co-curing method layers the prepreg composite material into the desired form along with the

photovoltaic film, consequently subjecting the part to the standard curing process (K̋. Jason Maung et al., 2010). The earlier mentioned curing process for prepreg composite materials requires a higher temperature and pressure than that of atmospheric.

2.2.4.1.4 EMI and Radiation Shielding Electromagnetic interference and radiation exposure can create undesired disturbances in the operations of the electronic systems (Gibson, 2010). Materials used in the shielding of electronic components against EMI and radiation are assessed in shield effectiveness (SE). Metallic and non-metallic materials have been used for shielding; however, due to the advantages of reduced weight the non-metallic materials have been favoured (Gibson, 2010). The non-metallic shielding materials are polymers and polymer composites (Gibson, 2010). A review on relevant research papers on fibre fillers by (Gibson, 2010) indicates the potential use of an intrinsically conducting polymer (ICP) based matrix. Alternatively, conductive material fibres such a carbon-fibre can be employed in order to shield electronics. Thus, using a carbon composite material will provide a natural shielding effect for internal electronics due to its conductivity.

2.2.4.1.5 Application of multifunctional composites in CubeSats After consultation with the personnel at the FSATI division at CPUT, a keen interest was expressed by all about the prospect of developing MFC structures for CubeSats. All the non-structural functions that were discussed in the previous paragraphs have the potential to optimise the CubeSat package within their development programs. Features, such as embedded electronic circuits or tracks, to route power and communication signals throughout the satellite, permit for a reduction in basic electronic requirements on the PCB-surface thus allowing a greater area for other more complex PCB-based electronics. The ability to adjust the thermal conductivity of the composite panels concedes control of the thermal environment within the satellite to create an optimal condition for the electronic components. Radiation and EMI shielding functions offer protection to any sensitive electronics that have a high risk of damage from exposure to these elements. The potential seamless incorporation of thin film solar cells into the external area of the composite skin mitigates the need to mount additional panels onto the satellite to support the solar cells. This potentially reduces the net weight of the satellite. Although the weight of the structure is not listed as a function above, research has shown that a weight reduction of up to 57% can be achieved through the use of MFC for routing wiring harnesses (D̋iPalma et al., 2004). This reduction in weight will allow more payload for the electronic systems on-board the satellite.

2.3 Space Operational Environments

There is a significant difference between space and the earth environment. The earths atmosphere provides a great deal of protection and calm to the environment which we experience on the surface. While there is no rain or weather in space, still other factors that we are not familiar with, are now introduced. The satellite deals with the earths environment during its creation, assembly and launch. Once in orbit tough,

the effects of radiation, debris and thermal environment can cause components to function inversely and can occasionally be implicit. If missed, this will show up as an emergent property of the system. The environment to which the satellite will be exposed to thus needs to be considered in the structural design of a spacecraft. The section to follow discusses the key theory points and factors that have an influence on the mechanical structural design. These sections cover every single detail of the space environment; even so, it highlights key considerations during the design of the spacecraft structure.

2.3.1 Ground Segment Environments

The satellite will be exposed to ground segment environments during its time on earth. These environments are familiar to us as the context that we are consistently dealing with in most fields of engineering.

2.3.1.1 Pre-Launch Stage

The pre-launch stage of the satellites can be quite lengthy: anywhere between five to ten years (Fortescue et al., 2011).During this time the design, manufacture and assembly of the satellite take place. Careful consideration of the materials characteristics on earth and its interaction with the atmosphere need to be taken into account. Components manufactured in the early phases of the build can be stored for months on end before assembly or integration with another component. The time and conditions that the components are stored in need to be considered, particularly in the case where moist conditions can cause corrosion. Materials that corrode or degrade in the earths atmosphere may be fitting in the space environment, but the time it spends on earth and exposure to the atmosphere needs to be planned for to ensure the components don't degrade before they reach space.

2.3.1.2 Launch Environments

The launch of a satellite is an extremely violent process and is likely, from a vibrational and shock point of view, the most dangerous time in a satellites lifespan (Fortescue et al., 2011). Initially, the vibrations are caused by the SRBs (Solid Rocket Boosters) firing together with the acoustic reflection of the ground (Fortescue et al., 2011). As the launch vehicle travels further from the surface, the acoustic reflections become less, however, the internal mechanisms operating create large amounts of vibrations. For example the fuel pumps for the liquid fuel rocket produces vibration patterns as the demanded flow rate is extremely high (Fortescue et al., 2011). Further into the launch, the speed of the vehicle increases and the aerodynamic noise intensifies with respect to the velocity. The shock loads are created by the explosive pyrotechnics that are activated to decouple the SRBs and various stages of the launch vehicle. The explosive actions are also generally followed by the jettisoning of the stage components to ensure it breaks away from the launch vehicle cleanly.

Significantly, during the launch, the atmospheric pressure drops as the launch vehicle ascends. As an example, the Ariane 5 has venting ports that control the de-pressurisation to 2 KPa/s (Fortescue et al., 2011). It is additionally reported by (Fortescue et al., 2011) that at certain stages of the launch the de-pressurisation rate can reach up to 4.5 KPa/s. The de-pressurisation of closed compartments on the satellite must also be done as the vehicle ascends to prevent a relative pressure build up, for example in electrical boxes or housings.
Further information and design related data of the launch conditions is discussed further in the spacecraft structural design section later in this chapter.

2.3.2 Space Environment Conditions

Space conditions, as earlier stated, are somewhat different to the earths environmental conditions. Aside from the obvious lack of atmosphere in space, there are other environmental conditions that influence the structural design aspects of spacecraft. These points are discussed in the sections that follow.

2.3.2.1 Solar Radiation

The Sun in the solar system provides almost all the heat that is available. It is only logical that it is the dominant force in the solar system in which everything quite literally revolves around. The Sun is essentially a very large thermonuclear fusion reactor (Fortescue et al., 2011). Some statistics on the Sun are; diameter is 7×10^8 metres, mass is approximately 2×10^{30} kg and has a power output of 3.85×10^{26} Watts (Fortescue et al., 2011).

The solar spectrum covers a wide range of wavelengths, from radio waves to gamma rays. Each range of wavelengths is emitted by the different solar atmosphere levels. The lower level solar atmosphere is called the *chromosphere* and the upper level is the *corona* (Fortescue et al., 2011).

One of the environmental effects created by the Sun is *solar winds*. Solar winds are created from flows of plasma that are expelled from the Sun's atmospheric flux (Fortescue et al., 2011). The solar winds can be related to the Sun's activity level and an indication of the Sun's activity are *sunspots* that appear on its surface. Solar winds generally travel at approximately 450 km/s and have a density of roughly 9 protons/cm^3. Also related to the sunspots is the level of disruption on the surface of the Sun and in turn, the level of radiation emitted by the Sun is generally higher during this time. Solar flares activity and coronal mass ejections are also at a higher frequency during this time. Solar flares are pulses of radiation from the Sun that occurs when a build-up of magnetic energy is discharged in the solar atmosphere. Coronal mass ejections are bursts of solar energy, solar mass and magnetic field energy from the surface of the Sun in a "tail" of fire and generally releases the plasma flux which becomes the solar winds.

2.3.2.2 Earth Orbit Environment

The first point that must be made about the earth's orbital environment is the link to the radiation exposure as discussed in the previous section. The radioactive ions and particles travel at high speed in the solar wind condition, however the electrons and ions carry their own currents which interfere with the earth's own core magnetic field and this forms the overall *magnetosphere* (the magnetic atmosphere of the earth), as shown in figure 2.6 (Fortescue et al., 2011).

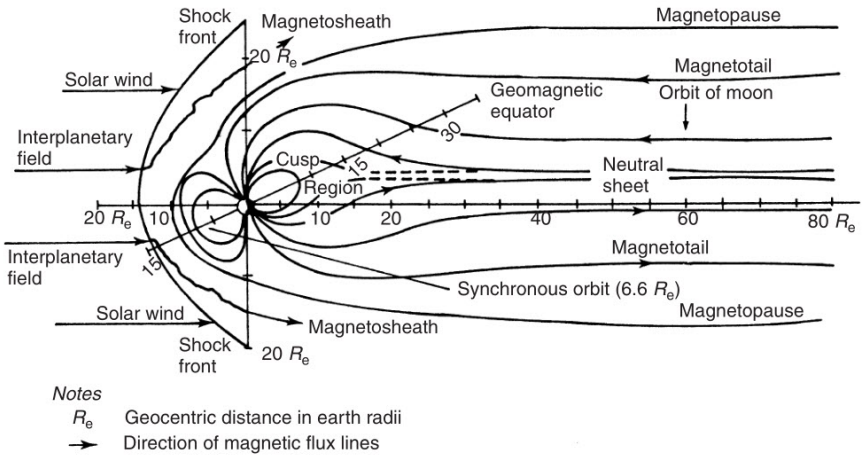

Figure 2.6: The earth magnetosphere and the influence of solar wind partials. (Fortescue et al., 2011)

The earth's magnetic field also traps some of these radioactive ions and electrons in "belts" in particular areas. The *Van Allen* radiation belt is an example of this and it generally follows the contour of the earth's magnetic field lines. In the case of LEO satellites the consideration of the *South Atlantic Anomaly*, which is an area of concentrated radiation that is geometrically located close to the earth and at lower altitude levels (Fortescue et al., 2011). With a LEO and low *Beta* angle (angle of the orbit inclination relative to the solar axis), it is likely that the satellite will pass through this radiation region every orbit.

The effect of the radiation is mainly on the structural material and the electronic subsystems of the satellite. The structural effects of radiation can be seen on most materials, for example, zinc or cadmium metals can form small metallic spikes when exposed to radiation at even small levels (Fortescue et al., 2011). The note must be taken that "heavier" particles such as protons and neutrons cause much larger damage to materials than that of the "lighter" electrons.
The electronic effects cause *Single event effects* (SEEs) (Fortescue et al., 2011). This can consist of single event upsets and single event latch-ups. A single event upset can be caused when a radiation particle strikes a sensitive electronic component, where the induced charge is large enough to create a change in the logic state of the device. This is a less severe issue as it can generally be cleared by resetting the device. A single event latch-up is very similar to that of a single event upset, however, in this case, the

device is locked into a particular state, where even when the device is powered down the logical state is still held fixed. A severe issue from single event latch-ups can be a single event burnout (Fortescue et al., 2011).

Another major factor that affects the structural materials of a spacecraft is *atomic oxygen erosion* at LEO. Due to the LEO being just off the atmospheric zone of the earth, there is still the presence of molecular density which can be significant (Fortescue et al., 2011). At LEO altitudes the main species of the atmosphere are atomic oxygen or helium. The relative velocity of these atoms is at approximately 8 km/s due to the orbit of the satellite (Fortescue et al., 2011). The impact of these atoms on the structure of the satellite has an erosion effect. Some metals like silver react with oxygen and cause corrosion. The types of materials used must be selected with this environment in mind, although for most other metals the erosion factor is small enough that the effects would only be visible after the lifespan of most CubeSat missions (a few years to yield any noticeable effect). An interesting point highlighted by (Fortescue et al., 2011), states that the atomic erosion effects actually increases the fatigue strength of metals by an order of magnitude. The two theories that have been hypothesised is that the oxidisation prohibits crack growth and propagation and the other is that the absorption of oxidisation and gas diffusion into the material bulk changes the material properties (Fortescue et al., 2011).

Finally, the last point is the presence of space debris. The debris in space has been created over the years by space activities and now poses an issue to active satellites. The important note is that this factor creates the chance of debris impact on the satellite. More details on this is provided in the impact section of the spacecraft structural design later in this chapter.

2.3.2.3 Thermal Environment

In space, there is only thermal radiation that can be received and dissipated by the satellite (Fortescue et al., 2011). Convection of heat is not possible due to the lack of atmosphere. Conduction of heat between parts of the satellite itself is possible. The heat input from the sun is radiation and the near-earth environment experiences a radiation level of approximately 1371 W/m^2 (Fortescue et al., 2011). The earth also has an albedo (reflectivity of the earth's atmosphere) which has a magnitude of 200 W/m^2. Solar wind provides negligible heating levels at LEO (Fortescue et al., 2011). Frictional heating is also negligible, although there is atomic density at LEO, the amount is so small that the friction levels created are very small. The rate at which the atoms strike that satellite does not induce a significant heating effect on the satellite.

2.4 Multifunctional Composites

Multifunctional Composites (MFC) (also referred to as "Smart Composites") systems are designed to perform more than one "primary" function simultaneously (Thomas

and Qidwai, 2004). This material's main design purpose is to reduce the redundancy of combined subsystems by "embedding" other materials into the main structural elements of a composite material to drastically alter its thermal, electrical, shielding and/or create energy harvesting functions. Ultimately, composite materials now not only have the traditional function of providing structural support to components but also have the ability to perform other main functions such as electromagnetic interference shielding and thermal insulation for electronics all from a single part.

MFC materials can also have various mechanical properties adjusted along with the addition of non-structural functions (Gibson, 2010). As taught in engineering, material structural functions consist primarily on strength, fatigue strength, ductility, stiffness, energy absorption, damping, and thermal stability. Non-structural functions would namely be electrical conductivity, thermal conductivity, material condition sensing and deformation, energy harvesting, energy storage, self-healing capabilities, electromagnetic interference (EMI) shielding, biodegradability and multiple other functions (Gibson, 2010).
For the application of MFC materials in nano-satellite structures the relevant MFC functions that will be focused on in this research thesis have been broken down into the subsections that follow.

2.4.1 Composite Materials

The composite structure forms the primary structural base for multifunctional composites, without this structure there would essentially be no composite part at all. In the previous "background" section of the report, the general concept of a composite material was highlighted. Composite materials primarily consist of a combination of two different materials, namely; the fibre and the matrix (or resin).

The purpose of this section of the literature review is to explore further into composite materials and the research, design and information relevant to the scope of this report. This section will focus on the design and structural applications of composite materials and briefly touch on the thermal and manufacturing methods used for composites. The thermal, manufacturing and shielding (Electromagnetic) will be covered in more detail in subsections that follow.

2.4.1.1 Reinforcement Materials

Fibre reinforcements are the load carrying component of a composite material (Rosato and Rosato, 2004). The stresses applied to composite materials are transferred from the weaker resin matrix to the much stronger reinforcing fibres. In order to produce an effective reinforced plastic part, the elongation of the fibre must be less and the stiffness modulus must be higher than the matrix. This is required to allow most of the stresses to be transferred to the fibre material. The diameter of the fibre strands also has a large impact on the effective stress transfer in the composite material. The smaller the diameter of the fibres, the larger the surface area of fibre is in contact with the resin matrix, thus allowing better load transfer between materials.

2.4.1.1.1 Reinforcement types and configurations There are many types of reinforcement fibres and resin matrix materials that can be used in composite materials. The resin matrix types are discussed further in a later section. A few common reinforcement fibres used in industry are:

- Glass Fibres
- Carbon Fibres
- Graphite Fibres
- Ceramic Fibres
- Aramid Fibres (Kevlar)

Fibreglass is one of the most commonly used fibre reinforcements in the industry, this is due to its relatively low cost and its ability to provide good strength to weight ratios. However, all the fibres listed above are available in either discontinuous, 1D or 2D textiles continuous fibres.

Discontinuous fibres are obtained by chopping continuous fibres or producing it directly into short fibres form to reduce cost. Typical examples of this are chopstrand mat. Advantages of this discontinuous fibre mat is that is can be subjected to loads in various directions and leans itself to easier manufacturing processes (Barbero, 2010), however, the quality of the composite part is not as high as a continuous fibre setup, as there are larger and more inconsistent resin cavities between the fibres. Also, the load transfer between the short fibres has to travel at some point through the sections of the resin matrix, which in turn lowers the load carrying capability of the composite system. An ideal application for this type of composite is for low stress components, examples such as mould casings, small boat hulls or pickup truck load bed canopies. Chop-strand mat is typically used with glass fibres as the overall cost would be less and the strength properties that high-performance composite fibres provide would be wasted in this configuration type. Figure 2.7, show an example of chop-strand glass fibre mat.

Figure 2.7: Chop-strand mat.
(AMT-Composites, 2015)

Continuous fibres, however, are preferred for high-performance applications where carbon, graphite or aramid fibres are used. Continuous fibres consist of single plane fibres 1D or 2D fibres generally woven into a textile configuration, for example:

1D textiles:

- Strands - is a bundle of untwisted continuous fibre filaments.
- Yarn - is a twisted strand.
- Tow - is a carbon fibre strand.
- Roving - is a collection of parallel strand, either twisted or untwisted.

2D textiles:

- Plain weave
- Twill weave
- Satin weave
- Stitched fabric
- Basket weave
- Continuous-strand mat
- Tri-axial weave

2D textile fibre fabrics are created by a group of woven or non-woven tows or rovings. The woven fabrics use very similar patterns to that used in the fabrics for the clothing industry. Non-woven fabrics generally consist of fibres which are either bonded together (using adhesive in some locations) or stitched together in different directions (uni-axial, bi-axial, etc). Figure 2.8 shows the different types of continuous fabric's which are available.

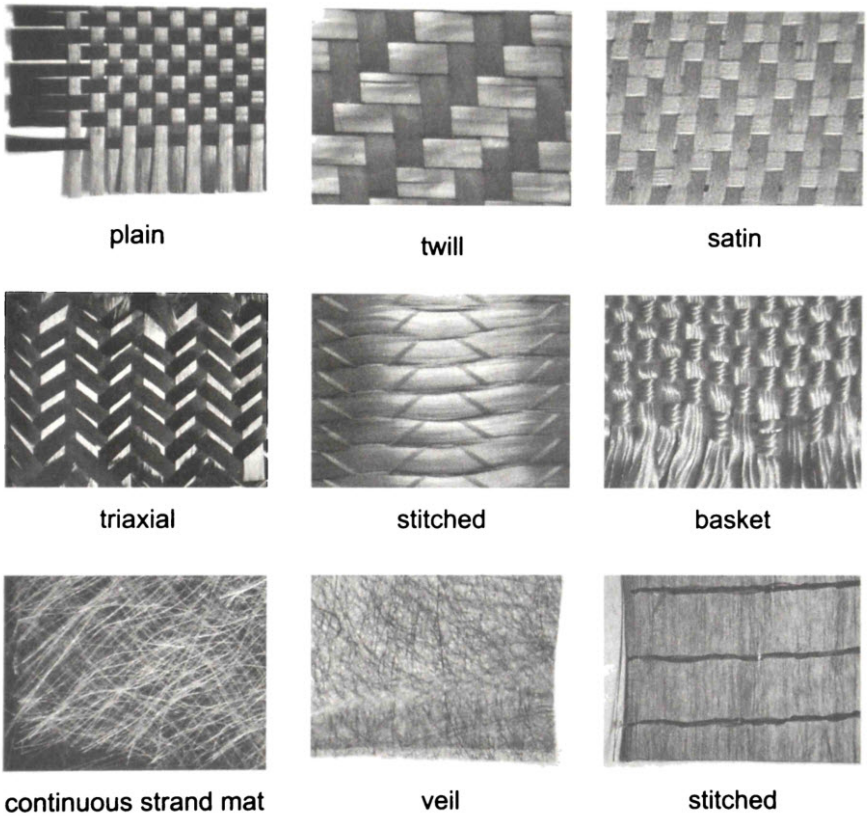

Figure 2.8: Continuous strand fabrics.
(Barbero, 2010)

For this thesis, the focus of the reinforcement material will be on carbon fibres, as that is the primary fibre that will be used to design the MFC CubeSat structure. Carbon fibres are discussed in more detail in the sections that follow.

2.4.1.1.2 Carbon Fibre Carbon fibres are lightweight and strong fibres with good chemical resistance (Barbero, 2010). They have been the reinforcement of choice in the aerospace market due to its properties. Carbon fibres can vary in their properties, depending on raw material composition and the manufacturing process used to create them. Two main types of raw materials are used to create carbon fibre: polyacrylonitrile (PAN) and pitch. Pitch fibres are cheaper than PAN fibres, however, pitch fibres are about half as strong in tensile loading and one-third as strong in compressive loading when compared to PAN-based fibres (Barbero, 2010). PAN-based fibres also offer a wide range of stiffness and strength values, which is another reason why it is a popular choice for aerospace applications.

Using a high modulus fibre allows the composite properties to imitate materials such as steel or aluminium (Barbero, 2010). However, to use the carbon composite to only replace an existing material such as steel or aluminium will lead to an inefficiently designed composite part. Rather than using the composite material as a "replacement" material, it needs to rather be used as an enabling material. Thus the composite material now not only produces a better strength to weight ratio part but also allows

other design features to be improved. This is where the use of multifunctional technology can now be included in the overall design intention. Not only does it allow for MFC technology, but can also in some application reduce the cost of manufacture of parts, as a single more complex part can now be created in the place of multiple metal components that would have once need to have been assembled. Being generally stiffer than glass fibres, carbon fibres provide better fatigue characteristics by reducing the amount of strain subjected to the polymer matrix for any given load (Barbero, 2010). The economic use of carbon fibres can sometimes be hard to justify, particularly where the components that are intended to be made of carbon fibre are not weight critical. Another important property of carbon fibre is that it has good electrical conductivity properties. Generally when in contact with electrically charged of energised equipment, the carbon fibre layers are separated from the metallic components by means of a layer of glass fibre material.

One of the latest research areas in composite technology is that of carbon nanotube CNT technology. This is one of the most interesting developments in the composite industry due to the properties that are being achieved with the structures. CNT are the arrangement of carbon atoms that is controlled during manufacture so that a perfectly cylindrical atomic structure of about 1 nm in diameter and 1 μm in length are achieved in such a way that the strong carbon bonds are orientated along the cylindrical axis (Barbero, 2010). This microstructure arrangement produces extraordinary strength in the fibre material by almost eliminating the material defects in the microstructure which is generally the limiting factor for most materials. Reports of the material modulus of about 1000 GPa and their strength being about 30 GPa, far exceeds any material made before it. However, the major limiting factor of the CNT fibres is their cost. Due to the cost of manufacture, the use of CNT in industry does not exist. They are extremely expensive and have not yet been able to be mass produced cheaply. Future developments and manufacturing improvements will hopefully see CNT fibres become a more affordable material for use in composite parts.

2.4.1.1.3 Carbon Fibre Properties Carbon fibre properties as mentioned in the previous section vary in terms of their raw materials that they comprise of as well as the manufacturing technique used to create them. For this particular research, the use of conventional carbon fibres either pitch or PAN fibres will be used for the materials of the CubeSat structure. Composites are also uni-directional materials, thus the maximum strength of the material is only available in a plane parallel to the length of the fibres. More detail on the orientation and component design of the carbon fibre materials will be covered in more detail in a subsection further on in this thesis.

The properties of carbon fibre materials are provided by manufacturers and are specified in which plane the strength and modulus of the material were measured relative to the fibre length. Unlike steels composite properties are not generally given or found very easily due to their complex nature. When working with metals (homogeneous material) which are made to a standard, properties of particular metal compounds can be generalised as the measured property difference between metals is fairly low. By also being a homogeneous material, metals have a constant modulus and strength in all planes of the material elements. Composites do not have very much consistency

Type	No. of filaments per tow	Tensile strength			Tensile modulus[a]			Elongation	Mass per unit length	Density
		ksi	MPa	kgf/mm²	msi	GPa	kgf/mm²	%	Tex (g/1000 m)	g/cm³
T300	1,000–12,000	514	3530	360	33.4	230	23,500	1.5	66–800	1.76
T300J	3,000–12,000	611	4210	430	33.4	230	23,500	1.8	198–800	1.78
T400H	3,000–6,000	640	4410	450	36.3	250	25,500	1.8	198–396	1.80
T700S	12,000–24,000[b]	711	4900	500	33.4	230	23,500	2.1	800–1650	1.80
T800H	6,000–12,000	796	5490	560	42.7	294	30,000	1.9	223–445	1.81
T1000G	12,000	924	6370	650	42.7	294	30,000	2.2	485	1.80
M35J	6,000–12,000	683	4700	480	49.8	343	35,000	1.4	225–450	1.75
M40J	6,000–12,000	640	4410	450	54.7	377	38,500	1.2	225–450	1.77
M46J	6,000–12,000	611	4210	430	63.3	436	44,500	1.0	223–445	1.84
M50J	6,000	597	4120	420	69.0	475	48,500	0.8	216	1.88
M55J	6,000	583	4020	410	78.2	540	55,000	0.8	218	1.91
M60J	3,000–6,000	555	3820	390	85.3	588	60,000	0.7	100–200	1.94
M30S	18,000	797	5490	560	42.7	294	30,000	1.9	745	1.73
M40	1,000–12,000	398	2740	280	56.9	392	40,000	0.7	61–728	1.81

[a] Measured using the impregnated strand test method

[b] T700S – 24,000 is temporary value, subject to change.

This information can be used just for material selection purpose

Table 2.1: Examples of different types of carbon fibre materials.
(Rosato and Rosato, 2004)

when sourcing material data (Rosato and Rosato, 2004). Due to material variation from manufacturer to manufacturer, the different types of carbon fibres available, all the different possible matrix combinations that can be used with the carbon fibres, relevant material data to a specific application is very difficult to come by. It is in almost every case highly recommend that material data for a specific fibre/resin system should be obtained in order to accurately predict/simulate the final composite material properties within the design. As a reference, Table 2.1 lists material data specifications for different types of carbon fibre.

2.4.1.2 Matrix Materials

Matrix materials have many functions, it binds the fibres together thus allowing the transfer of the load from the weaker matrix material to the stronger reinforcing fibres. Matrix materials generally carry transverse loads, intralaminar shear and bearing stresses (Barbero, 2010). Within a composite structure, there are a few characteristics that are primarily governed by the matrix material properties, such as working temperature range, chemical resistance, abrasion resistance, weathering capabilities, heat and electrical conductivity (Barbero, 2010).

Matrix materials can be polymers, metals or ceramics. For the purpose of this thesis, the composites referred to throughout this report will primarily refer to polymer based composite structures. Polymer matrix materials are the most widely used in industry due to its relatively easy manufacturing techniques and low tooling costs. The polymer matrix can be either thermoset or thermoplastic plastics. Widely used are the thermoset plastics, primarily polyester or epoxy polymers.

The composite parts or reinforced plastic parts are better equipped to deal with continuous loading and to withstand creep in the material. When compared to standard

plastic parts, which are largely affected by creep when used as a loaded component, reinforcing the plastic virtually eliminates creep in the plastic material (or now composite) component (Barbero, 2010).

Polymer matrix composites (PMC) are similar to aluminium and steel during the selection process for a particular application. Before the selection of a particular polymer for an application, the working requirements of the material and the conditions that the part will be subjected to will have to be known in order to make the correct choice. Polymers are also not all the same, and much like steels that also vary in the properties available, such as hardness ratings or tempered states, polymers are also available in a variety of material property specifications. The polymer that will be focused on in this thesis will be the two thermoset plastics mentioned earlier, polyester and epoxy resin systems. These two thermoset plastics will be focused on as they are the most commonly available resin systems in the general composite manufacturing industry. The thermoset resin systems will be covered in more detail later on.

2.4.1.2.1 Thermoset Resins: are formed by an irreversible chemical process where a resin system is turned into a cross-linked polymer matrix (Barbero, 2010). A resin system is the uncured form of the polymer matrix system (liquid form). Once the resin system has cured it forms a solid plastic composition. Between thermoset and thermoplastics, the thermoset plastics are commonly used more often than thermoplastic resin systems due to their relative ease of use and general cost. Thermoset resins do not soften when heated like thermoplastics do. Thermoset resins are stored in separate parts and are mixed on demand when required during manufacture. Resin systems are generally available in a "Part A and Part B" format, where part A of the mix would generally be the resin itself and the part B would be the hardener/catalyst required to commence the transformation of the polymer as mentioned above.

Terms used with resin systems such as; shelf life, which refers to the time that the unmixed resin system can be stored, or pot life which refers to the usable time of the mix resin system. "Gel time" refers to the gelation rate of the resin mixture and depends on the curing system, catalyst used and reactivity of the resin (Barbero, 2010).

Depending on the choice of the resin system, catalyst and mixture ratios, the curing time of the resin can be from minutes to hours. During the reaction or transformation phase of the resin, the process can be either exothermic or endothermic depending on the type of resin system. During the curing phase of thermoset resins, they experience a volumetric shrinkage of the plastic material. This particular property is of high importance to any designer of composite parts as the volumetric shrinkage will affect the dimensions of the final part that is produced. Volumetric shrinkage must not be mistaken for thermal expansion or contraction of the material, volumetric shrinkage occurs due to the availability of free volume in the polymer matrix during the curing cycle of the polymer composition (Barbero, 2010). The amount of volumetric shrinkage of the material depends on the type of thermoset resin system used. Depending on the resin type and manufacturing process used, the mould of the composite part may have to be offset in order to compensate for the shrinkage and create the desired final part as designed.

The most common type of thermoset resin systems on the market are polyesters, vinyl ester, epoxy and phenolic. In general, all resin systems provide a higher thermal insulation than most other types of construction materials (Barbero, 2010). Vinyl ester resins typically stretch further before failure thus allowing for a better transfer of load to the fibre reinforcement and also have improved corrosion resistance when compared to polyester resins. Polyester resins have a very wide range of properties that can be matched to a specific application of the part. Phenolic resins are normally used in applications requiring properties of smoke and flame exposure to be controlled, phenolic resins also tend to be more difficult to work with during manufacture. Lastly, epoxy resins are considered high-performance resin systems due to their good elongation to failure and high service temperatures are higher than most other thermoset resin systems used. Table 2.2 shows the characteristics and limitations of various different thermoset resins. The two sections that follow will be looking at epoxy and polyester resin systems in more detail, as a resin composition from one of these two resin systems will be considered due to the properties, cost and availability.

2.4.1.2.2 Polyester Resin: systems are the most commonly used in industry, second most being epoxy resins (Rosato and Rosato, 2004). Polyester resins have a broad scope of manufacturing processes that it can be used in, ranging from hand lay-up to geometrically complex moulds used in resin transfer moulding. Polyester resin can be either thermoset or thermoplastic, thermoset polyester resins are referred to as "unsaturated polyester resin" and thermoplastic polyester resins are conversely "saturated polyester resin". Polyester resins are a popular choice as it provides a good balance between mechanical, electrical and chemical resistance properties at a relatively low cost (Rosato and Rosato, 2004). Unsaturated polyester resins offer a very wide range of chemical compositions (e.g. orthophthalic, vinyl esters, and blends). Polyester resins are also one of the more easier resin systems to handle during manufacture.

Polyester resins cure by peroxides that initiate a radical copolymerization reaction (Rosato and Rosato, 2004). The curing process can occur at room temperature or at elevated temperatures (60-90 C). Polyester resins can also be cured by UV or light radiation exposure (Barbero, 2010). Polyester resin systems consist of generally 3 parts, the unsaturated polyester resin base, a catalyst system and the addition of accelerators when required. Accelerators can speed up the curing time of the polyester resin, but must not be added to the catalyst system. The accelerator needs to be added to the unsaturated polyester base prior to the addition of the catalyst system.

Resin systems that are manufactured and cured at room temperature often need to be post-cured in order to achieve full curing strength. This applies to epoxy resins as well (covered in the next section). Polyester resins in the industry are often used with glass fibre reinforcing materials as the combination of polyester resin and glass fibre provides a cost effective composite material with a well-balanced performance output. Polyester resins can also have additives mixed into the resin system in order to improve UV degradation, reduce flammability, smoke/toxic gas output during burning, etc. (Barbero, 2010)

Resin type	*Characteristics*	*Limitations*
Epoxy	Excellent composite properties Very good chemical resistance Good thermal properties Very good electrical properties Low shrinkage on curing Can be B-staged (prepreg)	Long cure cycles Best properties obtained only with cure at elevated temperature Skin sensitizer
Phenolic	Very good thermal properties Good fire properties (self-extinguishing) B-stage possible Good electrical properties	Color limitation Alkali resistance Contact with foodstuffs
Polyester	Wide choice of resins – easy use Cure at room temperature and elevated temperature Very good composite properties Good chemical resistance Good electrical properties	Emission of styrene Shrinkage on curing Flammability No B-stage possible
Polyimide and polyamide-imide	Excellent thermal properties Good composite properties Good electrical properties Good fire properties	Restricted choice of color Arc resistance Acid and alkali resistance
Polyurethane	Good composite properties Very good chemical resistance Very high toughness (impact) Good abrasion resistance	Nature of isocyanate curing agents Color Anhydrous curing No B-stage
Silicone	Very good thermal properties Excellent chemical resistance Very good electrical properties Resistant to hydrolysis and oxidation Good fire properties (self-extinguishing) Non toxic	Lack of adhesion Long cure cycles Can only be cured at elevated temperature
Vinyl ester	Good fatigue resistance Excellent composite properties Very good chemical resistance Good toughness	Emission of styrene Shrinkage on curing Flammability No B-stage

Table 2.2: Characteristics and limitations of different thermoset resins. (Rosato and Rosato, 2004)

2.4.1.2.3 Epoxy Resin: systems are widely used in industry due to the excellent mechanical, electrical and corrosion/chemical resistance properties that they exhibit. Epoxy resins also shrink far less than other thermoset resin systems (1.2-4%) (Barbero, 2010). Due to their superior properties, epoxy resins are generally used with higher performance fibre materials such as carbon, Kevlar, etc. Epoxies are quite versatile resin systems which offer great adhesion to other materials and a high strength to weight ratio (Rosato and Rosato, 2004). A wide range of epoxy resins are available that allow for curing at either elevated (50-100 deg C) or room temperatures. With the correct compositions, epoxy resins can withstand high temperatures (up to 290 C), but also provide excellent electrical insulating properties (Rosato and Rosato, 2004). Epoxy resins are used in electrical components and systems as a means of potting and encapsulating components.

Epoxy resin systems generally have longer curing times. High-performance applications generally see heated curing conditions in order to achieve the highest performance levels from the epoxy matrix. Applications of epoxy resins are almost endless in the composites industry but are seen primarily in the aerospace, chemical plant, high-performance car part and other various industrial applications such as circuit boards or tooling surfaces (Rosato and Rosato, 2004). Another use of epoxies are for surface coating of materials that require a combination of flexibility, toughness and chemical resistance that is virtually not seen with any other plastic material.

2.4.1.3 Conventional Composite Design Methods

Composite material design requires concurrent material and structural design. The properties of the material can be changed and customised to match or work with the structural requirements of the component. As previously mentioned, composite materials are made up of two primary components, thus composites therefore, requires a different design approach, as opposed to the conventional materials (such as steel) would require. Composite properties (e.g stiffness, thermal expansion, etc.) can vary across a wide range of values depending on the material choices and combinations (Barbero, 2010).

In the previous sections, the different reinforcement and matrix materials were separately discussed as were their individual properties were also discussed. The properties, however, need to be combined to predict the overall properties of the manufactured composite part. To perform the combination we use micro-mechanics formulas to generate properties for any combination of fibre and matrix materials. Although micro-mechanics can predict the stiffness of a composite material very accurately, it does not apply so well for predicting the strength of the composite material combination. Thus, it is critical for experimental data to be collected from composite test samples of the final composite part. Another point that has to be noted is that the type of manufacturing process also affects the strength of the composite part, as different manufacturing processes produce different quality parts (generally different fibre to resin ratios in the final component). Manufacturing processes used for composite parts are discussed in more detail in a section that follows. It is recommended to review the manufacturing processes used to produce composite components before proceeding

to the details of the design processes, as the manufacturing techniques background knowledge of the reader at this point is assumed to be known.

Generating experimental data for any given composite material combination requires a fairly large investment in order to produce a sufficient range of data to extract values to base designs on. One great disadvantage of using experimental data to base designs on is that if there is any change to the materials, manufacturing process or any other factor that could affect the properties of the composite material, then an entirely new experimental program for the new material or process used, is needed in order to get credible data again (Barbero, 2010). For composites materials designs the exact experimental data for the combination is not available. Then by using the material properties provided by the suppliers of both the fibre and resin matrix, micro-mechanics is then used to predict the lamina properties (Barbero, 2010). The accuracy of the micro-mechanics predictions can be evaluated by a few selected tests on material samples (Barbero, 2010). This combination of micro-mechanics and limited physical testing is ideal for small companies or limited resources to perform full-scale experimental programs. After the laminae properties are known, the next step is then to predict the laminate properties using macro-mechanics formulas. Once again the laminate properties can be verified with a few selected physical tests. This is generally recommended as the manufacturing process and quality can sometimes be difficult to represent in a formula basis. The section that follows discuss the mechanic's theories in composite materials in further detail.

2.4.1.4 Micromechanics

Micromechanics in composite materials is a study that takes into consideration the interactions between individual materials that together form the final composite material component. Micro-mechanics allows designers to study and predict the properties of composite materials depending on an array of conditions. Micromechanics is generally used to predict the stiffness with relatively good accuracy, however, cannot predict the strength as well (Barbero, 2010). Micromechanics formulas provide the designer with a way to estimate or find the material properties of the composite material so that after a specific composite construction material properties have been characterised, the material data can easily be used during the design phase.

As already mentioned, composite materials have directional properties and thus depend on the orientation of the material. With the use of micromechanics, a general formula specific to a particular composite material layup can be created in order to find the material properties at any angle of the material. Micromechanics formulas are used to find the various material properties required for the next step which is the ply and macromechanics sections. The different calculation methods for the various material properties will be explored in the paragraphs to follow.

2.4.1.4.1 Volume and Mass Fractions Are controlling parameters of a composite material. The ratio of fibre to matrix has a great effect on the overall properties that will be exhibited by the composite material. The ratio of fibre to matrix material

is given by either volume or mass fractions. When producing composites it is generally easier to measure the mass fraction of the composite, as the material data generally has the weight per area of dry fibre material, then by weighing the final part, the mass fraction can be found. However, later on in this section, the formulas used in micro-mechanics are mainly based on the volume fraction, thus the mass fraction needs to be converted to a volume fraction (Barbero, 2010).

The amount of fibre by weight is defined as:

$$W_f = \frac{\text{weight of fibre}}{\text{total weight}} \tag{2.1}$$

The amount of matrix by weight is defined as:

$$W_m = \frac{\text{weight of matrix}}{\text{total weight}} \tag{2.2}$$

The amount of fibre by volume is defined as:

$$\nu_f = \frac{\text{volume of fibre}}{\text{total volume}} \tag{2.3}$$

The amount of matrix by volume is defined as:

$$\nu_m = \frac{\text{volume of matrix}}{\text{total volume}} \tag{2.4}$$

Sum of the weight fractions:

$$W_m + W_f = 1 \tag{2.5}$$

The density of the composite material is defined as:

$$\rho_c = \rho_f \nu_f + \rho_m \nu_m \tag{2.6}$$

Where:

ρ_f: density of the fibre
ρ_m: density of the matrix

The composite material density in terms of the weight fraction (provided the density of each material is known):

$$\rho_c = \frac{\rho_f}{W_f} + \frac{\rho_m}{W_m} \tag{2.7}$$

Thus using equation 2.6 and 2.7, the volume fraction can be found from:

$$\begin{aligned} \nu_f &= W_f \frac{\rho_c}{\rho_f} \\ \nu_m &= W_m \frac{\rho_c}{\rho_m} \end{aligned} \tag{2.8}$$

The accurate measurement of the overall fibre volume fraction of a laminate can be done experimentally, using acid digestion methods (Barbero, 2010). This is a lengthy and time-consuming process. The alternative is to use a formulation to find the overall fibre volume fraction as shown in 2.9.

$$V^{o}_{fibre} = \frac{w}{\rho_f h} \tag{2.9}$$

Where:

w - is the weight per unit area of the fabric.
ρ_f - is the fibre density.
h - is the thickness of the fabric reinforcement.

2.4.1.4.2 Isotropic Material: Materials of this type are the most common used in industry, such as aluminium, steel, copper, etc. Isotropic materials have an infinite number of planes of symmetry, thus the material properties are not dependent on the orientation of the material (Barbero, 2010). For isotropic materials, the two main material properties that are generally given are; by Youngs Modulus (E) and by its Poissons ratio ν. Other than these two properties, other material properties can also be found, such as the shear modulus (G).

2.4.1.4.3 Anisotropic Material: Unlike an isotropic material, anisotropic materials have properties that vary depending on the orientation of the material during testing. Anisotropic materials can be homogeneous or heterogeneous in composition. Anisotropic materials can also include transversely isotropic materials, which refers to a material with transversely equal properties to the fibre direction (i.e $E_2 = E_3$) (Roylance, 2000). An organic example of an anisotropic material is wood, where the planes that run with the grain of the wood has different properties to that of the planes transpose to that and across the grain.

2.4.1.4.4 Orthotropic Material: Has three mutually perpendicular x-y-z planes of elastic symmetry (Rosato and Rosato, 2004). A unidirectional fibre reinforcement composite can be considered an orthotropic material if one of the planes of symmetry is perpendicular to the fibre direction and the other two can be any pair of planes parallel to the fibre direction (Barbero, 2010). Materials that have elastic properties that are not equal in any of the directions is considered to be orthotropic. ($E_1 \neq E_2 \neq E_3$) (Roylance, 2000).

2.4.1.4.5 Stiffness: In the mechanics of materials approach to solving a composite material problem, the combination of two materials (the composite) can be calculated to an equivalent homogeneous material (Barbero, 2010). This approach requires that the material properties in various directions need to be identified, as in this case, the Youngs Modulus and Poissons ratio does not fully define the representative material. Extracted from (Barbero, 2010), the following material properties are required as a minimum to define the representative material:

E_{11} : Modulus of elasticity in the fibre direction.
E_{22} : Modulus of elasticity in the direction transverse to the fibres.
G_{12} : In-plane shear modulus.
G_{23} : Out of plane shear modulus.
υ_{12} : In-plane Poisson's ratio.

Since the stiffness matrix "S" is symmetric, the following relationship will be true ($\nu_{21}/E_2 = \nu_{12}/E_1$) (Roylance, 2000). The following equation (2.10) applies for the relationship between the stress, strain and stiffness matrix:

$$\begin{Bmatrix} \epsilon_1 \\ \epsilon_2 \\ \gamma_{12} \end{Bmatrix} = \begin{bmatrix} 1/E_1 & -\nu_{21}/E_2 & 0 \\ -\nu_{12}/E_1 & 1/E_2 & 0 \\ 0 & 0 & 1/G_{12} \end{bmatrix} \begin{Bmatrix} \sigma_1 \\ \sigma_2 \\ \tau_{12} \end{Bmatrix} \tag{2.10}$$

2.4.1.4.6 Longitudinal Modulus: Refers to the material modulus in the fibre direction E_1. The longitudinal modulus can be predicted relatively well (Barbero, 2010) by the "Rule of Mixtures" (ROM) (2.11) equation. The equation is based on the assumption that the strain in both the fibre and matrix are equal, thus implying that the bond between the matrix and fibre is perfect. The assumption is required in order to replace the individual heterogeneous material modulus with an "equivalent representative" material modulus (Barbero, 2010).

The Rule of Mixtures (ROM) equation:

$$E_1 = E_f V_f + E_m(1 - V_f) \tag{2.11}$$

The equation is derived from the assumption that the strain is equal in both materials and using the combination of the basic pressure and strain equations, the ROM equation is formed.

2.4.1.4.7 Transverse Modulus Refers to the overall modulus of the material in a direction transverse to the fibre direction. Once again the same assumption that the stains in both materials are the same in order to maintain a balanced equation system (Barbero, 2010). For this set of formulas, the section of the material transverse to the fibre direction is considered, as seen in figure 2.9. The fibres thickness ($V_f W$) is now represented as a uniform fraction of the overall combined material thickness (W).

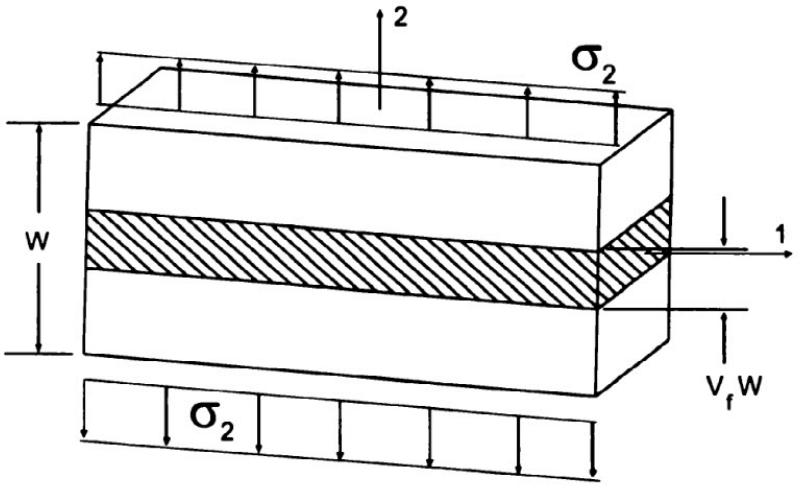

Figure 2.9: Composite material representation with a transverse load applied to it. (Barbero, 2010)

Thus, the equations to find the transverse modulus as discussed in (Barbero, 2010) are represented below:

The strains in the fibre and matrix material (equal):

$$\begin{aligned} \epsilon_f &= \frac{\sigma_2}{E_f} \\ \epsilon_m &= \frac{\sigma_2}{E_m} \end{aligned} \tag{2.12}$$

Combining the relative strains acting in each material, the total elongation is then:

$$\epsilon_2 W = \epsilon_f V_f W + \epsilon_m V_m W \tag{2.13}$$

Now applying Hooke's Law and since the stresses are equal ($\sigma_f = \sigma_m = \sigma_2$) the equation now becomes:

$$\epsilon_2 = \frac{\sigma_2}{E_f} V_f + \frac{\sigma_2}{E_m} V_m \tag{2.14}$$

Now by applying Hooke's law to the formula above and considering this is now an equivalent material:

$$\frac{1}{E_2} = \frac{V_m}{E_m} + \frac{V_f}{E_f} \tag{2.15}$$

Equation 2.15 is known as the "Inverse Rule of Mixtures" (IROM) (Barbero, 2010). Due to the simplicity of the IROM equation, it does not produce very accurate values or predictions for the transverse modulus. The values that are produced are good enough for basic and quick reference guides before proceeding to the design phase of the material. For design calculations, a modified version of the IROM formula is used. The Halpin-Tsai formula 2.16 is a semi-empirical formula and produces a more accurate prediction.

$$E_2 = E_m \left[\frac{1 + \zeta \eta V_f}{1 - \eta V_f} \right] \tag{2.16}$$

Where:

$$\eta = \frac{\frac{E_f}{E_m} - 1}{\frac{E_f}{E_m} + \zeta} \tag{2.17}$$

And ζ is an empirical parameter obtained by comparative plot matching values from equation 2.16 with the results obtained from a complex empirical analytical solution outside the scope of this thesis. As a general rule $\zeta = 2$ produces a good fit for round and square shaped fibres. For a case where the fibre is rectangular, using $\zeta = \frac{2a}{b}$. Where "a" and "b" are the dimension of the rectangular section of the fibre (Barbero, 2010). Other formulas of predicting the moduli can be used such as the stress partitioning parameter (SPP) or periodic microstructure model (PMM). Figure 2.10 shows a graphical comparison between the various models that can be used to predict the material moduli.

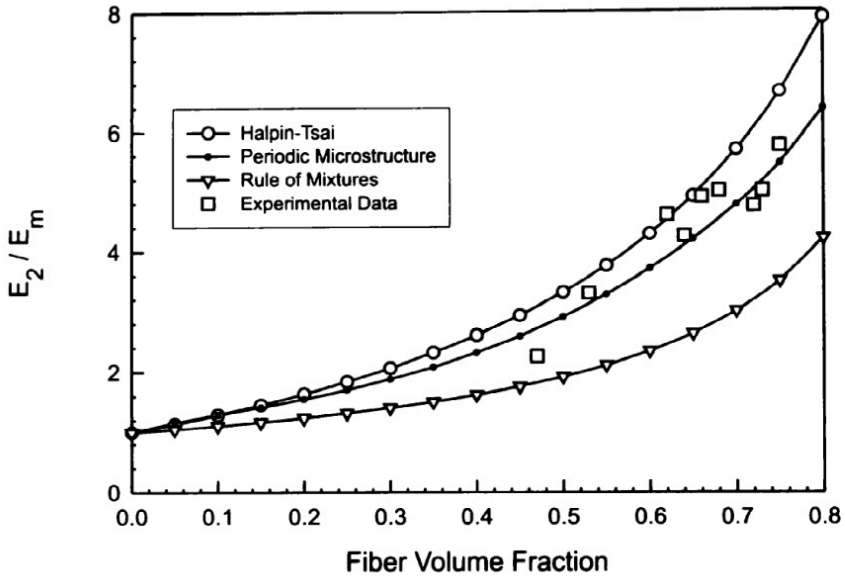

Figure 2.10: Comparison of composite models used to predict values of moduli. (Barbero, 2010)

2.4.1.4.8 In-Plane Poisson's Ratio For design purposes the In-Plane Poisson's ratio can be calculated using a variation of the rule of mixtures theory (eq. 2.18), discussed in a previous section. This is due to the fact that the Poisson ratio's of the two individual materials (fibre and matrix) are not vastly different, thus this prediction of the overall In-Plane Poisson's ratio will suffice for the design phase of a composite material.

$$\upsilon_{12} = \upsilon_f V_f + \upsilon_m V_m \tag{2.18}$$

2.4.1.4.9 In-Plane Shear Modulus The In-Plane Shear stress σ_6 in Figure 2.11, extracted from (Barbero, 2010) shows the deformations due to the various stresses present between the fibres and matrix material in different sections of the material.

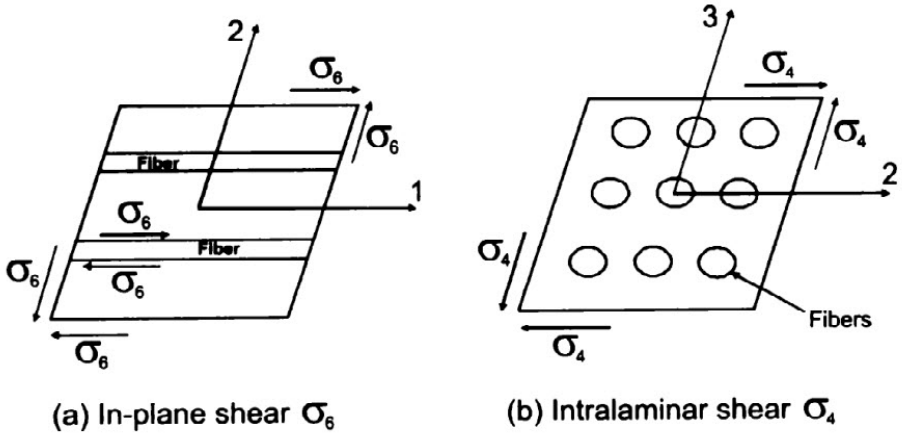

Figure 2.11: Induced stresses in the material in different section planes. (Barbero, 2010)

The inverse rule of mixtures (IROM) can be used to approximate the in-plane shear modulus, much the same as was done for the transverse elastic modulus. Where:

$$\frac{1}{G_{12}} = \frac{V_m}{G_m} + \frac{V_f}{G_f} \tag{2.19}$$

The equation can be re-written into:

$$G_{12} = \frac{G_m}{V_m + V_f \frac{G_m}{G_f}} \tag{2.20}$$

However, as mentioned in the transverse elastic modulus section, these equations do not yield very accurate values or values that can be used to base design calculations on. Other modified equations such as the "cylindrical assemblage model" and the periodic microstructure model formula's listed below (Barbero, 2010):

Cylindrical assemblage model in-plane shear modulus equation:

$$G_{12} = G_m \left[\frac{(1+V_f) + (1-V_f)\frac{G_m}{G_f}}{(1-V_f) + (1+V_f)\frac{G_m}{G_f}} \right] \tag{2.21}$$

Periodic microstructure model equation:

$$G_{12} = G_m \left[1 + \frac{V_f(1-\frac{G_m}{G_f})}{\frac{G_m}{G_f} + S_3(1-\frac{G_m}{G_f})} \right] \tag{2.22}$$

Simplified Periodic microstructure model equation:

$$G_{12} \cong G_m \left[1 + \frac{V_f}{\frac{G_m}{G_f} + S_3} \right] \tag{2.23}$$

where:

$$S_3 = 0.49247 - 0.47603V_f - 0.02748V_f^2 \tag{2.24}$$

These equations yield far more accurate values that can be obtained from the IROM base equations. More on the periodic microstructure model is discussed in a later section. In the case of a symmetrical material setup, there will be two planes with the same section planes, thus:

$$G_{13} = G_{12} \tag{2.25}$$

2.4.1.4.10 Intralaminar Shear Modulus In figure 2.11, this is now the representation of σ_4 as seen in part (b). The Intralaminar Shear Modulus can be found using the following equation:

$$G_{23} = G_m \frac{V_f + \eta_4(1 - V_f)}{\eta_4(1 - V_f) + V_f \frac{G_m}{G_f}} \tag{2.26}$$

Where:

$$\eta_4 = \frac{3 - 4\upsilon_m + \frac{G_m}{G_f}}{4(1 - \upsilon_m)} \tag{2.27}$$

These equations are generally accurate enough to base design calculations from. In this case, the fibre geometry is not exact with taking into account its form. For the most accurate calculation the use of the periodic microstructure model will yield the most accurate values. However, implementing the PMM can be a lengthy process and thus the equations above can be a quicker alternative.

2.4.1.4.11 Periodic Microstructure Model (PMM) Yields quite accurate predictions for the material moduli of a composite reinforced plastic (Barbero, 2010). The formulas required for this model are complex in nature and a full in-depth investigation into the derivation of these formulae is not the subject of this thesis. Due to the models' complexity, a number of computer programs in C++ and MATLAB are available from various composite research sites and sources. If further information regarding the derivation and base formula are required, the PMM method is covered in greater detail in the periodic microstructure model section available from (Barbero, 2010). The method uses equations to find the linear-elastic behaviour of the composite material, a stiffness matrix is created for the material and the final properties of the material are found from the compliance matrix. Certain aspects of the PMM will be used for

determining the overall woven composite properties, however, the previous literature covers a sufficient amount of the PMM that will be used and developed upon from this point.

2.4.1.5 2D Woven Fabric Numerical Modelling Methods

Woven reinforced fabric composites are widely used in the automotive, aerospace, marine and many other industries. The most commonly available textile fabrics are woven, braided, knitted and non-woven fabrics, as previously covered in the literature review section. The properties and characteristics of woven fabric composites are different when compared to unidirectional (UD) composite reinforcements. The UD textiles are mainly focused on in most of the literature on composite material calculations. The properties of 2D woven fabrics, although it is classed as a 2D fabric, the paths and geometry of the weave creates a 3D profile effect as each fill and wrap undulate over and under one another. The rest of this section discusses the various approaches investigated by other authors to model the behaviour of woven composites.

The first paper that was examined was by (Ansar et al., 2011), this paper covered the theory of modelling 3D woven composite fabrics. 3D woven fabrics refer to generally three sets of tows used to construct the fabric, a fill, a wrap and a tow or binding that runs through the thickness of the fabric. Thus, there are tows in the coordinate directions of x,y and z. The fabric, through its section, is divided into unit cells. Unit cells are the minimum sectioned areas of the fabric that contains an entire range of the fabrics tow geometry. The fabric is then divided into RVE's (Representative Volume Elements) in order to simplify the overall model. In the case of an FEA performed on a computer based application, it is expected that the meshing size of the model's material would coincide with the size of the RVE's. Each element in an FEA model would represent the RVE as each of these elements have the material properties that would be entered into the material data properties in the FEA program. The article presented by (Ansar et al., 2011) provides a clearer understanding of how the relationship of a 3D woven fabric theory can be extrapolated to an FEA model of a 2D fabric material. A discussion of the tow section profiles and the assumptions made regarding them are covered as well. Tow's can be considered either rectangular, circular, lenticular or elliptical (Ansar et al., 2011). The mode of the practical samples dealt with in the lab and what is available for this research the tow profiles are of a lenticular profile shape and would be the closest representation of the real world composite in this case. The actual application of the theory from this paper is not applicable for 2D fabrics, however, the theory and developments of the RVE used through the thickness can be applied to the undulation and 3D inherent architecture.

The paper presented by (Tan et al., 1997) makes statements regarding the use of the various types of textile composites and the inherent characteristics of each material. According to (Tan et al., 1997) woven fabrics exhibit good dimensional stability in the wrap and fill directions, but also provide higher out-of-plane strength which can carry secondary loads not subjected to the principle loading plane. It is also stated that woven fabrics have a low shear rigidity which results in good formability of the material. It is also stated that woven fabrics exhibit low in-plane shear tolerance. A statement

regarding braided fabrics was also made by (Tan et al., 1997) that the formability is not as desired as woven fabrics, and is also unstable under axial compressive loads. Lastly, it is claimed that knitted fabrics are often not used as reinforcements as the material has low in-plane properties due to the influence of the looped geometrically construction of knitted fabrics on the overall volume fibre fraction.
A further section presented by (Tan et al., 1997) discusses the finite element and theoretical analysis modelling of fabric reinforced composite materials. The general procedure of a finite element method is to sub-divide the textile composite into representative elements and represent the entire reinforced textile by reassembling the unit cells as accurately as possible. The application of the CLT is used here and is presented in the paper by (Adumitroaie and Barbero, 2011a) discussed later on.

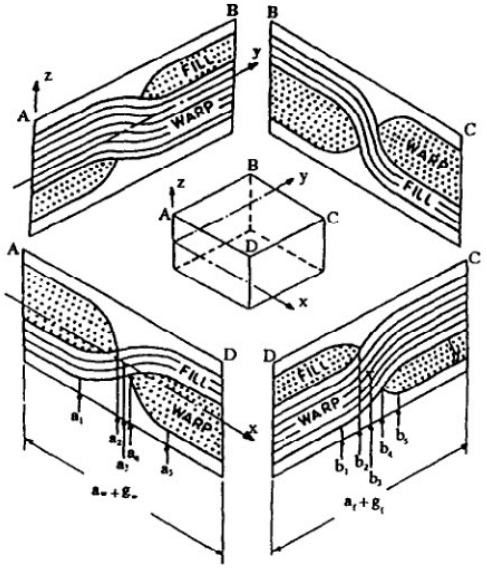

Figure 2.12: 2D projected diagram of a unit cell representation for a plain weave composite.
(Tan et al., 1997)

Figure 2.12 shows a clear image of how the 3D view of a unit cell representation can be seen from different perspectives. It is important to establish a reference coordinate system and to indicate which plane is represented when creating a 2D diagram of the unit cell cross-section.

One of the theories investigated by (Tan et al., 1997) was the assumption that the tow undulation of a plain weave composite could be represented by a sinusoidal curve, however, this proved to be inaccurate when modelled and could not provide accurate values of stress or strain. The commonly used approach in each of these papers is based on the assumption of an iso-strain condition. The iso-strain approach seems to yield the best conformance between numerical models, as it has been reported in the literature that the iso-stress assumption is not accurate due to the vast difference in yield stress of the two constituting materials.
Tan et al. (1997) reviews the fibre undulation model (mosaic model) which was applied by (Chou et al., 1989) in order to predict the in-plane stiffness "C11". The fibre undulation in a plain weave is the most severe case as the tow undulates every cycle to achieve and "up and under" weave profile. The continuous angle change of the tow reduces the fibres resisting the in-plane applied load. The FE results showed a good correlation between when the fibre undulation was taken into consideration when plot-

ted against the experimental data obtained. Thus it is clear that the fibre undulation does affect the properties of the lamina when considering woven fabrics.

A paper by (Chaphalkar and Kelkar, 2001) presents a CLT model for twill weave composites. The consideration of the fabric geometry is very similar to that of the previous models in other papers, where the fabric is sub-divided into a unit cell and RVE are used when considering the tow cross-sections. The assumptions made in this model are that the tows are uniform through the fabric and that the materials experience and iso-strain condition. The tow geometry is heavily considered when finding the overall volume fibre fraction. The geometry is calculated using the integration function applied to an infinitesimal portion of the fabrics unit cell in a representation geometrical mathematical model. The process is not as generic as the one presented by Adumitroaie and Barbero (2011a) in the section that follows, however, similar fabric properties are considered, such as the gap between the tows, tow profile, height and width. The micro-mechanics model used to predict the effective tow properties was the Composite Cylinder Model (CCM) presented by (Hashin, 1983). The model provides some generality for the use of twill weave fabrics. The mathematical model presented is very broad still and would require more work to develop when compared to the work of Adumitroaie and Barbero (2011a) that follows. There is also no significant evidence that this model is any better than the model by Adumitroaie and Barbero (2011a). The support of the model by Adumitroaie and Barbero (2011a) is greater and is covered in three separate papers/books.

The paper by Adumitroaie and Barbero (2011a) discusses the problem of the 3D architecture that is inherently created by the weaving process, although the fabrics are classified 2D. This paper, has the intended focus area on twill and satin weave fabrics. Most literature on woven fabrics looks at plain-weave textiles due to its availability in the industry. The waviness of any composite fabric creates new or complex stress-strain fields that result in a new form of damage and material failure patterns when compared to unidirectional reinforcements (Adumitroaie and Barbero, 2011a).
The purpose of the research of the paper by Adumitroaie and Barbero (2011a) is to create a generic numerical model to find the lamina properties for plain, twill and satin weave composite reinforcements. Most research papers deal with specific types of twill weave fabrics (as the construction can vary). Various papers also use different methods of measurement or characterising the fabrics to create the input data for the calculations. Parameters such as the gaps between the wrap and fill fibres, the cross-section profile of the tows used and the undulation angles or bending of the tows (waviness) as it crosses the fabric. A review of various authors approaches to modelling the fabric geometry is covered in (Adumitroaie and Barbero, 2011a). A discussion of the alterations and improvements to the numerical modelling techniques is covered, however, in most cases, it is for only the plain weave fabrics. (Adumitroaie and Barbero, 2011a) discusses the undulation model improvements made of the articles by (Ito and Chou, 1997) and (Ito and Chou, 1998) for only plain weaves. Notably, the addition of further material architecture attributes, for example, the consideration of a phase shift between plies and the nesting of the plies. This has a direct effect on the amount of matrix material considered to be in the layup and the overall volume fibre fraction that influences the strength characteristics of the lamina.
Generally the greater the number of fibre attributes that are considered in the model,

the prediction accuracy will also be greater. However, the increased number of factors will add further complexity and more computational power required to solve for the solution (Adumitroaie and Barbero, 2011a). During the paper, a review of a repetitive unit cell (RUC) is used to consider only a complete section of the woven fabric profile. The RUC is the smallest area of the 2D fabric that has a full representation of the woven geometry as depicted in Figure 2.13. The dotted rectangular section indicates the smallest area of the fabric that is needed in order to be repeated to form the completed fabric profile.

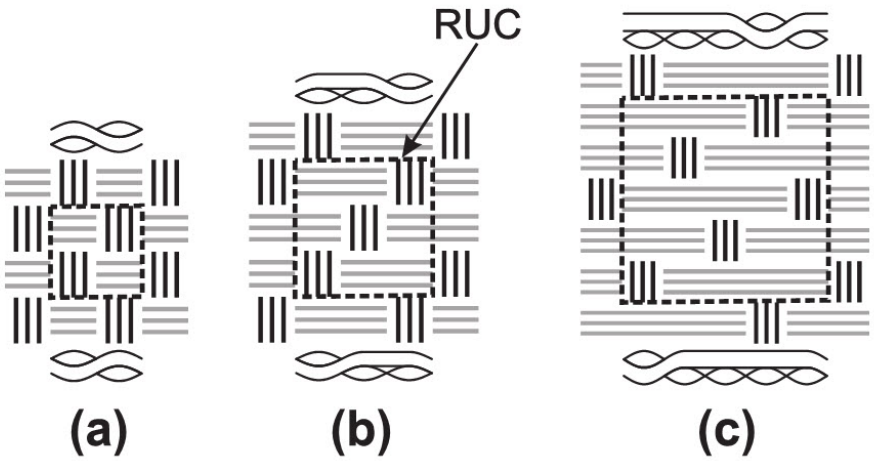

Figure 2.13: RUC for a) Plain b) Twill c) Satin weaves.
(Adumitroaie and Barbero, 2011a)

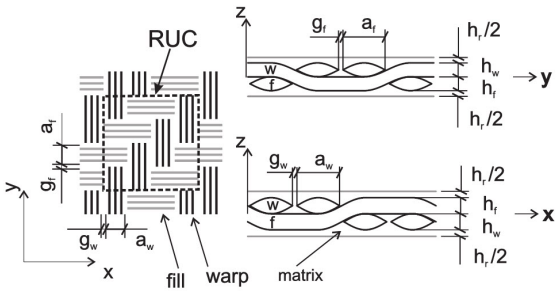

Figure 2.14: RUC of a 2/2 twill weave fabric geometric parameters.
(Adumitroaie and Barbero, 2011a)

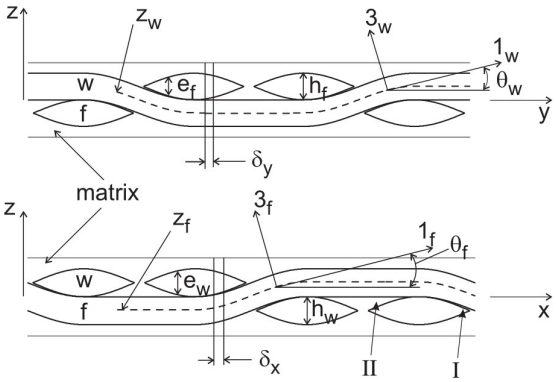

Figure 2.15: RUC a 2/2 twill weave fabric geometrical representation.
(Adumitroaie and Barbero, 2011a)

Figures 2.14 and 2.15 shows the general parameters and geometry that relativity easily characterises the fabric. Changes to these parameters (the fill and wrap gaps for example) will have an affect on the performance and workability of the fabric. The drape-ability, permeability of the fabric by the resin during its transfer, and the overall performance of the composite ply (as the overall volume fibre fraction will be influenced).

The work presented by (Adumitroaie and Barbero, 2011a) focuses more on the development of the generalisation of a numerical model for all woven composite, but this research paper only requires the theory related to the twill weave layups and that will be the scope of the literature focus in this case. The summary of this section characterises the reinforcement fabric into simple and easy to measure parameters that will be used in the CLT numerical algorithms covered in the next section. The properties include: the fill and wrap gaps, the tow width and height, tow fibre undulation angles, tow thickness and fabric thickness.

Overall for the FEA model of the composite material, only each individual lamina is being considered in determining the mechanical properties of the plies. Although this is not a true representation of the ply stacking thickness, in the case of an out of phase shift between the layers, it is sufficient enough to provide an indication that is lower than the real world value by a certain margin due to the inaccuracy of the overall volume fibre fraction. This can be used logically as a FOS (Factor Of Safety) in the composite design process. Due to the high strength to weight ratio requirement, the most optimal setup needs to be obtained for the construction. The implications of damage mechanics are considered only on a very light level as this is an entire research area on its own within composite technology. The key in the aerospace industry is not to design too much redundancy into the components to make them overly strong and heavy, but also to allow enough margin in the design for slightly more loading than what is expected. The working condition of nano-satellites once in space are very low stress in terms of direct loading, but rather focus needs to be more of the effect of the environmental conditions on the materials deterioration.

A supporting document by (Adumitroaie and Barbero, 2012) provides a comprehensive overview for the CLT applied to prediction of stiffness and strength properties for plain weave fabrics. This is indicated to the reader as further information should it be required and will not be discussed here further as is not required for the research presented in this thesis.

2.4.1.6 Classic laminate theory model for fabric composites

Presented in the woven composite geometric theory in (Adumitroaie and Barbero, 2011a), the mechanical properties calculations in (Adumitroaie and Barbero, 2011b) and the fabric reinforced composites chapter in (Barbero, 2010), the application of the classic laminate theory is covered in a fair amount of detail.

The article (Adumitroaie and Barbero, 2011a) discusses the principles of the fabric geometry and architecture, where the mechanical properties and the numerical algorithms required are discussed in (Adumitroaie and Barbero, 2011b). In the book by (Barbero, 2010), both the geometric profile and the numerical calculations are discussed. In this section, however, the focus of the literature content is on the mechanical properties and algorithms formulated to find the lamina properties of the final woven composite ply.

Initially, the use of micromechanics formulae is required in order to determine the

properties for each tow used in the fill and wrap that make up the textile fabric. Building on the detailed review of the micromechanics models already presented, then next stages of applying the CLT are covered in this section.

After the micromechanics models have been applied to find the tow composite fibre properties with respect to its own material coordinate system (infused with the resin), the next stage is to evaluate the tows within the fabric construction in terms of the fill and wrap configurations.
The transversely isotropic compliance matrix of the tow needs to found using equation (2.28).

$$S = \begin{pmatrix} 1/E_{11} & -\nu_{21}/E_{22} & -\nu_{31}/E_{33} & 0 & 0 & 0 \\ -\nu_{12}/E_{11} & 1/E_{22} & -\nu_{32}/E_{33} & 0 & 0 & 0 \\ -\nu_{13}/E_{11} & -\nu_{23}/E_{22} & 1/E_{33} & 0 & 0 & 0 \\ 0 & 0 & 0 & 1/G_{23} & 0 & 0 \\ 0 & 0 & 0 & 0 & 1/G_{13} & 0 \\ 0 & 0 & 0 & 0 & 0 & 1/G_{12} \end{pmatrix} \tag{2.28}$$

Now a rotation matrix for the fill and wrap needs to be constructed. Equation (2.29) and (2.30) represents the rotation matrix for each case, where the fill undergoes a clockwise rotation due the undulation (by θ_f) of the tow through the fabric and the wrap undergoes firstly a 90° rotation relative to the fill direction and then undulates as well as (by θ_w) it crosses the fabric (Adumitroaie and Barbero, 2011b).

$$\theta_f = \begin{pmatrix} cos\theta_f & 0 & sin\theta_f \\ 0 & 1 & 0 \\ -sin\theta_f & 0 & cos\theta_f \end{pmatrix} \tag{2.29}$$

$$\theta_f = \begin{pmatrix} 0 & cos\theta_w & sin\theta_w \\ -1 & 0 & 0 \\ 0 & -sin\theta_w & cos\theta_w \end{pmatrix} \tag{2.30}$$

Using reference terms for the elements in the rotation matrix: $\theta_{f,w} = \begin{pmatrix} l_1 & m_1 & n_1 \\ l_2 & m_2 & n_2 \\ l_3 & m_3 & n_3 \end{pmatrix}$

In general terms for each rotation matrix the transformation matrix from laminate to material coordinate system can be calculated to be:

$$T_{f,w} = \begin{pmatrix} l_1^2 & m_1^2 & n_1^2 & 2m_1n_1 & 2l_1n_1 & 2l_1m_1 \\ l_2^2 & m_2^2 & n_2^2 & 2m_2n_2 & 2l_2n_2 & 2l_2m_2 \\ l_3^2 & m_3^2 & n_3^2 & 2m_3n_3 & 2l_3n_3 & 2l_3m_3 \\ l_2l_3 & m_2m_3 & n_2n_3 & m_2n_3 + n_2m_3 & l_2n_3 + n_2l_3 & l_2m_3 + m_2l_3 \\ l_1l_3 & m_1m_3 & n_1n_3 & m_1n_3 + n_1m_3 & l_1n_3 + n_1l_3 & l_1m_3 + m_1l_3 \\ l_1l_2 & m_1m_2 & n_1n_2 & m_1n_2 + n_1m_2 & l_1n_2 + n_1l_2 & l_1m_2 + m_1l_2 \end{pmatrix} \tag{2.31}$$

Equation (2.31) can now be taken and reduced for the fill as equation (2.32) and the wrap with equation (2.33).

$$T_f = \begin{bmatrix} c_f^2 & 0 & s_f^2 & 0 & 2c_f s_f & 0 \\ 0 & 1 & 0 & 0 & 0 & 0 \\ s_f^2 & 0 & c_f^2 & 0 & -2c_f s_f & 0 \\ 0 & 0 & 0 & c_f & 0 & -s_f \\ -c_f s_f & 0 & c_f s_f & 0 & c_f^2 - s_f^2 & 0 \\ 0 & 0 & 0 & s_f & 0 & c_f \end{bmatrix} \tag{2.32}$$

$$T_w = \begin{bmatrix} 0 & c_w^2 & s_w^2 & -2c_w s_w & 0 & 0 \\ 1 & 0 & 0 & 0 & 0 & 0 \\ 0 & s_w^2 & c_w^2 & 2c_w s_w & 0 & 0 \\ 0 & 0 & 0 & 0 & -c_w & -s_w \\ 0 & c_w s_w & -c_w s_w & c_w^2 - s_w^2 & 0 & 0 \\ 0 & 0 & 0 & 0 & s_w & -c_w \end{bmatrix} \tag{2.33}$$

Where:

$s_f(x) = sin\theta_f(x)$
$c_f(x) = cos\theta_f(x)$
$s_w(y) = sin\theta_w(y)$
$c_w(y) = cos\theta_w(y)$

Thereafter, the transformed compliance matrix ($\bar{S_{f,w}}$) can be found using equation (2.34), this is now with respect to the material coordinate system (x,y,z).

$$\bar{S}_f(x) = (T_f(x))^T \cdot S \cdot T_f(x)$$

$$\bar{S}_w(x) = (T_w(x))^T \cdot S \cdot T_w(x) \tag{2.34}$$

For each transformed compliance matrix, a 6x6 matrix would have resulted for the fill and wrap. Applying the plane stress assumption to the compliance matrix we will only consider the terms of the matrix that correspond with $i, j = 1, 2, 6$. The reduced stiffness matrix in the laminate coordinate system for the fill and wrap will be:

$$\bar{Q}^f = \begin{bmatrix} \bar{Q}_{11}^f & \bar{Q}_{12}^f & 0 \\ \bar{Q}_{21}^f & \bar{Q}_{22}^f & 0 \\ 0 & 0 & \bar{Q}_{66}^f \end{bmatrix} = \begin{bmatrix} \bar{S}_{11}^f & \bar{S}_{12}^f & 0 \\ \bar{S}_{21}^f & \bar{S}_{22}^f & 0 \\ 0 & 0 & \bar{S}_{66}^f \end{bmatrix}^{-1} \tag{2.35}$$

and

$$\bar{Q}_w = \begin{bmatrix} \bar{Q}_{11}^w & \bar{Q}_{12}^w & 0 \\ \bar{Q}_{21}^w & \bar{Q}_{22}^w & 0 \\ 0 & 0 & \bar{Q}_{66}^w \end{bmatrix} = \begin{bmatrix} \bar{S}_{11}^w & \bar{S}_{12}^w & 0 \\ \bar{S}_{21}^w & \bar{S}_{22}^w & 0 \\ 0 & 0 & \bar{S}_{66}^w \end{bmatrix}^{-1} \tag{2.36}$$

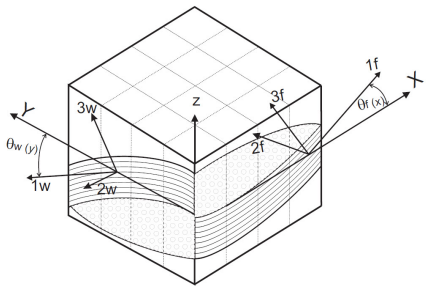

Figure 2.16: The material coordinate system vs. the laminate coordinate system (x,y,z).
(Barbero, 2010)

The reduced stiffness matrix is the inverse of the reduced compliance matrix in terms of the laminate material coordinates. Figure 2.16 provided in the book by (Barbero, 2010) shows the material coordinate system vs. the laminate coordinate system (x,y,z).

Now taking the theory presented and the formulations provided by (Barbero, 2010) and (Roylance, 2000), a combined and simplified formula can be created to find the extensional stiffness matrix [A] as seen in equation (2.37)

$$[A] = \frac{4}{(a_f + g_f)(a_w + g_w)} \sum_{k=1}^{N} \left[\bar{Q}_{ij}^{f,w}\right] \times \left(\frac{Z}{2}\right) \tag{2.37}$$

Where:

N is the in-plane traction.
Z is the thickness of the final lamina.
$a_{f,w}$ is the width of the tow for the fill and wrap.
$g_{f,w}$ is the gap between the fill and wrap tows.

The final matrix that is needed is the laminate compliance matrix $[\alpha] = [A]^{-1}$ Once the laminate compliance matrix is known, the lamina properties of the fabric composite can then be found using formulas (2.38) to (2.41) below.

$$E_x = (\alpha_{11} h)^{-1} \tag{2.38}$$

$$E_y = (\alpha_{22} h)^{-1} \tag{2.39}$$

$$\nu_{xy} = -\frac{\alpha_{12}}{\alpha_{11}} \tag{2.40}$$

$$G_{xy} = (\alpha_{66} h)^{-1} \tag{2.41}$$

Now, $G_{xy} = G_{12} = G_{13}$, thus G_{23} can be used from the micro-mechanics equation (2.26) as the tow fibres are still in the same transverse plane and direction as it was

when considering the tow fibre configuration.
Thus, the input parameters for the FEA composite model are known ($E_{11}, E_{22}, \nu_{12}, G_{12}, G_{23}$).

2.4.1.7 Macromechanics

Marco-mechanics modelling refers to the assembly of the composite plies to make up the overall laminate. The macro-mechanics theory produces overall laminate property data that can be used to analyse the stresses and strains in the material manually using formulations and algorithms. For the purpose of this research, the mathematical algorithms will only progress to the point where the representative lamina properties are known. The data for each lamina can then be entered into an ABAQUS FEA model which will assemble and analyse the macromechanics of the composite model. This provides a far less time-consuming operation and an accurate indication of the stress distribution due to the loading through the laminate construction.

2.4.2 Embedded Circuits and Electronics

Embedding electronics and electronic circuits in composite materials open up many new possibilities for multifunctional components to be designed, that allows the seamless integration of mechanical components with the electronic subsystems of the product that is being designed. An article created by (S̋eong Jang et al., 2010) analyses the construction of a multifunctional composite that included embedded electronics within is design. A full thermal analysis of the components, radiation shielding methods and a manufacturing layout is documented within the article.

The conventional design method of subsystems has been based on the idea that each subsystem is separately linked together in the final assembly process (As seen in Figure 2.17). For example, the wiring loom in a motorcar gets installed once the outer body of the car as been assembled. The same applies to electronics on aircraft, boats, appliances, etc. The aerospace industry, in particular, continues to seek greater ways of optimising space (volume) utilisation and at the same time producing ever lighter and stronger materials from which to build components from. The two main subsystems in any aerospace system are generally the electronics and the mechanical structure. MFC research is now exploring ways of using embedded FPC's to route the wiring loom and some basic electronic systems between the structural composite material of a component. In the article done by (D̋iPalma et al., 2004), an MFC panel that included the wiring loom between the composite layers and has surface mounted connectors for access to the conducting loom to provide the various connection requirements to the electronic boards as shown in Figure 2.18.

Figure 2.17: Aluminium panel with conventional type wiring harness attached. (ĎiPalma et al., 2004)

Figure 2.18: Composite panel with embedded wiring harness. (ĎiPalma et al., 2004)

In the article done by (ĎiPalma et al., 2004), a reported mass saving of approximately 57% was measured by using the composite panel as opposed to the conventional aluminium panel and harness construction. This amount of weight saving would be extremely beneficial in the aerospace application as a reduction in mass of components allows less energy requirement for the flight model or makes more payload available for other components or systems to be included in the overall design package. The addition of other components or added systems will potentially increase the overall functionality of the air or spacecraft being designed.
The composite panel in Figure 2.18 consists of an FPC with a 150-conductor wiring harness between layers of a moulded composite fibre material (ĎiPalma et al., 2004).

2.4.2.1 Flexible Printed Circuits and electronic systems

Conducting tracks that have been used during the construction of the composite panels in the article by (D̈iPalma et al., 2004) are Flexible Printed Circuits (FPC's). FPC's is the manufacture of copper conducting tracks on a flexible substrate material. The flexible substrate is a plastic based material and is usually either a polyimide, polyether ether ketone (PEEK) or conductive polyester film. FPC's are ideal for use in multifunctional composite panels as they will deform and flex with the composite materials as the component is subjected to loading. FPC's can be manufactured in almost any track configuration that will fit within the available open area of the composite panel.

The overall advantages and disadvantages of FPC's in general, based on information from (Coombs and Holden, 2007) are highlighted in the columns below:

Advantages:

- Thin.
- Bendable.
- High-density wiring in small spaces.
- Low total cost of components (Compared to PCB based circuits).
- Allows for 3D wiring in components.

Disadvantages:

- Fragile.
- Dimensionally unstable, unless constrained by a support or structure.
- Can be complex to design and manufacture.
- Difficult to handle during manufacture and assembly.
- Difficult to rework if required.

FPC's can be made to very precise measurements and allows many individual conducting tracks within a small surface area of a single layer of substrate material. In multifunctional composite panels, only a single layer of conducting tracks will be used during the investigation due to the following:
Firstly, the creation of multiple layered conducting tracks will create a great potential for a thickness problem within the multifunctional material. The thickness issues have a high probability of reducing the flexibility of the multifunctional composite part due to the spread of the copper tracks away from the neutral bending axis of the material.
Secondly, a single layer of FPC tracks will provide enough individual connections required between the various CubeSat electronic components housed within the nano-satellite.
Finally, the addition of multiple layers of FPC tracks will greatly increase the chance of the multifunctional composite panels having structural de-lamination between the structural fibres of the composite panel and the FPC house between the structural fibres.
After logical evaluation, the ideal initial investigation setup should be based on a single layer of FPC conducting tracks that will be manufactured between the structural layers of the composite component.

A single layer FPC can also be sub-divided into further categories, the main ones being: High-density FPC for small spaces, Lightweight/3D based wiring or reliable wiring (Long flexing endurance) (Coombs and Holden, 2007). High-density FPC's are quite expensive and sacrifice reliability. For mechanical shock and vibration reliability the

	Polyimide	Polyester	Thin glass-epoxy	LCP	PEEK
Maximum operating temperature	>200°C	<70°C	~105°C	~90°C	>200°C
Standard thickness	12.5, 25, 50, 75, 125 μm	25, 50, 75, 100, 125, 188 μm	100, 150, 200 μm	(50 μm)	(50 μm)
Soldering	Applicable	Difficult	Applicable	Possible	Possible
Wire bonding	Possible	No	Difficult	Difficult	Possible
Color	Brown	Transparent	Transparent	Transparent	Milky
Moisture absorption	High	Low	Low	Low	Low
Dimensional stability	Acceptable	High	High	Good	High
Flexibility	High	High	Low	High	High
Cost	High	Low	Medium	Low	High

Table 2.3: Comparison between FPC substrate materials.
(Coombs and Holden, 2007)

preferred flexible specification as outlined by (Coombs and Holden, 2007) handbook, should be the high bond strength of conductors and between the layers that form the flexible circuit component.

The traditional FPC materials used for construction are based on thin film materials such as polyimide and polyester films. For its great flexibility, rolled annealed copper foil is used as the major conductor material. Base substrates are typically polyimide or polyester film, thin glass-epoxy or resin-coated paper. The base substrate is the material to which the conducting tracks will be placed on. Conductor materials that are used in FPC's are mainly electro-deposited copper foil, rolled annealed copper foil, stainless steel or aluminium foil. The copper clad laminates are either epoxy or acrylic based adhesives. The cover layer used for the FPC's are generally the same as the base substrate material, as generally two substrate laminates are used, one on either side of the conducting tracks which in itself becomes the coverlay material. Adhesives used to bond the layers together are primarily epoxy, acrylic, phenol or pressure-sensitive adhesives (PSA's). By increasing the thickness or number of coverlay or substrate layers used in the FPC, the stiffness property of the FPC can be adjusted.

Table 2.3 shows a comparison between FPC substrate materials that are generally used for various electrical applications. If the budget of the electrical application allows for it, the polyimide film has the most versatile mechanical properties of the all the other materials.

In Table 2.4 and 2.5 a chart of the detailed properties of the various polyimide films used in FPC's is displayed.

Importantly the adhesion properties of the cover-lay materials used in the construction of the FPC's must be highlighted and information provided, as this will be a determining factor as to whether the resin system of the structural composite material system will accept the material surface and bond to it. If the structural epoxy matrix of the composite does not fully bond to the FPC coverlay material, the parts created run the risk of de-lamination between the structural layers of the laminate. Table 2.6 shows the comparison of adhesive materials for flexible circuits.

In flexible printed circuits there is also very thin copper conducting tracks that are

		Kapton H™	Apical AV™	Kapton E™	Apical NP™	Apical HP™	Upilex S™
Manufacturer		DuPont	Kaneka	DuPont	Kaneka	Kaneka	Ube
Thickness (μm)		12.5, 25, 50, 75, 125	12.5, 25, 50, 75, 125	12.5, 25, 50, 75	12.5, 25, 50, 75	12.5, 25, 50, 75	12.5, 25, 50, 75, 125
Tensile strength (kg/mm^2)	MD	25.2	25.0	28.3	30.0	28.6	39.4
	TD	22.3	27.0	25.4	32.0	29.0	40.2
Elongation (%)	MD	85	119	16	82	40	22
	TD	83	114	32	73	38	21
Tensile modulus (kg/mm^2)	MD	336.1	305.9	785.5	407.9	654.0	897.3
	TD	321.4	312.2	622.4	428.3	661.0	912.1
CTE (ppm) (100–200°C)	MD	27	35	3	17	12	14
	TD	31	31	12	13	11	15
CHE (ppm) (50°C, 35–75% RH)	MD	15	16	5	13	8	9
	TD	16	15	8	12	6	10
Heat (%) shrinkage (200°C, 2 h)	MD	0.18	0.08	0.03	0.06	0.06	0.07
	TD	0.20	0.03	0.02	0.02	0.02	0.10
Water absorption (23°C, 24 h)		2.8	2.9	2.2	2.5	1.1	1.9
Alkaline resistance		17.4	25.9	5.5	22.9	4.2	~0
Chemical etching		Possible	Possible	Possible	Possible	Possible	Difficult

Table 2.4: Properties of the various polyimide films used in FPC's. (Coombs and Holden, 2007)

Manufacturer	DuPont	Nikkan Industry
Grade	Pyralux LF	CISV
Adhesive	Acrylic	Epoxy
Lamination temperature	180°C	160°C
Storage condition	Room temperature	Refrigerator
Bond strength (kg/cm)	1.3	1.0
Surface resistivity (Ω)	$1.0 \times \exp 13$	$3.0 \times \exp 14$
Volume resistivity (Ω*cm)	$1.0 \times \exp 14$	$1.2 \times \exp 16$
Soldering resistance	288°C × 5 min	280°C × 10 s
Flammability	No	UL-94-V-0

Table 2.5: Basic properties of the various cover-lay polyimide films used in FPC's. (Coombs and Holden, 2007)

	Thermosetting epoxy and acrylic resin	Hot-melt-type polyimide resin	Pressure-sensitive adhesives (PSAs)
Reliability	High	High	Acceptable
Bond strength	High	High	Acceptable
Creep	Small	Small	Large
Soldering	OK	OK	OK
Application process	Complicated	Complicated	Simple
Process temperature	160–180°C	>330°C	Room temperature
Material cost	Low	High	Low
Total cost	High	Very high	Low

Table 2.6: Comparison of adhesive materials for flexible circuits. (Coombs and Holden, 2007)

	ED foil	HD-ED foil	RA foil
Manufacturer	Furukawa Electric	Furukawa Electric	Japan Energy
Grade	STD foil	HD foil	RA
Thickness (μm)	9, 12, 18, 35, 70	18, 35	12, 18, 35, 70
Tensile strength (kg/mm^2)	TD 34	TD 32	MD 21.5 TD 18.9
Elongation (%)	TD 9	TD 23	MD 12.8 TD 9.5
Surface roughness (μm)	8	10	<3.5
Cost	Low	Middle	High

(Data measured for 35 μm Thick Foils).

Table 2.7: Basic material properties of copper conductors used in FPC's. (Coombs and Holden, 2007)

laminated between the various film layers of the FPC component. These copper conductors provide the electrical connections required to form the connection "bus" that connects various electrical board to one another. It is important to note that when the multifunctional composite component that has the FPC bonded into it is subjected to a load, the stresses induced in the copper tracks of the FPC must not exceed the design stress of the material in order to maintain its design reliability specification. The data provided in Table 2.7 will be referred to when creating the Finite Element Analysis model of the multifunctional composite in order to specify the material properties of the copper tracks in the FPC.

This thesis will be limited to the mechanical aspects of the flexible printed circuits as to remain within the scope of the mechanical engineering field. The internal copper track design and construction itself is not part of the scope of this thesis, as the standard design conventions currently used in the design process of the FPC's will be unchanged during the design and manufacture of the multifunctional composite structures.

Electronic circuit mechanical design of FPC boards has a few important areas that should be highlighted. The design consideration of stress distribution within an FPC board has to be taken into account when considering any design that involves the use of FPC boards. Much like any beam or section mechanical engineering, when subjecting the FPC section to bending there is a compressive and tensile stress layer that is created above and below the neutral axis of the bend line. In figure 2.19 in part a) of the figure, the different layers in a common FPC board layout are shown in a symmetrical layup along with the tensile and compressive face indication while subjected to bending. In part b) of the figure the visualisation of the material deformation is shown in an unsymmetrical case. It must be noted that in the unsymmetrical case of the board layout, that the copper conducting layer tends not to stay in-line with the neutral axis of the FPC material layup.

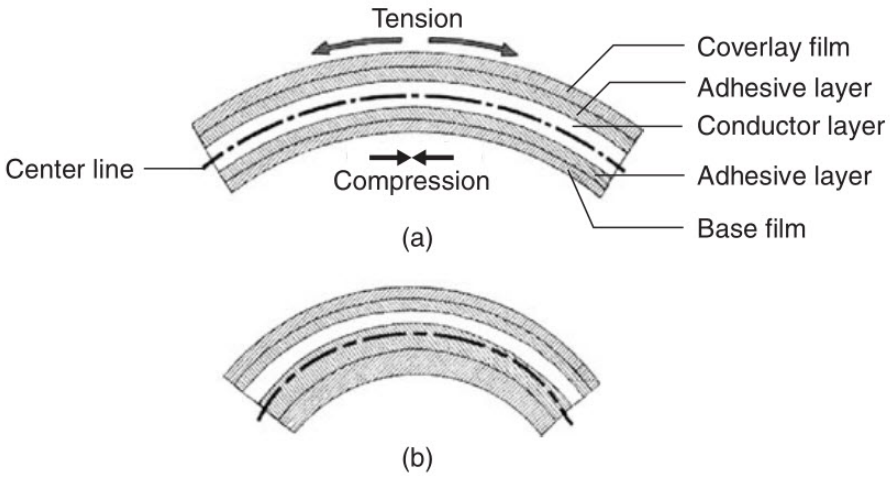

Figure 2.19: FPC board materials layup and reaction during bending.
(Coombs and Holden, 2007)

Looking at the basics of the mechanical stress diagrams, the design of any FPC board should make use of a conducting layer that remains on the neutral axis during bending thus requiring a symmetrical material layup. This would be advised in order to produce minimal stress in the conducting layer, as the conducting layer will have to provide key communication and electronic connection. This design intent will, in turn, increase the flexing lifespan of the board. The size of the bending radius of the FPC board also has a direct effect on the flexing life of the FPC, however, in the use of FPC materials for multifunctional composites, there will be almost no bending radius when compared to the application of FPC's in the commercial environment. By having the conducting layers between the composite material layers, the bending radius will be limited to the maximum bending radius of the composite material used as the structural support.

The wiring harness requirements and positioning vary depending on the electronic requirements of the subsystems within the spacecraft. The circuit layout within the multifunctional composite panel will have to be calculated by the electrical engineers designing the internal electronic subsystems and the required location of the connecting tracks. The aim from a mechanical point of view is to prove that the overall system of combining the FPC within the composite material is feasible and manufactureable while still producing good mechanical properties to be used as an assembly structure. The design, manufacture and construction of the FPC boards will remain as per industry standard already laid out and adapted for use as a multifunctional component.

By keeping these sections standard, methods that are currently being used and that are well known by electrical engineers can continually be used in order to have ease of adaptability for electrical engineers systems into a multifunctional mechanical design. The main priority of the FPC design is to provide detailed background on the FPC cover layers in order to find a suitable method of adhesion to the epoxy matrix used in the manufacture of the composite structure. The section to follow will explore the field of thermal conductivity within multifunctional composites.

2.4.2.2 Embedded Transformer (Coated Wire)

An alternative to a flexible circuit board construction using copper foil sandwiched in the composite laminate is to use small gauge enamel coated transformer wires. The wires can be placed between the composite material layers and allow a controlled electrical connection from one side of the composite to the other. Enamel coated wire or also called magnetic wire is commonly available from most electronic component suppliers and is widely used for electromagnetic coil windings. Magnet wire is also used for the windings in a transformer. The wires are available in a range of different sizes and the sizes are listed in a particular *gauge* of wire. The enamel coating provides a non-conductive insulation layer which prevents electrical shorting when multiple coils are wound around a core in a transformer for example. Thus, for the application between the layers of the carbon composite material, this material can be considered as it has a built-in protective layer against possible shorting with the carbon material. Appendix C.4 shows the common sizes of magnetic wire that are available in the industry.

2.4.2.3 Thin PCB Copper Layer Board

Traditional PCB's have a copper cladding on either one or both sides of the board. Various board thicknesses are available off the shelf. Different configurations of thin PCB materials can be layered in a way to create multi-layered PCB's.

This section will review the fundamental knowledge of PCB's required for the MFC panel design and configuration layout. Apart from the option of FPC's and transformer wire integration, a simpler alternative which is to use existing PCB materials in the MFC design, as they are already well known and used in almost all electrical applications in some form or another. The consideration of PCB integration allows for a more traditional approach to electronic design and consideration on the electrical engineers part.

For the interest of this research only single sided boards (SSBs) will be focused on, however, in this area of the structural design, there is room for further development and enhancement of the electrical conductors' integration into the multifunctional panels. It must be noted that further development by electrical engineering researchers into possibilities of multi-layered board integration on to MFC panels will allow much further expansion of the PCB and electrical capabilities.

2.4.2.3.1 Single Sided Boards SSBs as previously mentioned on have circuitry on one side of the board. Boards come in a variety of thicknesses and typically range from 0.1 mm to 1.6 mm. Although boards with double sided copper cladding can be used (where one side has connection tracks and components and the other is just connection track), this section will focus on the SSB with a single sided copper cladding as well. SSBs are also referred to as print-and-etch boards, as it is common for these boards to have a screen printed track layout on the copper surface and the exposed areas of copper are chemically etched away (Coombs and Holden, 2007).

Typical SSB materials are FR-2 grade paper (cotton) composite laminates. The structural material of the PCB is commonly referred to as the sub-straight material. Generally, SSBs are used for low cost, high volume production items (Coombs and Holden, 2007). However, from local suppliers, SSB materials are also in FR-4 composite material laminates. On one side of the board, a copper foil is applied. The sections that follow expand further into the FR-4 material and common copper foils used on SSBs.

2.4.2.3.2 FR-4 Composite PCB material FR-4 is a woven glass composite material with an epoxy resin system, as listed by the NEMA material grades. NEMA (National Electrical Manufacturers Association) is an association of United States based manufacturers of electrical equipment, with many of the electrical components standards conforming to the regulations set out by this association.

FR-4 is the most commonly used PCB material today (Coombs and Holden, 2007). Due to the excellent mechanical, electrical and thermal properties of FR-4, it is extremely versatile and has a very wide field of uses in industry. Applications ranging from computers, networks, telecommunication, automotive, aerospace and many others (Coombs and Holden, 2007).

In the tables and listing of standard FR-4 materials provided in (Coombs and Holden, 2007), which are used for PCB's, there is more than one FR-4 material listing. The key factors remain relativity unchanged, where FR-4 material consists of a woven fibreglass, epoxy resin system and is flame-resistant. The different temperature ratings of the material require different resin systems to be used and each resin system or configuration of the FR-4 material needs to be specified.

As covered in the previous sections, the composite material theory applies to the FR-4 material much the same way as it would to any woven fabric composite. In this case, the material is fibreglass. However, due to the fact that PCB material already comes prepared from the suppliers and the exact geometry, tow type, tow dimensions and fabric properties are not completely listed by the suppliers, the PCB composite material is very difficult to apply the basic micromechanics models too. The fabric would have to be evaluated for a specific batch and reverse engineered to determine the fabric properties. In the electronics world, the properties, standards and specifications to which the manufacturers of PCB material have to conform to are very strict. Thus, to look up the already documented material properties by the manufacturer is far less tedious to do. In addition, due to the fact that the PCB material itself is not constructed in the design covered in this research, only the assembled composite material properties and characteristics are important when calculating the material properties of the primary composite structure material.

The FR-4 PCB material properties and specifications are very well documented in electrical engineering handbooks. The handbook by (Coombs and Holden, 2007) specifies the properties of a large range of PCB materials commonly used in industry, this includes the copper foil material properties and various additives that can be used to alter the properties of the PCB material.

Copper PCB Layer:				
Property	***Symbol***	***Units***	***Value***	***Data Source***
Young's Modulus	E_cu	Pa	1.18E+11	
Shear Modulus	G_cu	Pa	4.40E+10	
Density		g/cm^3	8.9	
Poisson's Ratio		-	0.35	
Coefficient of Thermal Expansion		µ/m °C	16.8	
Thermal Conductivity		W/m/C	3.9	
Fatigue Strenght (50e6 cycles)		Pa	2.00E+07	
UTS		Pa	2.00E+08	

Table 2.8: Copper Foil Material Properties.
(Chapman, 2016)

The FR-4 material data can be extracted from (Coombs and Holden, 2007) throughout the various chapters, but Appendix C.1 and C.2 contains a copy of a condensed data sheet of NEMA grade FR-4 PCB material.

2.4.2.3.3 Copper Foils The primary conductive material used on printed circuit boards is copper foils. In rigid or flexible printed circuit boards, a copper foil layer will be used as the primary conductive material that the electronic circuitry is cut into. The copper foils are available in a range of different thickness's which is used by industry manufacturers on PCBs. The copper that each manufacturer uses will differ in chemical composition very slightly, however, this discrepancy is so small that it can be neglected unless a special type of copper foil is used in a specific application. However, for general electronic PCBs, the copper foils data presented in Table 2.8, where the data was extracted from the copper conductor electrical engineering handbook by (Chapman, 2016).

For each variation of PCB available from each supplier, the specification of the copper layer thickness must be obtained from the supplier. The copper layer thickness can be taken into account when assembling the FEA numerical model for simulating the material properties. The material properties presented in Table 2.8 can be used for the copper foil layer of the PCB.

2.4.2.4 Fatigue fracture of copper conductors

The fatigue characteristics of copper conductors follow the primary mechanical engineering practices as learnt for most isotropic metals at undergraduate level. Cyclic stress loading of the material which reaches stress levels near that of the yield stress of the metal will inevitably decrease the expected life span of the material under the working conditions (the number of cycles till failure). The effect is set on by the cold working effects on the material as it enters the plastic deformation regions of the stress-strain graph. The cold working of the metal will produce a harder material, however, the material will become more brittle as the hardness increases. Particularly in the case of bending where the stress levels will induce work hardening of the material and

the ductility of the metal is reduced, which in turn will affect the performance of the metal to bend under normal loading conditions.
The effect of extended exposure to a loading below its yield can induce a creep or cold flow condition in the metal.

An article presented by (Ḧyonny Kim et al., 2005) covers the fatigue testing of embedded copper conductors in multifunctional composite structures. The research is experimental based, where MFC samples were produced with a copper foil layer embedded in the middle of the composite material layers. Mechanical tests both static and dynamic fatigue tests were conducted, where a power supply of 3 volts DC was monitored across the sample to determine whether the copper connectivity had broken in the material. It was reported that the addition of the copper material to the composite material has very little structural effect on the overall UTS.
After establishing the UTS of the composite samples using the static tests, a range of fatigue tests was done. The reported results show that at 75% of the UTS and after 1000 cycles the failure mode was the composite material structure, however at 65% of the UTS and after 1100 cycles, the failure mode was the copper conductor which was embedded in the sample. The failure modes have been separated in the report to indicate that although the electrical function may have failed, the structural properties of the composite section of the samples were still intact and able to carry a load. Observing the logarithmic data as graphically presented by (Ḧyonny Kim et al., 2005), at approximately 70% of the overall UTS of the material and 1000 cycles both the copper and composite material would fail. The samples are a glass epoxy composite with the copper foil embedded in the layup construction. 70% of the UTS, in this case, is approximately 340 MPa, which would be the ultimate fatigue strength of copper at 1000 tensile stress cycles. In the case of a carbon composite construction, the overall UTS will increase however the fatigue failure of the copper would most likely remain at the same stress to cycle ratio and at 340 MPa. The copper fatigue failure limit will have to be considered relative to the carbon composite that is used.

2.4.2.5 PCB Mechanical design requirements

The mechanical design requirements of a PCB is very similar to that of the structural requirements and testing defined in the spacecraft structural design section later in this chapter. However, as a comparison, the book by (Coombs and Holden, 2007) is electrically orientated (not directed specifically to spacecraft) and highlights the following key mechanical design requirements:

- Dimensioning and tolerancing
- Mechanically mounted PCBs
- Shock and vibration.
- Board deflection.
- Natural frequency.

All the design requirements listed above are addressed in the spacecraft structural design section and have almost exactly the same consideration. Due to the fact that the topic of this thesis is the design of a composite spacecraft structure, the requirements from the spacecraft point of view will be taken, as this is the predominant area for the requirements' guideline as opposed to that of the PCB field. Although the concept behind the configuration of the material mimics that of a PCB construction, the focus is on the space qualification and requirements field.

2.4.3 Thermal Conductivity of Materials

Among the most important non-structural features of a multifunctional composite structure, is the thermal properties of the material. In certain cases, it can be beneficial for a material to be insulating or conductive. The problem with most structural designs is that without changing the material from which the structure is made of, it is very difficult to change the thermal conductivity of the material drastically. In certain applications, there are options of various coatings and compound materials that can be used in conjunction with the primary structural material in order to aid the conductive properties in either capacity. With the use of composite materials, a range of materials can be stacked in between the composite structural layers formed by the primary fibre components. This allows not only a single material base to have drastically different thermal conductivity coefficients in a single panel, but also allows the possibility for the thermal material to be positioned in specific locations depending on its requirement.

Thermal conductivity can be a critical factor when working in harsh thermal environments such as space. Without the protection of the earth's atmosphere, the temperature fluctuation in space is at quite a high rate. More about the space environment is discussed later on in a further subsection. The placement of the thermal materials can be arranged to optimise the internal environment for the electronic subsystems. The electronic components of a nano-satellite system are the most vulnerable to changes in temperature. In most cases, the mechanical materials can cope with a wide range of temperature variance without effect to the integrity of the structure. Electronics, however, have an optimal operating window that will provide the best life span of the electronics but also prevent electronic failure. The temperature fluctuation of the environment that surrounds the electronics must also be reduced to a minimum, as larger changes in temperature create thermal expansion problems between the electronic components. The subsections that follow will now evaluate each of the critical thermal topics relating to satellite design, namely; thermal effects on electronics, composites thermal properties and operating environment.

2.4.3.1 Thermal effects on electronics

One of the factors that needs to be taken into account when considering the thermal effects on electronic components is the effect of the thermal expansion difference between the components and the stress loading on the solder joints. The solder joints

are connections between the electronic components and the substrate circuit board in order to provide for the connections between multiple electronic components. Solder is a metallic material that usually melts in temperature between 183-215 degrees Celsius (Coombs and Holden, 2007).
In this particular study, the electronic requirements will remain the same as that of the electronics mounted to the internal PCBs of the satellite. Any electronics mounted to the MFC structure will be within proximity of the existing electronic components on the PCBs. The CubeSats operate in the LEO (Lower Earth Orbit) where the temperature fluctuations are not as severe as deep space.

The thermal control of spacecraft is very important to ensure that the electronics are within their thermal operating window. Typical operation ranges of electronic components are between -15 to +50 degrees Celsius (Fortescue et al., 2011). Different electronic components require finer thermal control and have smaller thermal operating ranges. For example, the typical operating range of rechargeable batteries is 0 to +20 degrees Celsius (Fortescue et al., 2011).

Components currently used in CubeSats are already space qualified and in most cases already have space heritage. Therefore, any electronic components intended to be mounted on the MFC material will undergo the same requirements and checks as that of the components used on the internal boards of the satellite's electronic systems.
The thermal environment that satellites are exposed to was discussed in the operational environments section earlier in this chapter.

Many factors have to be considered in the thermal environment of the satellite and it is important that the satellite maintains and regulates its thermal condition to maintain a balance. Heat is radiated to the satellite by the environment but is also generated by the internal electronic subsystems during operation. The orbital environment of the satellite must be known and the heat generation of the subsystems needs to be accurately defined before any thermal analysis of any accuracy can be performed. Thus, the design of the components needs to be matured to subsystem level requirements and specifications. The thermal balancing of the satellite is an entire field of study on its own and will not be the focus of this thesis, however, it is important to keep these thermal requirements in mind and is one of the key driving considerations in any structural design.

2.4.3.2 Composites thermal properties

The importance of thermal balance in the satellite has been highlighted in the previous section. In order to perform the thermal analysis of the overall satellite, the thermal properties and characteristics of the structure need to be known. The objective of this section is to deal with the multifunctional composite material thermal property determination.

The composite material thermal coefficient calculations have been extracted from the book by (Barbero, 2010), which covers the numerical calculations for various cases in

very fine detail.

Composite materials have two coefficients of thermal expansion. However, equations (2.42) and (2.43) below are for UD fibres and do not consider the fibre undulations of woven fabric carbon fibres. Thus the equations that follow adjust the thermal coefficients by considering the fibre undulation effects on each tow and wrap.

$$\alpha_1 = \frac{\alpha_A V_f E_A + \alpha_m V_m E_m}{E_1} \tag{2.42}$$

$$\alpha_2 = \alpha_3 = \alpha_T \sqrt{V_f} + (1 - \sqrt{V_f})(1 + V_f \nu_m \frac{E_A}{E_1})\alpha_m \tag{2.43}$$

Where $\alpha_A, \alpha_T, \alpha_m$ are the transversely isotropic fibre and isotopic matrix thermal expansion coefficients. E_A, E_m, ν_m are the elastic constants of the isotropic fibre and matrix and the Poisson's ratio. V_f is the volume fibre fraction.

Using equations (2.44) to (2.48) the local fill and wrap thermal coefficients can be found.

$$\alpha_x^f(x) = \alpha_1 c_f^2 + \alpha_2 s_f^2 \tag{2.44}$$

$$\alpha_x^w(y) = \alpha_2 \tag{2.45}$$

$$\alpha_y^f(x) = \alpha_2 \tag{2.46}$$

$$\alpha_y^w(y) = \alpha_1 c_w^2 + \alpha_2 s_w^2 \tag{2.47}$$

$$\alpha_{xy}^f = \alpha_{xy}^w = 0 \tag{2.48}$$

Then the next stage is to use the hygrothermal forces using the CLT principles covered earlier.

$$\begin{Bmatrix} N_x^T \\ N_y^T \\ N_{xy}^T \end{Bmatrix} = \triangle T \int_{-h/2}^{h/2} [\bar{Q}(x,y)] \cdot \begin{Bmatrix} \alpha_x(x,y) \\ \alpha_y(x,y) \\ \alpha_{xy}(x,y) \end{Bmatrix} dz \tag{2.49}$$

$\bar{Q}$ is found using equations (2.35) and (2.36). "h" is the height of the final lamina. The representative volume element (RVE) using the isostrain method again the average in-plane load becomes:

$$\{N\}^{T,M} = \frac{4}{(a_f + g_f)(a_w + g_w)} \int_0^{(a_w+g_w)/2} \int_0^{(a_f+g_f)/2} \left\{N^{T,M}(x,y)\right\} dxdy \tag{2.50}$$

Using the values obtained in Equation (2.50) together with the inverse of the extensional stiffness matrix, the thermal coefficients of the woven lamina can be found using equation (2.51).

$$\begin{Bmatrix} \alpha_x(x,y) \\ \alpha_y(x,y) \\ \alpha_{xy}(x,y) \end{Bmatrix} = [A]^{-1} \begin{Bmatrix} N_x^T \\ N_y^T \\ N_{xy}^T \end{Bmatrix} \tag{2.51}$$

The [A] matrix is found using equation (2.37) presented in an earlier section covering the composite material calculations.

2.4.4 Energy Harvesting Capabilities

Solar panels are the primary forms of power for CubeSats. The solar panels are mounted on the surface of the CubeSat structure and in some cases are attached to deployable panels to allow the best angle toward the sun for maximum power harvesting. The deployable options are in most cases used with a CubeSat that has an attitude control system to maintain the best position of the satellite relative to the sun during the time in which it is exposed to the sun's rays.

In the case of the MFC structural material, the conventional type solar panels can be mounted to the exterior surface of the material in much the same way that it would have been attached to a conventional PCB backing board. Through-holes in the MFC material can be made to allow the electrical connections to reach any layer of the composite construction and attach to the copper conducting material to reroute the electrical power toward the battery charging unit in the CubeSat. Solar panels can be bonded to the outside of the satellite as a means of fastening, using epoxy adhesives between the panels and the composite external layer. The correct preparation of the composite material surface would be required to provide the optimum bond layer strength. Thus, the same methods used for the current applications of solar panels to PCB material on CubeSats will remain the same when using the new MFC material configuration.

2.4.5 Electromagnetic Compatibility and Radiation shielding

Electromagnetic Compatibility (EMC) is a reference to electromagnetic emissions and susceptibility. For example; radiated and conducted emissions and susceptibility (Fortescue et al., 2011). Electromagnetic interference (EMI) is the radiated and conducted EMI that is produced by the system. Radio frequency interference is a type of EMI that can be induced in the system. Electrostatic Discharge (ESD) is the discharge of static electricity in the system that can lead to component and subsequently system failure. All of these types of interferences have to be considered and managed in the system design as it can involve my different areas of the satellite. A systems approach to this problem is recommended in order to manage with all the variable factors in EMC (Fortescue et al., 2011). Electromagnetic Pulse's (EMPs) are also large threats to electronic systems and can destroy electronic equipment. EMI shielding is created by layers of electrically conductive material (Fortescue et al., 2011). In the case of the MFC using carbon fibre, the fibres are electrically conductive and by including

a layer of copper foil, would mimic or better the performance of standard PCB material. EMC has been notoriously difficult to model and simulate because of the very high level of detail required for accurate results (Fortescue et al., 2011). Thus, for this thesis research it important that it is mentioned and needs to be tested for when the development of an engineering model of an MFC structure is created and integrated with electronic subsystems. Physical EMI test can also be done when a representative prototype has been created. The research conducted in this paper does not have the sufficient funding allocation to allow for a representative model to be built and tested, thus the basics of the EMC have been listed here, however, would need to be taken further once the research project has been taken to the correct level.

Radiation shielding for the internal electronics is required to reduce the dose level to a manageable number of the electronic components or low enough to have very low probability of a single event upset occurring. Usually, the first step is to find the curve for a 1D dose based on the depth on a spherical shell of aluminium (Fortescue et al., 2011). From this curve, the dose experienced behind the spacecraft structural thickness is read with a margin of safety. With composite materials, the shielding is not uniform and difficult to calculate. As a solution for this the inclusion of tantalum or tungsten is placed in the region were low dose levels are required. For the MFC the same thing can be done by having a thin layer of tungsten in the areas of the CubeSat where the radiation shielding is required. Physical radiation testing of the composite should be done, however, this is potentially not available due to the limited test facilities available locally.

2.4.6 Manufacturing Techniques

For composite materials, there are many methods that can be used to produce parts. For many years, composites have been used in industry and research conducted to improve the overall manufacturing and handling process required to complete a final part, the composite manufacturing process has evolved inherently. A few common processes used widely in the industry are:

- Hand-Layup
- Autoclave
- Out of Autoclave
- Infusion moulding (aka Resin Transfer Moulding RTM)
- Open Moulding

The facilities available in the labs do not provide access to Autoclave manufacturing methods. Also, due to the relative inconsistency of Hand-Layup and Open Moulding, these three manufacturing techniques will not be covered in this section. The most applicable to the application of a CubeSat composite panel manufacturer would be infusion moulding (primarily vacuum assisted) and possibly Out of Autoclave manufacturing techniques. The infusion manufacturing process is available and the Out

of Autoclave manufacturing process may become available in the near future. Thus, these two processes are covered in more detail in the sections that follow.

2.4.6.1 Infusion Moulding

The composite sections of the CubeSat will be manufactured using the vacuum infusion moulding process.
The *infusion moulding process* (also sometimes referred to as vacuum assisted resin transfer moulding) allows the dry materials to be vacuum drawn prior to the addition of any resin. The resin is then drawn into the mould while under a vacuum. Rather than starting with excess resin in the part and drawing it out (such as seen in the hand layup vacuum bagging process), the infusion moulding starts with no resin at all and introduces it to the mould. Ideally, any excess resin that is introduced to the part would be drawn out (Hopper, 2003). This lowers the overall weight of the part, minimises waste resin, increases the strength of the part and maximises the ratio of fibre to resin.

Another benefit of infusion moulding is time. Even though there are ways to increase the working time, this can still be a challenging factor in very large parts is that it takes time to construct and layup. Problems such as locating leaks in the vacuum bag have to be considered. Then the time at which the bag is applied also affects how much resin is removed from the part, due to the increasing viscosity of the resin as it begins to gel. The infusion moulding process is also generally cleaner than most of these processes, as there is no resin handled or applied by hand with brushes or rollers which could and most like will splash and splatter around the area of the mould.

With any laminating process, there are also drawbacks to infusion moulding process. First of all the set-up of the process is more complicated than vacuum bagging. In vacuum bagging, only the vacuum tubes have to be placed in position. With infusion moulding, the setup of the resin inlet pipes relative to the vacuum pipes has to be planned out carefully (Hopper, 2003). The placement of these pipes varies from part to part and theres no fixed method of setting the pipes up either. Unique parts can become a bit of a trial and error process to perfect resin infusion. This point leads to the next drawback which is that parts can be destroyed very quickly (Hopper, 2003). Although the setup time is unlimited and that there are dry runs that can be done on the mould, there is still the possibility of a leak occurring or air getting into the resin inlets, which can create air bubbles or the air could also create locks which could lead to resin pooling in the part. Although most time these problems can be fixed during the infusion of the resin, one should not expect to resolve the problems every time. Due to the potential problems that can arise with infusion moulding, a trial and error approach should be used to perfect the setup (Fibre-Glast, 2013). Smaller trial runs with less material are advised during this trial and error period to eliminate wasted material and cost (Fibre-Glast, 2013).

Figure 2.20 shows the overall setup of a typical infusion moulding process. The setup involves the required equipment and materials, as well as their specific placement to form the system.

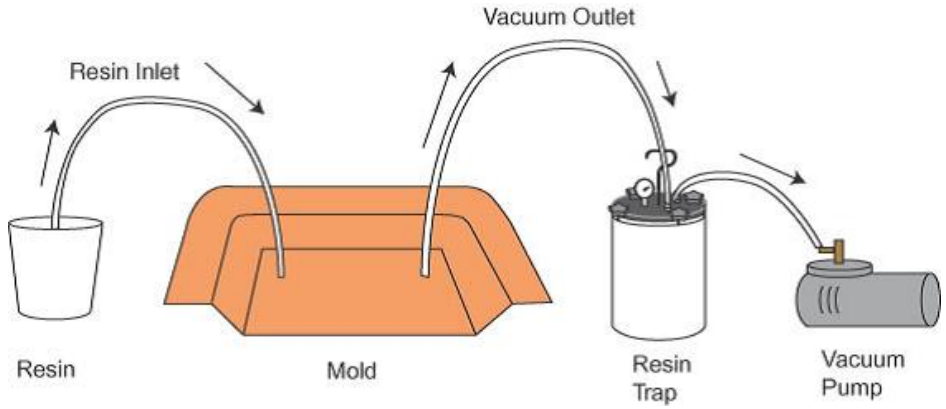

Figure 2.20: Typical Infusion System Set-up.
(Hopper, 2003)

The vacuum bag on the mould is connected to the vacuum pump via the resin trap. Once the vacuum pump is switched on it evacuates the resin trap and the vacuum bag on the mould. Initially, the resin inlet pipe will be blocked to evacuate as much air as possible in the vacuum bag and the resin trap. Once a good vacuum level (80 to 90 %) has been reached the resin inlet pipe is opened, with the end of the pipe in the resin bucket. The resin flows into the mould as the pressure of the resin is at a higher level (at atmospheric) than the mould. The resin inlet pipe is opened with the end of the pipe already in the resin to prevent air entering the mould once the resin begins to be drawn in. Air is not wanted in the mould as it creates voids in the finished part, which can weaken the component and also creates an undesirable finish on the surface of the component. This is not the only way the setup can be done, but just shows a general setup used to perform the infusion process.

2.4.6.2 Out of Autoclave

The *out of autoclave* process is the process where generally prepreg composites are stacked into a mould with a vacuum bag over the top of the mould layup. The mould is then subjected to a vacuum in much the same way the infusion process was done, however, the difference now is that the complete mould vacuum assembly is placed into an oven to raise the ambient temperature. This process cures and bakes the part while still under a vacuum and creates a more accurate and better quality part than the room temperature infusion process described in the previous section. It is recommended that this process is used for any engineering model components or flight grade components if an autoclave is not available.

The only difference between a conventional autoclave and an out of autoclave process is that in the autoclave process the oven itself is also pressurised, creating a higher relative pressure on the surface of the mould (more than 1 bar) and thus producing a much better quality part. Autoclaves and prepreg carbon fibre are used for high-performance space components, however out of autoclave process can also do a good enough job and may be more accessible than the autoclave machine.

2.4.6.3 Machining of Composite Materials

Composite materials are generally machined with diamond-coated tools. In most cases, it is not recommended to machine holes through a carbon laminate as it creates stress concentration areas and also breaks the continuity of the fibre tows that run the length of the laminate. Normal machine tools and bits can be used to machine composites, however, they tend not to last as long and become dull in a short span of time. Composite parts that are manufactured, are done with the intended shape already formed and only the edge or profile trimming is required after the curing process to finish off the dimensioning of the part. The machining processes that are most applicable are routeing, milling, sanding and drilling operations. These processes will cover the majority of the required machining work in this research. The process of machining will use the standard machining methods and use specialised tools or bits if they are available. The correct protective gear and clothing must be worn to ensure that the harmful composite dust that is created during machining from irritating the skin, eyes or being inhaled by the machinist. Adequate ventilation must also be available in the machining areas, thereafter standard machining safety must be practised.

2.5 Spacecraft Design Theory

2.5.1 Introduction

Spacecraft design is an extremely large and complex operation. The roles of systems engineers and specialists in each engineering discipline involved are vital to achieving a design of spacecraft that will operate successfully in space. The focus area of the theory presented in this section will be on the structural design considerations and processes for spacecraft, to keep it in line with the topic of this thesis. The majority of the theory presented here is extracted from the book by (Fortescue et al., 2011). This book provides a great collection of spacecraft design theory and experience directly from industry projects. The section of spacecraft structures has been written by an engineer from EADS Astrium, which is a large spacecraft company based in Stevenage in the United Kingdom. The company has many years experience in building very reliable GeoSync telecommunication satellites, which have a guaranteed operational lifespan of 15 years. The theory covered in the book by (Fortescue et al., 2011), generalises the design factors for all types of spacecraft.

In addition, the book by (Brown, 2002) also covers the spacecraft design aspects and the chapter on spacecraft structures cover much the same points and theory that the book by (Fortescue et al., 2011) does. Between the two book previously listed, the bulk of the required information for this thesis is adequately covered.

The main design factors and considerations in spacecraft structural design are covered in the sections that follow and specifically deal with information and factors most relevant to the CubeSat design process. Any structural design begins with a

good configuration specification/definition, material selection, type of manufacturing method, analysis and simulations, and lastly, requirements verification using virtual engineering models as they become mature enough to provide reasonably accurate predictions.

2.5.2 Design Factors and Considerations

The concept design of the spacecraft structure is the first area of approach in the overall development cycle. The concept design will provide a clearer vision and indication of the direction in which the design cycle is headed in. A number of "sub-factors" need to be considered before the structural concept design can begin. The "sub-factors" will aid in the constitution of the spacecraft structural requirements which need to be achieved or met in order to develop a successful structure.

The major factors that need to be considered are the launch vehicle interfacing, mounting of equipment, environmental protection, alignment, thermal and electrical conductivities, accessibility and mass. (Fortescue et al., 2011). In a recent discussion with a spacecraft systems engineer, a statement that was made was that if you can strictly control the mass of the spacecraft, then one-third of the design work would be completed inherently. Now although the structure only forms part of the overall weight specification, the means by which the design is done may be restricted to the amount of redundant material that is designed into the PCB's for example. The structure itself naturally would be optimised as far as possible to limit any unnecessary weight. Many of the design factors that needs to be considered are covered by the CubeSat standards, however, the effect of the standards and its implementation will be discussed in the relevant section later on.

2.5.3 Material Choice

The material choice for any structure is always a tricky and complex decision to make. Each material that can be considered has its relative pros and cons. The application of the structure determines which material would address the most amount of mechanical issues with the least compromise. The key selection criteria that comes to mind for a mechanical engineer, are generally; specific strength, specific stiffness, corrosion resistance, fatigue and fracture strength, thermal expansion and conductivity properties and the ease of manufacture and handling requirements of the material (Fortescue et al., 2011).

The specific mechanical properties are important particularly in the aerospace industry, as the mass factor is critical to the cost and capability of the spacecraft. Logically the lighter the materials the easier launching of the structure is and/or more capacity of payload. The corrosion resistance of the material needs to be considered with respect to the environments the spacecraft will be operating in and the environments it will ultimately be exposed to. As an example, a spacecraft when being constructed on earth will come into contact with the atmosphere unless constructed in a complete vacuum

chamber, which would be unrealistically costly to achieve. However, conditions in space need to be considered in terms of the corrosiveness of the environment. The main factor is the consideration of the out-gassing effect on the materials as it is subjected to the vacuum of space and the thermal cyclic loading as the satellite orbits the earth.

The fatigue strength of a material is considered when a dynamic load is applied to the structure repeatedly over its lifespan. The load may be from devices or due to the operation of the satellite in working conditions. The thermal cyclic loading must also be considered once again, particularly if the orbital parameters and altitude of the satellite results in a path transverse to the earth's dawn-dusk line. This will induce a temperature fluctuation on each orbit which will create a thermal expansion and contraction of the materials. If the satellite is also constantly positioned in a specific orientation via attitude control mechanisms, the relative surfaces will experience a differential temperature. The "hot" and "cold" spots or areas on the satellite at a single time will induce a stress in the material and tend to warp the material or the structure if not analysed and controlled.

Finally, the manufacturing process that will be used to produce the various components and parts required for the structure needs to be considered. For metals, the machinability of the materials is generally considered for example, where composites are moulded into their relevant shapes. Composite components are trimmed or routed around the edges to specification, however, with filament tows in fabrics, composites cannot be machined as the fibres would be "cut" and the structural integrity would be compromised. Composites are also difficult to apply specific tolerance to, as they tend to shrink and deform/warp as the material cures. The amount of distortion of the components and the amount of shrinkage is linked to the type of matrix resin material chosen for the composite construction.

As a specific note of the composite material application, carbon fibre exhibits properties of hygroscopic absorption when exposed to moisture. The water absorption can add up to 2% of weight in normal atmospheric conditions, which does affect the strength of the material (Fortescue et al., 2011). Then, when the component is exposed to the space environment the water content is then released which adds to the out-gassing properties of the material. Carbon fibre composites are known to be brittle and require careful consideration of stress points or concentrated loads applied to the material (Fortescue et al., 2011). When compared to aluminium or titanium materials, they have sufficient ductility to dissipate and absorb the stress into the rest of the material. For this reason, you will find that most carbon fibre parts are simple and use metallic fittings or ends where the component will attach to the structure (Fortescue et al., 2011). For example, newer racing bicycle frames will be constructed from carbon fibre, however, the areas where the front forks or the suspension parts are mounted are metallic inserts. This allows the ductile properties of the metal to absorb and transfer the stresses more evenly into the carbon composite section.

2.5.4 Numerical Analysis

The creation of a finite element model which can be used for analysis is a key part of the design and development process (Fortescue et al., 2011). The model is used to:

- determine stresses and strains induced by the loads.
- predict the overall natural frequencies of the structure.
- determine the stiffness and deflection requirements corresponding with the sub-assembly needs.
- be used by launch providers to validate the design and spacecraft compatibility with the launch vehicle.

On the market, there are many FEA software packages available to use to simulate spacecraft structures. Common to all the software packages is the selection of the type of elements that will be used in the analysis procedure. The model or assembly of a complete spacecraft is generally constructed by bringing together various sub-assemblies (Fortescue et al., 2011). The main elements are shell elements, 1D elements and 3D elements. Each element can have different formats such as hexagonal or tetrahedral element shapes for 3D elements, or triangular or quadrilateral elements for 2D shell elements. Further discussion and explanation of the types and details of the elements used for the analysis are covered in a later section of this thesis.

Important factors to consider is to model a portion of the structure in order to reduce the computational expense and the overall run time of the simulation. The main point that will be mentioned here is the consideration and placement of the loads in the FE model. The major loads that must be considered are the launch loads, vibration and shock loads that the structure will experience. The most dangerous time for any satellite is the launch stage. The launch vehicle exerts a g loading on its payload (in this case it is the satellite itself) including a vibration pattern as the solid rocket boosters (SRB's) are running. Shock loads are experienced as the SRB's break away from the spacecraft when the explosive bolts and jettisons are activated. Table 2.9 illustrates the various loading conditions at the different stages of the Ariane 5 rocket.

In addition to the g loads and shock loads, the payload of the launch vehicle will also experience acoustic noise and randomised vibration patterns due to the aerodynamic noise of the rocket travelling through the atmosphere (Fortescue et al., 2011).

As a simplification of the many complex vibrations that are experienced during launch, a sine vibration pattern is used at a range of frequencies (Fortescue et al., 2011). Components are subjected to tests on a large 'shaker' (vibration bed) that is controlled to run through frequencies from 5 Hz right up to 100 Hz. The frequencies are increased at a rate of two octaves (doubles) every minute until 100 Hz is reached. Table 2.37 shows the sine vibration environment for the Ariane 5.

The acoustic noise and random vibration patterns are validated and tested for, how-

Critical flight event	Acceleration (g)			
	Longitudinal		Lateral	Additional line load (N/mm)
	Static	Dynamic	Static + Dynamic	
Lift off	−1.8	+/− 1.5	+/− 2	10
Maximum dynamic pressure	−2.7	+/− 0.5	+/− 2	14
SRB end of flight	−4.55	+/− 1.45	+/− 1	20
Main core thrust tail off	−0.2	+/− 1.4	+/− 0.25	0
Max. tension case: SRB jettisoning	+2.5		+/− 0.9	0

Note: The minus sign with longitude axis values indicates compression.

Table 2.9: Launch loads of the Ariane 5 rocket.
(Fortescue et al., 2011)

Sine	Frequency range (Hz)	Qualification levels (0-peak)	Protoflight levels (0-peak)	Acceptance levels (0-peak)
Longituinal	2−5*	12.4 mm	12.4 mm	9.9 mm
	5−50	1.25 g	1.25 g	1 g
	50−100	1 g	1 g	0.8 g
Lateral	2−5	9.9 mm	9.9 mm	8.0 mm
	5−25	1.g	1 g	0.8 g
	25−100	0.8 g	0.8 g	0.6 g
Sweep rate		2 oct./min	4 oct./min	4 oct./min

Table 2.10: Sine vibration representation for the Ariane 5 rocket.
(Fortescue et al., 2011)

ever, the predictions of individual components are not very accurate as the assembled satellite will exhibit a different response characteristic to that of the individual parts. For that reason, the satellites critical components and larger assemblies are generally tested for random vibrations.

For individual components, the simulation of the structure's natural frequencies and the dynamic response under loading are evaluated. From this data, the critical frequencies are recorded for each component and if required a damping can be implemented should it be needed. The interfacing to other components, its relative natural frequencies and any generated frequencies must also be considered to avoid incompatibility or to determine the level of damping required between components.

The factor of safety also needs to be built into the design of the spacecraft structure. Unlike most industries, the aerospace industry cannot allow for over redundancy in the design, thus that factors of safety are marginal. As an example, the Ariane 5 launch vehicle has a FOS 1.25 (Fortescue et al., 2011). The most commonly used proof factor of safety in the industry is 1.1 (Fortescue et al., 2011), but anything between 1.0 and 1.5 is also acceptable.

The FE models can also be used for thermal analysis of the structure in its operation environment in orbit. The thermal environment in space has been previously discussed in the beginning sections of this chapter. The parameters and conditions can be models along with the satellite itself and simulated in these conditions to evaluate the thermal response of the structure.

2.5.5 Design Verification

Any structural design for a spacecraft needs to be verified in terms of its design, meeting the requirements initially set out. The major requirements of the structure would ultimately be a strength and stiffness specification. When the structure is tested it should conform to the designed factor of safety or produce results very similar to that of the mathematical models. This ensures that valid tests are being done and that the numerical models are relatively accurate in terms of predicting the real world scenario. The key requirements to be physically and virtually tested for are, the static strength, sine vibration responses and the natural frequencies (Fortescue et al., 2011).

During the testing phase a dedicated test model is generally produced, as the testing procedure requires in most cases specialised areas machined out to attach the probes and measurement devices to (Fortescue et al., 2011). For vibration tests engineering models can be used (Fortescue et al., 2011), however, it is advised that when using the engineering models, dummy masses should be included into the model to represent any missing components or sub-assemblies that are too fragile or not yet ready for testing. In most testing operations the used for non-destructive testing methods are employed to reduce the cost of testing and the number of test components required. The comparison of the natural frequencies can be done between the physical model and the numerical model to provide further verification of the FEA models produced.

2.5.6 Impact Protection

One of the points that needs to be mentioned is the consideration of debris in space impacting the satellite structure. In recent years various countries have launched satellites and have had failures or accidents in space that have built up a large debris field. In 2007 the Chinese tested an anti-satellite weapon on one of their own satellites which created thousands of pieces of debris in lower earth orbit (LEO). After attending various satellite related conferences, the key focus areas in space exploration and technologies is the management and reduction of space debris. The debris field creates great hazards for active satellites orbiting in the near area and needs to be considered by satellite designers.

The highest density of debris is in LEO and must be considered when designing larger and more expensive satellites. CubeSats are not protected against impacts as they do not cost enough to warrant a protection system. CubeSats also have very limited space available to create protection layers.

The typical size of debris considered in impact scenarios are that of around 1 mm in size (Fortescue et al., 2011), this is due to the fact that tracking these debris particles are very difficult and can't always be avoided. Larger pieces of debris can be tracked and satellites with propulsion systems can be manoeuvred to above a collision. The typical impact speed of the smaller 1 mm particles is around 2 to 5 km/s (Fortescue et al., 2011), which is an extremely high velocity. This is an extremely high-speed impact and will definitely destroy a CubeSat if the particle is larger than 1 mm in size. CubeSats also don't generally have propulsion systems, thus cannot be moved in orbit to avoid a collision path. Another advantage of larger satellites is that space is available for multiple layer protection devices and materials that are spaced away from the main structural material to provide a protective catch net (similar to a bullet-proof vest). CubeSats don't have the space available to add such systems of protection.

2.5.7 Composite Material Testing Methods

To determine the material properties of a composite material, a set of standards can be followed which governs the manner in which tests are conducted. The ASTM (American Society of the International Association for Testing and Materials) standards are widely used in the composite industry to conduct the various material tests. The standards were first created by an American society and adopted as the general testing standard across the world. Although there are other standards available for testing of composite materials, most of the companies and suppliers of composite material follow the ASTM standards when conducting their tests.

Many material tests are available to test for specific material properties, tests such as; tensile tests, compressive tests, bending tests, fatigue strength and many others. In this thesis research, the focus of the tests will be on the tensile and bending test procedures, the primary material properties required for a good comparison to the numerical models can be determined from these two tests. The other limitation is due to the machinery and equipment currently available at the University.

In the interest of not repeating the ASTM standards that are available from most academic libraries or companies that distribute the standards to industry, the key specifications and information will be highlighted in the sections that follow.

2.5.7.1 Tensile Testing

The initial sections of the standards (ASTM Standard D3039, 2014) run through the abbreviations and some terminology used in the document. Thereafter, details of the types of apparatus needed to perform the tests are given. The individual pieces of equipment are specified and its specific purpose to the test procedure, however, in this case, a tensile testing machine is available where majority of the machinery and sensing equipment required is already setup and contained within the machine itself. The available machine includes the equipment such as the force gauges, strain gauges, distance measurement devices, clamps, etc. The machine itself is computer controlled and can be programmed for specific load rates on the specimen, while also recording the data from the various sensors. Figure 2.21 shows the machine available in the material testing lab at the University.

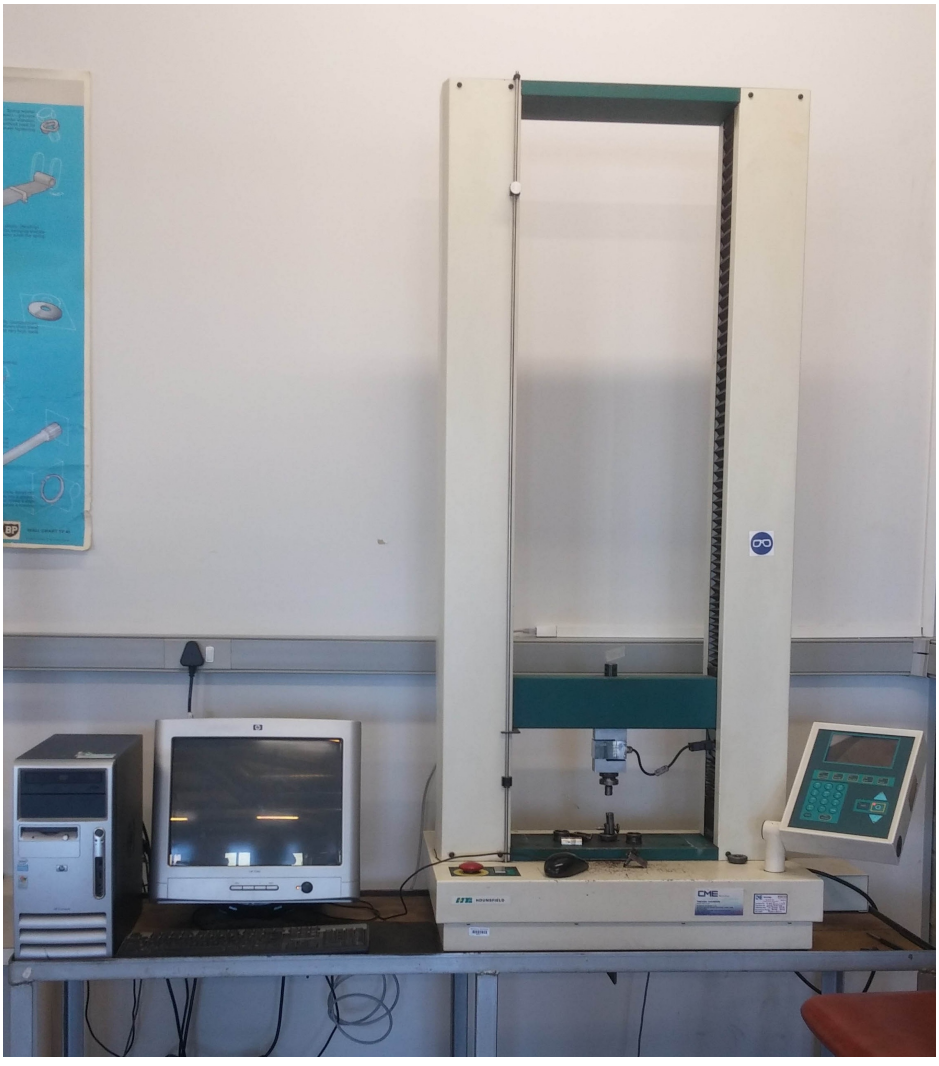

Figure 2.21: The older bend test machine available at the engineering lab.

Parameter	Requirement
Coupon Requirements:	
shape	constant rectangular cross-section
minimum length	gripping + 2 times width + gage length
specimen width	as needed[A]
specimen width tolerance	±1 % of width
specimen thickness	as needed
specimen thickness tolerance	±4 % of thickness
specimen flatness	flat with light finger pressure
Tab Requirements (if used):	
tab material	as needed
fiber orientation (composite tabs)	as needed
tab thickness	as needed
tab thickness variation between tabs	±1 % tab thickness
tab bevel angle	5 to 90°, inclusive
tab step at bevel to specimen	feathered without damaging specimen

Table 2.11: Tensile Specimen Geometry Requirements.
(ASTM Standard D3039, 2014)

Important to note is the specification of the sample size and geometry specifications. Table 2.11 summarises the geometrical requirements of the test samples. No specific sizes are actually given, thus allowing the variation in the sample size to vary as the case or scenario requires it to. As a general size guideline, the recommended specimen width is 25 mm and a length of 250 mm. The thickness is specified to be 2.5 mm, however, this depends heavily on the material layup and configuration as to what thickness is ultimately achieved.

The addition of thickening "tabs" can be bonded onto the specimens to limit the chance of slipping occurring during the test which will add inaccuracies. This should be done in the case where the specimen material thickness is very thin and difficult to grip in the test machine clamps. A drawing representing the specimens can be seen in Figure 2.22.

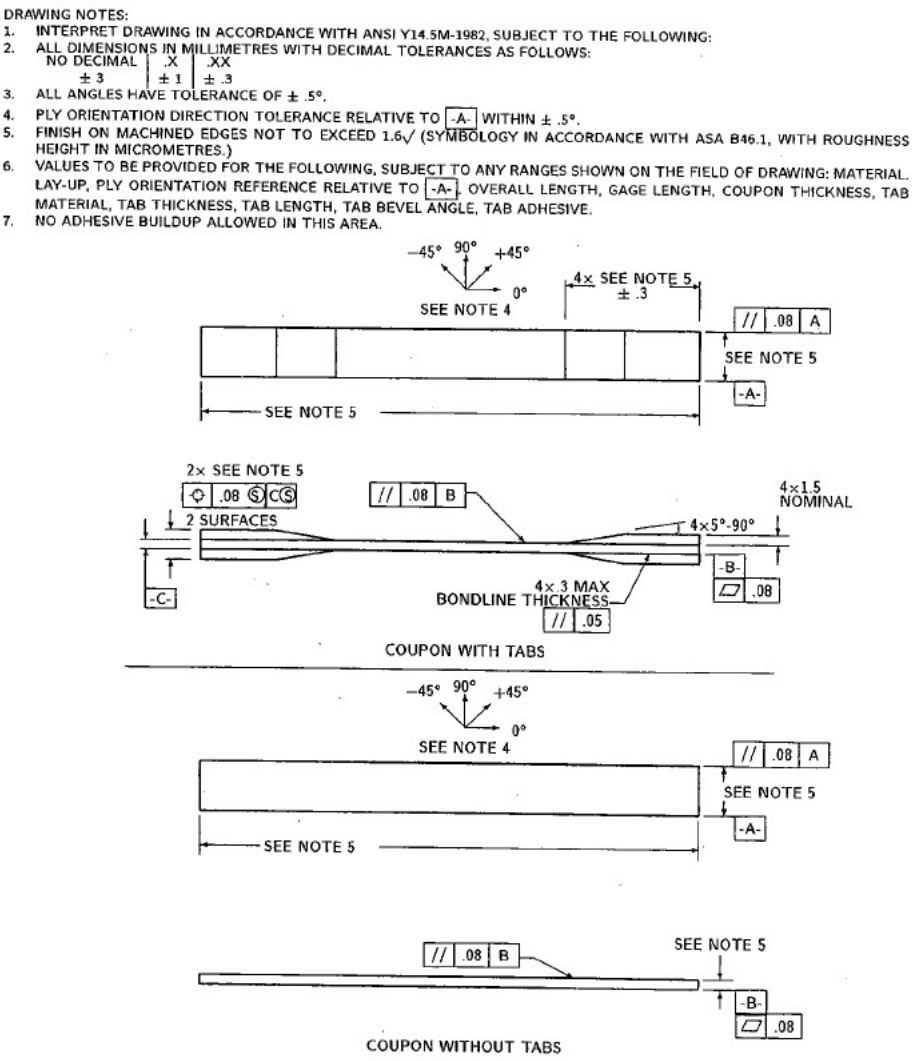

Figure 2.22: The tensile test specimen drawing.
(ASTM Standard D3039, 2014)

The number of specimens required is governed by the user depending on the accuracy and the type of output data required from the tests. It is important to ensure that the machine is calibrated and in good working order. As for the test procedure, the specimens are clamped into the machine ensuring that they are securely fastened. The specimen should then be pre-tensioned very lightly to ensure that there is no slack or play between the clamps of the machine and the load cell. Any play or movement other than that of the specimen stretching initially would create misreading of the specimen elongation. The machine would then be zeroed and the test would be commenced at the specific load rate until the specimen has failed. The application of the load on the specimen should be such that the strain rate is maintained at a constant (ASTM Standard D3039, 2014).

The material properties such as the tensile modulus, the strain and UTS can be determined from the data. According to the standards (ASTM Standard D3039, 2014), the average coefficients of variation for the strength should be no more than 5.11%, the Modulus 2.22% and the failure strain 5.94%. Any value beyond this deviation would

be considered inaccurate and not ideal in terms of practical material data results.

2.5.7.2 Bending Tests

The standards (ASTM Standard D790, 2015) make use of a three-point bending test to determine the flexural properties of the fibre reinforced material. Most of the sample equipment and apparatus used in this test was used for the previous tensile test procedure. The same machine in the material testing lab here at the university can be used, however, the three point bending jig has to now be mounted on the bed of the machine and the loading tube to the plunger attached to the load cell.

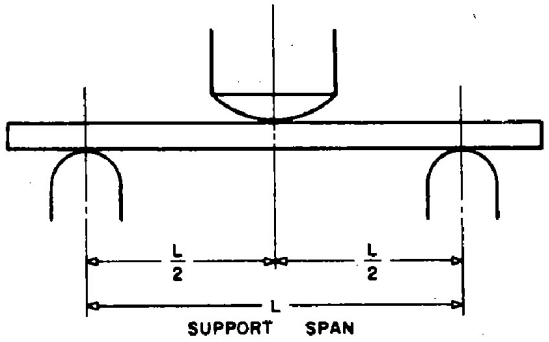

Figure 2.23: Bend test setup diagram. (ASTM Standard D790, 2015)

In the summary of the standards, it states that specimens shall be deflected until rupture occurs in the outer surface of the test specimen or until the maximum strain of 5.0% are reached (ASTM Standard D790, 2015). The procedure employs a strain rate of 0.01 mm/mm/min. The specimen geometry can once again be user defined, however, the load must be applied at the mid-span of the specimen. Figure 2.23 illustrates the specimen loading setup that should be used for the three-point bending test.

Guidelines have been provided for the specimen geometry, if the specimen's thickness is less than 1.6 mm, then the recommended span between the supports should be 51 mm. The overhang on each end of the specimen past the supports should be at least 10% of the supported span and in no case less than 6.4 mm. The overhang allowance should be sufficient to not allow the specimen to slip through the supports (ASTM Standard D790, 2015). The guideline for the number of test specimens that should be tested is a minimum of 5, however, more is preferable.

Formulas for calculating the rate of the cross-head motion is described in equation 2.52.

$$R = \frac{ZL^2}{6d} \tag{2.52}$$

Where:

R : Rate of crosshead motion (mm/min).
L : Support span (mm).
d : Depth of the beam (mm).
Z : Rate of straining of the outer fibre (will be equal to 0.01 mm/mm/min).

The flexural stress can be found using equation 2.53.

$$\sigma_f = \frac{3PL}{2bd^2} \tag{2.53}$$

Where:

P : Load (N).
L : Support span (mm).
d : Depth of the beam (mm).
b : Width of the beam tested (mm).

The modulus of elasticity from the bend tests can be found using Equation 2.54 and can be compared to the modulus found in the tensile tests that were done.

$$E_b = \frac{L^3 m}{4bd^3} \tag{2.54}$$

Where:

E_b : Load (N).
L : Support Span (mm).
d : depth of the beam (mm).
b : width of the beam tested (mm).
m : slope of the tangent to the initial straight-line portion of the load deflection curve (N/mm).

Finally, the standard deviation of the results obtained from the tests should ideally be no greater than 5%. It is important to note that the measurements of the specimen's dimensions need to be recorded before the tests begin and the deviation of the dimensions should be recorded as well. The specimens should be created as uniformly and accurately as possible to ensure that the minimal amount of deviation in the results can be caused due to the geometrical tolerance inaccuracies.

2.6 Summary

The theory literature review gives the reader supporting information required to build a complete understanding of the research effort attempted here. The chapter begins with a review of CubeSats and a brief background of their application and existence. The standards associated with CubeSats are reviewed in terms of the general, structural and mechanical requirements. A further review of the current CubeSat structures and the current research into new structure technologies has been covered to establish the direction in which this research intends to build towards. The potential areas of interest and application of other technologies for secondary functions such as integrated circuitry or energy harvesting have been explored.

Thereafter, a review of the space environment and the factors that need to be considered for the operating conditions in with the CubeSat will be placed. Environmental factors have been considered throughout the life cycle of the satellite, from initial development in the earth's atmosphere to the working conditions in space.

Following on that, a review of the material mechanics of composite materials has been given considerable coverage as this section forms a large part of the primary objectives of this research from a mechanics point of view. Emphasis has been placed on the micro-mechanics behind composite materials as it is the primary driver for the FEA software to perform macro-mechanics operations of the material when assembling the simulation model.

Due to the nature of this composite material being researched and developed, electronic PCB theory has been covered, as the two materials share many similarities and new methods could be formed through adaptations of existing theories used on conventional PCB materials. The manufacturing process of composite material has been covered, as a novel manufacturing technique has to be created for the new MFC material as budget and equipment limitations play a decisive role in the final manufacture plan.

The chapter concludes with a review of well known and industry implemented spacecraft design theory based on the systems engineering practices. Many forms of literature have been created to cover the systems engineering practices applied to spacecraft development. The final section focuses on the most relevant areas of systems engineering applicable to this research, such as the design process, verification and validation through numerical and empirical testing.

Chapter 3

Research Methodology

3.1 Multifunctional Composite Design

The subsections that follow covers the selection of the materials, the calculations and the design process that is involved with multifunction composite structures. Reference to the theory chapter is made extensively and the application of the presented theory is addressed in this chapter. A very important point to raise is that the design process is extremely difficult to capture in a report. The creative process and idea creation to address the requirements is unique to every designer. Throughout this section, the designs and ideas are discussed and the logic behind each concept is broken down. The intention of every concept design is to address the requirements of the structure in the most efficient and complete way. The requirements referred to are the CubeSat standards and the mechanical requirements for general spacecraft as covered in the theory chapter.

3.1.1 Material Selection Considerations

The material selection for the use in satellites have many factors to consider. The requirements from the CubeSat standards state that the interface to the P-POD must be aluminium in order to conform to the set standards, thus aluminium will be used in the design for certain sections. The multifunctional composite design will be done with a 2/2 twill weave carbon fibre. Carbon fibre has been selected due to its specific strength versus fibreglass as well as some of its inherent properties. The theory section covered the EMI shielding capabilities of carbon fibre, due to its electrical conductivity. In the standard "off the shelf" aluminium frame design, the standards FR4 PCB panels are used as the side panels of the CubeSats, by using the carbon fibre where the FR4 material would be, would only increase the EMI shielding efficiency. The rigidity offered by carbon fibre is also greater than that of the FR4 material, due to it's higher specific strength. Another advantage is that the carbon fibre design will be lighter than that of the FR4 PCB material. A disadvantage is the cost of the carbon fibre, however, the cost is marginally more expensive than standard PCB material when

considering the potential material advantages that carbon fibre brings.

The 2/2 twill weave carbon fibre was chosen primarily due to the availability of the material at the university, however, the woven composite is preferred to the unidirectional carbon fibre due to its distribution of the fibres in two directions. The exact load direction that the CubeSat will experience is not completely defined, thus by selecting a woven carbon fabric, it provides a material coverage in more directions and increases the out-of-principle plane strength properties. The in-plane strength of the material will be lower than that of the unidirectional composites, however, transverse properties will increase providing better universality of the components. As a reference to illustrate the effect of the rotation of a woven composite lamina, Figure 3.1 is a graph of the woven fabric elastic modulus versus the rotation angle of the fabric (for the case that 50 percent of the tow fibres are in the fill direction and the other 50 in the wrap).

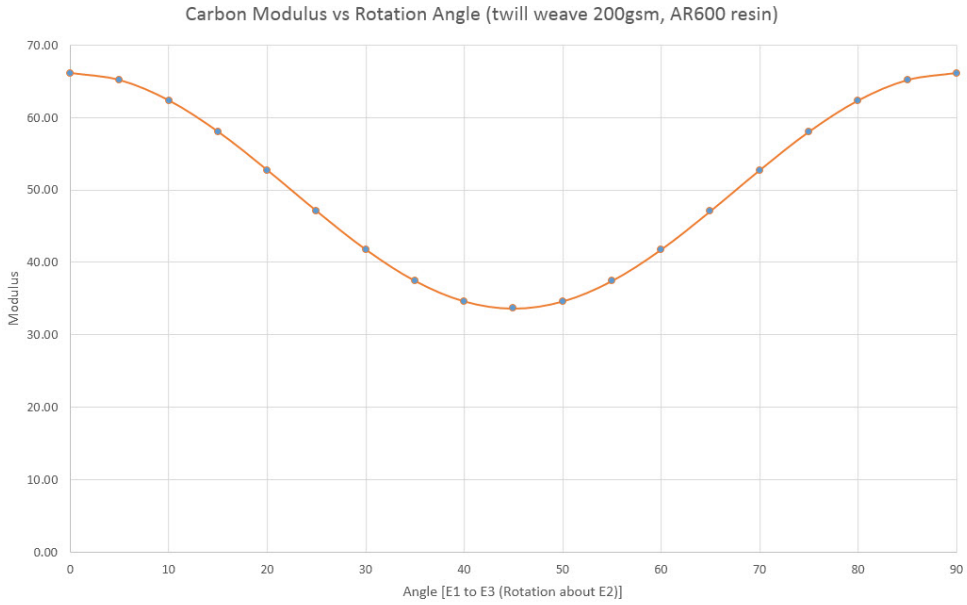

Figure 3.1: Graph of the composite material elastic modulus versus rotation angle.

The final key factor that must be considered is the out-gassing properties of the selected materials. Carbon fibre is used by most spacecraft builders for selected components. NASA has a handbook where the materials that have accepted out-gassing properties are listed. The main out-gassing properties will be dependent heavily on the matrix material selected and the manufacturing process. Ideally for the flight model of the CubeSat a high-grade prepreg carbon fibre, as listed by NASA to have approved out-gassing properties should be used. Due to the cost of the recommended prepreg material, a more cost effective and readily available material must be chosen to produce a "mockup" model as a proof of concept prototype. It will not require any rework to switch the material at a later stage to a higher grade carbon fibre to ensure that the engineering model will pass the out-gas testing. A readily available matrix material to complement the dry woven carbon fibre matting is AR600 epoxy resin. The AR600 resin system will be used with the twill weave carbon to produce the required components.

3.1.2 Material Configuration Concepts

3.1.2.1 Core Material Design

The initial material configuration concept was to use a core material in a sandwich laminate configuration. The idea behind the concept was to include a core material to reduce the weight of the composite panel and at the same time increase the rigidity of the panel by increasing the second polar moment of the geometry with the increased thickness.

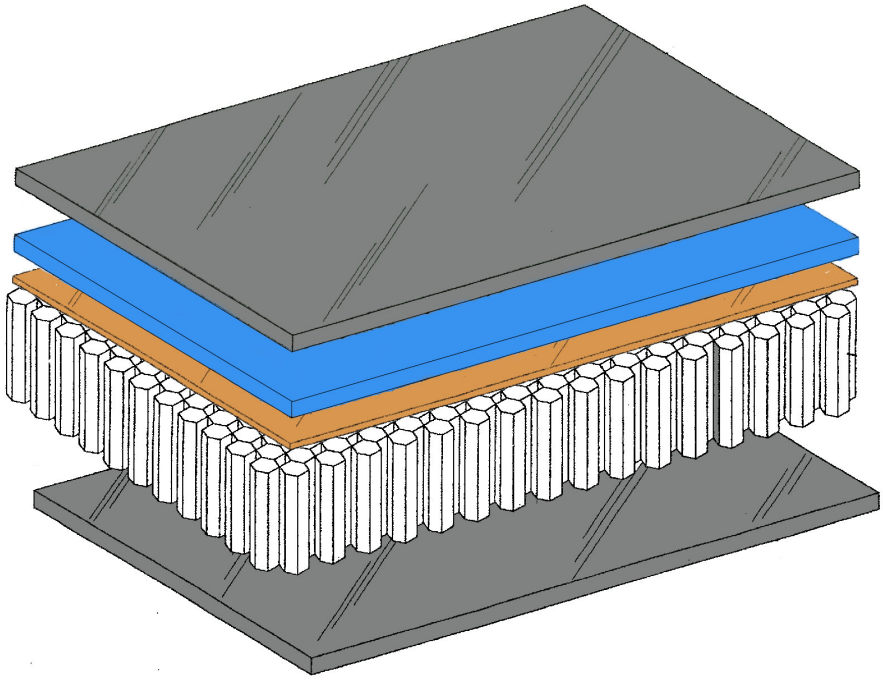

Figure 3.2: Core Material Configuration Concept.

Figure 3.2 is a neatened up representative diagram of the proposed sandwich laminate configuration for the composite material layering. The top and bottom layers are woven carbon fibre fabric, the blue layer is fibreglass, the orange layer is the electrically conductive copper wires or foil and the white layer is the honeycomb core material. The carbon layers are located on the outer surfaces of the panel and are intended to be the main load bearing layers of the construction, particularly in the case of bending, where the higher stresses will be on the surface of the composite panel. The fibreglass layer has only been included as a separation layer between the carbon fibre and the copper layer, due to the electrical conductivity of carbon fibre. The addition of the fibreglass layer adds a further factor of safety by ensuring a separation of the two electrical conductive materials. The fibreglass layer will also assist in terms of the load capabilities of the composite panel. The electrical layer will primarily be either copper wires or a machined (laser cut) copper foil to form conducting tracks. Further information on the electrically conductivity layers and configuration will be discussed further in section 3.1.4.

The core material proposed is a honeycomb foam core material called "Soric". The core material has a very low density and is very thin at only 2 mm thick. The "Soric" core allows resin to flow through its thickness in controlled areas to aid the infusion process, the controlled resin flow areas remain full or resin which cures. The resin in the specific areas of the foam core creates a hexagonal profile which is propagated across the foam layer and forms a honeycomb structure from the resin matrix that cures. "Soric" core material is relatively inexpensive and readily available from local suppliers.

The primary reason that the core material concept was not chosen is the integration of the composite panel in the nano-satellite structure concept design. A secondary concern is also the out-gassing properties of the core material as it is unknown at this stage. Although it is possible to integrate the core material panel, the thickness poses a challenge for the nano-satellite format (1U to 3U) of the structure by taking up a fair amount of the internal space available for internal electronic boards or external deployable panels. For larger satellites (larger than 3U) this type of composite construction may be better suited, as the relative size of the structure versus the material thickness is more in proportion. The added rigidity of the thicker panel will also assist when larger spans of composite panels are required for the structures. Future work can still be done to source thinner core material (at this stage only 2 mm was available). A logical explanation is that for composite panels thinner than 2 mm, the use of only composite material stacking to achieve the thickness becomes more prominent as the panel will require a minimum number of layers to cope with a reasonable size load without experiencing large distortions or flexing of the panels.

3.1.2.2 Copper mid and surface layer laminate design

Following on from the previous chapter, the removal of the core material and replacing it with a fibreglass layer to once again create an insulating protection layer between the carbon fibre and the copper. This composite panel construction method can be used in the case where the conductions tracks would run through the laminate. In both cases, the copper layer in-bedded between the composite layers increases the chances of delamination during the load application to the composite material. Thus, the final construction would be carbon fibre surface layers and fibreglass a layer below each carbon layer which sandwich the copper conductive layer in the middle of the laminate.

Finally, the chosen material layup concept for the structural development is illustrated in Figure 3.3.

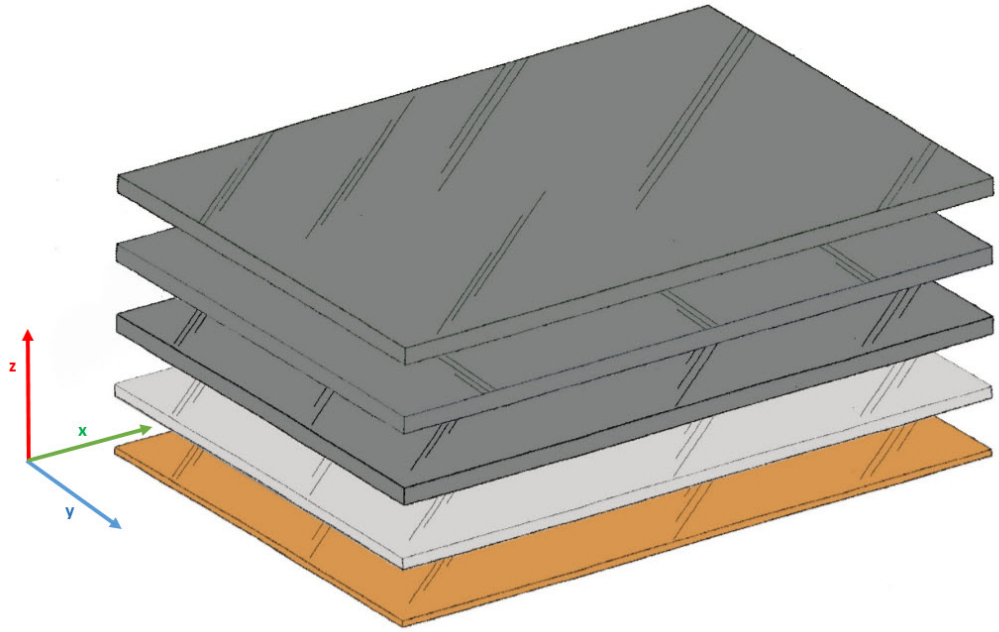

Figure 3.3: Surface-conduction layer composite panel, with 3 carbon fibre fabric layers.

The carbon fibre layers are orientated relative to the x-axis as follows:

- Top layer is at 0 degrees
- Second carbon layer is at 45 degrees
- Third carbon layer is at 0 degrees

The x or y-axis of the material coordinate system will be aligned to one of the structural assemblies coordinate axis systems, thus the 0 degree material layers will have maximum strength in the vertical and horizontal directions of the side panels of the CubeSat for example (the y and z-axis respectively, in the CubeSat diagram in Appendix A.3).
The 45-degree carbon layer is included to provide a better out-of-principle plane strength to the composite laminate in the case where loads are not applied exactly in the vertical and horizontal axis of the overall CubeSat. Due to the woven nature of the carbon fabric, 50% of the tows will run in the positioned orientation and the other 50% will run along an axis 90 offset to the positioned axis (i.e. 0/90 deg and 45/-45 deg tow fibre directions in each fabric layer for this case). The 45-degree layer orientation provides a more symmetrical distribution of the strength if observed from a rotational point of view about the z-axis in the layup diagram (Figure 3.3).

The white layer in Figure 3.3 represents the epoxy adhesive layer used to bond the copper foil layer to the surface of the structural carbon composite layers. The epoxy layer is *Araldite AV4076*, which is an industrial grade adhesive used for high-performance composite bonding. The key material data is provided in Appendix C.3 and shows that the material has a high elasticity which will provide a better flexibility conformance and resist delamination when the panel is subjected to bending loads. Further

material data can be read from the products comprehensive data sheet available on the manufacturers' website. The material data is summarised in the FEA section later in this chapter.

The final orange layer represented in Figure 3.3 is the copper foil layer which will have the required tracks or circuitry machined or laser cut in the same fashion as a conventional PCB would be machined.

Specifics about the material data is discussed in the composite material property prediction section that follows and the isotropic materials are covered in the FEA section, as the isotropic materials' data can be read directly off manufacturer specification sheets.

As a final note of the concept design for the material layup, the surface conductive layer design lends itself to a simple parametrization of the carbon fabric layers. The 3 layer carbon layup design as discussed in the previous paragraphs can have one of the layers removed if found that it is not required. Structural analysis will be done based on a payload assumption as it has not been fully determined for the specific mission that this concept structure may be implemented on. Thus, one of the carbon layers can be removed if required to reduce weight and increase the space available for possible deployables, should the two remaining layers of carbon fibre provide adequate rigidity and load capabilities. Figure 3.4 illustrates the parametric change that potentially can be applied to the composite panel based on the loads of the complete mission design structure. As an additional note, the reduction of the laminate to two layers would now make in non-symmetrical, this would influence the stiffness and the overall loading characteristic of the laminate. There would now be less fibre strength in the 0/90 deg plane. If the compromise in strength is still within an acceptable limit, one has to bear in mind that this change would also reduce the manufacturing cost of each panel.

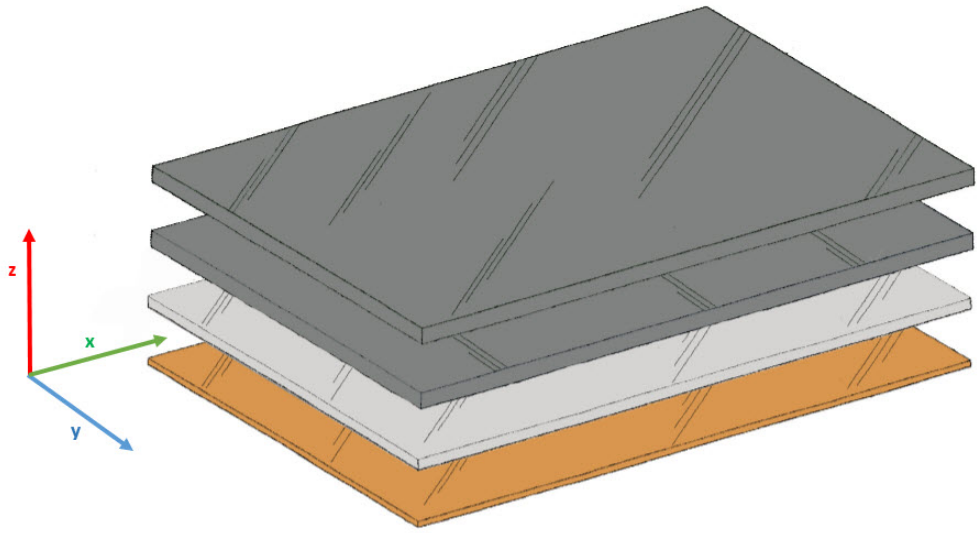

Figure 3.4: Surface-conduction layer composite panel, with a reduced 2 carbon fibre fabric layer construction.

The 45-degree layer will still be maintained and in the 2 layer case will become the top layer of the composite laminate, along with the second 0-degree fabric layer followed by the copper foil bonded to the carbon layers with the epoxy adhesive.
Both the 3 layer carbon and the 2 layer carbon panels will be considered in the FEA of the overall structure covered in section 3.3.

3.1.3 Composite Material Property predictions

In this section, the methodology used to produce the theoretically predicted properties of each lamina used in the makeup of the overall composite panel is explained. An adapted theory as presented in an article by (Adumitroaie and Barbero, 2011b), is used to create the mathematical algorithm for predicting the defining material properties. The theory is also covered in Chapter 9 in the book by (Barbero, 2010) in quite some detail, the mathematical modelling and fibre reinforcement prediction methods are highlighted and only the relevant areas of the theory are discussed in detail. After reviewing a range of literature (as covered in the literature review section), the adapted process was mainly drawn upon from these two sources.

3.1.3.1 Micromechanics

It is important that before any mathematical predictions can be done the material data needs to be known. The data should ideally be sourced from the manufacturer specifications for the specific fabric construction and material make up that is currently being used. Further information not available from the manufacturer should then be sourced from various other literature, such as articles, papers or books which can provide a good level of accuracy in terms of representative material data.

Carbon Fibre Tow:	[from: AS4C_400.pdf and Carbon fibre Twill weave.pdf and BOOK]			
Property	***Symbol***	***Units***	***Value***	***Data Source***
Young's Modulus	E_f	Pa	2.31E+11	AS4C_400.pdf
Shear Modulus	G_f	Pa	Calculated in Algorithm using Isotropic formula	
Density	Rho_f	g/cm^3	1.78	AS4C_400.pdf
Poisson's Ratio	nu_f	-	0.2	Intro to Composite Material Design - Ever.J Barbero [pg 62]
Coefficient of Thermal Expansion	Te_f	ppm/ºC	-0.63	AS4data.pdf
Thermal Conductivity	Tc_f	W/m/C	6.83	AS4data.pdf
Electrical Resistivity	Er_f	ohm.cm	1.70E-03	AS4data.pdf
weight/length	w	g/m	0.2	AS4C_400.pdf
Tow Cross Section Area	CSA	mm^2	0.11	AS4C_400.pdf
UTS [Fibre]	UTS_f	Pa	4.66E+09	AS4C_400.pdf
Tensile Strain	Str_f	%	1.8	AS4C_400.pdf
Composite Lamina Thickness (dry)	tc	mm	0.2	AS4C_400.pdf
Composite Lamina Thickness	n_theta		0.5	Composite ROM presentation
Fibre Undulation Angle (fill)	theta_f	deg	4.4	Measured (SW sketch)
Fibre Undulation Angle (wrap)	theta_w	deg	4.4	Measured (SW sketch)
Infused composite thickness	z	mm	3.00E-01	Measured
Separation between tows (wrap)	g_w	mm	0.1	Measured
Separation between tows (fill)	g_f	mm	0.1	Measured
Tow width (wrap)	a_w	mm	2	Measured
Tow width (wrap)	a_f	mm	2	Measured

Table 3.1: Carbon Fibre DATA collected from various data sources.

Resin Matrix [AR600]:	[from: AR600 AH2338.pdf and BOOK]			
Property	***Symbol***	***Units***	***Value***	***Data Source***
Young's Modulus	E_m	Pa	2.76E+09	Data sheet
Shear Modulus	G_m	Pa	Calculated in Algorithm using Isotropic formula	
Density	Rho_m	g/cm^3	1.088	Measured
Poisson's Ratio	nu_m	-	0.38	Intro to Composite Material Design - Ever.J Barbero [pg 68]
Coefficient of Thermal Expansion	Te_m	µ/m °C	5.60E+01	Data sheet
Thermal Conductivity	Tc_m	W/m/C	3.50E-01	Engineeringtoolbox.com
UTS	UTS_m	Pa	6.90E+07	Data sheet
Tensile Strain	Str_m	%	6.8	Data sheet

Table 3.2: AR600 Resin DATA collected from various data sources.

Figure 3.1 lists the primary data obtained from the manufacturers' data sheets for the carbon fibre twill weave fabric and the tow data. The tows used for the fill and wrap in the fabric are exactly the same and is the AS4C 3K tow from "Hexcel". The physical fibre parameters in terms of the tow width, the gap between the tows and the undulation angle have been physically measured and remodelled as a sketch in SolidWorks (Figure 3.5) to find the fibre undulation angles. All measurements were done after manufacture of the composite material in order to achieve the most accurate dimensions relative to the manufacturing process used. More accurate measurement solutions are available, such as 3D CT (computerised tomography) scan of the material, however, this technology was not accessible by our department at this time.

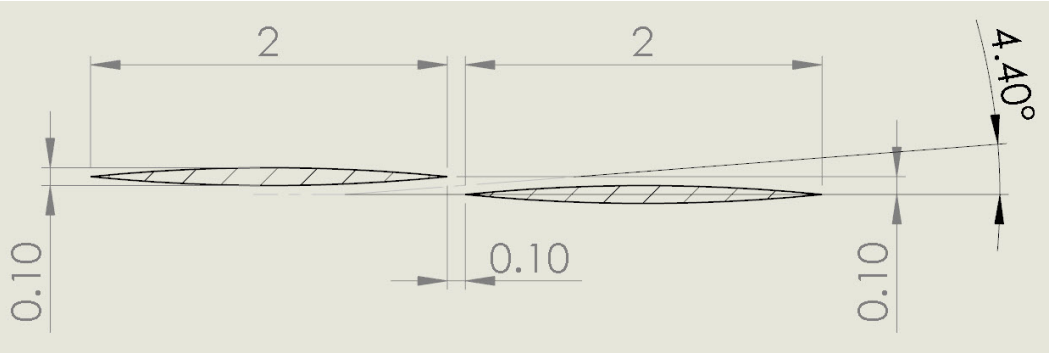

Figure 3.5: SolidWorks evaluation sketch of a section view of the fibre tows.

The shear modulus for both the fibre and resin has been calculated using the isotropic relationship (3.1), as this is specific to each individual homogeneous material.

$$G = \frac{E}{2(1+\nu)} \tag{3.1}$$

The formulation and algorithms for the theoretical calculations that follows were programmed into MATLAB to produce the final material data set of the lamina. A further discussion of the MATLAB program is covered in a subsection later.

It is important to stress at this point that the objective of the micromechanics modelling is to produce the lamina properties (E_{11},E_{22},G_{12},G_{23},υ_{12}), which is required as an input for the ABAQUS FEA composite material model.

The mechanics of materials approach uses RVE (Representative Volume Equivalent) elements and produces an equivalent homogeneous anisotropic material, which is the result of the combination of two isotropic materials.

Building from the basis of the known material data, the first important property that must be established is the overall volume fibre fraction of the woven fabric lamina. For this calculation, equation (2.6) is used as presented in the previous literature section. The specific geometry of the fabric and the properties of the tow will directly influence the volume fibre fraction.

The next stage is to calculate the fibre tow properties using the micromechanics models. The fibre tows are only considered for this level of modelling as the woven geometrical aspect of the fabric composition will be accounted for later in the overall ply combination. The properties are taken from the tow level of the fill and wrap and assembled into the overall fabric construction to derive the lamina properties.

First off the in-plane Young's modulus (E_{11}) can be found using equation (2.11), based on the rule of mixtures. Thereafter, the transverse Young's modulus (E_{22}) using equation (Halpin-Tsai-eq). The refined semi-empirical adjusted formula of Halpin-Tsai produces a more accurate solution than the IROM equation. Since the equations will be implemented into a computerised program, the extra computational time needed is marginal. However, if this calculation was going to be performed by hand over a number of iteration, the Halpin-Tsai formulation would then pose to be more tedious when compared to the IROM formula.

To find the in-plane Poisson's Ratio (υ_{12}), formula (2.18) can be used. An approximation of the Poisson's Ratio is generally sufficient enough for design purposes (Barbero, 2010). The Poisson's Ratio of the fibre and matrix materials are not vastly different, thus the deviation would be very little from what the actual composite composition would be.

Using equation (2.23), the in-plane Shear modulus (G_{12}) can be found. Once again the IROM provides a formulation that produces a "rough" value of the shear modulus, however, the simplified version of the PMM (Periodic Microstructure Model) formulation produces a more accurate solution. As shown by (Barbero, 2010), the PMM formulation provides a good agreement between the theoretical predictions and the experimental data.

The next process is to find the overall lamina properties, which will be done using an adapted application of the Classical Laminate Theory (CLT). The application of the adapted theory used is covered in the section that follows.

3.1.3.2 Adapted Classical Laminate Theory approach

The classical laminate theory of fabric reinforced composites as presented by (Adumitroaie and Barbero, 2011b) and (Barbero, 2010), which is outlined in the literature review under the composite materials section.

A summarised overview of the material prediction algorithm developed and used begins with the calculation of the tow properties using micromechanics formulas as reviewed in the previous section.
Thereafter, the application of the CLT requires that the tow compliance matrix needs to be found using equation (2.28). The rotation matrix for the fill and wrap tows need to be found using equation (2.29) and (2.30). The fill rotation matrix only considers the undulation angle rotation about the wrap tow, however, the wrap rotation matrix accounts for the 90-degree rotation relative to the fill tow, as well as the undulation angle rotation about the fill tows.

Using the method outlined by equation (2.31), the relative transformation matrices (T_f and T_w) can be found using equation (2.32) and (2.33), for the fill and wrap tows respectively.
The transformed compliance matrix for the fill and wrap tows are found using equation (2.34). Reducing the transformed compliance matrix to the elements related to (i=1,2,6) in the matrix and then finding its inverse produces the reduced stiffness matrix for the fill and wrap tows as shown by equation (2.35) and (2.36).

Using equation (2.37) to assemble the two reduced stiffness matrices into the extensional stiffness matrix [A]. The inverse of matrix [A] produces the laminate compliance matrix "alpha". The values from the laminate compliance matrix can be used to determine the woven fabric lamina properties as listed by equations (2.38) through to (2.41).

The properties required for the input as the composite lamina material data in the ABAQUS FEA is now known. The orientation and stacking of the laminate layers can be defined in ABAQUS to solve the macromechanic characteristics.

3.1.3.3 MATLAB implementation

The numerical formulas to predict the lamina properties were implemented in MATLAB to solve for the solution. The data for the initial variables are read in from the EXCEL spreadsheet and assigned to the corresponding variable name in MATLAB. Figure (3.1) and (3.2) show the data within the spreadsheet.

The data is entered into the spreadsheet with a specific unit of measurement, as listed in the spreadsheet, which is the required units for the formulations that follow. The data for each variable is linked to a specific block in the spreadsheet, where only the numerical value is extracted into MATLAB.

The micro-mechanics formulas as discussed in a previous section are entered in the logical order and makes reference to the variable values required to solve and determine the new set of variables. The tow properties found by the micromechanics models are kept and not overwritten in the MATLAB program and thus allows any of the variables to be recalled at any time.
The CLT formulas then follow the tow properties which require a few larger 6x6 matrices to be calculated in the program.
For the reduced compliance matrix, the specific values that correspond to the values

of i=1,2,6 are extracted by manually calling the relevant values from the full 6x6 compliance matrix. This method chosen as the process of calling the values is not iterative or dynamic, thus the value location will remain fixed regardless of the data input.

The individual values of the [A] matrix are individually specified in MATLAB using the assembly formula (2.37). The inverse of [A] is found, along with the lamina values, which is outputted to the screen in MATLAB after running the script so that it can be entered directly into the ABAQUS FEA model.
Appendix B contains a copy of the MATLAB algorithm created and used to find the lamina properties of the twill weave carbon fibre fabric used to construct the satellite components.

3.1.3.4 Composite Material UTS Prediction

A simple method can be used to determine the approximate UTS point of the composite material that has been designed. The UTS point will be predicted for the panel design using 3 layers of carbon fibre fabric reinforcement, as this will be that material that will be virtually simulated in the FEA program and physically manufactured for the material sample testing and the mock-up model.
The UTS calculations will only consider the properties of the carbon fibre tow strengths, this is due to the fact that the ultimate tensile strength point is expected to be the point of failure for the composite laminate. Composite materials do not exhibit plasticity characteristics after the UTS has been reached, such as the case for most metals. At or just before the UTS of the material, it is expected that matrix cracking will have occurred already and the majority of loading will be held by the carbon tows momentarily before failure.

Therefore, before any calculations can be done, a summary of the required material data is needed:

1. Carbon Fibre Tow Strength - 4.66 GPa (Provided from Table 3.1)

2. Lamina dry fabric thickness - 0.2 mm (Provided from Table 3.1).

3. The volume fibre fraction of each lamina is 0.5618 (extracted from the MATLAB material calculation program covered in section 3.2).

4. Fill/Wrap tow distribution in the fabric is 50/50 (due to the 2/2 twill weave construction).

Figure 3.1.3.4 illustrates a section view of the expected fabric construction. The blue and green section indicate the 50/50 fibre tow distribution in the fill and wrap directions.The construction of the overall laminate being considered can be seen in figure 3.3. The tensile test sample will have the first and third carbon fibre layers aligned in the direction of the tensile load application (0-degree tensile load application on the sample).

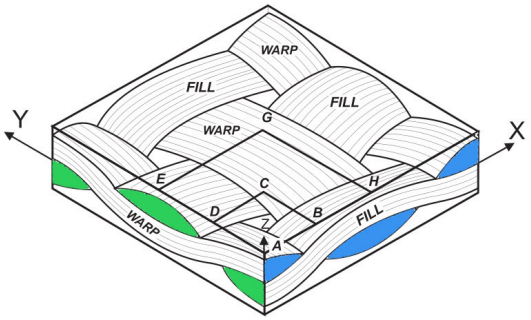

Barbero (2010)

The 45-degree middle layer of the composite material will not be considered, as the lamina's modulus will allow the layer to stretch beyond the point of failure of the first and third fabric layers. The 45-degree layer will then not cope at all with the remaining load requirement on its own and fail almost simultaneously with layers 1 and 3.
The effective fibre tow area that will carry the load needs to be determined between the two load bearing laminae.

Firstly, considering the volume fibre fraction, the effective fibre volume in the overall lamina (cannot consider the matrix material to carry any considerable load):

$$\text{Effective Lamina Fibre Area } = (0.0002 \times 0.025) \times 0.5618 = 2.809 \times 10^{-6} \quad (3.2)$$

The area of the black section shown in figure 3.1.3.4 has now been found with equation 3.2. It must be noted that the tensile test sample width is 25 mm.

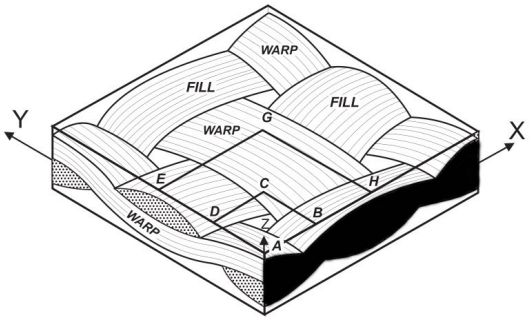

Barbero (2010)

Then taking into account that only 50% of the fibre tows are available to do work against the applied load:

$$\text{Effective Lamina Fibre Tow Area} = (2.809 \times 10^{-6}) \times 0.5 = 1.405 \times 10^{-6} \quad (3.3)$$

The area of the blue area shown if figure 3.1.3.4 is now known as the area of the fibre tow that will be loaded when the tensile load is applied.

Considering that there are two laminae's that will carry the applied tensile test load, the total effective fibre tow area is:

$$\text{Total Loaded Tow Area (in Laminate)} = (1.405 \times 10^{-6}) \times 2 = 2.809 \times 10^{-6} \quad (3.4)$$

The fibre loaded area (A_t) is known, as well as the maximum tensile stress of the fibre tow (σ_t), therefore the maximum applied force can be found:

$$\text{UTS Force} = \sigma_t \times A_t = (4.66 \times 10^{-6}) \times (2.809 \times 10^{-6}) = 13.09KN \quad (3.5)$$

Considering the fibre undulations of each tow in the fabric (shown in Figure 3.1.3.4), it is expected that the actual strength will be approximately in the region of 80 to 90% of the ideal strength of each lamina. This factor is considering the loading of the fibres in a slightly offset angle as the fibres are not laid perfectly straight, this factor must not be mistaken for an "imperfect" lamina construction which compensates for the presence of voids or defects. It would be expected that during the actual material testing that a deviation of the material strength will be seen between each test sample due to defects or voids present in the samples.

Thus, the expected force range for failure is:

$$80\% \text{ of the Force} = 13.09 \times 0.8 = 10.47KN \quad (3.6)$$

$$90\% \text{ of the Force} = 13.09 \times 0.9 = 11.78KN \quad (3.7)$$

The laminates expected force at failure is between 10.47 and 11.87 KN, without considering the effects of defects or voids.

3.1.3.5 Plasticity data prediction for the copper foil

The metallic copper foil component is expected to show signs of plasticity after the yield stress of the material has been reached. A simple, but effective formulation to create the plasticity profile of the copper's stress-strain relationship is the Ramberg-Osgood isotropic hardening equation 3.8. This will provide a good prediction of the plasticity profile for the copper foil layer.

$$G(\varepsilon^p) = \sigma_y + C(\varepsilon^p)^n \quad (3.8)$$

The index's C and n are the typical strength coefficient and strain hardening exponent respectively for annealed copper. These indexes can be found in reference tables in engineering handbooks. The σ_y is the yield stress of the material. The plastic strain

is increased by a set increment and the product of the equation is the corresponding stress for the given strain used in the equation. The material data for the copper foil has been presented in Table 2.8 and these parameters were used. A C++ program was written to produce the copper material plasticity data, which would be entered into ABAQUS. Figure 3.6 illustrates the predicted stress-strain graph produced for the material. Figure 3.7, 3.8 and 3.9 shows the C++ program that was written, the data input used for the program and the ABAQUS data input for plasticity.

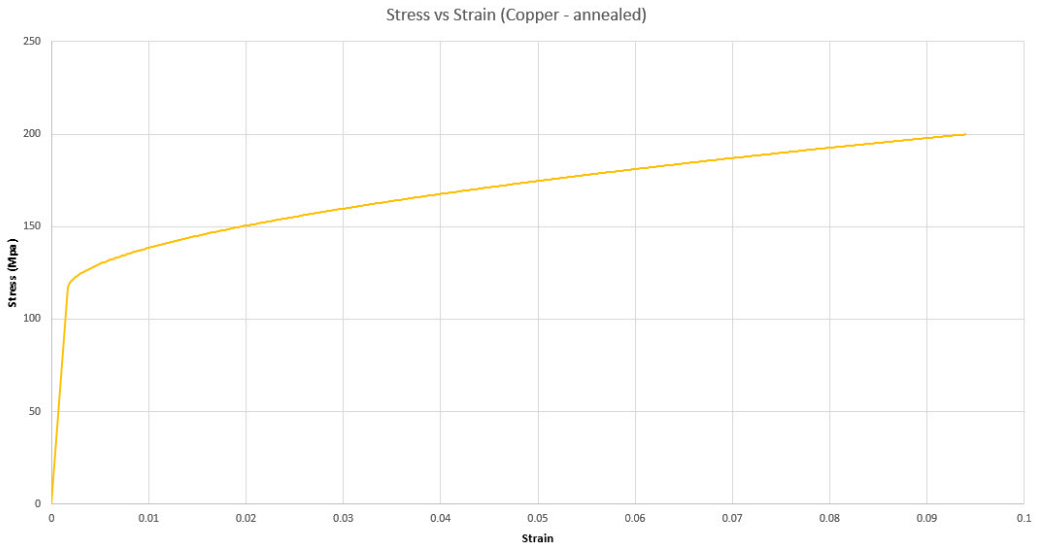

Figure 3.6: Predicted stress-strain graph for annealed copper.

Material Properties (Copper, annealed):			
Modulus of Elasticity (GPa):	118	n:	0.54
UTS (MPa):	200	C (MPa):	315
Yeild Strength (MPa)	117		

Figure 3.7: C++ material data input parameters.

```
#include <iostream>
#include <math.h>
#include <fstream>
using namespace std;

double G(double x)
{
    double C,n,Sigma_y;
    C=315e6;
    n=0.56;
    Sigma_y=117e6;
    return (Sigma_y+C*(pow(x,n)))/1e6;
}

int main()
{
    double strain;
    ofstream out_file;
    out_file.open ("Stress_vs_Strain.csv");
    out_file<<"Strain:"<<","<<"Stress:"<<"\n";
    strain=0;
    for (strain=0;G(strain)<=200;strain=strain+0.0002)
        {
            cout <<G(strain)<< endl;
            out_file<<strain<<","<<G(strain)<<endl;
        }
    cout<<"File written"<<endl;
    return 0;
}
```

Figure 3.8: C++ Program written to compute the material data.

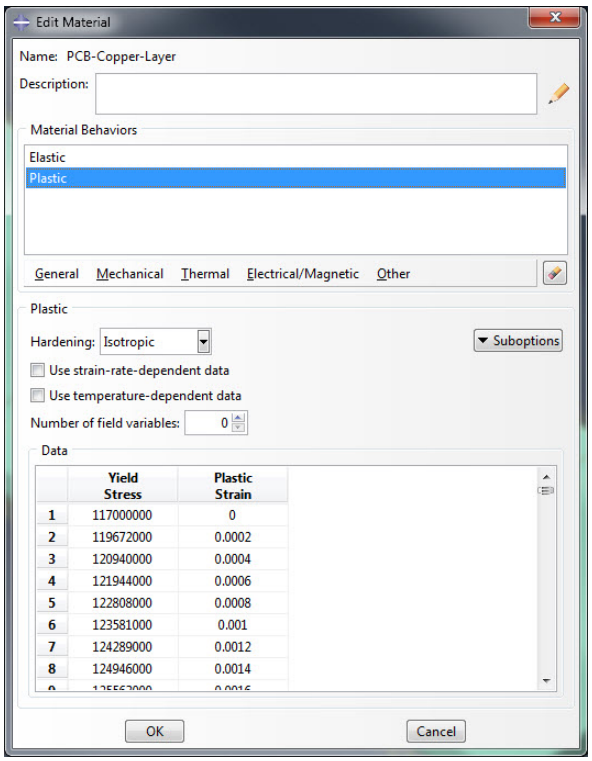

Figure 3.9: Plasticity data input for copper material in ABAQUS.

3.1.4 Electrical Integration

The electrical circuit integration into the composite material had a number of iterative processes to check a few key concerns before conducting in-depth investigations into a specific type of integration. The first key concern is the availability of copper conductors that can be in-bedded into the carbon fibre material. The second key issue was the manufacturability of the concept ideas of the integration plan. By prototyping and testing, the feasibility of the concept in these areas of concern would provide a good initial process of illumination. The idea is to reduce unnecessary effort spent developing an idea that later down the line fails due to previous concerns raised early on in the project.

Firstly, a discussion about the concept ideas for the electrically conductive copper track integration. Considering the materials available at the university labs, the following concepts were drawn up to be tested:

1. Placing enamel coated copper wires between the composite material layers.

2. Placing a pre-cut copper foil circuit (similar to the concept used for the copper foil layer in flexible printed circuits).

3. To manufacture a composite panel with a copper foil layer on a single outer surface of the composite.

The concepts listed above were considered to be the most feasible when taking into account the equipment and facilities available. No university funding was allocated for the purchasing of new equipment for the lab, thus in order to produce a prototype structure, the manufacturing requirements had to be within the laboratory manufacturing capabilities available. Another key driver is to maintain simplicity as far as possible, this will make the manufacture easier and less require less complex equipment. Maintaining simplicity in the design also increases the repeatability of the design should it become a commercial product in production later on.

The next subsections run through each concept, highlighting the key advantages and disadvantages in each case. The subsections are followed by a concluding paragraph on the concept that was chosen.

3.1.4.1 Concept 1

Concept 1, which is the enamel coated copper wires in-bedded between composite layers, the requirement for the enamel coating is to provide an electrical isolation. Carbon fibre material is electrically conductive which would interact with the bare copper wires and create electrical shorting conditions. It is therefore imperative that the enamel coating does not get damaged during the manufacturing process. The key driver for the use of enamel coated wire is due to its availability in many sizes at the electrical engineering department and ease of access.
One of the major concerns with the enamel coated wire is the manufacturability using the wire. The placement and alignment of the wires through a panel was very difficult

to do and maintain during manufacture. Materials tend to shift and move slightly during the composite manufacture process which therefore required a jig or holder to maintain the positions of the wires between the materials. An idea was to use a machinable core material that could have thin grooves machined into it to allow the copper wires to sit in, however due to the overall laminate thickness limitations, a core material couldn't be used which eliminated the idea. Apart from the core material being removed, it is not ideal to add a further manufacturing requirement to the core material as it becomes an additional process. Ideally, the material should have the least amount of machining requirement to reduce time and cost of production.

3.1.4.2 Concept 2

Concept 2, was to use a copper foil layer placed between the composite layers. Once again the first issue is to insulate the bare copper from contacting the carbon fibres. The conductivity issue could be solved by using thin plastic cover films on either side of the copper foil layer. One of the issues that now arises is that the plastic film/copper layer configuration added between the layer of composite creates a disruption in the bonding of the layers of the composite, the proposal would increase the likelihood of the composite layup de-laminating and weakening the structural integrity of the composite panel. The advantage is that the copper layer failure due to bending can be minimised as the copper foil can be positioned very close to the neutral axis during bending of the panel. A limitation of the design is the fact that components cannot be added to the copper circuitry to perform simple electrical operations. Components would create distortion of the fibre layers that cover the component side of the copper foil and reduce the fibre stacking efficiency and in turn the volume fibre fraction of the composite.

3.1.4.3 Concept 3

Concept 3, was a modification of the idea from concept 2, however considering a conventional PCB design. Firstly to simplify the manufacturability of the panel, the composite material would be created using conventional composite manufacturing techniques and then a full copper layer foil backing would be added to the one side of the composite panel with an epoxy adhesive. This would also reduce the delamination issues created by bonding copper foils between composite layers. The copper foil, in this case, is, in fact, a very thin PCB (0.2 mm) and the copper foil has an FR4 material backing. The FR4 composite material backing will aid the adhesion of the copper foil layer to the carbon composite material layer. Later in the FEA section, the FR4 material is taken into account. A further advantage is that the circuitry can be machined after the panel has been produced in the required electrical track configuration. In the case of concept 2, the track layout would have to be machined first then added between the composite layers. The copper foil on the other surface adds the added flexibility for later design modifications to the electrical tracks before having to machine them out. The epoxy layer would be vacuum bonded onto the composite material and the adhesive bond line thickness would be controlled with a bond line control mesh. The

disadvantage of the design is that the copper layer is now exposed to a larger tensile or compressive stress when the panel is exposed to bending loads. It would be expected after considering the theory presented in Section 2.4.2.4, that lower fatigue stress bending would cause a copper foil failure before a composite structural failure due to the surface stress the copper would be exposed to. The addition of composite layers would assist by increasing the rigidity and reducing the amount of bending the panel experiences. The manufacturing process of this concept is far easier as it does not require any specific positioning jigs for wires or copper foil layers relative to the material, apart from the overall alignment during the stacking and bonding process to the pre-made composite panel.

3.1.5 Thermal Characteristics

The thermal properties of the overall composite panel will rely mainly on the properties of the carbon composite section due to the relative volume of the carbon fibre material to the epoxy bond layer and the copper foil layer.

The calculations for the carbon composite layers thermal properties were done following the theoretical calculation process covered in section 2.4.3.2. The formulas were included in a MATLAB program in the exact same fashion as was done in section 3.1.3.3 for the composite structural properties. For the sake of saving time, this process is not repeated here again and the required sections referred to above, cover all the necessary information.

Once the carbon composite material thermal properties are known, a model can be created, as thermal conduction between the carbon layers, the epoxy and copper layers will take place.

3.1.6 Final material concept summary

The final material configuration was chosen based on the structural design requirements (discussed further in section 3.2.1), the material selection parameters and the electrical integration concepts. The use of carbon composite material has been chosen and using a 2/2 twill weave reinforcement due to its availability, strength and inherent properties offered by the material. As a consideration of the potential EMI protection and the requirement of the strength of the panel in various load orientations, at least two carbon fibre material layers will be used. The two layers will provide a better coverage of the load orientations if the layers rotational orientations are offset relative to one another and at the same time reduce the chance of a gap in the carbon layers to create a more uniform carbon lattice coverage. Three carbon layers will also be modelled as there is no design or configuration change apart from the panel thickness change. The model can be parameterised into a selection of two or three carbon fibre layers and the relative orientation of each ply. A core material was not used as the thinnest core material available would still create a laminate which overall thickness is too large to effectively implement in the structural design. The electrical

integration will use the third concept as presented in the electrical integration section (3.1.4), due to the number of relative advantages it has when compared to the first two concepts.

3.1.6.1 Material Manufacture Plan

The manufacturing plan has been kept as simple as possible to reduced cost, production time and production equipment required. The carbon composite laminate structure will be manufactured using a flat glass table top and the vacuum infusion process. Flat composite panels will be used to create the overall structure (this is discussed further in the CubeSat structure design section that follows). Once the carbon fibre structural laminate has been produced, the copper foil layer is then bonded to the rough surface (the surface not in contact with the glass table top), which is created by the "peelply" layer in the infusion process.

A modified infusion process will be used to vacuum bond the copper foil layer to the carbon fibre laminate. The table is pre-prepared with wax and PVA release agent. The carbon laminate is then placed on the external surface of the satellite structure (shiny smooth side) down on the table. The AV4076 Epoxy adhesive is then prepared in the required quantity to cover the surface of the composite laminate for a final bond line of 0.2 mm (note, extra epoxy needs to be mixed to allow for loss and to squeeze some adhesive out the sides of the laminate). No exact quantities are given here as this is done with experience and in accordance with the laminate size that is being bonded at the time. In the case of a new user attempting to produce these panels, the guidelines given above will be more than adequate to work from.
Once the epoxy has been applied the copper foil layer is then placed on top of the epoxy layer, with the assistance of a soft cloth to apply pressure across the surface of the copper foil ensuring no wrinkles or inconsistencies in the copper layer is present. After the copper foil has been smoothed down to a reasonable level by hand, the vacuum pressure plate is placed on top of the copper foil. The vacuum pressure plate is essentially a large flat rigid plate (can be aluminium or a thick wood sheet). The plate needs to be sufficiently thick to allow for little deflection when the vacuum is applied to its surface. The pressure plate needs to also be waxed to ensure it's released from the composite laminate during de-moulding. Spiral flow vacuum tubes and a plastic vacuum bag is then placed over the top of the complete bonded assembly with a perimeter of sealant tape in the exact same way it would be done in the general composite infusion process. The adhesive is then left to cure at room temperature for the specified curing time in the specification sheet while under a vacuum of approximately 80 %.

3.2 CubeSat Structural Design

3.2.1 Structure Design Considerations

The CubeSat structure that is designed must meet the requirements of the CubeSat standards and the requirements developed from the mission needs and objectives. Once again it must be noted that the design process is very difficult to fully document as there is no fixed why of designing concepts and coming up with ideas or innovations. However, a rule of thumb that is generally good practice is that the design must be kept as simple as possible while satisfying the requirements in the best and most efficient way.
Section 2.2.2.1 and 2.2.2.2 covers the CubeSat standards in quite some detail and will be adhered to in the design process. In addition to the CubeSat standard requirements is the mechanical requirements and considerations for spacecraft in general, which is covered in the spacecraft design (section 2.5).
The interfacing to the launch vehicle is covered by the CubeSat standards by designated design requirements such as the material type of the interface to the P-POD and the dimensions of the exterior surfaces.
The material choice for the composite sections has been discussed in the previous section. The composite sections, however, will have to be interfaced to aluminium sections to conform to the CubeSat standards. The CubeSat standards state that if the material is not aluminium, that it would have to undergo a weaver process and would require qualification tests. The qualification tests add further cost and time to the development process and thus the design will conform to the standards as close as possible.
In the design of the structure, the free parameters are how the interfacing of the composite will be done to the aluminium sections. The external design and method of interfacing will have an effect on the payload size and geometry. Spacecraft design theory does make mention that the deflection, vibration, environmental conditions, stress and strain under loading must be considered as well. The rigidity of the panels will have the greatest effect on the deflection when subjected to a load or in response to a load while in a vibration state. Static load testing and modal analysis of the complete structure is required to analyse the predicted performance characteristics of the concept design. More on the FEA of the structure is covered in a later section.

A few design notes that were made before any concept designs were done is that the payloads from suppliers have been standardised. Although there is no specific standard documentation or regulations for the geometry or placement of the internal PCB's for the electronic subsystems, the design will be of greater benefit if it can also accommodate the commercially available subsystem payloads. Thus, making the structure a more marketable item to industry should it prove worthy. Therefore, taking a look at the standard CubeSat chassis available from industry suppliers (Section 2.37), it would be wise to design a composite based structure with similar dimensions. Thinking in a systems engineering sense and considering the system life cycle, the structure needs to not only conform to the out-gassing standards but also the conditions in space. Not only that, but the structure must be easily manufacturable. The most

volatile time of the satellites life is the launch phase, where the greatest stresses and loads will be experienced by the CubeSat. In space, the largest contribution of the loads will be from the thermal stresses and thermal cycling as the spacecraft orbits the earth. Taking all of this information into account and designing concepts with a holistic overview, three main concepts were developed and are discussed further in the sections that follow.

3.2.2 Concept Designs

3.2.2.1 Concept 1

The first concept idea was to create a solid composite shell section, the side panels would be formed by a square tube profile essentially and then the top and bottom panels would be attached separately. The aluminium rails would be bonded onto the outer surface of the "rectangular tube" section at each corner, using a high-grade composite epoxy. A support angle section would be bonded onto the side panels and would provide the fastening points for the top and bottom panels. Figure 3.10 shows the complete concept 1 model, the model was created to provide a clearer vision of the idea from the initial rough sketches.

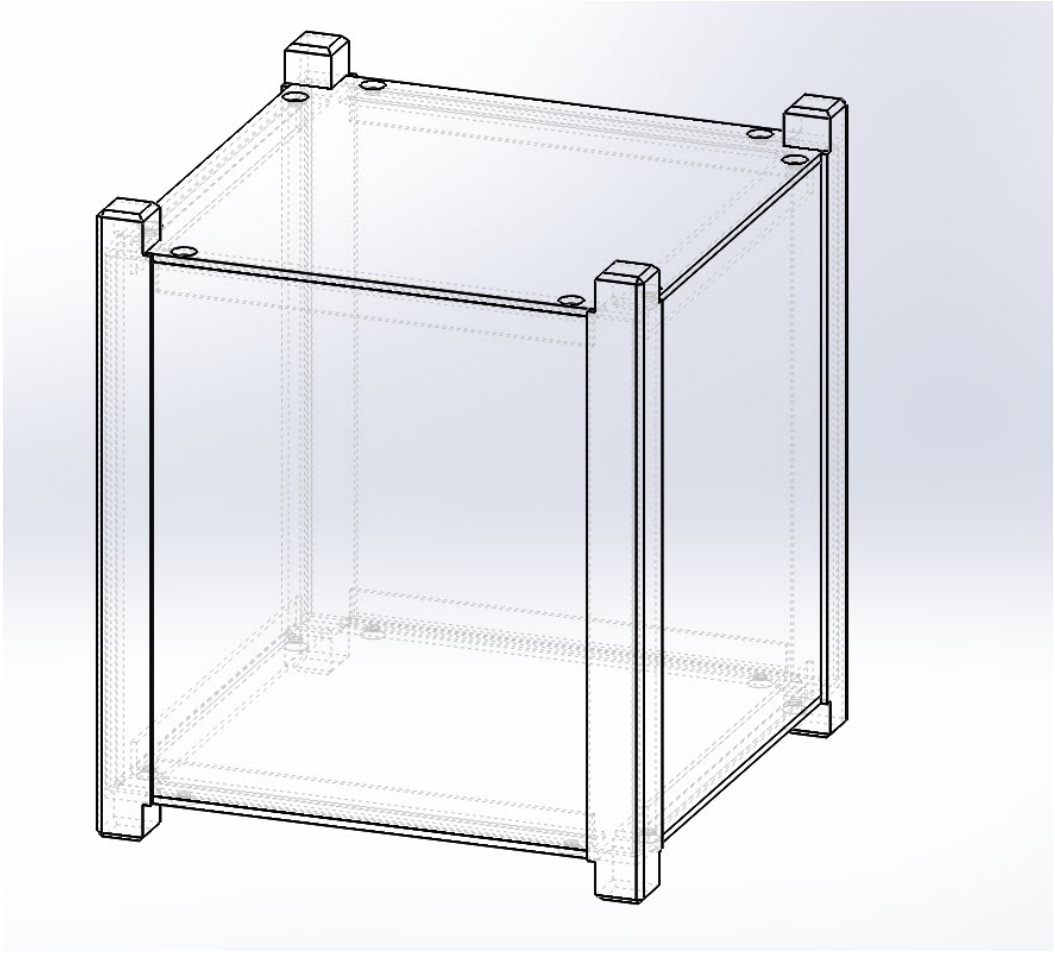

Figure 3.10: Assembled Concept 1.

Figure 3.11 provided an exploded view of the aluminium rail and the corner section of the composite shell it would be bonded to. The flat surfaces of the aluminium rail will meet up with the composite corner section. The rendered image shows the internal copper surface of the multifunctional composite material. A good view of the composite support "angles" bonded to the upper inner surface of the composite shell is provided in figure 3.11.

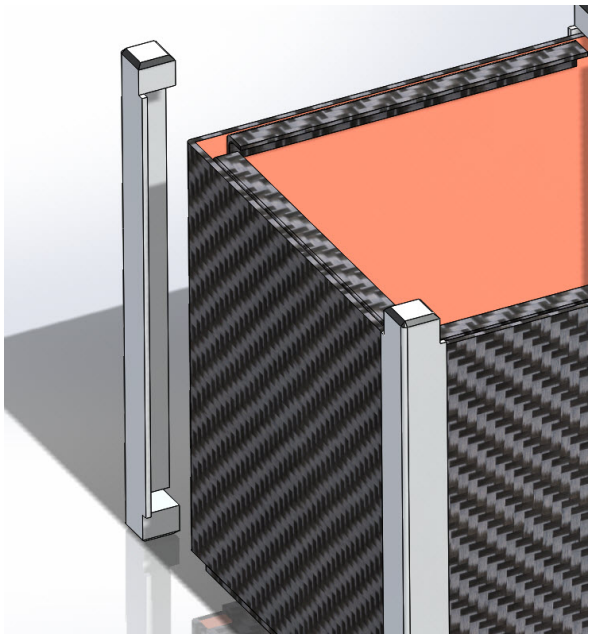

Figure 3.11: Concept 1 aluminium rails.

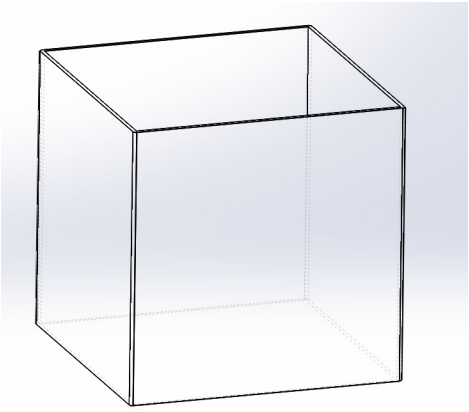

Figure 3.12: Single Composite Shell Section for Concept 1.

Figure 3.12 shows the composite shell section which is made from a solid rectangular tube of carbon composite. The intention is that the rectangular tube would be constructed using a cavity mould created with two halves and have an inflatable tube located on the inner surface to provide the pressure against the surface of the mould. This would create an exterior surface of the CubeSat with a smooth surface. Figure 3.13 shows an exploded view of all the parts used to make up the concept 1 model.

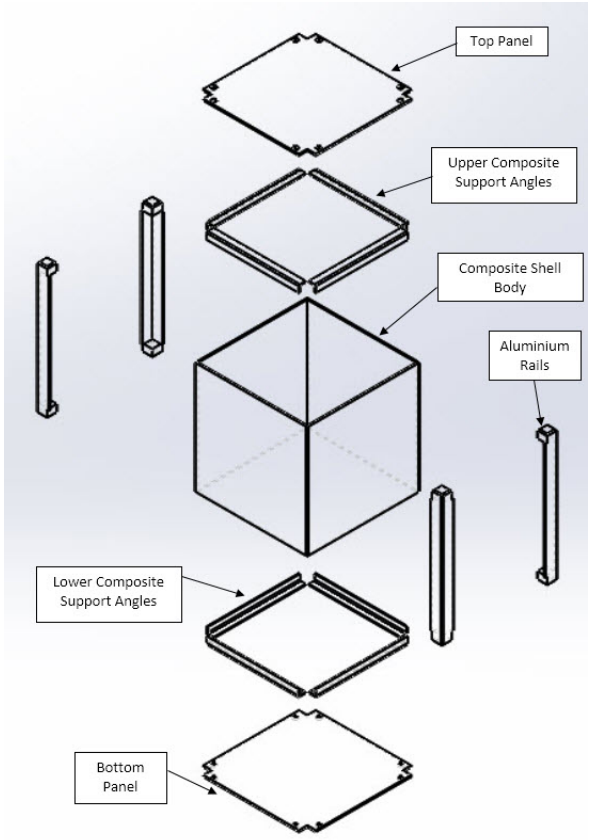

Figure 3.13: Concept 1 exploded view.

All the sections apart from the top and bottom panels (to allow access to the internal subsystems) would be bonded together using high-grade composite epoxy.
The main reason this concept would not work is the fact that achieving an accurate enough rectangular composite shell from the moulding process would be extremely difficult. The Norwegian University that tried this type of approach also reported tolerance issues with the outer dimensions of the composite CubeSat structure (Section 2.2.4). The equipment available at the laboratories also does not lend itself to this level of precision required. This full composite shell body design has a mass of 177 grammes, excluding the solar panels and other subsystems.

3.2.2.2 Concept 2

Concept 2 was to produce flat composite panels that slotted/located into grooves in the aluminium rails. This has been done to try illuminating some tolerance issues that would be experienced in *Concept 1*. The idea is that the aluminium would provide a better guide and alignment of the panels.
The assembled diagram of the concept 2 model is very similar to that of concept 1, with almost no visual difference from the exterior. Figure 3.14 provides a view of a de-slotted side panel and the locating groove in the aluminium rail.

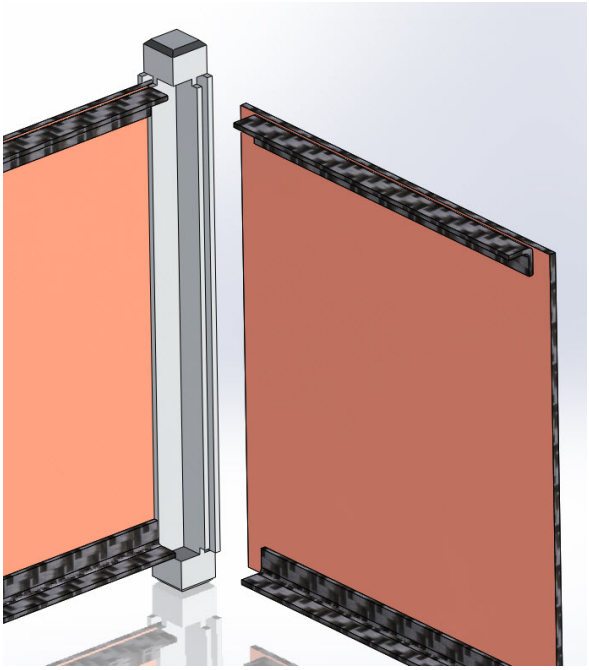

Figure 3.14: Removed side panel for Concept 2.

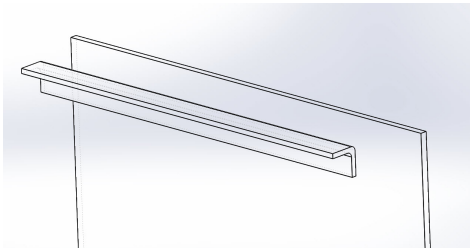

Figure 3.15: Composite Angle Support Section for Concept 2.

Figure 3.15 shows the composite support rail that would be bonded to the side panel. This is the same design as implemented in concept 1. Figure 3.16 provides an exploded view of the concept 2 model.

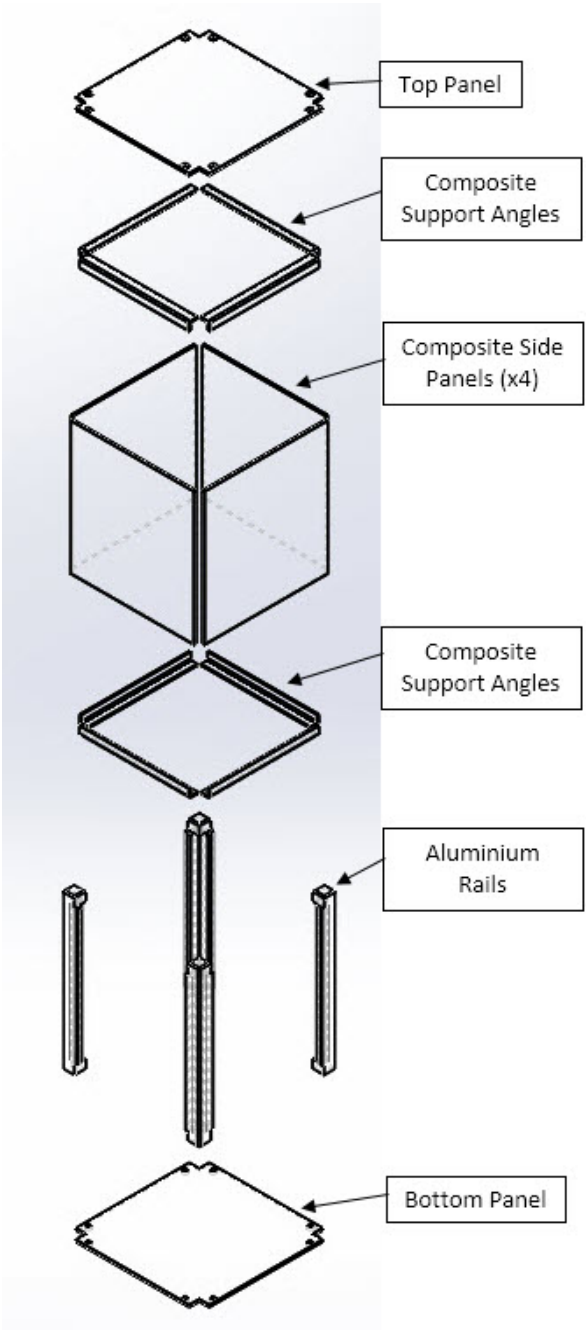

Figure 3.16: Exploded view for Concept 2.

The main reason that concept 2 was not chosen is due to the difficulties of the side panel alignment. Each side panel would have to be accurately positioned and bonded in place. Another key issue with the design of concept 1 and 2, is the accessibility of the internal subsystems by removal of the side panels. The configuration and the aluminium rail design in both cases do not lend itself to using screws due to the relatively thin wall thickness of the aluminium faces. The weight of this structural design is 201.6 grammes, excluding solar panels and other subsystems.

3.2.2.3 Concept 3

Concept 3 was developed for the need of removable side, top and bottom panels to provide all round access to any section of the CubeSat payload/internal bus. An alteration to both concept 1 and 2 was done to form the concept 3 model. The addition of countersink screws allows removable panels to be installed and secondly it provides an "automatic" or "natural" alignment of the side panels via the countersink self-locating geometry.

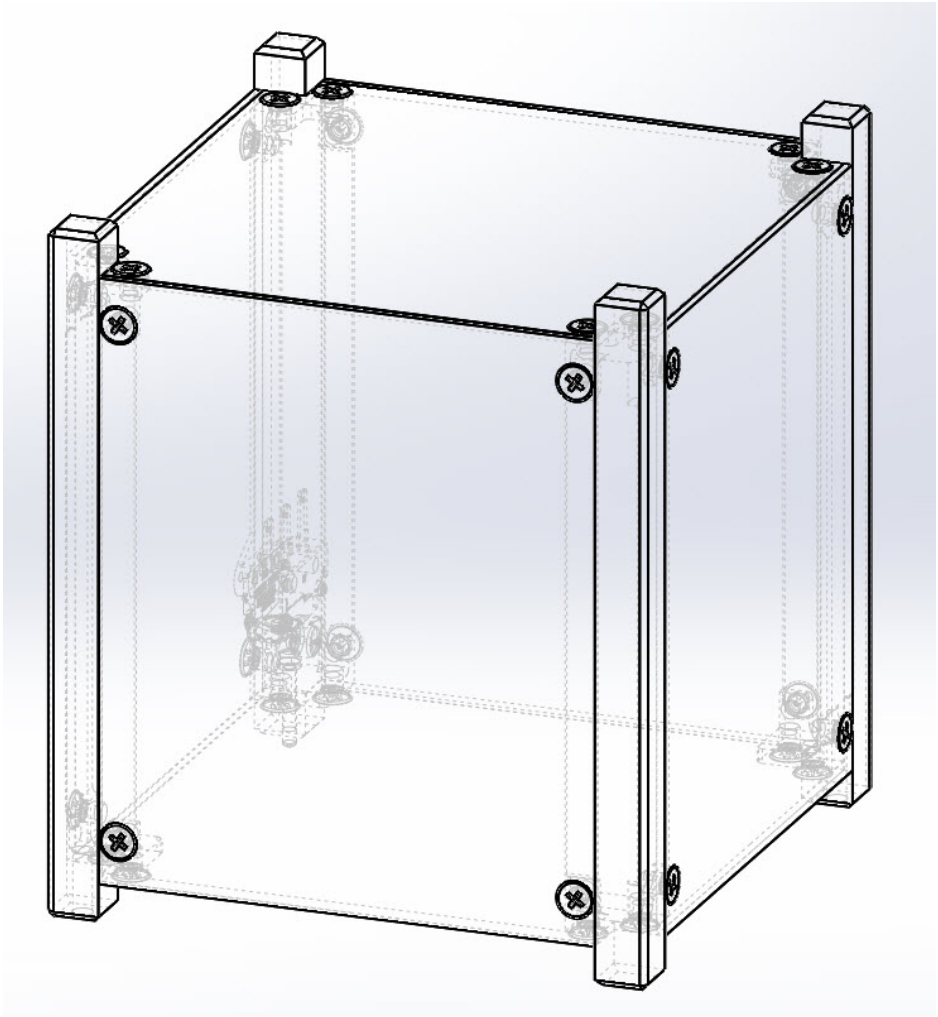

Figure 3.17: Complete Concept 3 view.

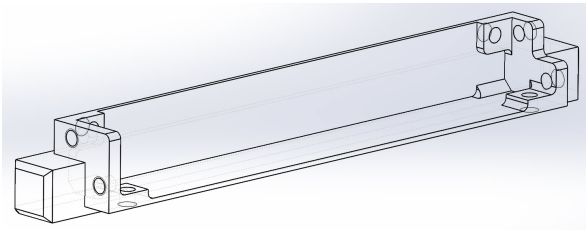

Figure 3.18: Concept 3 Aluminium Rail.

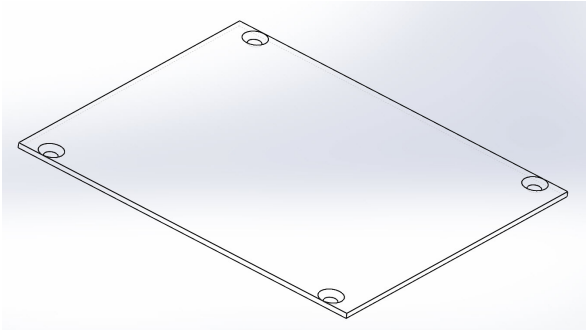

Figure 3.19: Concept 3 side panel with countersunk holes.

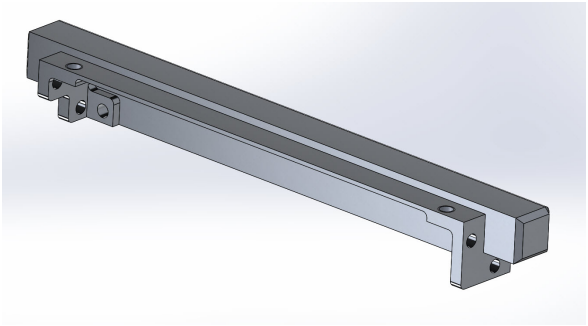

Figure 3.20: Concept 3 Aluminium Rail "step" and top profile view.

Figure 3.18 and 3.19 show the aluminium rail design and the side panel with the required countersunk holes. The aluminium rails have a stepped surface where the side panel is attached to, this gives the CubeSat structure a flush side panel to aluminium rail face transition and maximises the internal volume. The side panels are 1.4 mm thick when considering the 3 layer carbon fibre material layup, together with the epoxy adhesive layer and the copper foil layer. The step in the model has been created at 1.45 mm to provide a near flush finish to the structure. Figure 3.20 provides a view of the step in the rail as well as the top section of the rail with the mounting locations of the top and bottom panels.

The design relies on the aluminium section providing all the fastening and supporting function, however, should there be an excessive deflection in the side or top and bottom panels then a composite support angle section as seen in the concept 1 and 2 models can be added for further rigidity and provide additional fastening locations.
The aluminium rails will be constructed using 7075-T6 aerospace grade material. The 7075 provides a very high specific strength, low density and maintains great properties at low temperatures. The machinability of the material is still good. The T6 tempering extracts the peak strength of this aluminium compensation while still allowing a workable platform. The 7075 series aluminium has been widely used in the aerospace industry and has a great heritage record. See Appendix C.6 for a data-sheet on 7075-T6 material. The aluminium material data used in the FEA was extracted from the datasheet provided in the appendices.
The standard PCB material used to support the solar panels in a conventional CubeSat structure ranges from 1.2 to 1.6 mm in thickness and is attached to the exterior of an aluminium skeleton structure. This knowledge drove the composite design to be restricted to a 1.4 mm laminate thickness to provide a geometrical improvement over the conventional setup. In addition to the added internal volume, the mass of

the structure will be reduced. The solar panels can still be attached to the external surface of the composite panels and small pilot holes can be created to allow connecting wires to be attached to circuitry on the internal copper foil to route the power from the solar panels. Therefore, the structure does the task of performing multiple functions, electrical tracks/connections, solar panel support, mechanical structure and inherent EMI shielding due to the carbon composite. The countersunk screws will be 3 mm (M3) nominal thread size screws, made of stainless steel as they are commonly available and provide no magnetic interference for any payload or subsystem onboard the CubeSat.

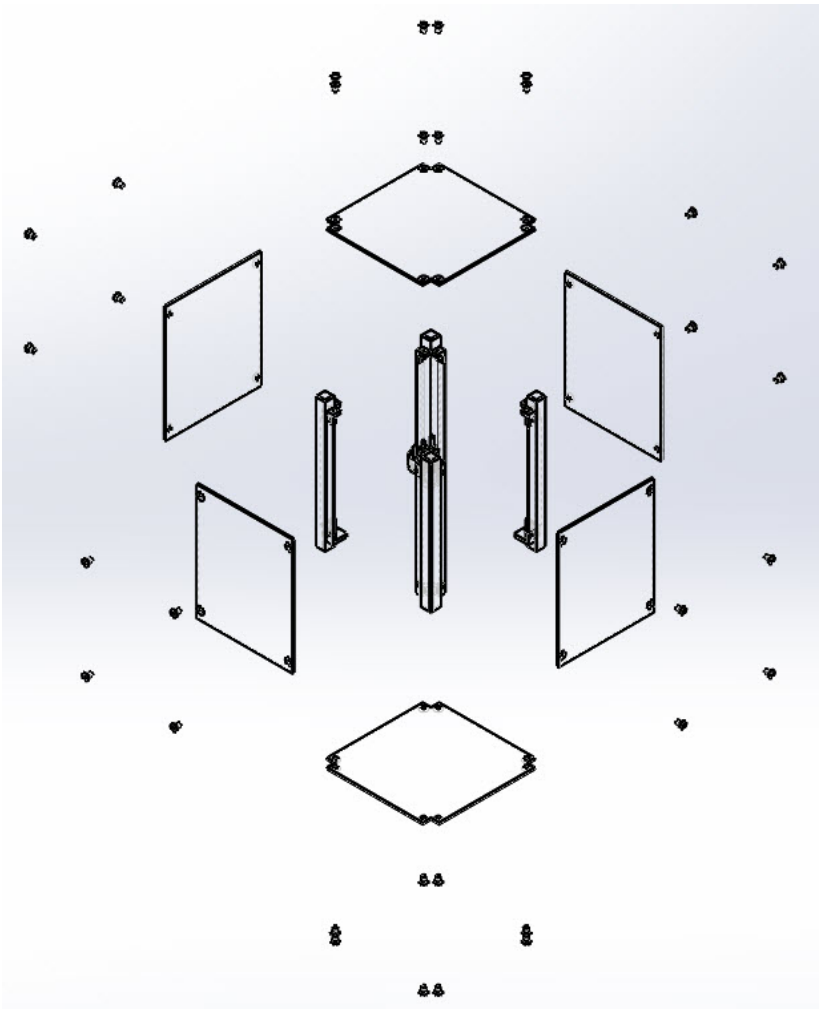

Figure 3.21: Exploded View of the Concept 3 model.

The manufacturing of the aluminium rails will be done using a CNC milling machine and the composite panels will be made using the infusion process (for the mockup model) on a flat glass table and then routed out using a PCB milling machine. The material is a very similar configuration and thickness, so the same machining process used for PCB's can be implemented on the side, top and bottom panels of the structure. For the engineering model, however, as previously mentioned, an autoclave with prepreg carbon fibre should be used that has an accepted out-gassing property from NASA or any other spacecraft developer. No specific type of prepreg material is listed here as it is open to selection when the time comes to select the adequate material.

The same theory can be applied to the prepreg twill weave carbon fibre fabric and the properties of the new prepreg would have to be entered into the programs and relevant software packages.

Overall the concept 3 design seems to provide a complete solution to all the requirements for the CubeSat and the potential issue of deflection or rigidity has been addressed with a reserved solution if required. The final design weight of this concept structure design is 196.7 grammes, which excludes the solar panels and other electronic subsystems. The predicted mass of the structure was calculated using the CAD software that is was constructed in and the known densities of the materials.

3.2.3 Structure Assembly Plan

The concept structures described in the previous sections have to integrate with the other subsystems that make up the overall satellite. In this section, a description of how this can be done is covered. As an example, using concept design 3 for this demonstration, a complete model including the electronic subsystem and Antenna Deployment System (ADS) unit has been created to illustrate the interfacing of these subsystems. Figure 3.22 provides a complete view of an assembled satellite (the solar panels have not been included to provide a better view of the internal components when the side panels are made translucent).

Figure 3.22: Overall view of the complete concept satellite with the subsystems.

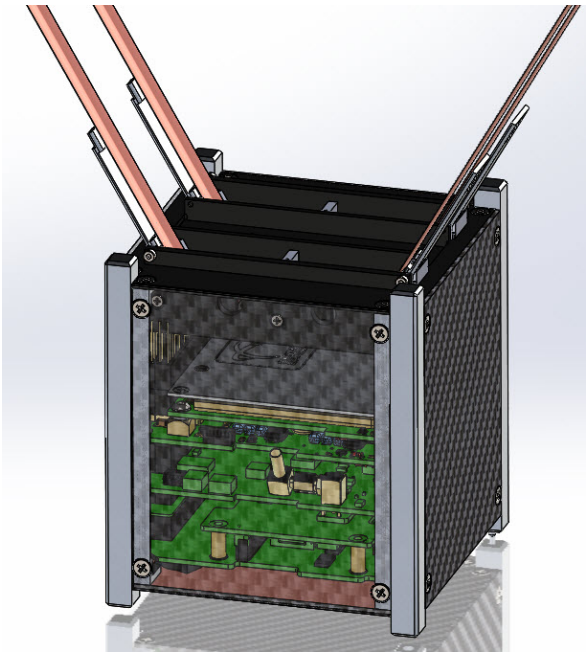

Figure 3.23: Closer view of the internal electronic subsystem within the structure (translucent side panel for a better view).

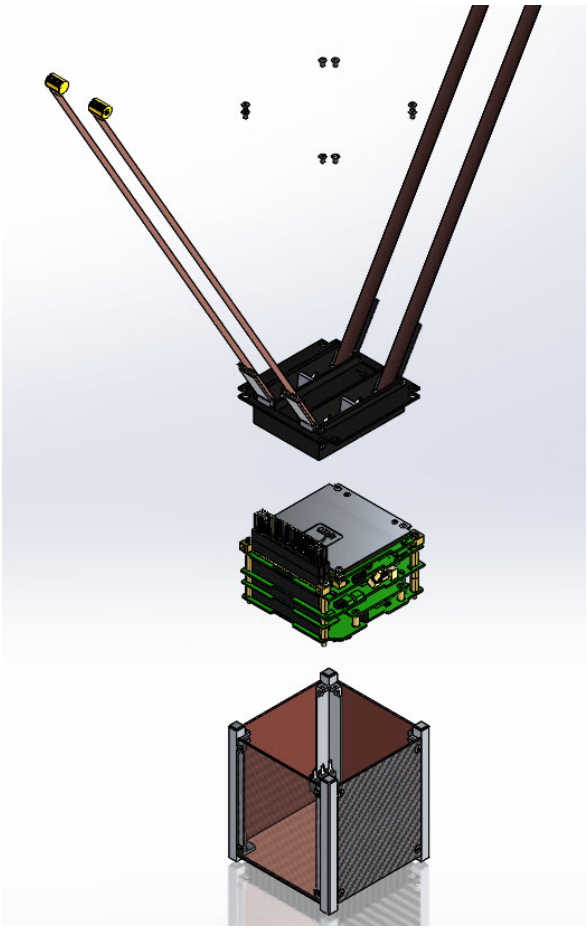

Figure 3.24: Exploded View of the subsystems of the satellite.

As can be seen in the diagrams above the subsystems can be accessed through a stacking process. The bottom of the electronic board stack would be mounted to the base section of the aluminium support rails. If required one or more side panels can be removed to access the screws that fasten the base PCB to the structural rails. The ADS subsystem is required to deploy communication antennas for the satellite. The ADS was primarily designed for use in a 2U CubeSat however it is placed in this model to provide a complete demonstration of the subsystem integration. Mention of solar panels can be directly placed on the surface of the carbon composite panel, however, an adhesive insulation layer should be used to prevent electrical conductivity between the solar panel and the composite panel in unwanted areas. Also, it must be noted that the solar panels are not simply bonded to the panel, but need to be especially "laid" on the surface of the panel and be bonded very carefully into position. Once again the objective of the multifunctional panels is to be integrated as a functional item in the electrical subsystem. The panels can provide both the support for the solar panels and in the unallocated space on the copper foil, components and circuit tracks can be mounted and machined into these areas to perform functions that were once taking up space on the main PCB stack in the CubeSat. The electrical side of the structural panels can be connected to the main electronic stack by using FPC connectors.

3.2.4 Cut-away Panel Structure Concept

A modified design of concept 3 was created with cut-out sections from the side panels and the top and bottom composite panel. Figure 3.25 and 3.26 show the modifications made to the concept 3 design. The objective of this design is to create a structure with a reduced overall weight when compared to the concept 3 design. The overall mass of the cut-away structure is 160 grammes, thus saving 31 grammes from the full panel design which equates to a 16% weight reduction.

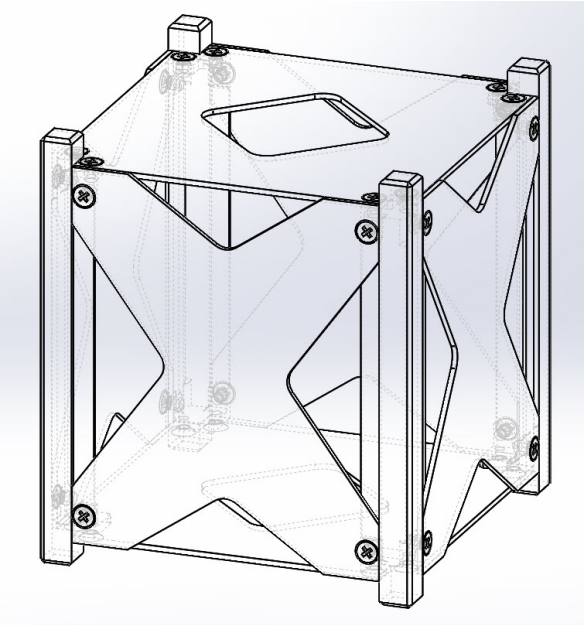

Figure 3.25: Cut Away Panel Concept structure wireframe view.

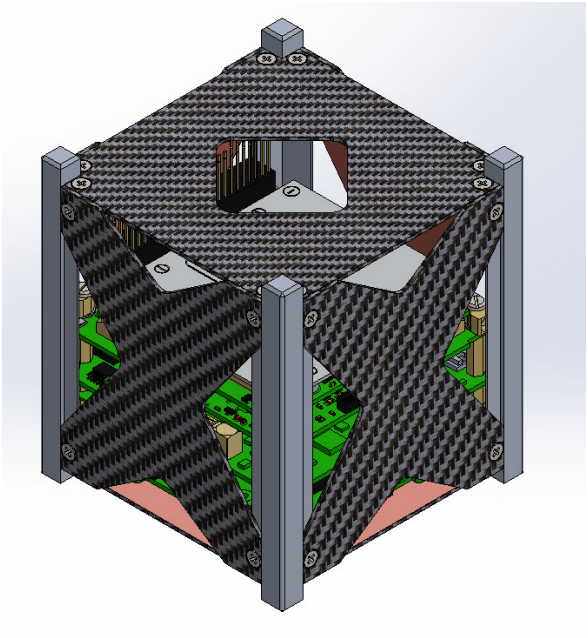

Figure 3.26: Cut Away Panel Concept structure with integrated electronic subsystems.

It is important that the structural rigidity is maintained, thus the profiles of the side panels have been created based on a cross-brace support profile and the top and bottom panels constrain the linear movement of the aluminium support rails. The centre section of the top and bottom panels has been removed to reduce the mass influencing the defection of the panel at its weakest point (furthest from the supports). The main advantage is the weight saving, however, the main disadvantage of the design is that the structure does not provide complete coverage and protection to the internal subsystems. For example, radiation shielding or EMI shielding of internal subsystems would not be complete due to the gaps that are present in the panels. Solar panels can still be mounted to the external surface of the available panel areas, where required, but may prove to be very tricky considering that the solar panel may not be fully supported by the panel. The exact same assembly plan as used for the full panel concept would be used in this case which simplifies the need for additional jigs or assembly plans to be followed. An FEA analysis of this structural design will also be done to evaluate the deflection characteristics of the revised cut away panels to ensure that the stresses and deflections induced in the panels remain at an acceptable level. The creation of this design is intended to provide an alternative option or configuration

idea for a CubeSat structure that may be desired over the full panel design, as it may aid or integrate with electronic subsystems more favourably.

3.3 Finite Element Analysis

The finite element analysis (FEA) of the composite material laminate has been done primarily in ABAQUS FEA software. A small thermal analysis has been done in NX Siemens Space Thermal workbench. A virtual tensile and bending test model has been created in ABAQUS, along with a structural model on which a static load analysis, Natural frequency and dynamic load response analysis has been conducted. A small impact test has also been done to view the stress and possible interaction characteristics if struck by debris. The construction of the composite material and structure remain the same for all the ABAQUS simulations and a brief explanation of the general simulation model will be explained.
Note, it is assumed that the reader has a background with FEA and a basic understanding of ABAQUS. The specific loads and analysis steps for each simulation will be expanded on in the relevant sections that follow. The complete overview of the NX Siemens thermal simulation is also discussed in a later section.

A mixed modelling or lamina level technique was adopted for the creation of the FEA model. The micromechanics of the composite as presented in section 3.1.3, is used as the lamina data input in ABAQUS. Each lamina will be modelled separately and stacked in a ply layering sequence to represent the material configuration that is chosen. The level of detail required for this model does not warrant the use of a micromechanics modelling approach where the fibres and matrix are modelled as well, this would create unnecessary complexity and computational expense to the process. The mixed modelling approach provides the opportunity to view each lamina that make up the overall laminate and evaluate its performance.

Continuum shell elements will be used to create the element structure of the FEA model. Continuum shell elements require the explicit geometry of the model and the laminate. Generally 3D solid elements would be used, however, continuum shell elements enforce the FSDT (First-order Shear Deformation Theory). Continuum shell elements only have displacement degrees of freedom (Barbero, 2013) and can, therefore, be stacked as well as connected to solid elements. Continuum shell elements discretize the 3D geometry in the same manner as solid elements would.

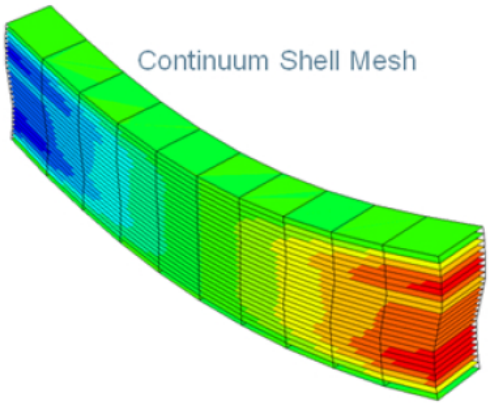

Figure 3.27: Example of continuum shell elements used to view the transverse shear stresses.
(Dassault-Systemes, 2014)

The main advantage of continuum shell elements is the fact they can be stacked, this allows an accurate elasticity solution to be solved. The stacking advantage of continuum shell elements outweighs the use of solid elements as continuum shell elements do not have aspect ratio problems (Barbero, 2013). The thinness of the elements (through the thickness of the layer) can be very small due to the incompressibility of the normals (Barbero, 2013).
The meshing of continuum shell elements is marginally more difficult when compared to generally shell elements, due to the fact that the thickness of the shell has to also be meshed. Figure 3.27 shows an example of the transverse shear stress colour plot through the thickness.

For the multifunctional composite, FEA model is first created by extruding a profile sketch with the required dimensions to the required thickness to create a 3D solid body. The body is then partitioned through the thickness to create the various layers at their relative thicknesses. Figure 3.28 shows the partitioned layers through the thickness of the part. The overall thickness is very close to 1.4 mm, where each carbon fabric layer (3 layers) is 0.3 mm thick, the adhesive layer is 0.2 mm thick, the FR4 material backing on the copper foil is 0.18 mm and the copper layer is 20 micron.

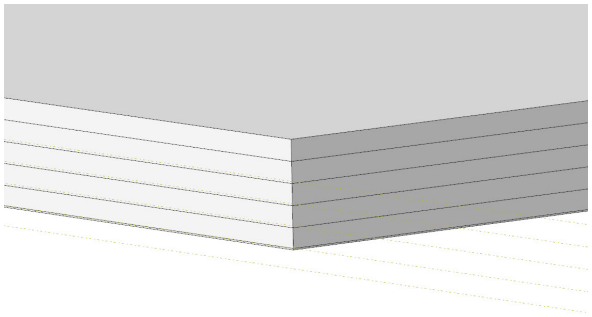

Figure 3.28: Partitioned MFC model through the thickness.

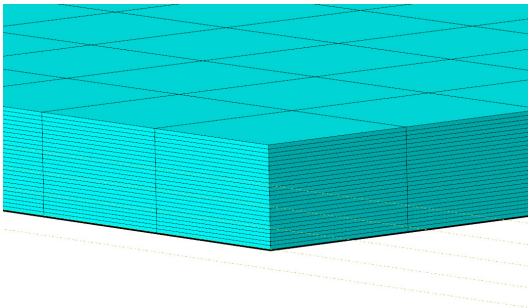

Figure 3.29: Continuum shell mesh of the composite laminate.

The mesh used for the model was created by using a global seeding of 0.0025 (model drawn in metres to maintain SI units) and the vertical edges (that run through the thickness) meshed to 5 nodes per partitioned layer in the part. This provides a fine enough resolution to view the shear stress transition through each lamina ply. After the meshing has been done, it is important that the stacking orientation should be assigned to the part regions in this module before proceeding to the composite layup. A structural or sweep mesh can be done to provide the best mesh results.

The material allocations and section assignment were done using a composite material layup in ABAQUS. Firstly before the composite layup can be done, the material properties of each layer needs to be created. The adhesive and copper material properties can be entered into ABAQUS using the general isotropic material type input (material datasheets can be found in the Appendices). The FR4 material and the carbon composite material ply properties will use a *lamina* material type. The FR4 properties can be found using the data-sheets (Appendix C.1) and the carbon lamina properties are the outputs of the MATLAB program written to determine the lamina properties using the micromechanics models. Figure 3.31 illustrates an example *lamina* material type input for the carbon fibre material. Figure 3.30 provides a summary of the material data collected from the various datasheets. All the data has been kept to standard SI units to eliminate conversion errors.

AV Epoxy [AV4076]:			
Property	***Symbol***	***Units***	***Value***
Young's Modulus	E_av	Pa	1.00E+09
Shear Modulus	G_av	Pa	5.00E+08
Density		g/cm^3	1.04
Poisson's Ratio		-	0.32
Coefficient of Thermal Expansion		µ/m °C	-
Thermal Conductivity		W/m/C	-
UTS		Pa	2.00E+07
Tensile Strain		%	5
Copper PCB Layer:			
Property	***Symbol***	***Units***	***Value***
Young's Modulus	E_cu	Pa	1.18E+11
Shear Modulus	G_cu	Pa	4.40E+10
Density		g/cm^3	8.9
Poisson's Ratio		-	0.35
Coefficient of Thermal Expansion		µ/m °C	16.8
Thermal Conductivity		W/m/C	3.9
Fatigue Strenght (50e6 cycles)		Pa	2.00E+07
Yield Stress		Pa	1.17E+08
UTS		Pa	2.00E+08
Tensile Strain UTS		%	9.40E+00
Fibreglass PCB Layer:			
Property	***Symbol***	***Units***	***Value***
In-plane Young's Modulus	Ep_11	Pa	2.00E+10
transverse Young's Modulus	Ep_22	Pa	1.80E+10
In-plane Shear Modulus	Gp_12	Pa	1.48E+08
Transverse Shear Modulus (y)	Gp_13	Pa	1.48E+08
Transverse Shear Modulus (z)	Gp_23	Pa	8.05E+09
Density		g/cm^3	1.85E+00
In-Plane Poisson's Ratio		-	0.136
Transverse Poisson's Ratio		-	0.118
Coefficient of Thermal Expansion	(-0.000001)	µ/m °C	15
In-Plane Thermal Conductivity		W/m/C	1.059
Transverse Thermal Conductivity		W/m/C	0.343
UTS		Pa	3.10E+08

Figure 3.30: Material Property summary from the datasheets.

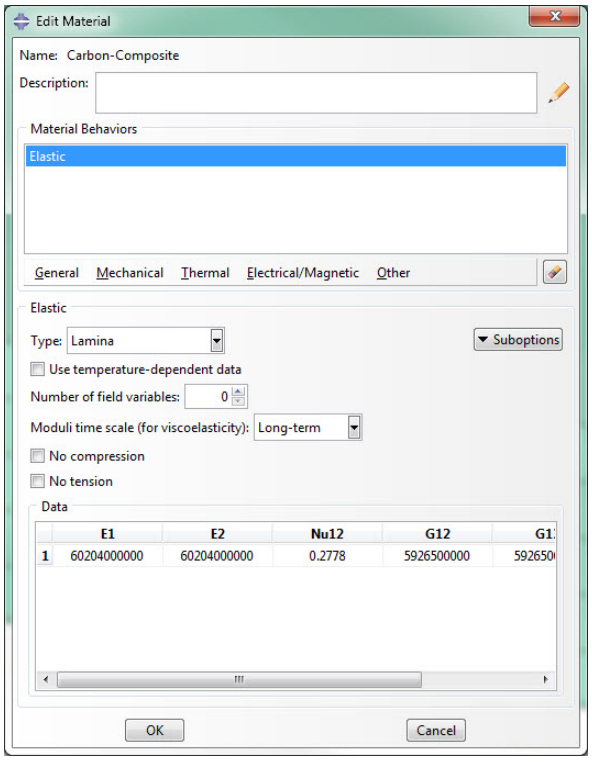

Figure 3.31: Lamina type material property input for the carbon fibre.

Once the material properties have been set up the next phase is to create the composite layup. Figure 3.32 shows the data inputs for the composite layup. The regions are selected accordingly in the view window of ABAQUS, the correct material properties are assigned to each designated layer in the composite. The element relative thickness should be the thickness of the lamina layer. It must be noted that the isotropic material layers are also included in the composite layup, however, the materials assigned to these layers are also isotropic thus it will not be an issue. The composite laminae need to have their rotation angles specified relative to the selected coordinate system. For the woven fabric composite laminae, the properties of E11 = E22, thus the angle can

be either 0 or 90 degrees. In this case, the alignment of the upper and lower carbon composite layers is 0 degrees and the middle layer at 45 degrees to those two layers. The rotation is about an axis normal to the ply surface. The FR4 composite backing layer has been positioned at 0 degrees. The isotropic material could effectively be aligned at any angle, as it is not affected by the rotation, however for consistency it has been positioned at 0 degrees as well. The coordinate system is based on the overall part rectangular coordinate system as it is a flat part. The stacking direction, in this case, is in the element direction 3 (z-axis through the thickness).

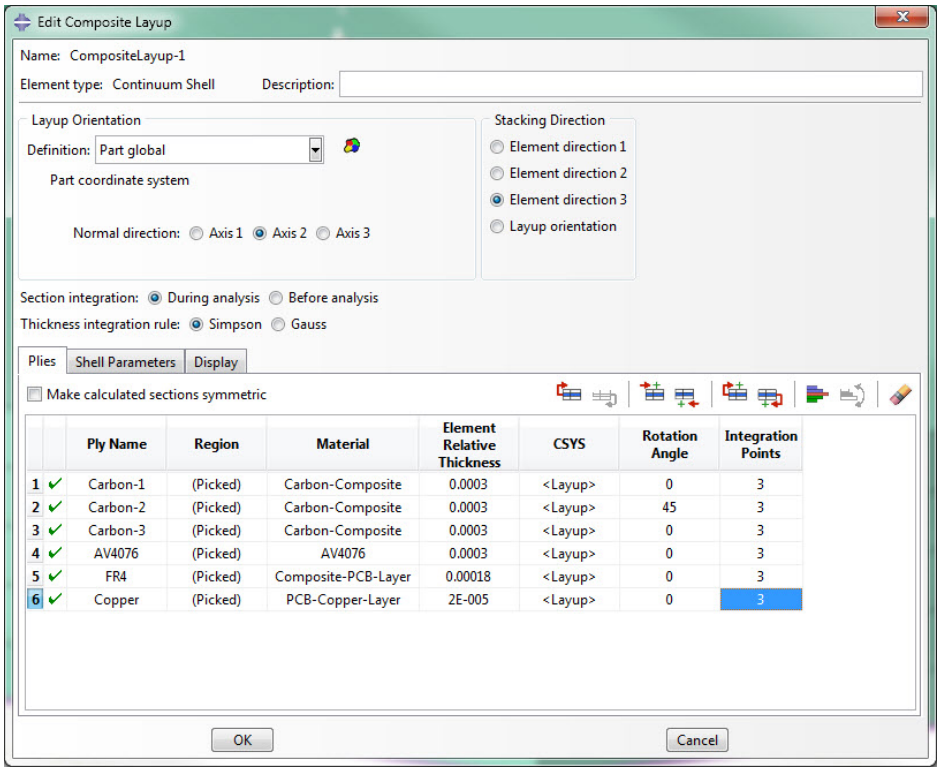

Figure 3.32: Composite Layup Properties.

Up to this stage, the setup of each simulation will follow the same material assignment and configuration process as previously described. However, for each simulation, the loads that are applied and the type of steps created will vary with each case. The sections that follow now explain the simulation details, the step, loads and boundary condition setup for each of the simulations that have been done. The results from the various simulations will be discussed further in the relevant results chapter that follows.

3.3.1 Progressive Failure Analysis Implementation

After further research into the prediction accuracies of the conventional composite laminate construction in ABAQUS, the addition of a progressive failure analysis tool (PFA) was used to increase the realism of the material response. It is well known that composite materials fail ply by ply after the main load bearing ply has failed. This

progressive failure yields a clear drop in the force supported by the laminate after the load plies fail, then a gradual step down profile as each of the remaining plies fail. This would be particularly visible in the bending tests as plies fail one at a time. It is expected that the tensile tests will yield a complete failure at UTS of the laminate. The PFA tool will, however, be used in the FEA predictions of the tensile test as well.

After some wide research into PFA plug-in tools for ABAQUS FEA, a tool produced by *Autodesk* appeared to lend itself to this application.

The *Autodesk HELIUS PFA* plug-in for ABAQUS was used to create the material properties for each lamina.

As opposed to inputting the data from the MATLAB program to predict the micro-mechanic properties of the lamina layers directly into an ABAQUS lamina material specification, the data was used to cross reference the input data for the PFA plug-in tool. Figure 3.33 illustrates an example of a 2/2 twill weave carbon fibre lamina data input into the PFA tool.

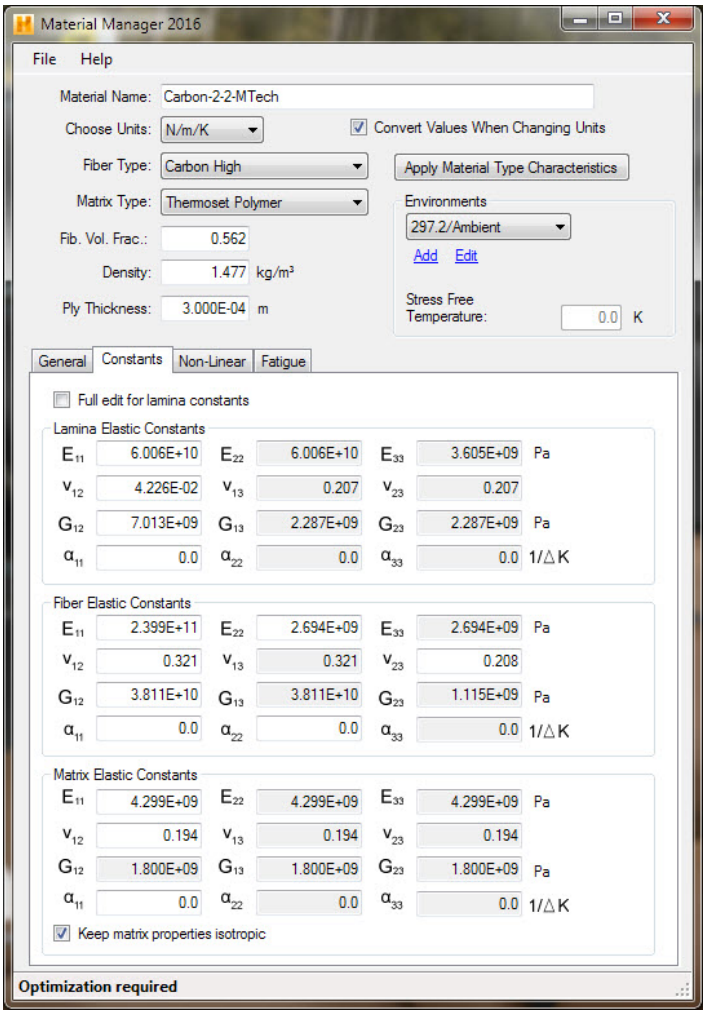

Figure 3.33: Input lamina data from the MATLAB program into the PFA tool, HELIUS PFA.

A standalone interface for the HELIUS PFA program allows the user to input lamina data and all know fibre and matrix material data in the relevant dialogue boxes on the program interface. The material was sourced from the material data sheets and the theory used to write the micro-mechanics material property predictions covered in section 3.1.3.

Once the material is saved in the HELIUS PFA Library, the material properties and specification are then loaded in the ABAQUS FEA model by importing the material from the HELIUS library through the plug-in interface. The ABAQUS job is set up as per normal methods, however before the job is run, it is required that an input file for the job is written. The input file is then run through a pre-process program before being reloaded as the job input file. The pre-process program writes in the required elastic constant equivalents for the imported composite materials which will allow the conventional ABAQUS solver to run the job.

The output of the job provides a clear indication of the stages at which each ply in the laminate fails and shows a progressive failure trend. The results of the various jobs that were run are shown in the next chapter.

An academic licence for this software plug-in was obtained for free from Autodesk and can be freely used for academic research purposes, however not for any commercial work or jobs.

3.3.2 Virtual Material Test Models

The virtual simulation of the material tests mimics that of the physical tests that will be conducted. Two primary material tests will be done for this material, that is a tensile and a bending test. The data from these two tests will be sufficient to provide a comparison of the physical data collected to the predicted characteristics of the specimens.

3.3.2.1 Tensile Test

Following the ASTM tensile testing guidelines and standards presented in section 2.5.7, samples measuring 250 x 25 mm were created at the thickness of 1.4 mm. The material part was modelled in ABAQUS and the composite material layers setup as covered in the previous section for this specific profile.
During the tensile, the specimen would be clamped between two vices and a tension force applied, thus creating a tractive force on the contact surface of the specimen to the vice clamps.

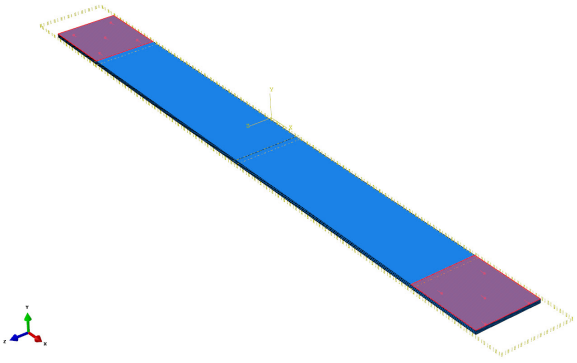

Figure 3.34: Tractive tensile load applied to the highlighted regions.

Therefore, a general static step was created, due to the applied load being slow enough that the strain rate does not have a significant effect. In this step, a tractive force on the portions of the surface that is in contact with the clamps is applied. One tractive force is applied to each surface of equal magnitude and opposite direction. The area to which the tractive force is applied was created using a face partition to isolate the surface area needed. Figure 3.34 shows the applied tractive force applied to the highlighted regions on both sides of the specimen. To provide consistency between the FEA model and the actual model the area on the actual specimen has been scribed to provide an alignment guide when testing.

No boundary conditions are required for this simulation due to the forces being equal and opposite to one another. The tractive force will be varied until the predicted UTS of the material has been reached, at which point the applied force will be recorded and

used for the comparison. A stress-strain plot will be created from the specimen data and compared to that of the physical samples.

3.3.2.2 Bending Test

Once again the ASTM testing guidelines and standards were followed when setting up the bending tests (section 2.5.7.2). A three-point bending test will be conducted on the composite specimens. However, due to the thinness of the material the standard 250 mm long sample is not recommended as the material will have too much flexure and the deflection would be too large before the material failed. It is stated that for materials less than 1.6 mm thick, that the distance between the supports is 51 mm. The sample should be long enough so that no less than 6.4 mm of the overhang is present on each end to prevent the sample slipping through the supports.

For this test, samples will be made at an overall length of 80 mm and a support span of 51 mm. The composite material assignment and layup process in ABAQUS remain unchanged from the initial section specification. The composite part has 3 face partition that is created, one on each end in the positions of the support pins and another in the centre plane of the laminate. These partitions will be used to align other components and apply boundary conditions too.

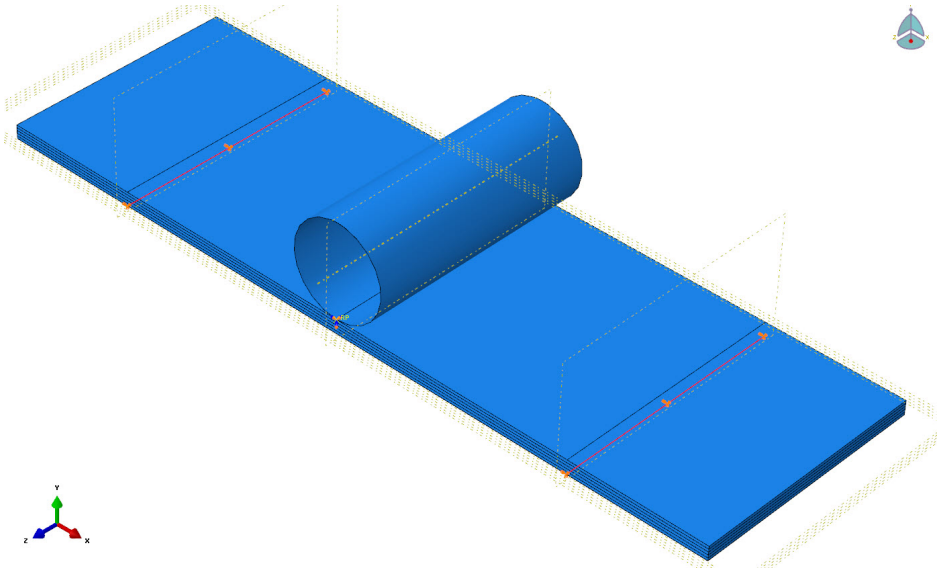

Figure 3.35: Job setup of the bend test in ABAQUS.

The composite part model is created with the previously mentioned specification, but also an analytical rigid part is created to represent the "Load" pin in the centre of the specimen. The rigid pin has a diameter of 10 mm and is approximately the same diameter as the pin on the physical test jig. The instance for both parts are created and the pin in translated into position above the centre line partition of the laminate. The load is applied in the form of a displacement of the rigid pins reference point. The deflection value will be initially set at 2 mm and then adjusted until the materials

UTS has been reached. The boundary conditions for the sample is a simply supported condition applied at the support face partition locations. The rigid pin also has an additional boundary condition on the reference point to enforce that the pin only moves in a downward deflection pattern. Figure 3.35 illustrates the complete FEA model with the positioned rigid pin, the composite sample and the boundary conditions that are applied.

3.3.3 Structural Analysis Models

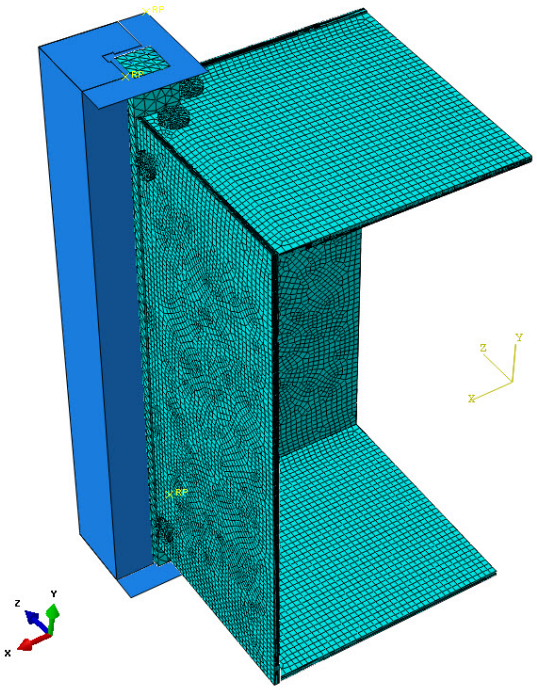

Figure 3.36: Quarter structure FEA model in ABAQUS.

The structural analysis of the complete structure was done on a quarter section model of the complete structure. Due to the structures symmetry about two planes, a section of the model was created to lower the total number of elements and boundaries of the model which in turn allows less computational expense and less simulation time required.
Figure 3.36 illustrates the complete quarter section FEA model, this can be compared to the full model diagrams of the structure shown in section 3.2.2.3. The side panels are dimensionally half the size of the actual panel size and the top and bottom panels are a quarter of the actual panel size. The origin of the model has been placed in such a way that the principle planes can be used to mirror the results in the result visualisation mode.

The geometry of the model was set-up symmetrically due to the nature of the structure. The symmetry of the composite material was also considered in the analysis model to ensure no loss in model accurate was seen. By doing this, the computation time and mesh requirements were also reduced significantly. The loading and boundary conditions are also symmetrically applied to the model. The boundary conditions made use of representative surface for the launching pod and considered to be ridged in this case. Contact conditions were setup between the launch pod surfaces and the Cubesat structure, thus considering the interaction conditions to the launch pod. A mesh refinement investigation was done in a brief analysis. One of the key limiting factors in this case is the limits of the number of allowable elements per model with academic FEA licensing. A similar mesh size was then used through-out the models to produce more consistent and comparative data. The reduction of the mesh size for example of the composite test samples yielded very little difference to the overall contour plots, however did exponentially increase computation time which was also available for limited times. Thus, the overall mesh used considered the computation

time required, accuracy of the results and limitation of licensing and finding the best balance for this situation.

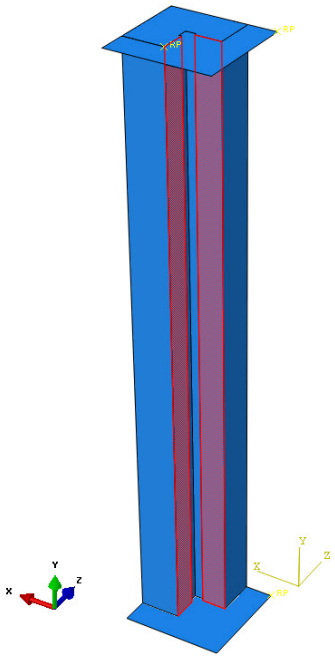

Figure 3.37: The P-POD reference surfaces, to simulate the actual interfacing conditions of the launch pod.

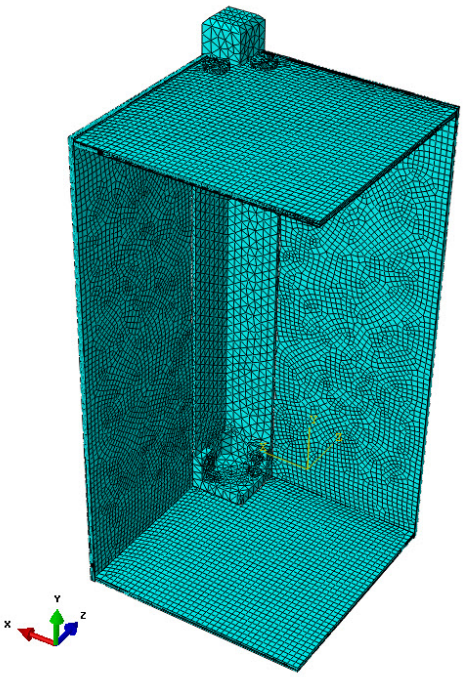

Figure 3.38: Internal View of the FEA structure model in ABAQUS, without the P-POD reference parts.

Figure 3.37 illustrates the P-POD parts that are made in the FEA model, these are analytical rigid surfaces that are used to create a representation of the P-POD surface that the CubeSat structure will interface with. The boundary conditions that need to be applied to the CubeSat surfaces are varying in the different displacement directions and rotations. The P-POD is assumed to be the fixed reference in this case and the POD parts have an encastre boundary condition applied to them. A contact relationship is then applied to the interfacing surfaces of the P-POD parts and the CubeSat structure to mimic that of the aluminium to aluminium contact condition that would be seen in the actual assembly. The top and bottom planes are there to potentially limit the movement of the CubeSat structure. The structure cannot protrude or deform into/past the P-POD surface, however, it can deform or "collapse" in on itself and away from the surface if the loads on the model permit it. In Figure 3.37, the interfacing surfaces are highlighted and the dimensions were taken from the CubeSat standard's documentation. Figure 3.38 provides an internal view of the FEA CubeSat structure and the aluminium rail's internal geometry. As a further note, all the parts have "part dependent" meshes. The composite material is set up as previously covered, the aluminium support rails and the bolts are 3D solid parts using 3D stress element types and a free tetrahedron mesh control.

The CubeSat assembly is fastened together with bolts as shown in Figure 3.39. The bolts, in this case, have been simplified to a button head design and a smaller button head on the internal surface of the aluminium rail. The actual countersink design proved to be too complex to model, as the countersunk head of the screw had many interfacing conditions for each layer of the composite material in the countersunk hole. Thus, a simplified button head was created with a mean diameter of the countersunk head that closely represents a similar pressure distribution of the bolt load on the composite material surface.

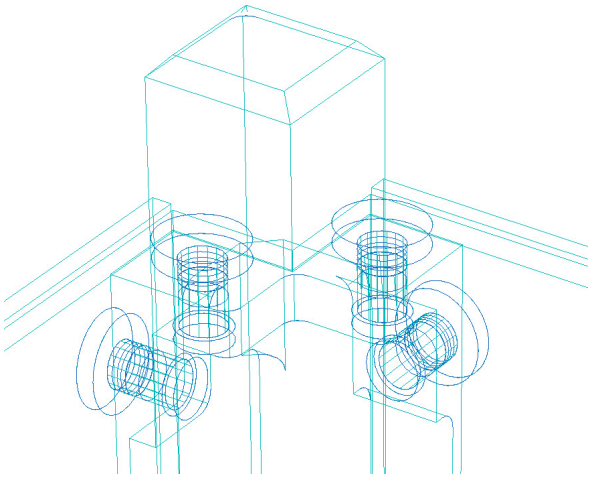

Figure 3.39: *Wireframe view* of the bolts that fasten the panels to the aluminium support rail.

The design of the structure has the screws threading into a female thread section in the aluminium rail itself, however once again the threaded section adds too much complexity for the computing power available to successfully solve the job in a reasonable simulation time and thus had to be simplified. A smaller button head was created on the internal side of the aluminium support rail to ensure that the screw would not move out of position when the loads were applied. A very high friction coefficient was applied to the bolt to aluminium contact condition to simulate the stress distribution of the loaded bolt in the aluminium material similar to a threaded state. The design incorporated stainless steel M3 screws that are designed to be torqued to 0.5 Nm as the aluminium thread section was not able to be very deep. A torque of 0.5 Nm on the screw creates a bolt clamping force of approximately 90 kg (Oberg et al., 2004), thus the ABAQUS model bolt load would be set to 880 Newtons of force.

Between all the composite panels, the aluminium support rails, bolts and the launch pod, contact conditions were specified based on a "Hard Contact" condition and the relevant friction coefficient based on the material type for the tangential behaviour. The friction coefficients between the materials are well researched and can be found in most engineering handbooks. The friction coefficients used for the contact conditions are as follows:

1. Aluminium to Aluminium - 0.4 (finite sliding).
2. Bolt to Composite Material - 0.3
3. Bolt to Aluminium - 0.98 (To represent a fastened threaded condition).
4. Composite to Aluminium - 0.28 (Which is a copper to aluminium condition due to the copper foil backing on the composite panels).

After the structural assembly was completed and the contact conditions specified, the encastre and symmetry boundary conditions are applied in the *initial* simulation step

and thereafter a general static load step is created to apply the bolt pretension loads. Based on the maximum rated bolt torque permitted between the stainless steel bolt and the threaded aluminium section, the corresponding bolt load was applied to the bolts. The bolt pre-load step in the simulation fastens the panels and also establishes the contact conditions between the various interfaces. The values of the maximum bolt torque and the clamping load was found using an open source engineering calculator available from (FUTEK-Advanced-Sensor-Technology, 2015). The profile of the screw, female threaded section and the corresponding materials are feed into the algorithm and the relevant values are computed for the user. The bolt load applied is 800 Newtons of force.

The general FEA structural model is now complete and additional simulation steps and the various load conditions required are added in, depending on the simulation being conducted. The subsections that follow cover the additional steps added to the simulation model for the different analysis that were run. Note, that the loads and boundary conditions from the initial and pre-bolt load steps are propagated to the other steps that follow in each type of simulation that is run.

3.3.3.1 Static Load Analysis

The static load analysis involves applying a *gravity load* in a general static step to the entire FEA model. The densities of all the materials have been added to the model to perform this calculation. Based on the spacecraft structural design theory presented in section 3.2, a large gravity load of 20 g is applied in the vertical direction for the static launch load simulation. The vertical direction reference is in the y-axis direction as seen in figure 3.37. The maximum static longitudinal load seen during launch is approximately 5G, thus using a factor of safety in the design of 2, the test load would generally be 10 g. Due to the fact that a shock load simulation will not be covered in this research, a larger factor of safety by the designer has been taken at this point to compensate for the shock load test. The response of the structure in terms of the stresses induced in the various materials and the deflection of the structural components will be recorded and evaluated.

A further consideration is if the CubeSat is launched in a horizontal position, with the side panels on the bottom and top surfaces. Due to space limitations and optimisation, CubeSat's have the possibility of being placed horizontally during launch. The effect of this orientation would be different to that of the vertical gravity load test, however, it is unlikely that this would be done as the launch pods have primarily been designed to function vertically. For the structural design purpose, the response of the structure during a horizontal launch was set up. The gravity load, in this case, is 10 g to provide a realistic representation and is lower due to the low probability of this type of launch condition.

3.3.3.2 Natural Frequency Analysis

The natural frequency analysis of the structure is a simple operation in ABAQUS, the static load test from the previous section is suppressed and a frequency step is created for the simulation. The first 10 eigenvalues are solved for, to compute the first 10 natural frequencies of the structure. The frequency range of interest is 0 to 100 Hz, as the spacecraft test data in the various literature presented does not cover frequencies beyond 100 Hz. The natural frequencies will be evaluated and considered in a design sense.

3.3.3.3 Dynamic Load and Response Analysis

Following the natural frequency step in the analysis covered in the previous section, a steady-state-dynamic modal step is created to measure the dynamic response of the structure under loading. Once again the frequency range of interest is 0 to 100 Hz. In this case, the range has been extended to 120 Hz to capture any response behaviour near the 100 Hz frequency that may be present. For each natural frequency found in the previous analysis, the dynamic response of the structural model will be measured. In this case, a gravity load is applied once again to the overall structure to simulate the frequency response will be under launch conditions. The vibrations and loading during launch would be the most likely time of the satellite's system life cycle where a modal response to a loading under a vibration pattern may create interfacing issues to the launcher or damage internal subsystems or even the structure itself if the response deflection is too high. No damping factors have been applied to the model, this has been done to produce a direct output of the frequencies of the CubeSat structure. It is however expected that for the physical tests done in the lab, that the air surrounding the equipment will have an inherent damping effect on the model. Due to the fact that facilities are not available to perform the tests under a vacuum, the interpretation of the data will have to account for this damping effect. The deflection and stress response to the dynamic loading condition will be measured and taken into account for the data output request from the analysis. The gravity load applied in the dynamic step is 20 g in the vertical direction for the same reasons as done for the static load analysis in a previous section.

3.3.4 Impact Analysis Model

A simulation model of an impact on the composite material was also done to show the characteristics of the material during impact. According to the literature reviewed in the theory section, the average impact velocity of debris in space is approximately 4 km/s. As an initial value, the "projectile" or debris will be set to impact the composite panel at 400 m/s which is at a similar velocity to that of a rifle. Once the model has been solved, the velocity will be increased to 1 km/s and then to 4 km/s to see the progression of the effect to the material. The debris in this test is a sphere of aluminium 1 mm in diameter and represents the majority of the debris field in space.

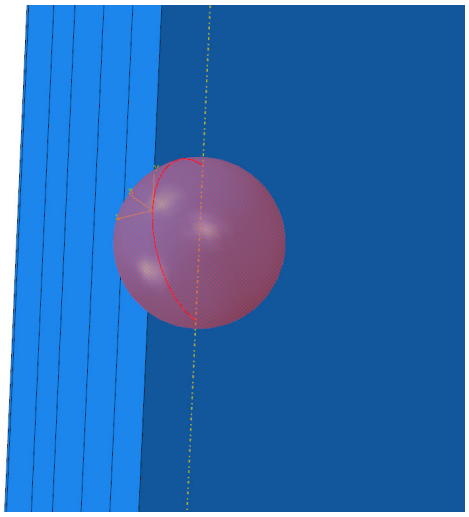

Figure 3.40: The aluminium debris sphere positioned in the centre of the half section composite side panel.

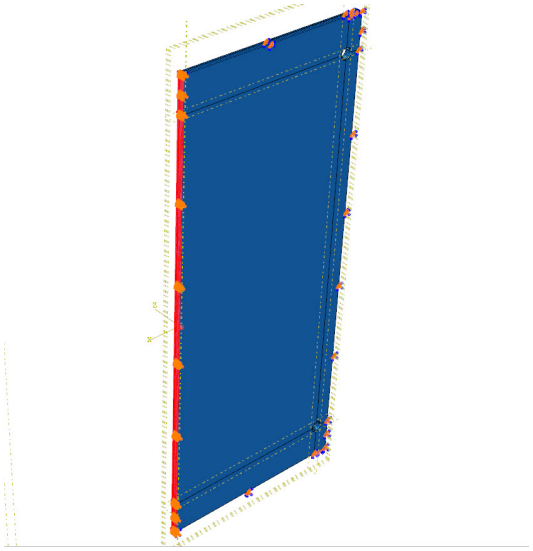

Figure 3.41: Boundary Conditions applied to the composite laminate.

A half section of the structural composite side panel has been modelled and a debris sphere placed at the midpoint of the centre section of the composite panel and in a direction to impact the outer surface, the composite surface (see Figure 3.40). A predefined field is used to apply the velocity to the debris section of the model. An aluminium material property is applied to the debris particle and the material properties can be read from any good engineering handbook.
The composite laminate has a symmetry boundary condition applied to the section plane in the middle of the panel. An encastre boundary condition is applied to the outer edges of the composite panel to fasten the composite panel in place and prevent it from drifting.
The impact of the debris happens within a dynamic explicit step in ABAQUS. Non-linear geometry is turned on and the time period is initially set to 2.5e-5 seconds with the 400 m/s projectile velocity. The velocity of the projectile will be increased as initially described and the response of the panel will be examined.

3.3.5 Thermal Analysis Model

An orbital thermal analysis was setup for the CubeSat Composite structure in NX Siemens Space Thermal Systems workbench. Having only view recently gaining access to this tool at the research centre, relatively simple, however representative simulations were designed for this particular CubeSat structure. At this time, the orbital parameters of the satellite mission that this structure is designed to be used on are yet to be defined. There are an array of options that can be considered for the final orbit panel and profile. However, two main orbit simulations have been setup for this structure; firstly an eccentric (circular) polar orbit which follows the dawn-dust line and secondly an orbit around the equatorial panel.

The first orbit setup which follows the dawn-dust line is a very unlikely plane to be

selected. However, when this case is selected it provides a scenario where should the attitude of the CubeSat maintain a single surface in the direction of the sun vector, a maximum temperature differential will be experienced across the structure of the satellite. The surface facing the sun vector will be the hottest point of the satellite and the surface on the opposite of the structure will be in continuous darkness and the coldest point of the satellite.
The second orbit case will simulate the temperature fluctuation of the structural during each orbit period across the equatorial plane. This orbital pattern will have the CubeSat structure reach a minimum and maximum overall structural temperature during each orbit period.

In each orbital simulation case, the temperature differential will be examined against the maximum and minimum operating temperature range of the materials used to construct the structure. A thermal stress plot is unfortunately not produced in these simulations and will require further processing or a different simulation setup and or package to do this. A thermal stress plot will not be sort after in this research attempt in an effort not to veer off the primary research objective, which is the overall design and analysis. Although this is a very important factor to analysis before the structure is finally built, an engineering evaluation of the properties of the composite material suggests that unless there is a substantial temperature difference in the structural components, the induced stresses will not be high enough to approach the fatigue limit of the construction materials. When evaluating the material data developed in a previous section for the composite material, the modulus of elasticity and the thermal coefficients of expansion are relevantly low which indicated that the material will be quite flexible and not sensitive to temperature induced stress unless large temperature differentials are reached. However, before a final flight structure is developed, further research should be conducted to analysis and optimise this, which overall detail would be too large of a scope to completely add to this research effort.

The NX Siemens Space Thermal model is quite simply setup in the sense that the materials are allocated to the structural geometry which is imported via a step file from the existing ABAQUS simulation models. The thermal properties of the composite material are extracted from the MATLAB program covered in section 3.1.5, which uses the exact theory from section 2.4.3.2. The thermal properties for the aluminium support rails of the structure are already available in a pre-defined material library built into the simulation software.

The simulation model consists of 3D solid components and a 10 node 3D tetrahedral mesh is used for all the components of the model. The mesh is part dependent and each component has an adjusted mesh seeding size to allow for an adequately small mesh to capture the temperature gradient change. Figure 3.42 illustrated the FE model of the CubeSat structure in NX Siemens, along with the mesh settings used for the composite panels.

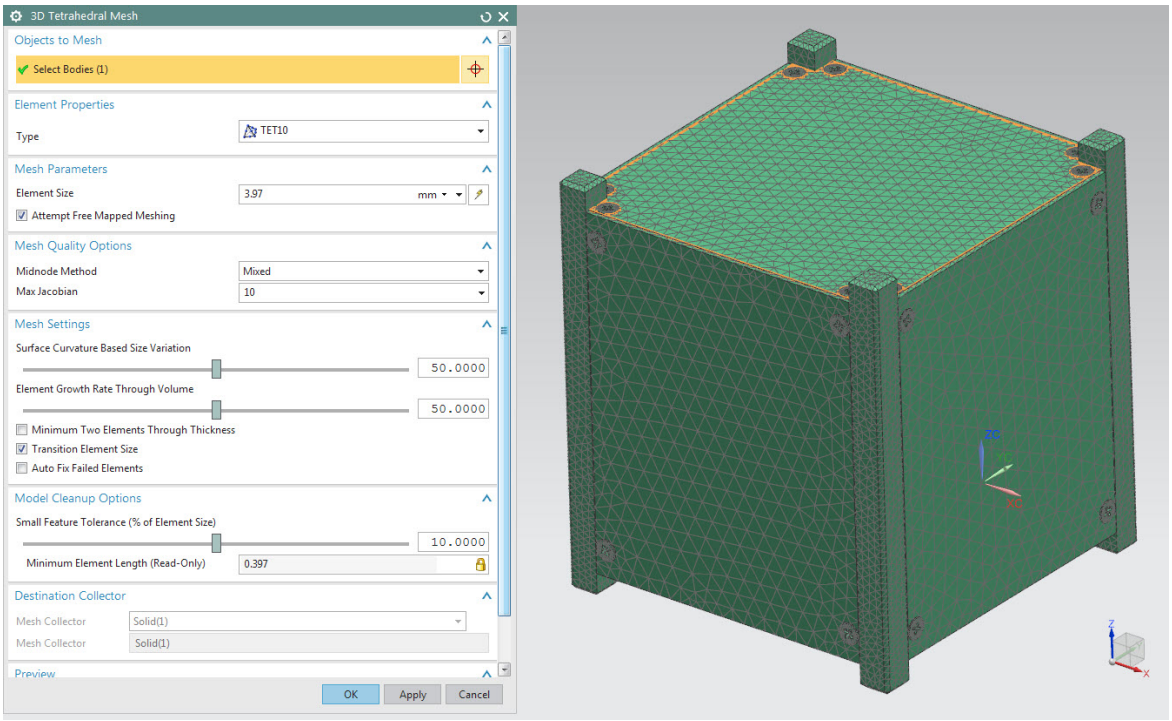

Figure 3.42: FE model setup and composite panel mesh settings in NX Siemens.

The orbital parameters for both orbital thermal simulations have been set as a circular orbit at an altitude of 500 km. The thermal radiation properties of the Sun, the albedo radiation from the earth's atmosphere and space environmental effects have already been pre-defined in the simulation software library. The standard orbital settings used as a default from the program has been used in both cases, apart from the orbit panel inclination angle which is different for each simulation case.

The internal thermal radiation from subsystem operations has not been included in this simulation. The addition of more material mass will aid in reducing the rate of change of the thermal levels of the structure during each orbit. However, the internal subsystems will also produce its own heat. Some electronic subsystem may also require heat sinks or heat pipes to remove heat from the microchip location. The thermal design cannot be continued and simulation of the thermal radiation from the internal subsystems cannot be included, as no electronic subsystem have been defined by the mission this structure is designed to fly on. Once the electronic subsystems are well known, then a detailed thermal model can be created to provide an accurate prediction of the thermal characteristics of the satellite. The attitude of the satellite will also govern how the heat pipes in the structure will be placed, as well as the orbital plane that the satellite is placed in. The objective of the simulation currently conducted in NX Space thermal workbench is to provide a preview of the plausibility of using this material within the thermal environment of space.

3.4 Prototype Production

To conduct the empirical testing and to produce a prototype mock-up, the materials need to be manufactured and machined to the design specifications. The sections that follow cover each of the topics relating to the actual manufacturing of the materials required to accomplish the objectives.

3.4.1 Physical Material Testing

The physical samples will be produced as defined in the design of the CubeSat material specification for the structure. A flat laminate of carbon composite is first produced, then the copper foil layer will be bonded to the carbon composite laminate. The complete MFC panel is then machined to the exact sample sizes required for tensile and bend testing of the material. The procedures outline from the ASTM standards will be followed for the tests and has been previously covered in the subsections of section 2.5.7.

Figure 3.43: The newer tensile test machine available at the engineering lab.

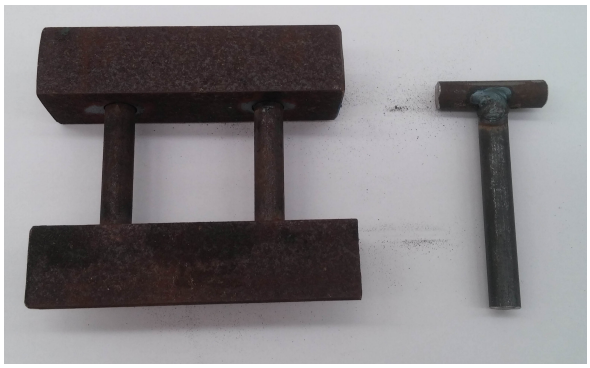

Figure 3.44: Bend Test jig for the composite sample testing.

The machine that will be used for the tensile and bending tests is shown in figure 3.43. A set of vice jaws is fitted to the machine in which the tensile composite samples are positioned and fastened. The bend tests are done using the jig shown in figure 3.44, the jig is very simple and appears crude, however, it is made to the exact specifications of the ASTM bend test standards. The bend test jig is positioned in the lower section of the material test machine and the push rod in the upper section of the machine.

The composite sample is positioned over the support pins of the jig and the push rod positioned to apply the load in the centre of the specimen. The position of the support pins and distance between the pins has been previously covered in section 2.5.7.

3.4.2 CubeSat Mock-up/Prototype Manufacture

The structure mock-up will be made using composite panels made to the designed specifications as covered in the material design section. The panel will consist of 3 layers of carbon fibre in the design orientations, an adhesive layer and finally, an FR4 backed copper foil layer on the panels inner surface. A commonly available carbon fibre twill weave fabric, as used for the data for the simulations will be used to manufacture the panels. This is a 2/2 twill weave carbon composite and 0.2 mm dry fabric thickness. (Data in Table 3.1)
The aluminium rail components will be 3D printed from ABS plastic. The 3D printed components will allow the mock up model to be tested for form and fit before the rails are machined from aluminium. The aluminium rails will be machined from 7075 aerospace grade aluminium, once the design of the prototype model has been confirmed using the 3D printed version. A mock-up ADS will be 3D printed as it will once again provide a visual form and fit analysis of the ADS unit into the MFC structure.
Both mock-up models will be fastened together using countersunk screws as it was designed to be constructed. The 3D printed mock-up model will use standard galvanised M3 countersunk screws and not the stainless steel screws, that will be used for the full version aluminium rail prototype. This is done to reduce the overall cost of the mock-up unit.

3.4.3 Modal Analysis Verification Test Plan

In order to verify the data produced by the numerical modal simulations done in ABAQUS, a vibration rig was designed and built to perform empirical modal data collection. The reason the jig was built was due to the fact that the modal test facilities do not exist at the university where this research is taking place and the varsity did not have the required funding to have the testing outsourced to an equipped facility. The vibration jig was personally funded and built for the purpose of this research.
A detailed description of the construction process and the engineering that took place to develop the test bench will be covered in a further academic paper that will cover specifically the modal test rig development. For the purpose of this research, an outline of the functions of the test bench is presented.

The vibration test bench was created using a large subwoofer speaker, mounted in a strong supawood box and driven by a large powerful automotive amplifier. The amplifier is powered by a large 12-volt truck battery to provide a constant direct current (DC) power supply to the amp, which will minimise the noise output from the amplifier. Figure 3.45 and 3.46 illustrates the main subwoofer box assembly with the bolt flange bonded in the centre of the speaker cone. The bolted flange allows for the

removal and potential to develop further mounting jigs for other components to be tested in the future.

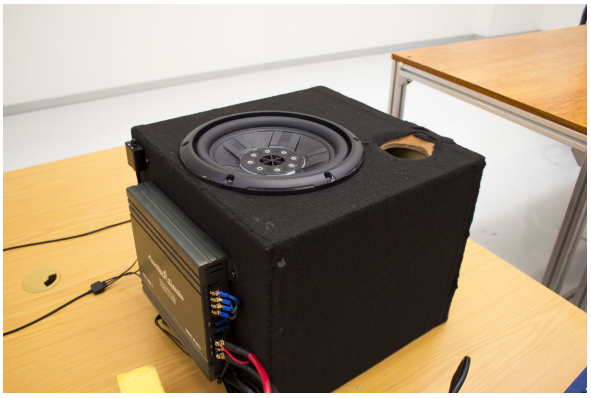

Figure 3.45: Subwoofer vibration rig, with power amp mounted on the side of the box.

Figure 3.46: Closer view of the bonded mounting flange in the speaker cone.

Figure 3.47 and 3.48 below shows the aluminium cage and speaker mounting system that was constructed to hold the CubeSat on the speaker. The assembly was attached to the speaker by means of mounting flanges bonded to the speaker cone that allows the bolting of the rest of the test rig assembly and the containment cage.

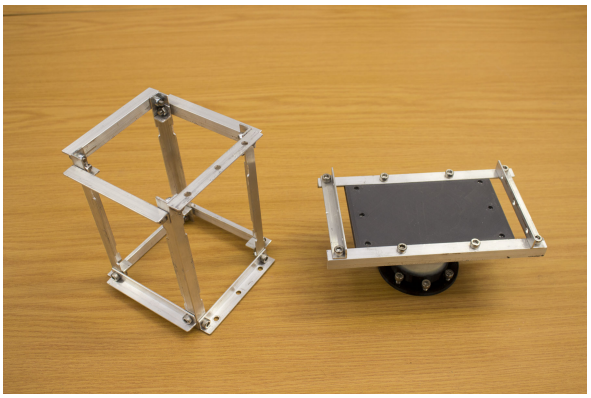

Figure 3.47: Aluminium CubeSat cage and the speaker interface mount.

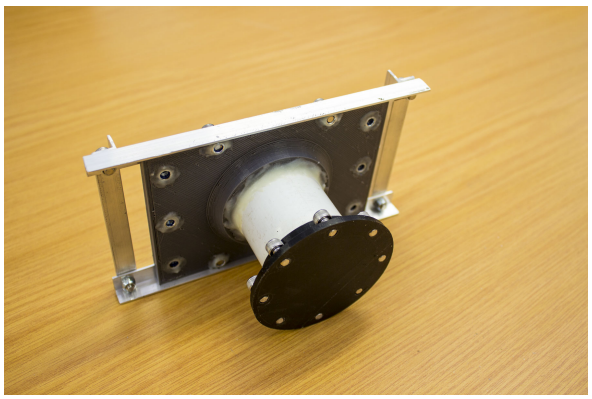

Figure 3.48: Bottom of the speaker interface mount.

The design of the aluminium cage assembly has been done in such a way to minimise the mass of the structure, however, maintain a high rigidity level that mimics the characteristics and the interface that the CubeSat would have with the P-POD used to launch the satellite in the actual conditions. Figure 3.49 and 3.50 illustrate the assembled vibration cage jig, with and without the CubeSat.

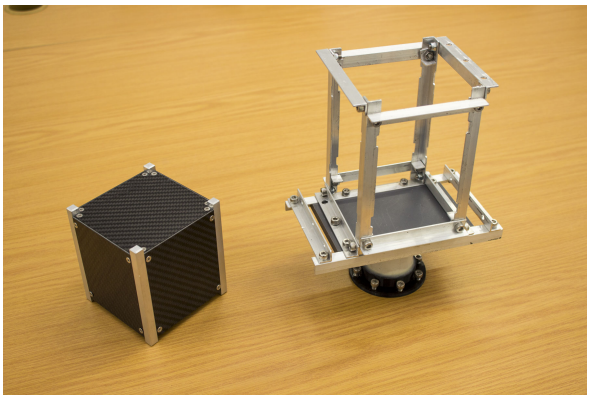

Figure 3.49: Aluminium CubeSat prototype and the empty vibration cage assembly.

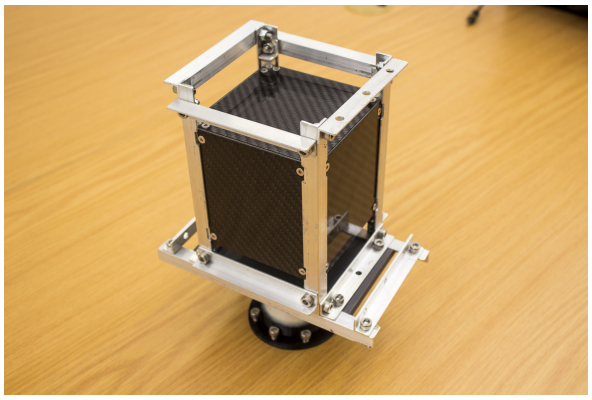

Figure 3.50: Fully assembled vibration cage with the CubeSat enclosed in the jig, the assembled mass is 690 grammes.

Once the test assembly has been completely constructed, the power amplifier is connected to an audio output jack on a computer. A MATLAB code was written to produce a sine wave output that ramps from 5Hz to 100Hz in 2 minutes, which follows the guidelines of the NASA test standards for sine wave vibration testing as mentioned previously in section 2.5.4. The amplitude of the output is governed by the power adjustment on the power amplifier itself. For this test, the amplification power is set as a constant. The objective is to measure any response from the satellite across this frequency range. To measure the response, an *Arduino* based accelerometer is placed on the top surface of the satellite and the acceleration data is recorded every millisecond. A plotting graph can be drawn using the *Arduino* program interface, however, a serial communication port recording program was used to capture the signal data from the *Arduino* board for further post-processing in Microsoft Excel. A control reading was measured at the base of the vibration jig assembly to provide a control data set as for the direct output of the speaker profile. The accelerometer was then placed on the top surface of the satellite for the actual measurement.

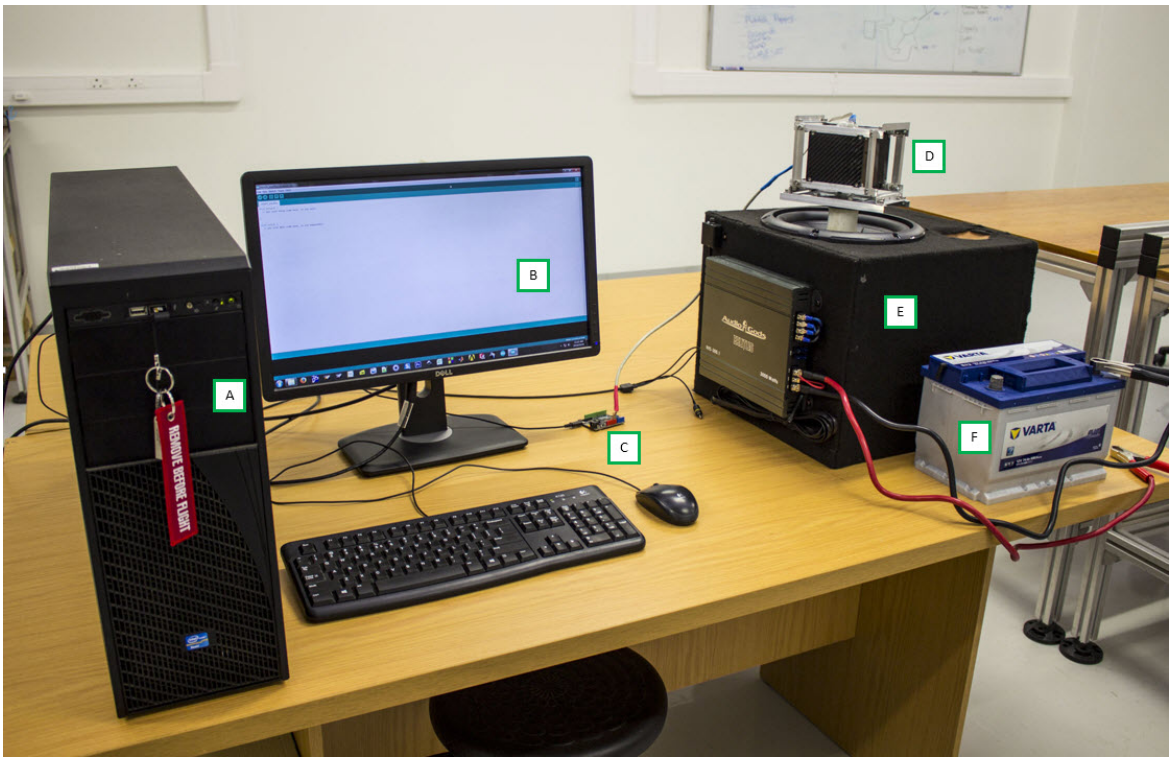

Figure 3.51: The full vibration test bench setup.

Figure 3.51 illustrates the complete test bench setup consisting of;

- A - Computer (output signal to speaker via audio jack and receive data from *Arduino*).
- B - *Arduino* software.
- C - *Arduino* board with an accelerometer attached.
- D - Vibration cage assembly with the CubeSat in a horizontal test configuration.
- E - Speaker assembly with mounted power amplifier.
- F - 12 volt DC battery to supply constant DC power.

Figures 3.52 and 3.53 show the two different design configurations of the cage assembly, with the accelerometer, mounted to the surface. The cage has been designed so that it can be mounted vertically or it can be turned 90 degrees to perform a horizontal axis test on the satellite. Control measurements were taken for both configurations before the actual tests were conducted and the accelerometer orientation was transposed onto the surface of the CubeSat to maintain the correct axis alignment for data comparison.

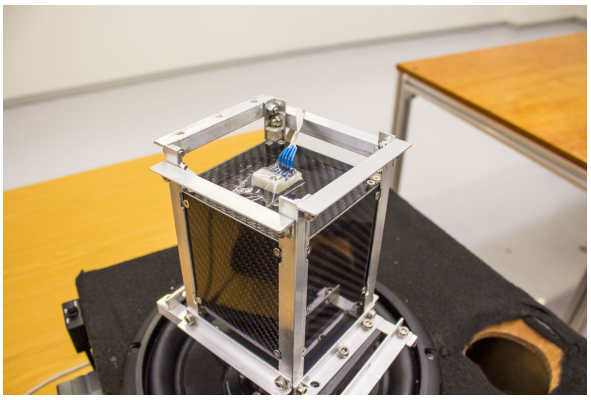

Figure 3.52: Vertical CubeSat vibration test configuration.

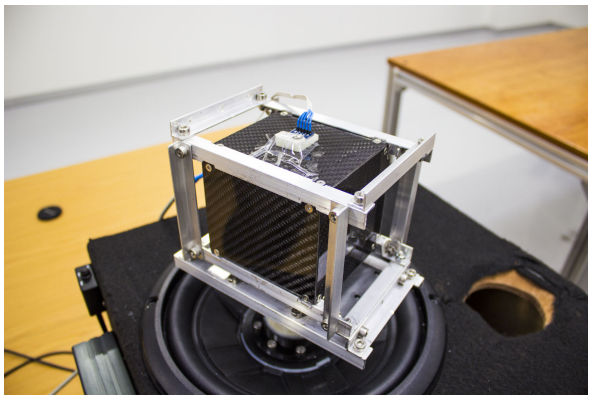

Figure 3.53: Horizontal CubeSat vibration test configuration.

Chapter 4

Numerical and Empirical Analysis Results

The purpose of this chapter is to present the data and results obtained from the numerical simulations and the empirical sample testing done on the composite material. The details for the set-up of each of the simulations has been described in Chapter 3. The discussion of the processed data and results will be covered in the following chapter. After the numerical analysis results section, the empirical results from the physical tensile and bending tests are presented and thereafter the manufacturing process that was used for the creation of the structural mock-up model.

4.1 Finite Element Analysis and Numerical Modelling

A number of FEA simulations have been performed across two different software packages. The majority of the simulations have been done using the ABAQUS FEA software package. Only the latter thermal orbit simulation has been done using *Siemens NX Space Thermal Systems*. Each of the simulations results have been presented in the marked sections that follow.

4.1.1 Virtual Material Tests

Using the *Autodesk Helius PFA* plug-in for ABAQUS, a specialist visual output (SDV1 Parameter) indicates the status of the material during the loading steps. The table below summarises the convention and data range indications.

0 to 1 - indicates the standard undamaged material state.
1 to 2 - indicates that matrix material failure/cracking has occurred.
2 to 3 - indicates that the fibres of the composite lamina have failed.

4.1.2 Tensile Test

The tensile test data presented in the FEA images below only consider the stressed zone of the sample (180 mm length) and not the full length of the sample. The last figure (4.8) illustrates the stress distribution considering the full sample length.

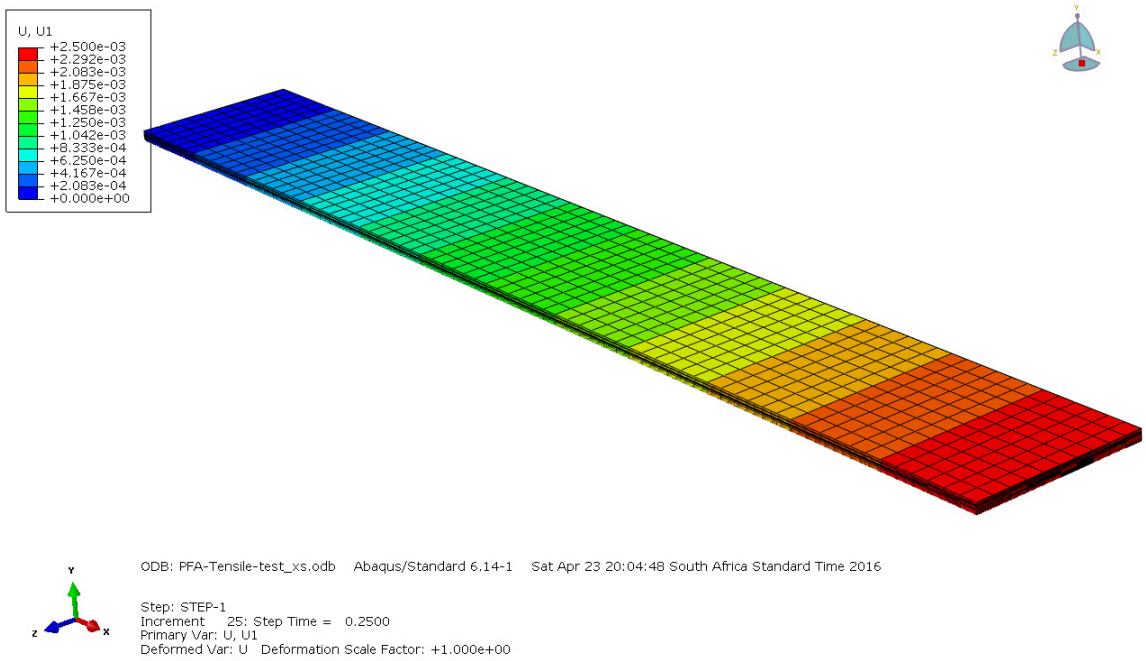

Figure 4.1: Deflection in the X-axis direction of the model (U1/Elongation).

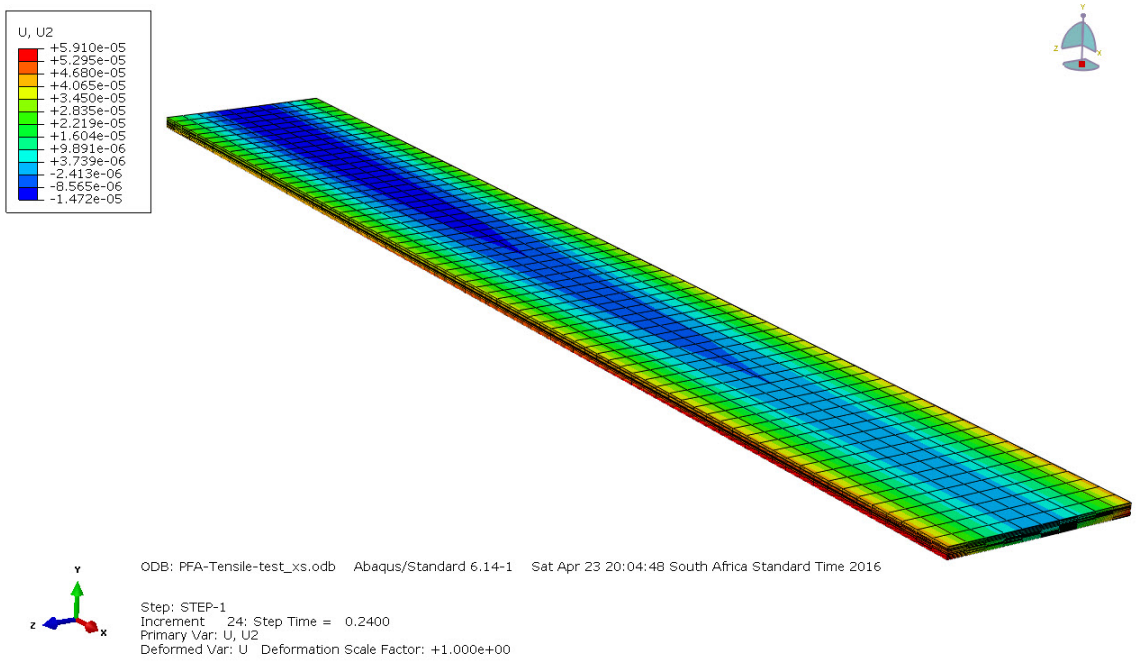

Figure 4.2: Deflection in the Y-axis direction of the model (U2/Bowing effect).

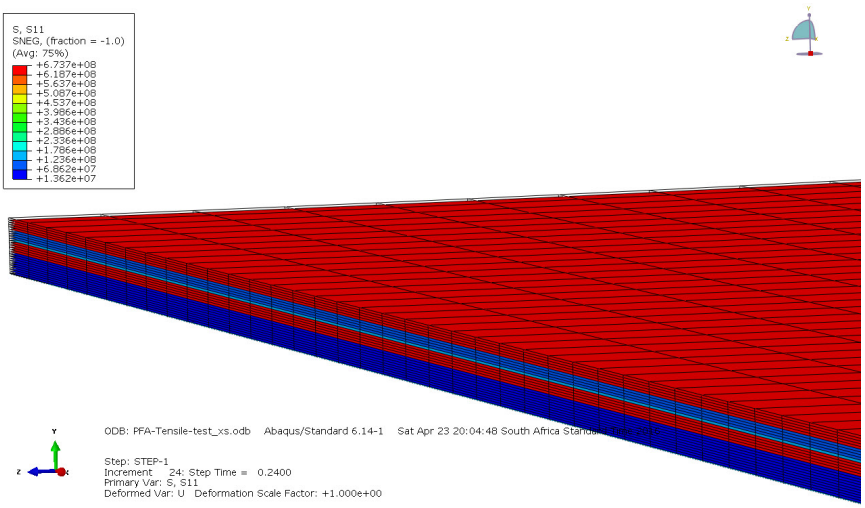

Figure 4.3: Maximum S11 (In-Plane Principle) stress in the material layers just before failure.

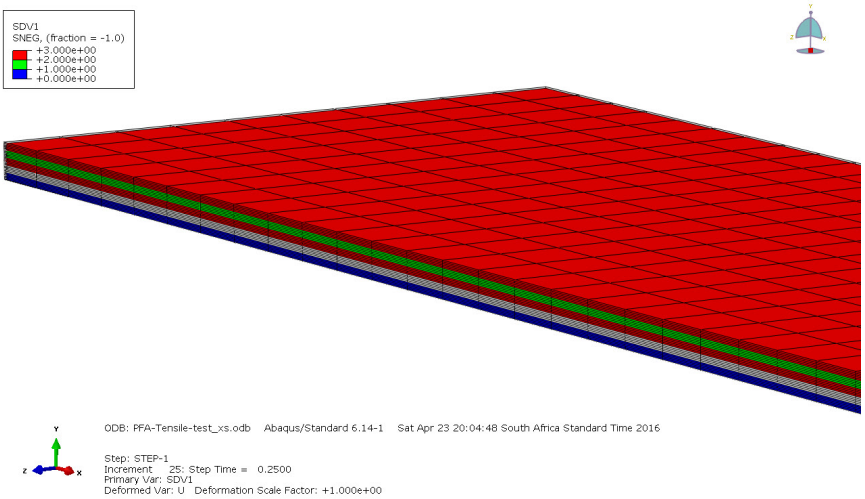

Figure 4.4: *Helius PFA* SDV1 indicates the material failure stages, this is the indication of the primary load lamina failure point.

In relation to the graph shown in Figure 4.6, the deviation seen at deflections of 0.8 and 1.5 mm are the points at which the matrix failure occurred in the primary (0/90 deg) layers and 45-degree carbon lamina layers respectively. Figure 4.5 provides an indication of the complete matrix material failure of all the carbon composite lamina at approximately 1.5 mm deflection.

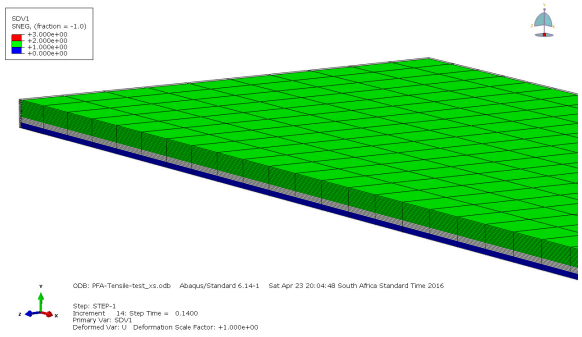

Figure 4.5: Complete matrix failure of all carbon lamina.

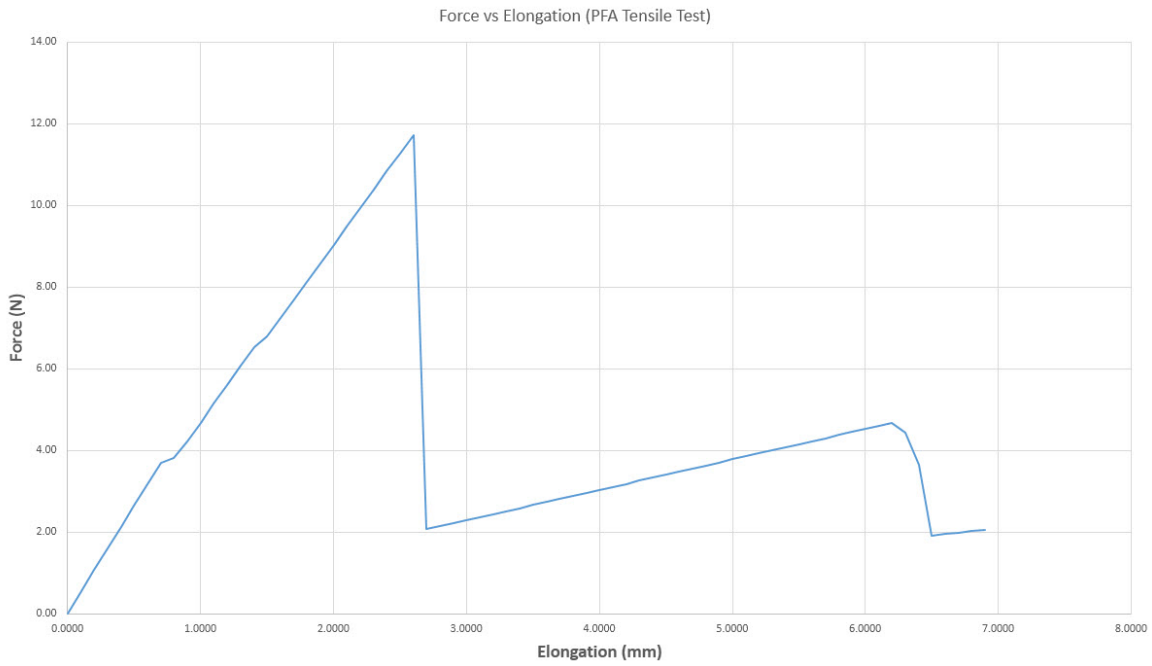

Figure 4.6: Force versus Elongation graph of the tensile material test performed in ABAQUS with PFA.

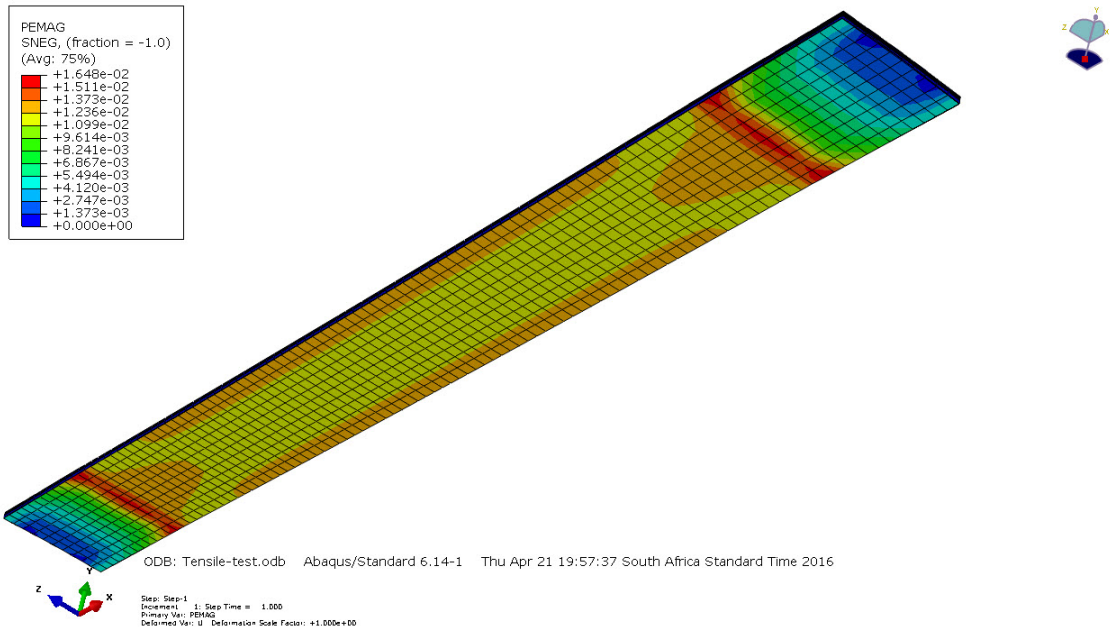

Figure 4.7: The magnitude of the plastic deformation of the copper foil layer (PEMAG).

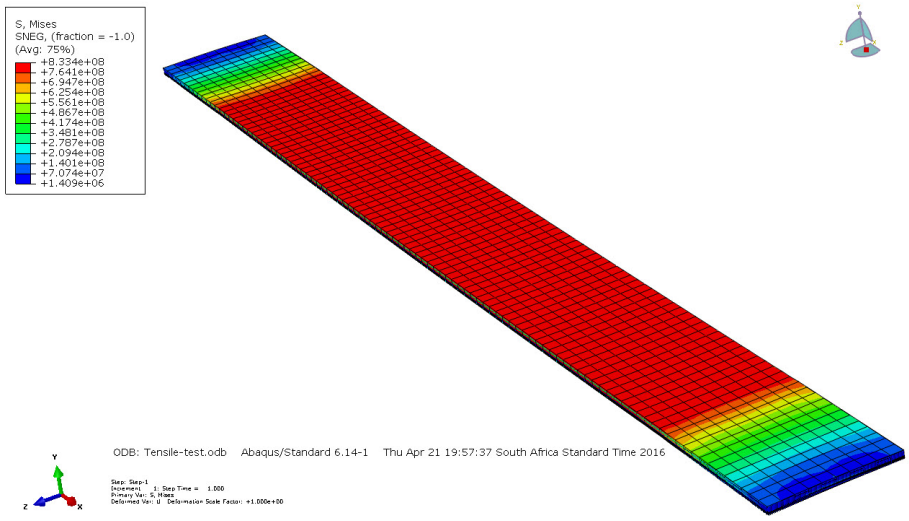

Figure 4.8: Stress distribution plot of the full model including the stress profile in the vice of the machine.

4.1.3 Bend Tests

4.1.3.1 Copper side up (compression)

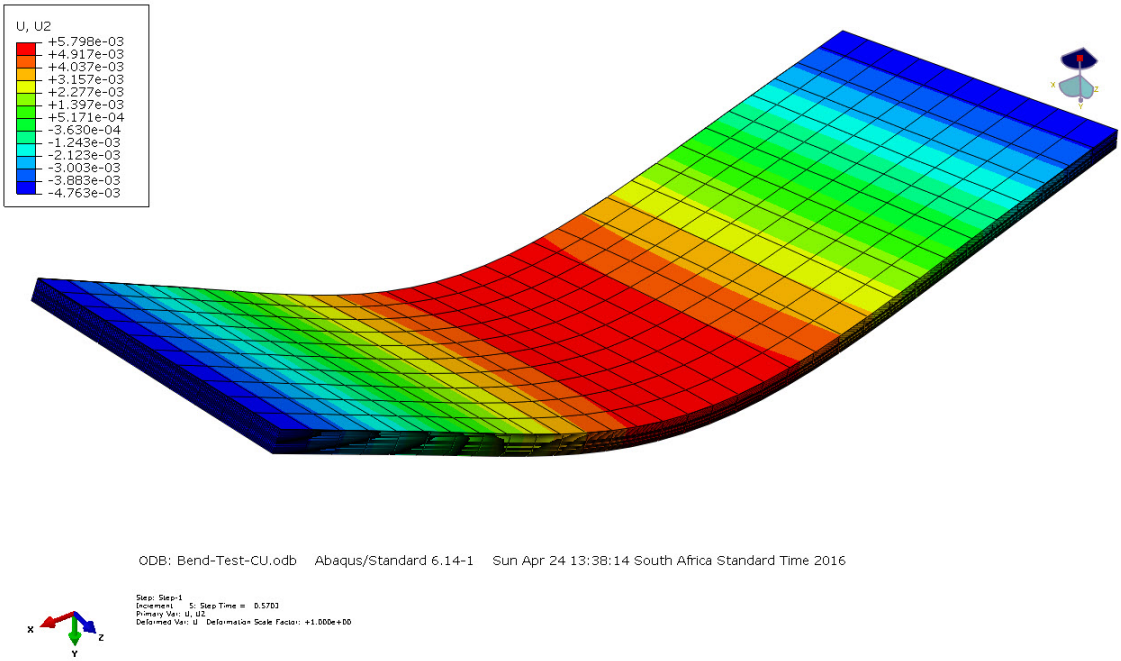

Figure 4.9: Downward Deflection of the sample in the Y-axis (U2), copper up.

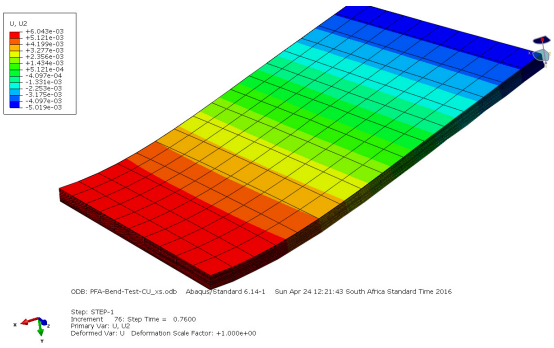

Figure 4.10: Half section deflection (U2) of bend test sample, copper up.

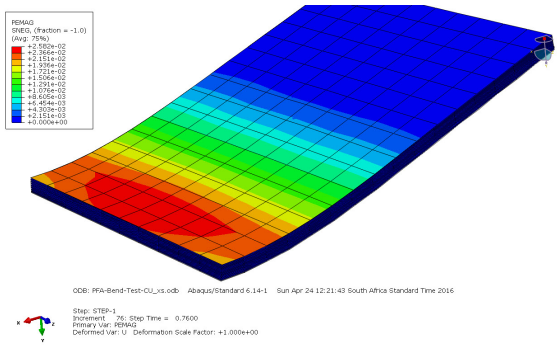

Figure 4.11: Half section bend sample magnitude of plastic deformation of the copper foil layer, copper up.

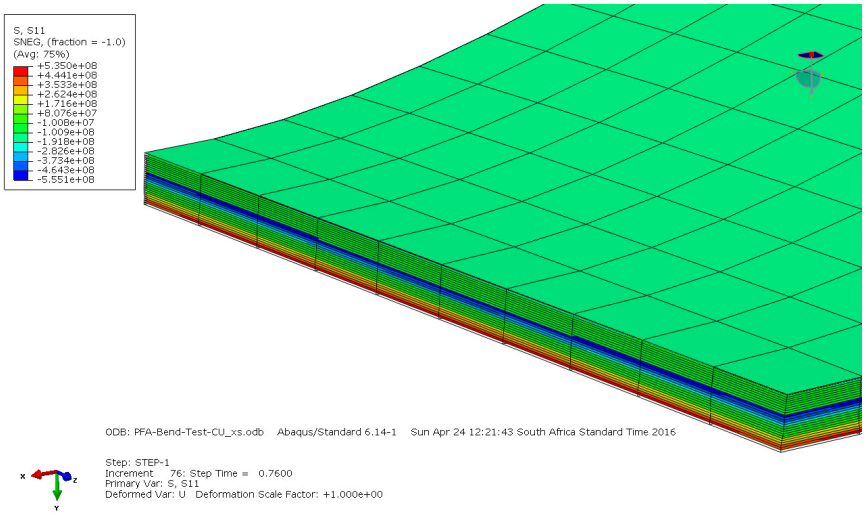

Figure 4.12: Half section bend sample maximum S11 stress (in-plane), copper up.

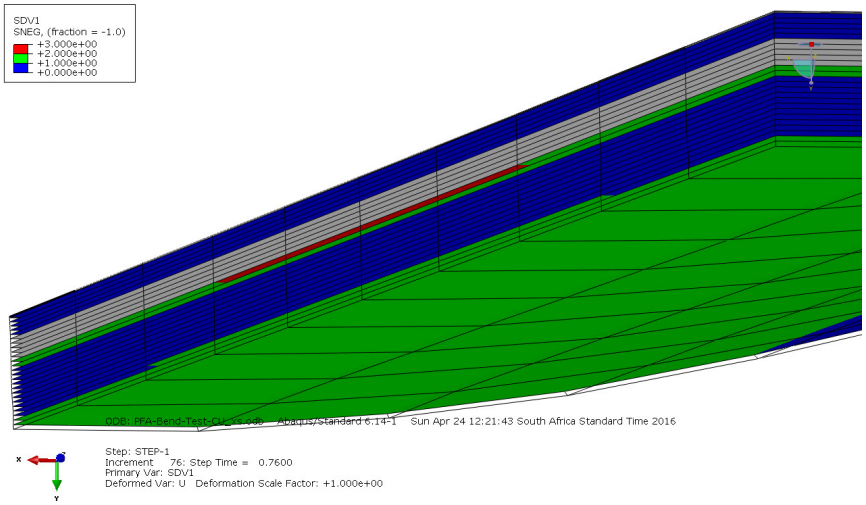

Figure 4.13: Half section bend sample SDV1 failure criteria plot, copper up.

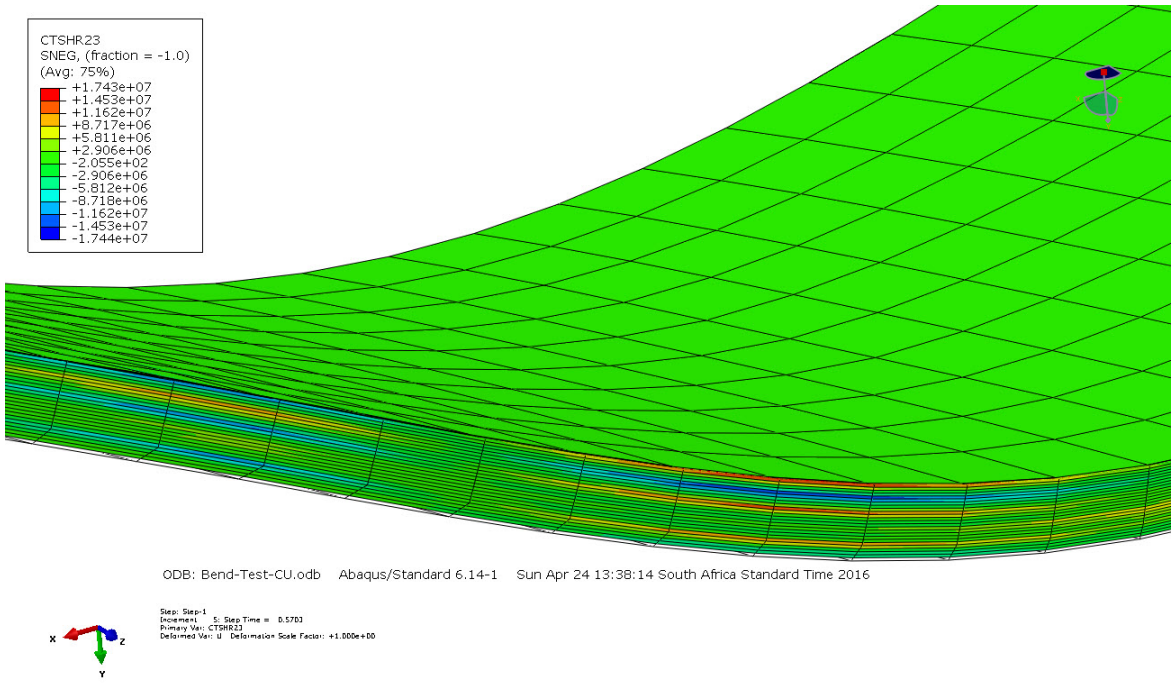

Figure 4.14: Half section bend sample transverse shear stress plot through the thickness, copper up.

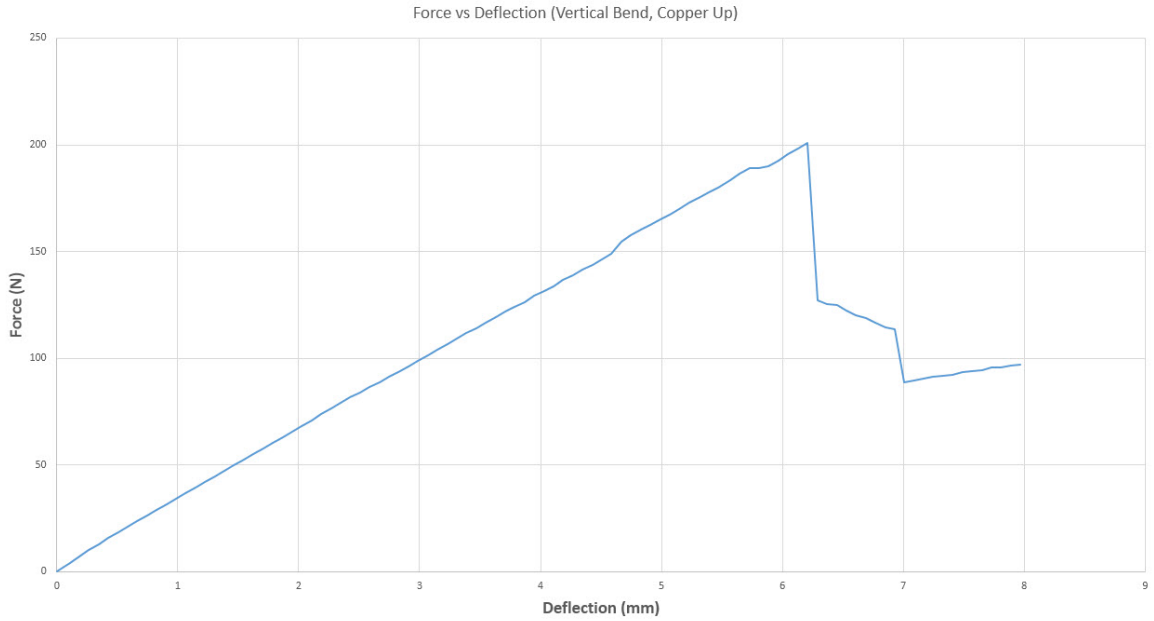

Figure 4.15: Force verse deflection graph, copper up sample.

4.1.3.2 Copper side down (tensile)

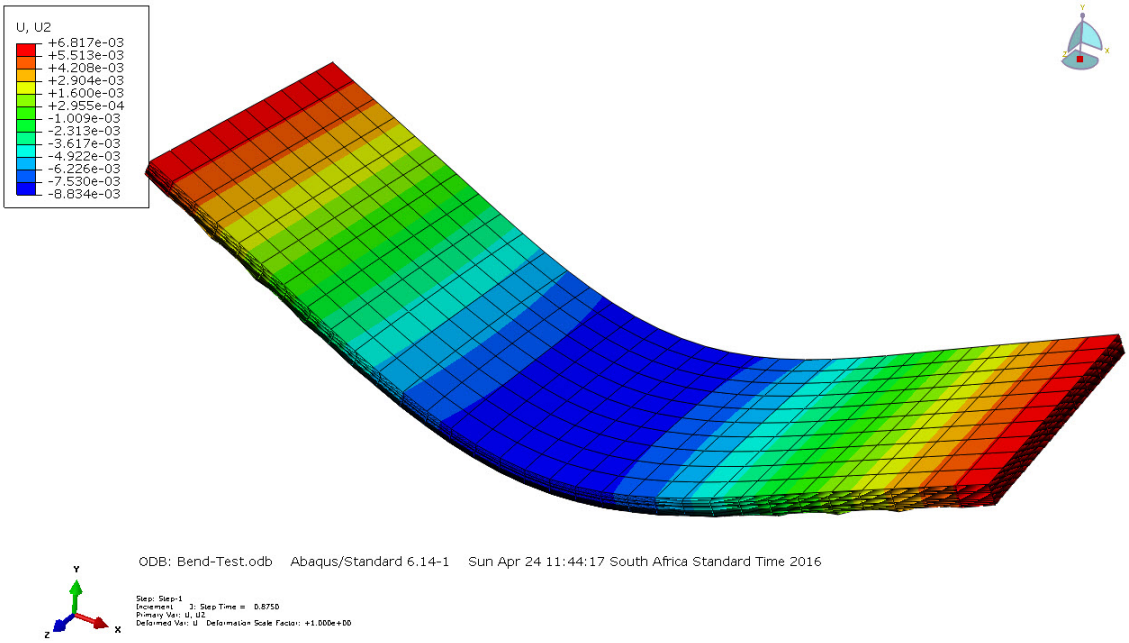

Figure 4.16: Downward Deflection of the sample in the Y-axis (U2), copper down.

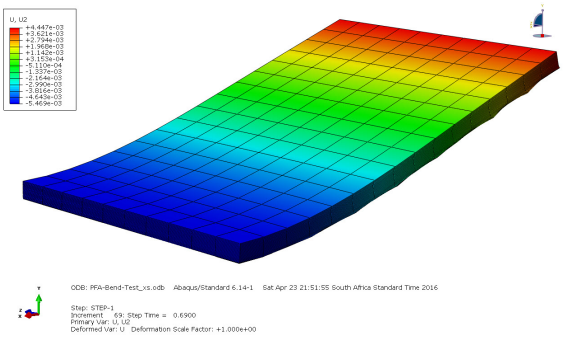

Figure 4.17: Half section deflection (U2) of bend test sample, copper down.

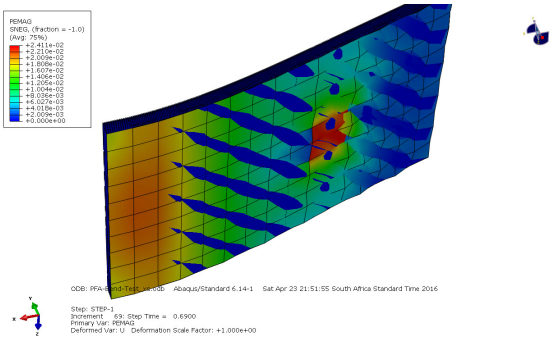

Figure 4.18: Half section bend sample magnitude of plastic deformation of the copper foil layer, copper down.

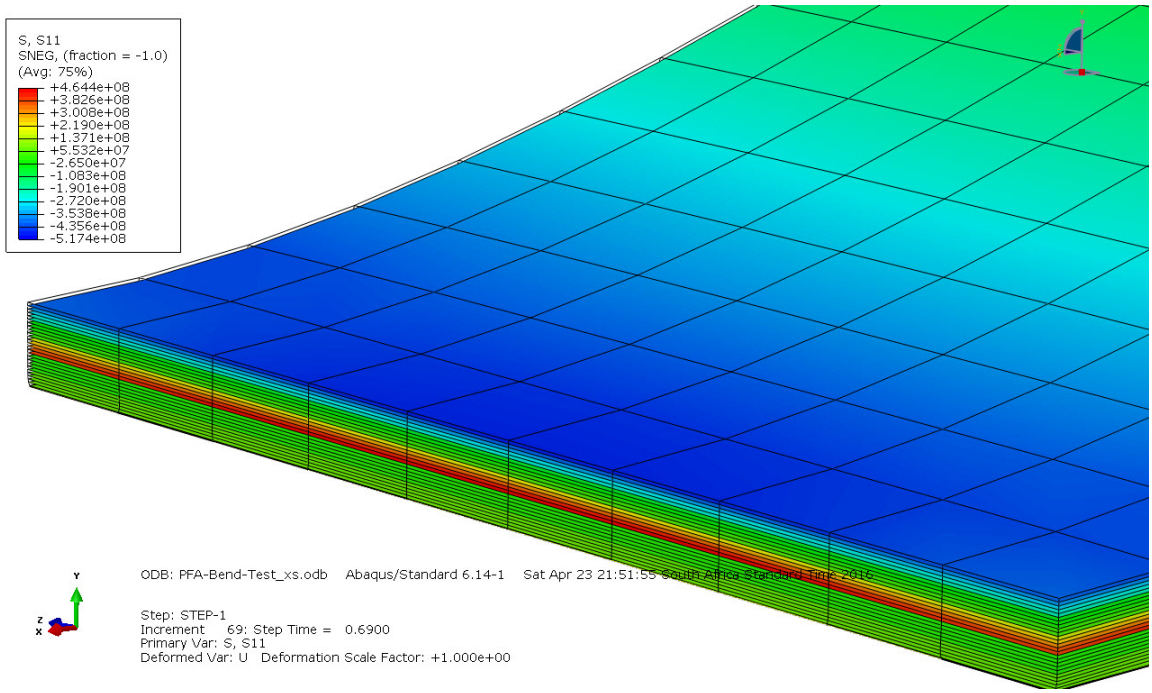

Figure 4.19: Half section bend sample maximum S11 stress (in-plane), copper down.

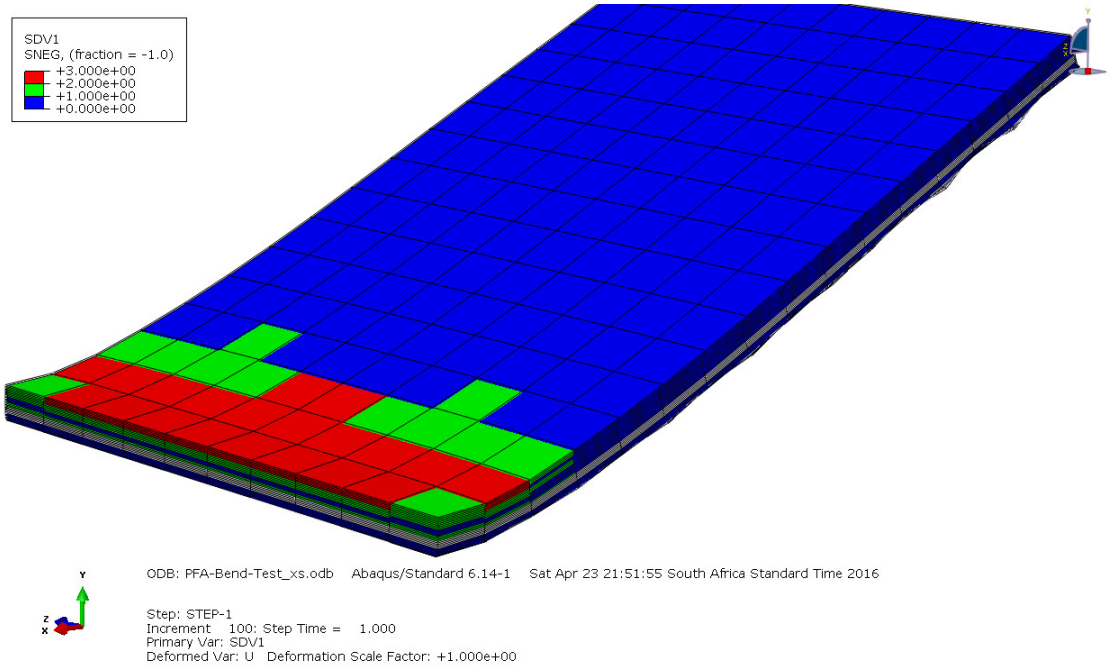

Figure 4.20: Half section bend sample SDV1 failure criteria plot, copper down.

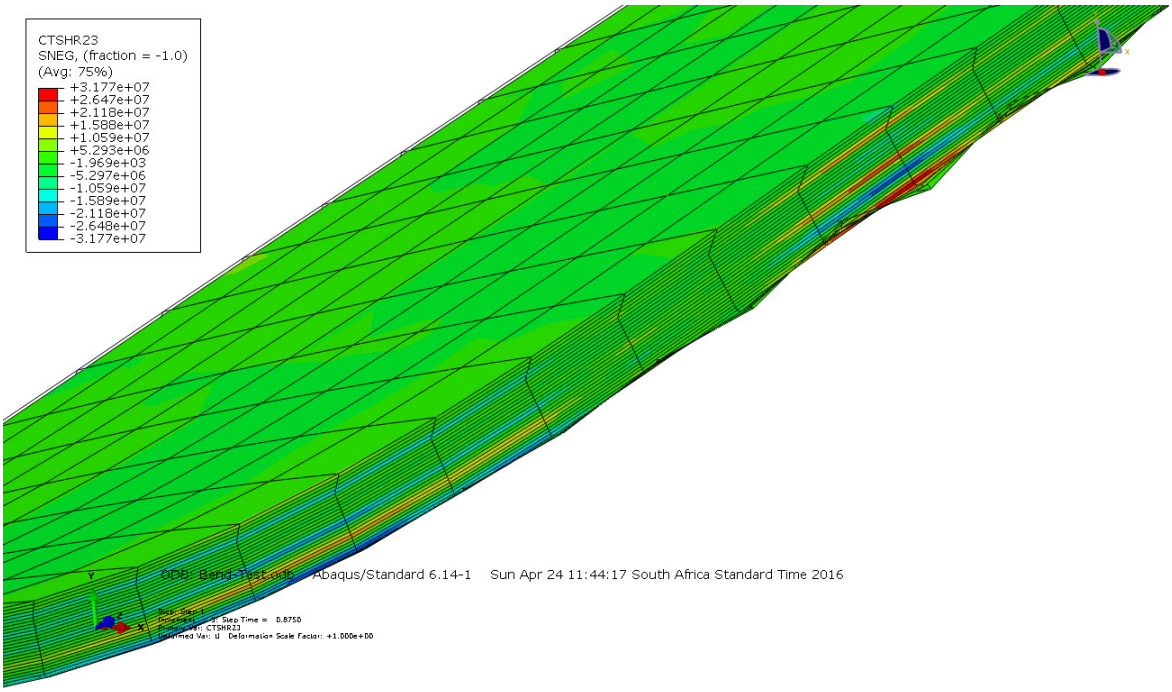

Figure 4.21: Half section bend sample transverse shear stress plot through the thickness, copper down.

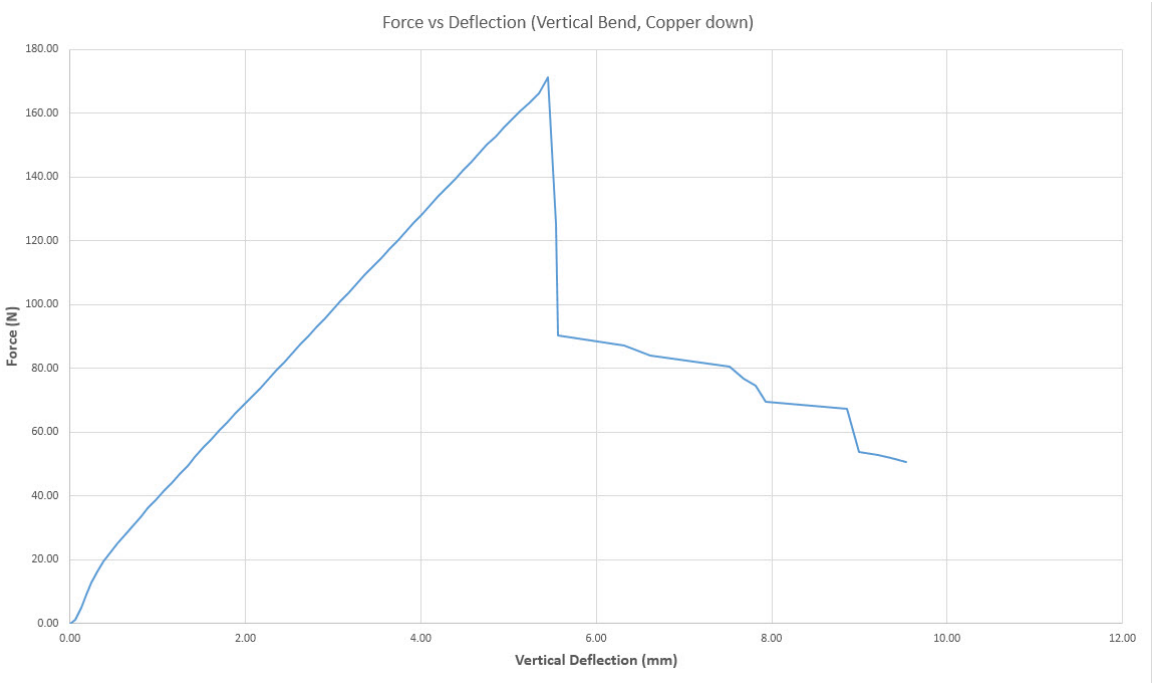

Figure 4.22: Force verse deflection graph, copper down sample.

4.1.4 Full Panel CubeSat Numerical Modal Data

The data presented in this section is for the full standard carbon CubeSat design that has the fully completed side panels without any weight reduction cutaways as

discussed in section 3.2.2.3. The main data of interest is the deflection and maximum stress induced in the components of the satellite structure.

4.1.4.1 Bolt preload conditions

For the bolt pre-loading applied to the screws used to fasten the panels to the CubeSat structure, the following ABAQUS simulation data was observed:

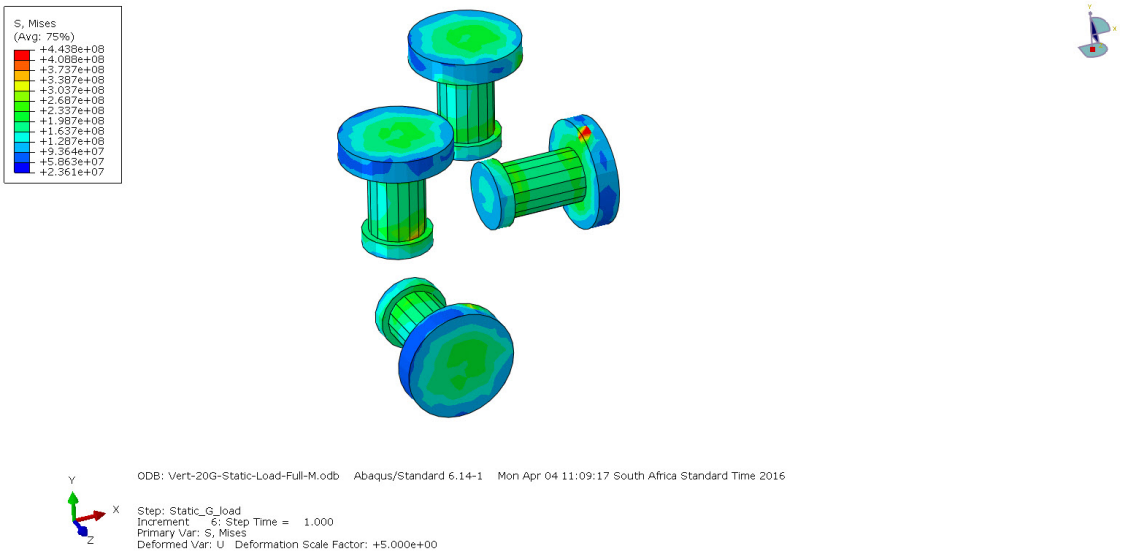

Figure 4.23: Maximum von Mises stress induced in the bolts due to the bolt loads applied.

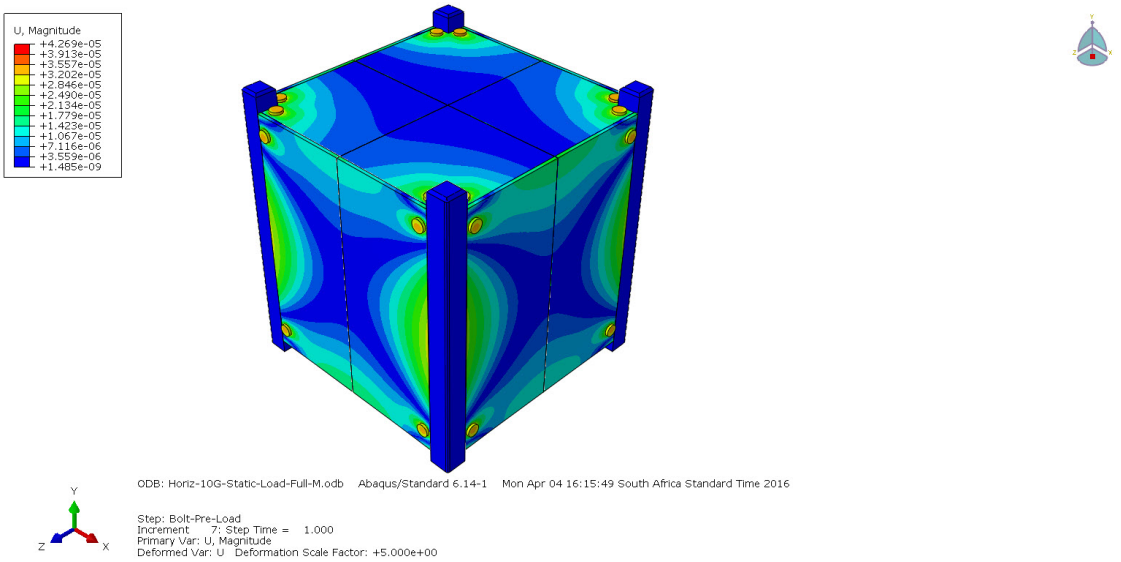

Figure 4.24: Maximum overall deflection due to the applied bolt loads.

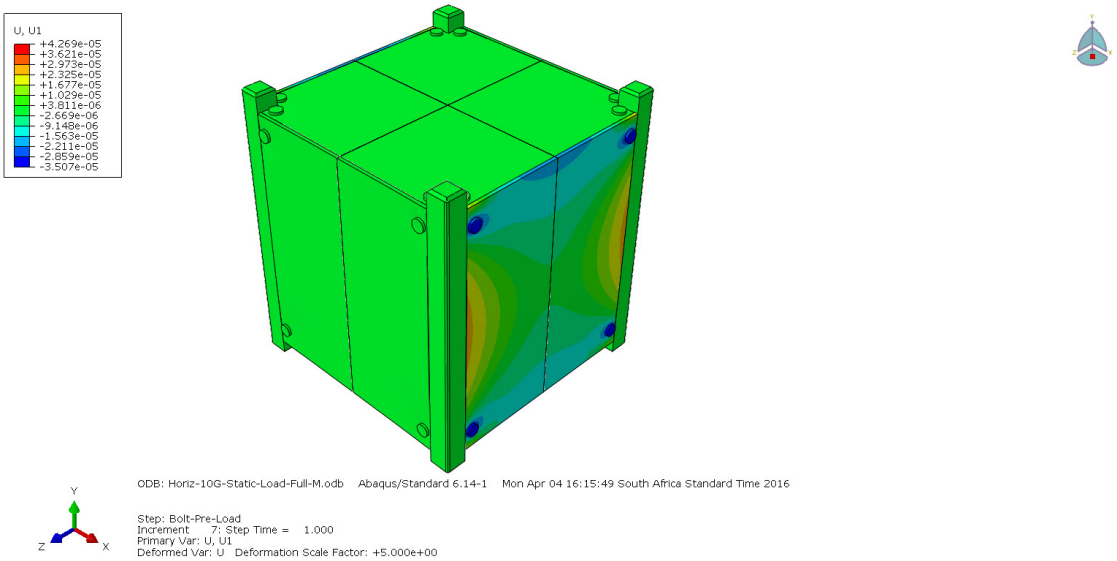

Figure 4.25: U1 deflection due to the applied bolt loads.

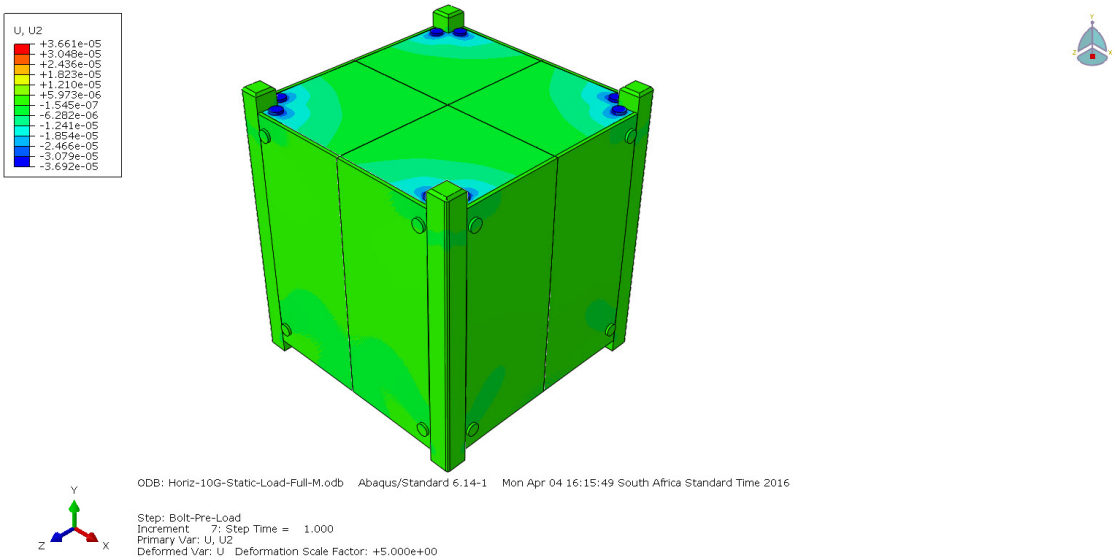

Figure 4.26: U2 deflection due to the applied bolt loads.

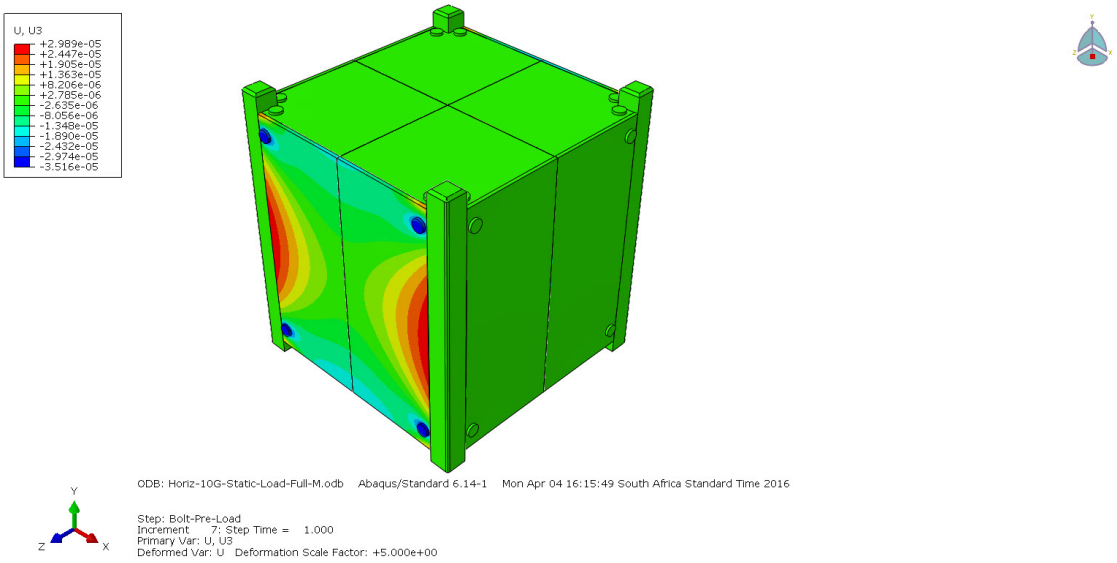

Figure 4.27: U3 deflection due to the applied bolt loads.

In this case, the maximum stress in the model occurred in the bolts them-self when the bolt loads were applied to the model and were virtually not affected by the applied loads in the simulations that follow, thus for each of the concept models considered the stress outputs were not repeated in the sack to save space in the thesis. The stress induced in the composite panels were so low that no practical data plot could be created.

4.1.4.2 Structural Static Load Results

4.1.4.2.1 Vertical Static Load The vertical loading as specified in the simulation description is the gravity load applied in a line parallel with the aluminium rails.

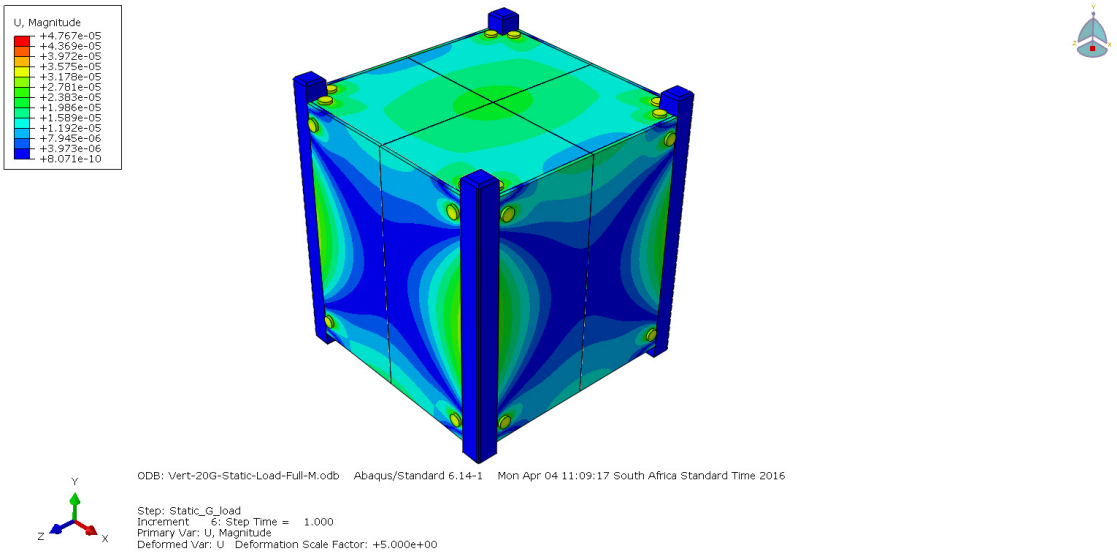

Figure 4.28: Maximum overall deflection due to the applied 20 g vertical static gravity load.

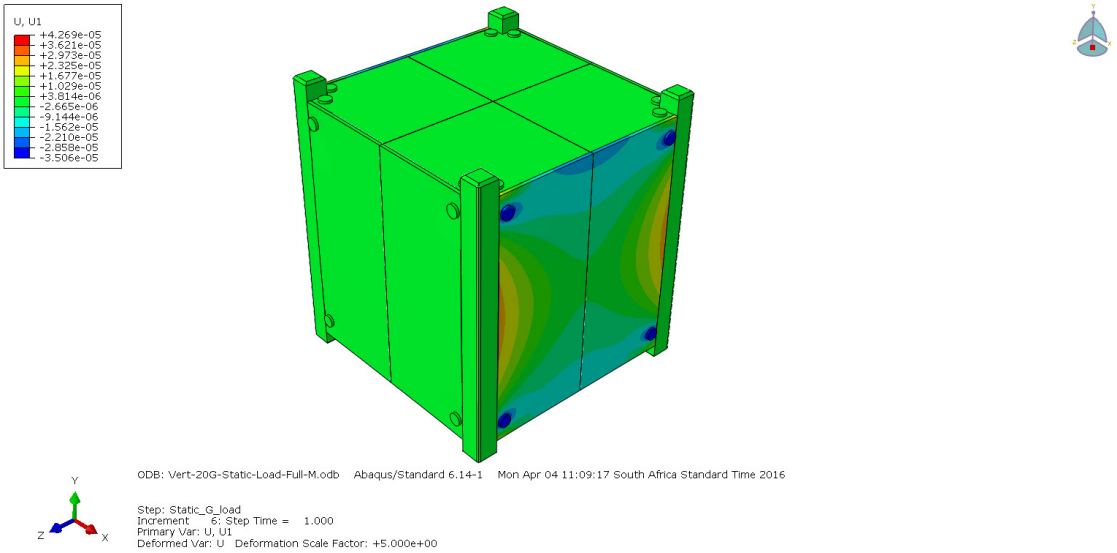

Figure 4.29: U1 deflection due to the applied 20 g vertical static gravity load.

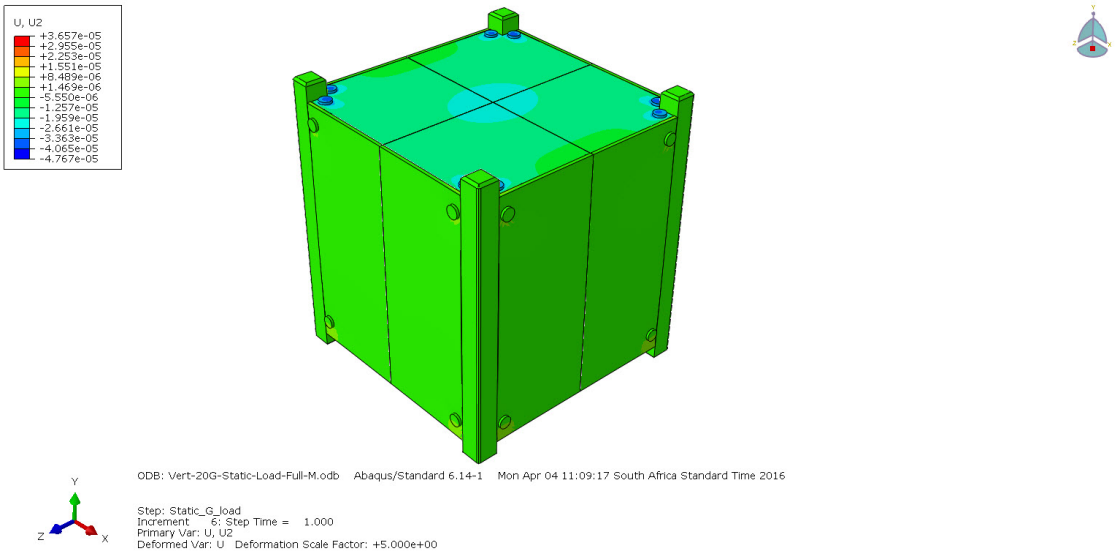

Figure 4.30: U2 deflection due to the applied 20 g vertical static gravity load.

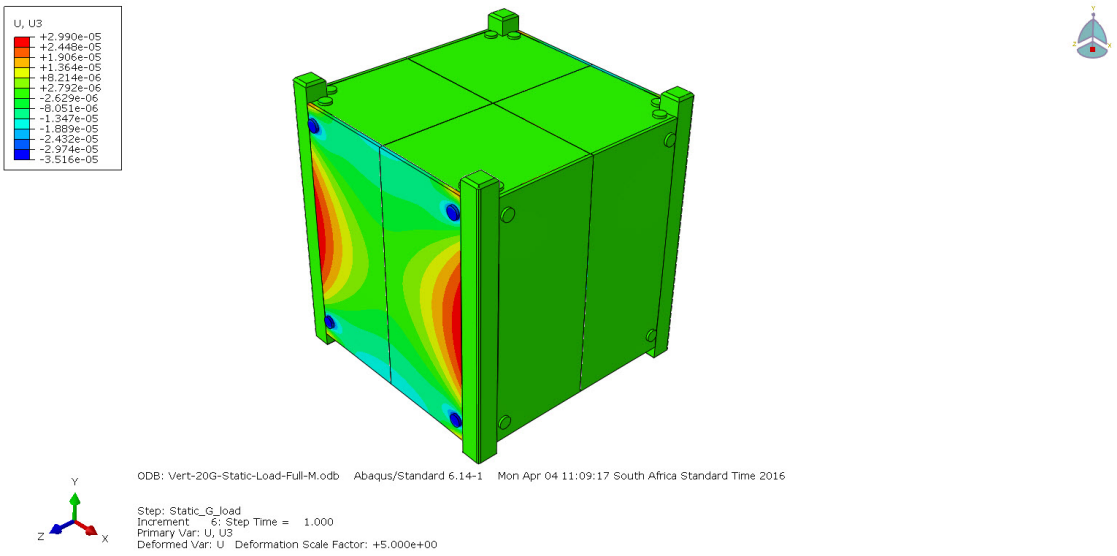

Figure 4.31: U3 deflection due to the applied 20 g vertical static gravity load.

4.1.4.2.2 Horizontal Static Load The horizontal loading is a 10 g gravity load applied in a line across the lines of the aluminium rails. (two possible axes could be used due to the satellites' symmetry).

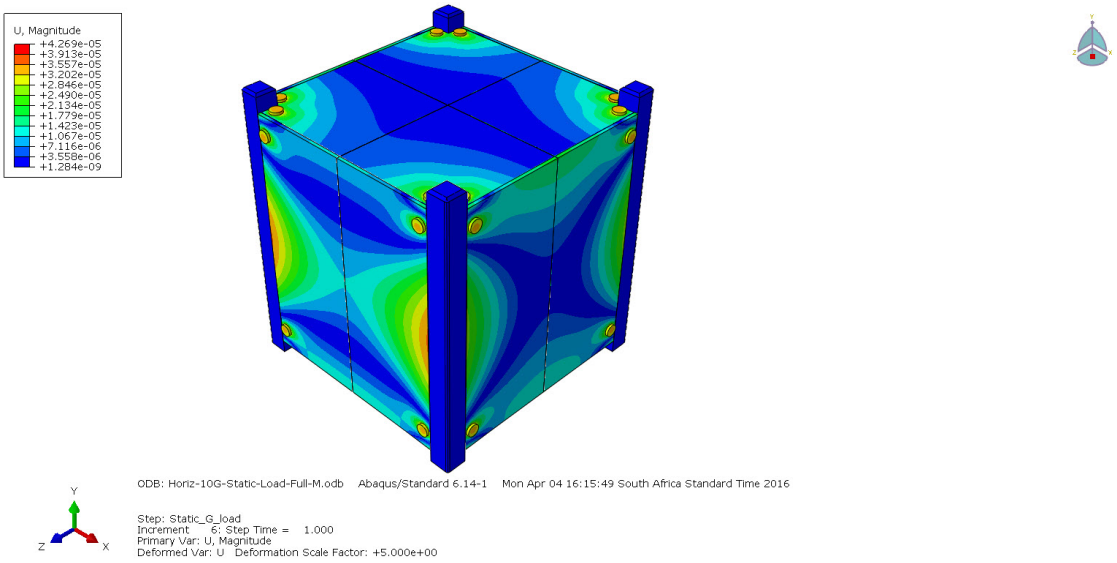

Figure 4.32: Maximum overall deflection due to the applied 10 g horizontal static gravity load.

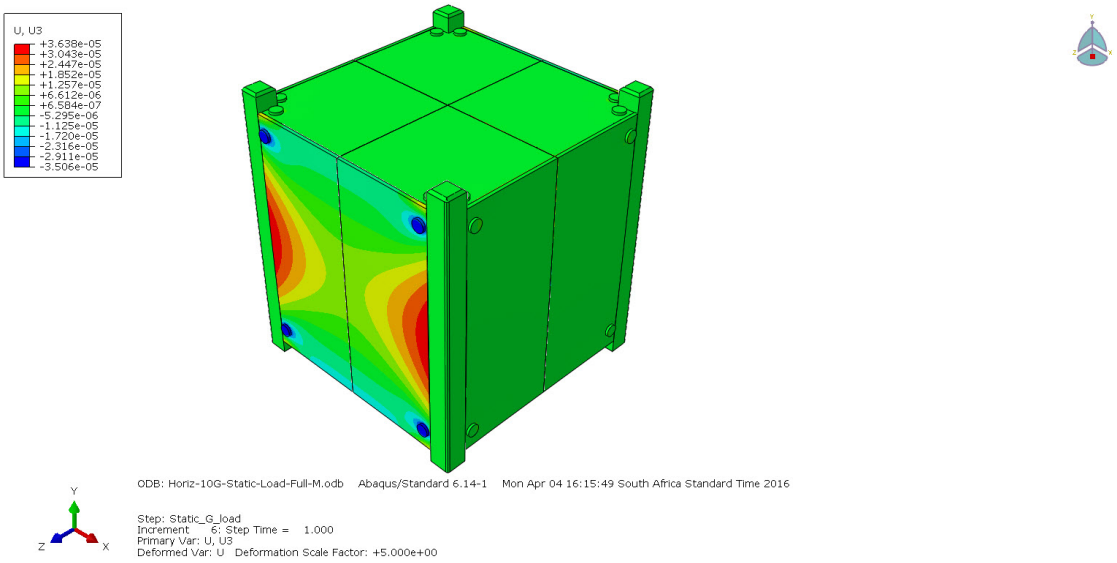

Figure 4.33: U3 deflection due to the applied 10 g horizontal static gravity load.

4.1.4.3 Conventional aluminium structure response to static loads

A conventional aluminium CubeSat chassis was subjected to a static acceleration load analysis to provide a means of comparison between the carbon fibre CubeSat that is being designed in this research effort and the commercially available aluminium structure The FEA model used tetrahedron mesh elements, with a 3D stress linear element type and general aluminium material properties assigned to the section. Quadratic elements were used to compare the difference in result and very little difference in the simulation results were found with a large increase in computation time per setup.

The vertical axis (parallel to the rails) was subjected to a 20 g static gravity load and the horizontal axis was subject to a 10 g gravity load. The loading and boundary conditions were setup in such a way as to recreate the loading applied to the composite CubeSat prototype, which will allow for the most accurately numerical analysis performance comparison. The sub-section below show the results for each simulation case.

4.1.4.3.1 Vertical Static Load .

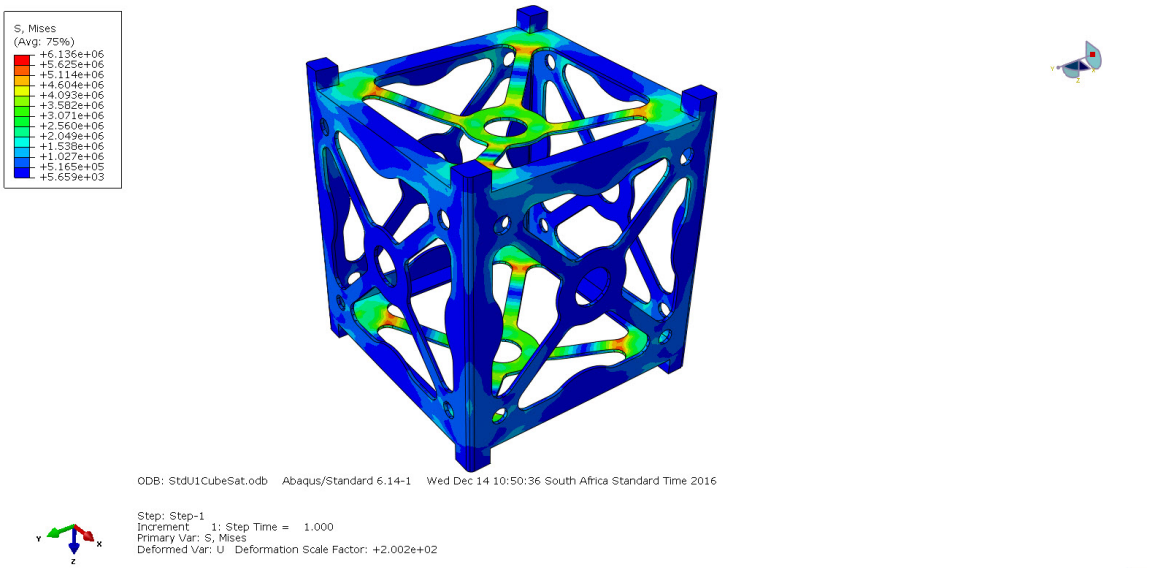

Figure 4.34: Maximum Von Mises stress due to the applied 20 g vertical static gravity load.

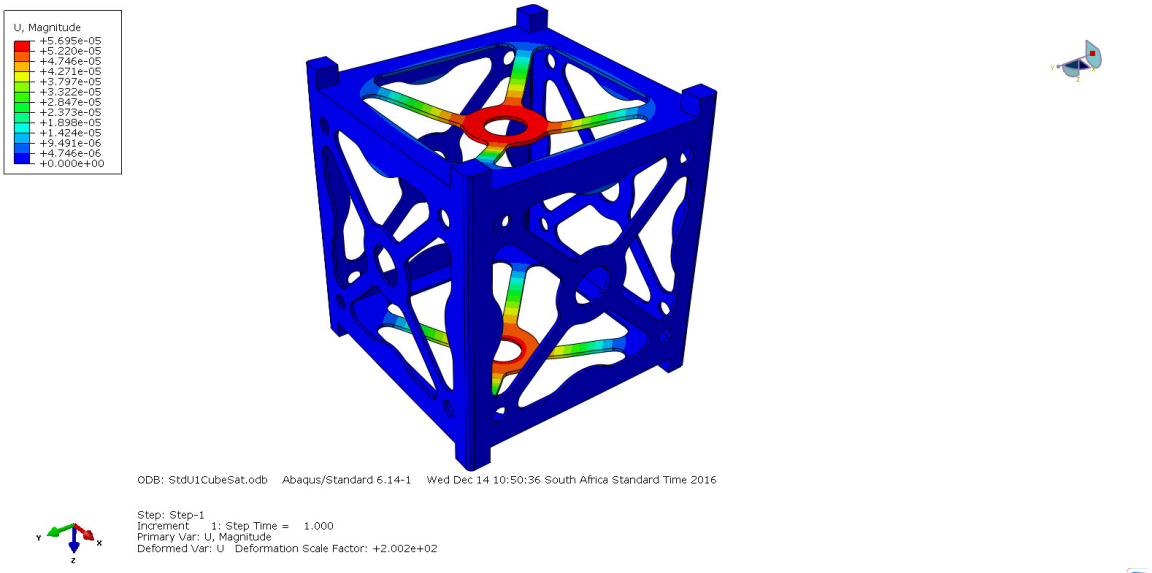

Figure 4.35: Maximum overall deflection due to the applied 20 g vertical static gravity load.

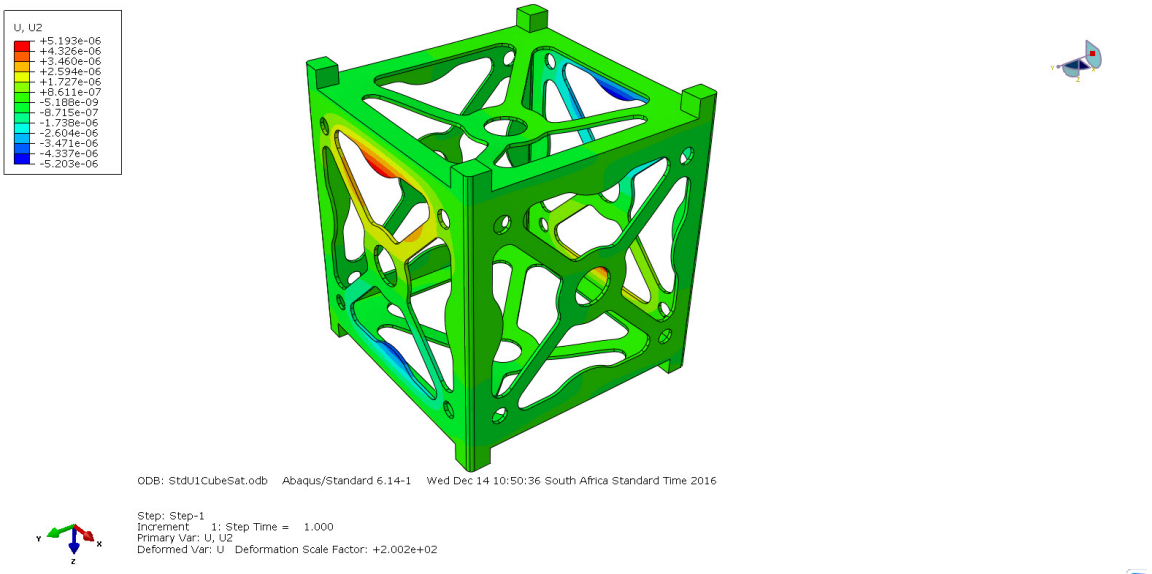

Figure 4.36: Deflection in the U2 (y) axis which has a symmetrical result in the x-axis.

4.1.4.3.2 Horizontal Static Load .

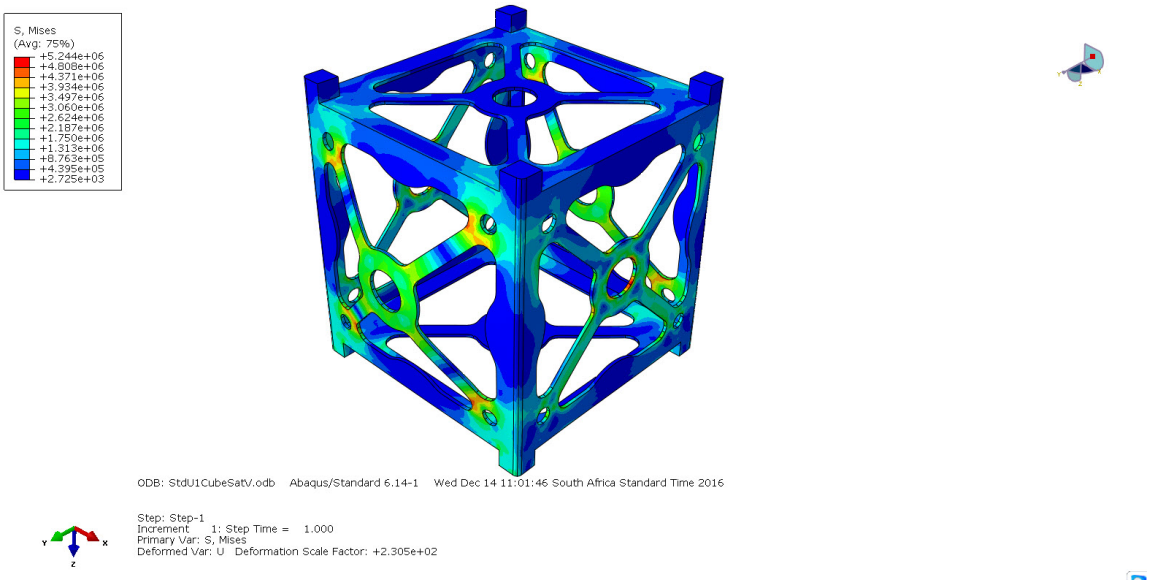

Figure 4.37: Maximum Von Mises stress due to the applied 10 g horizontal static gravity load.

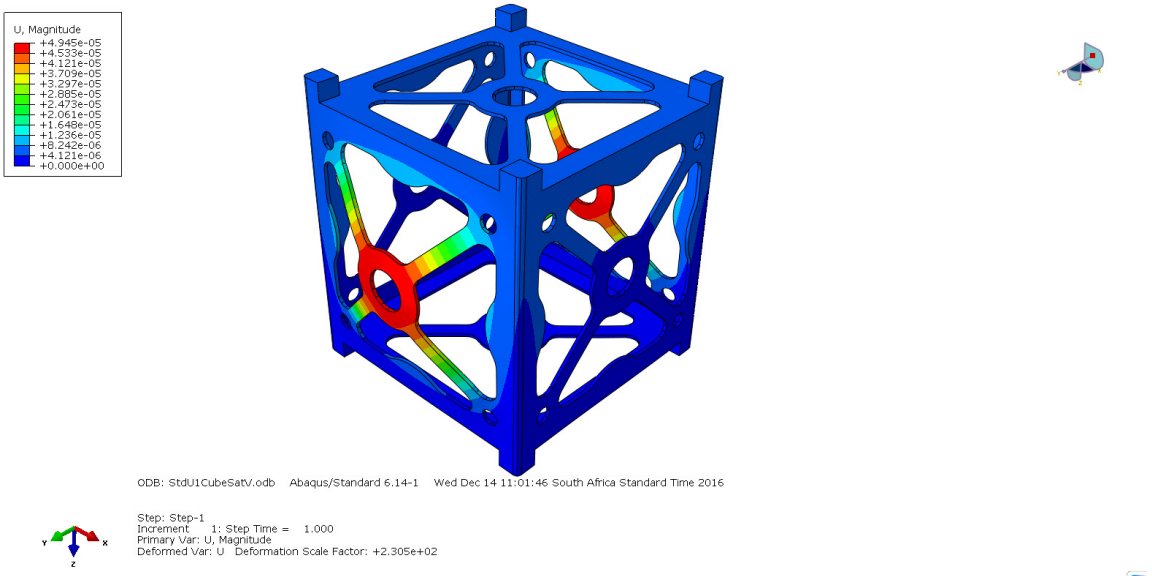

Figure 4.38: Maximum overall deflection due to the applied 10 g horizontal static gravity load.

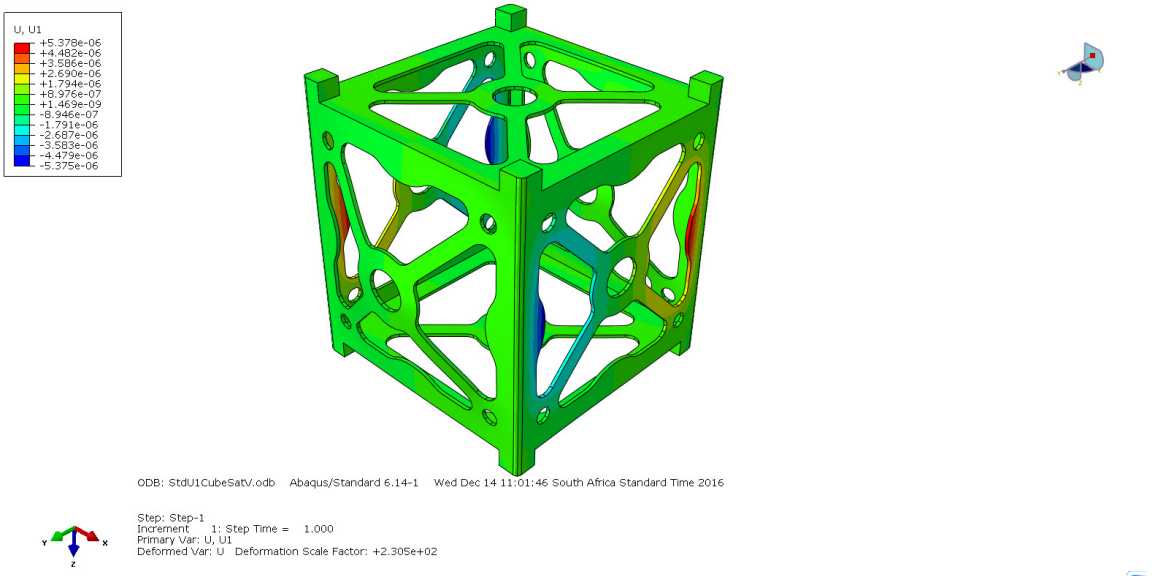

Figure 4.39: Deflection in the U2 (y) axis which has a symmetrical result in the x-axis.

4.1.4.4 Structural Natural Frequencies

The first 10 eigenvalues that represent the modes were outputted for the CubeSat structure. Below, each mode is shown and the frequency it occurred at, is also listed in the caption.

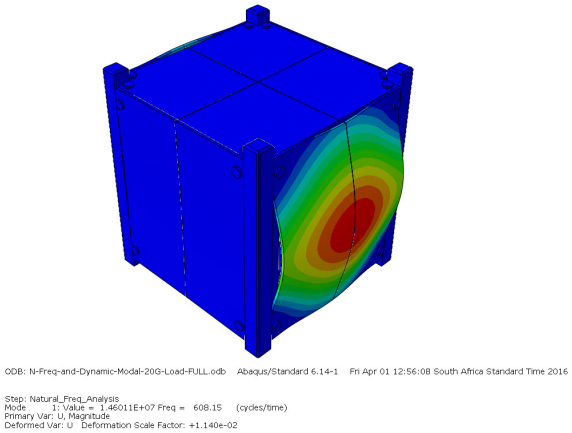

Figure 4.40: Mode 1 - 608Hz.

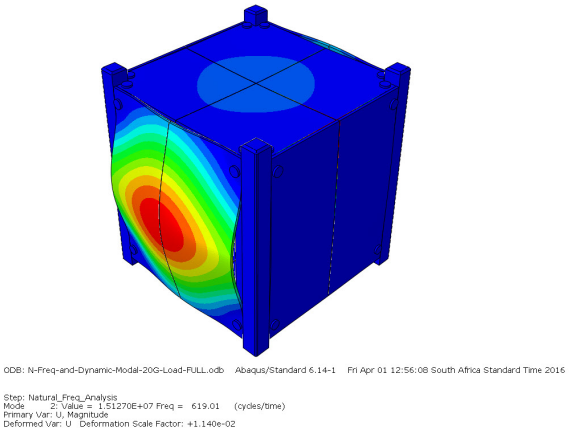

Figure 4.41: Mode 2 - 619Hz.

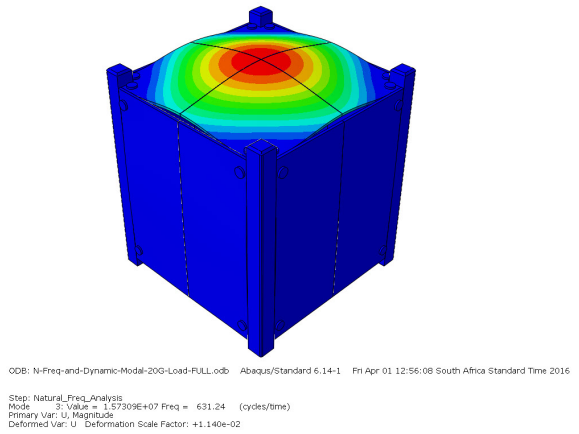

Figure 4.42: Mode 3 - 631Hz.

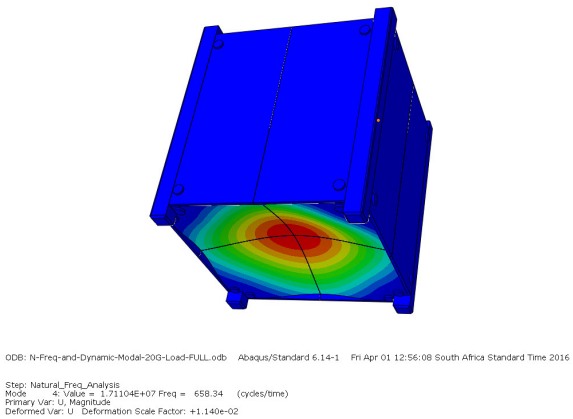

Figure 4.43: Mode 4 - 658Hz.

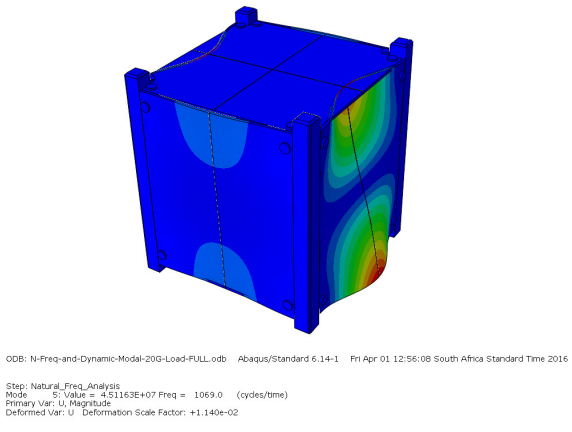

Figure 4.44: Mode 5 - 1069Hz.

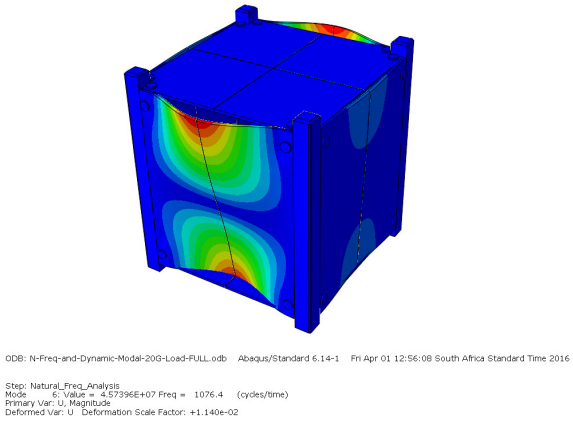

Figure 4.45: Mode 6 - 1076Hz.

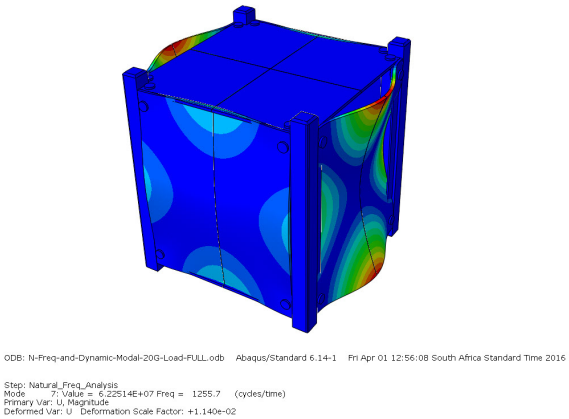

Figure 4.46: Mode 7 - 1255Hz.

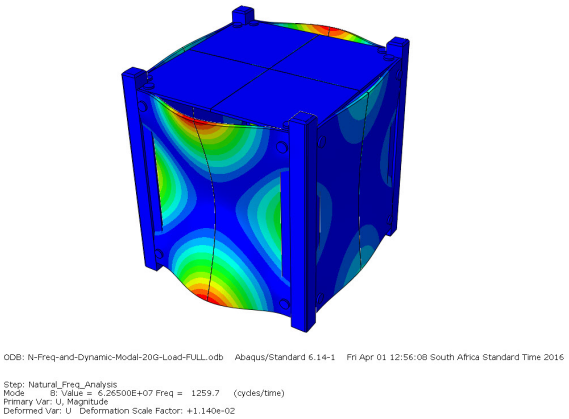

Figure 4.47: Mode 8 - 1260Hz.

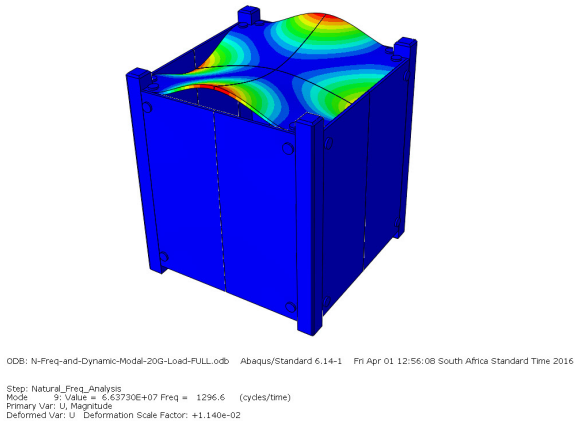

Figure 4.48: Mode 9 - 1297Hz.

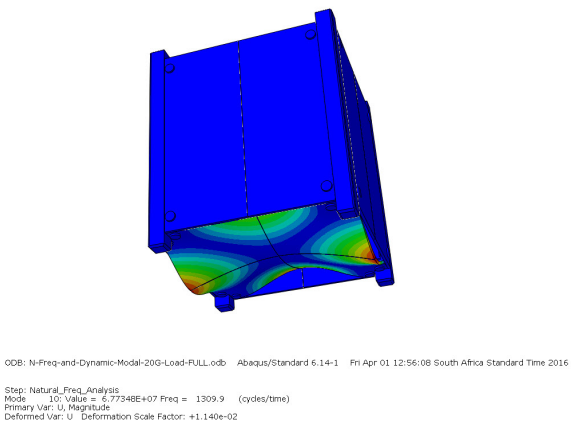

Figure 4.49: Mode 10 - 1310Hz.

4.1.4.5 Sine Wave Structural Dynamic Load Response

The data presented is the small responses observed at the various frequencies of the CubeSat structure and the overall deflection at that point. A sine gravity load of +5G to -5G was applied to the model over a time of 2 minutes sweeping from 5Hz to 120Hz in frequency.

4.1.4.5.1 Vertical loading .

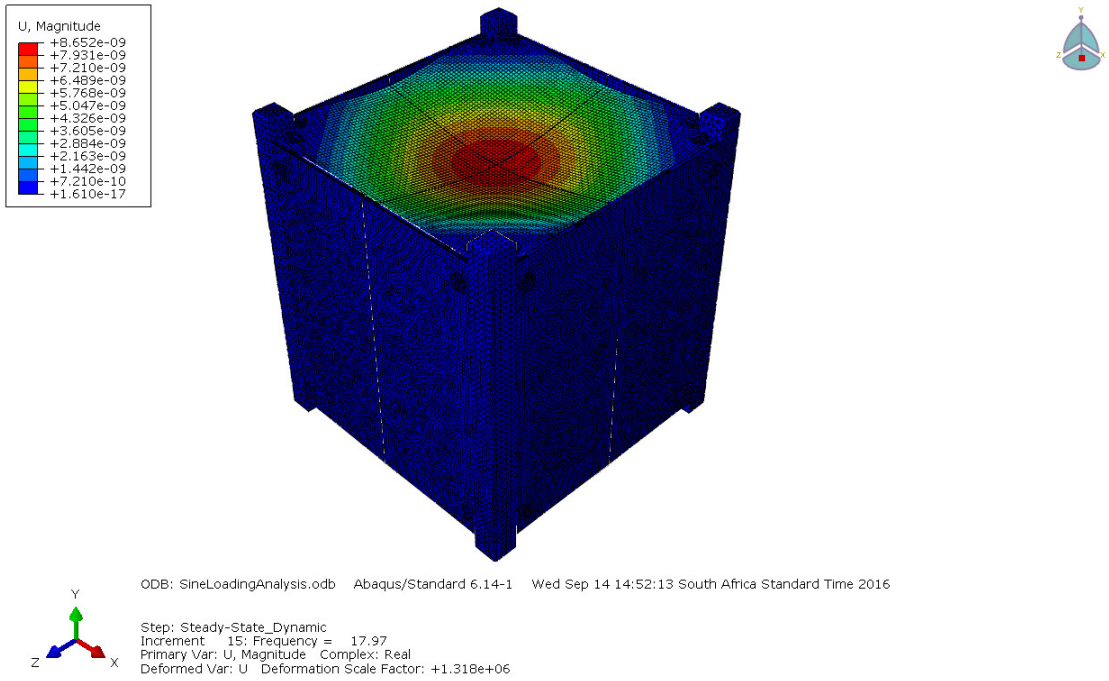

Figure 4.50: Response observed at approximately 18Hz

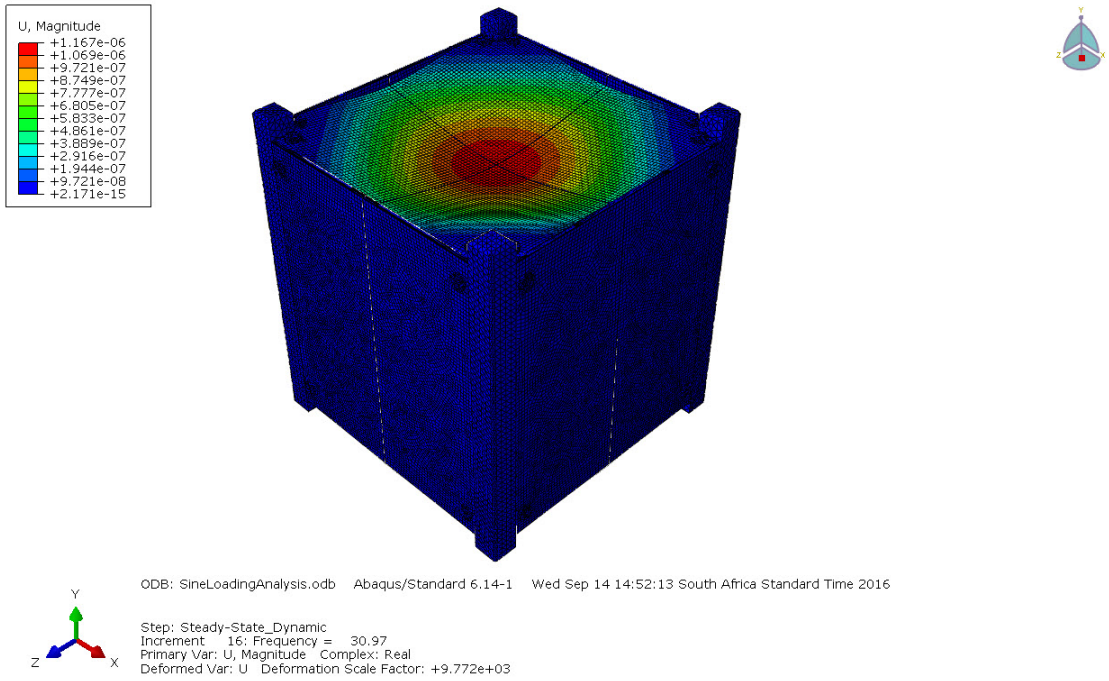

Figure 4.51: Response observed at approximately 31Hz

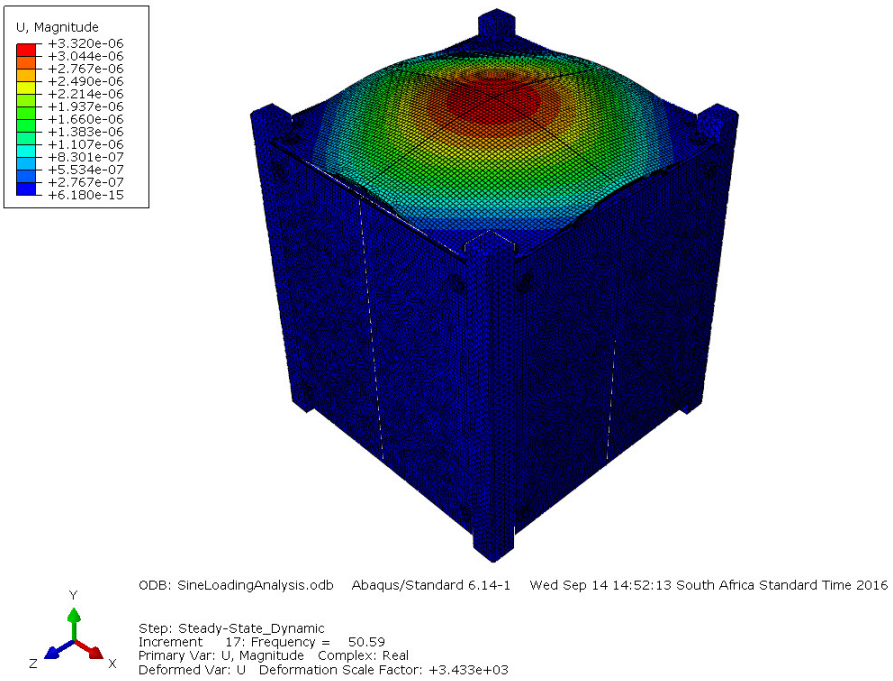

Figure 4.52: Response observed at approximately 50Hz

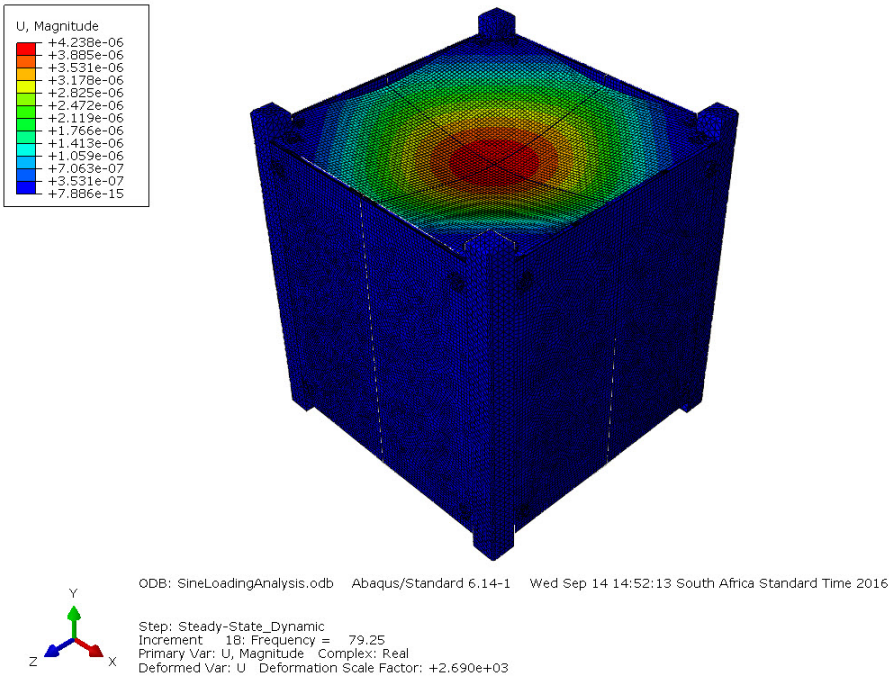

Figure 4.53: Response observed at approximately 79Hz

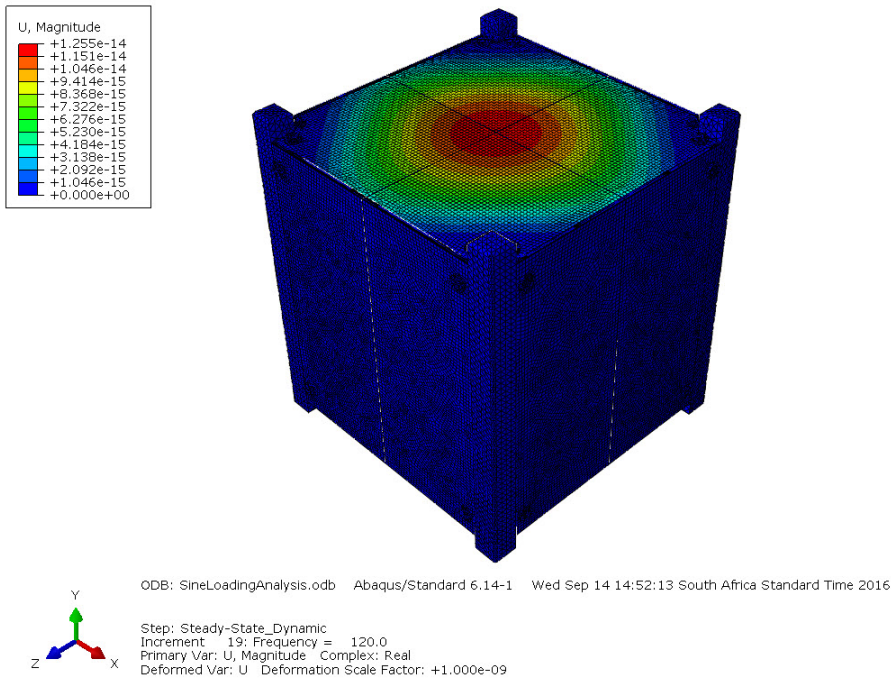

Figure 4.54: Response observed at approximately 120Hz

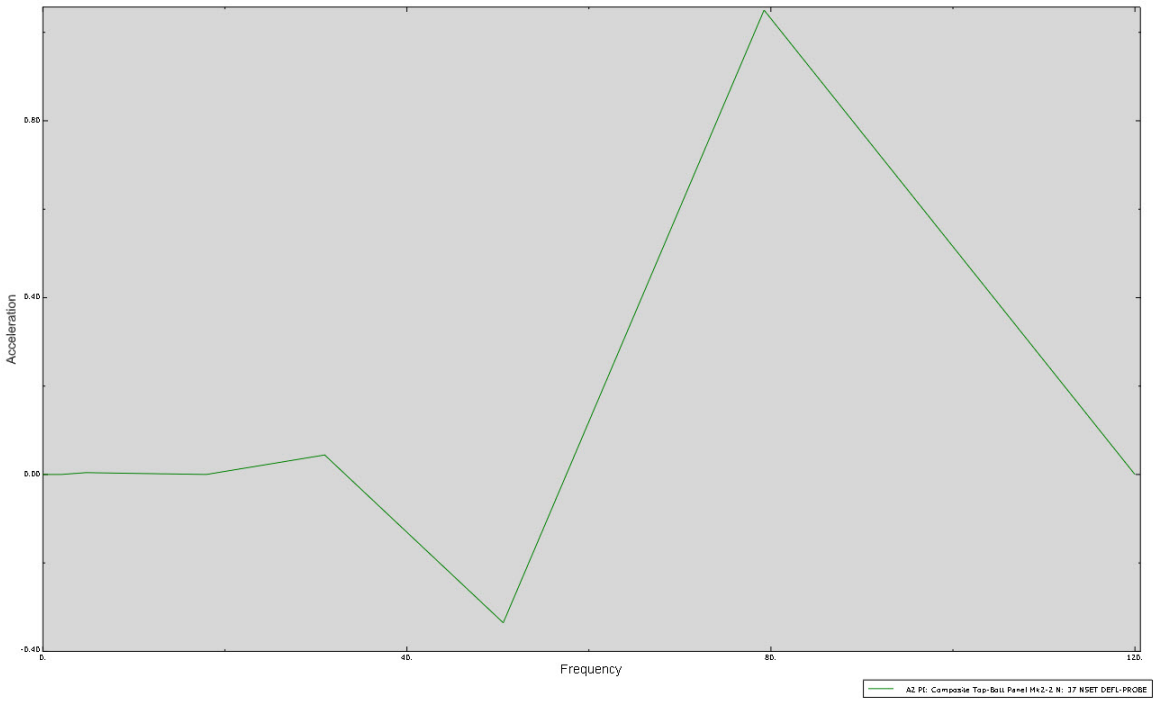

Figure 4.55: Acceleration versus time plot of the response points previously listed for a probe node on the surface of the satellite in the same location as the placement of the accelerometer in the physical tests.

4.1.4.5.2 Horizontal loading .

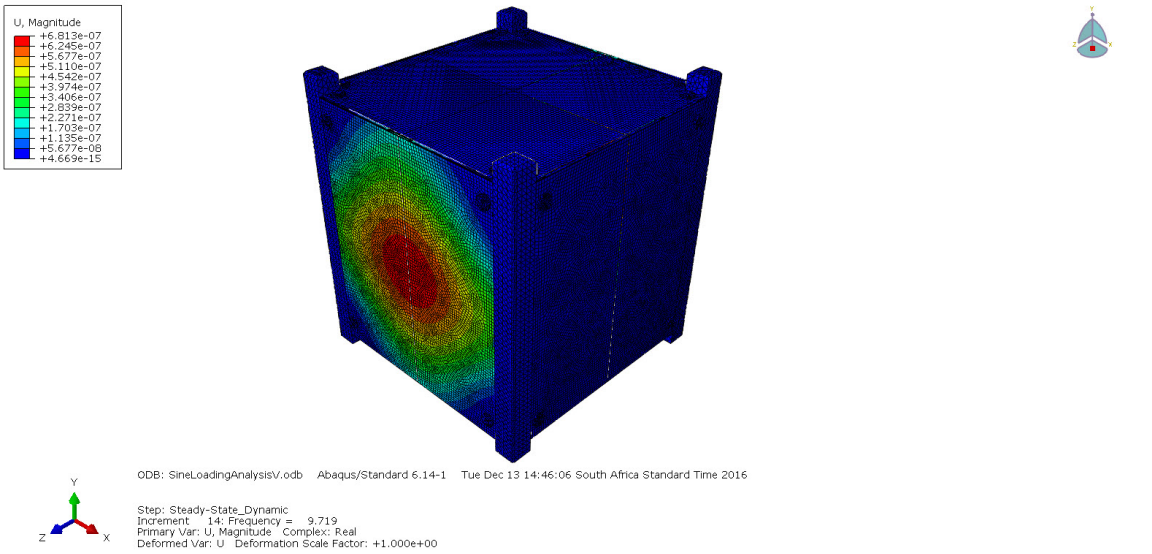

Figure 4.56: Response observed at approximately 9.7Hz

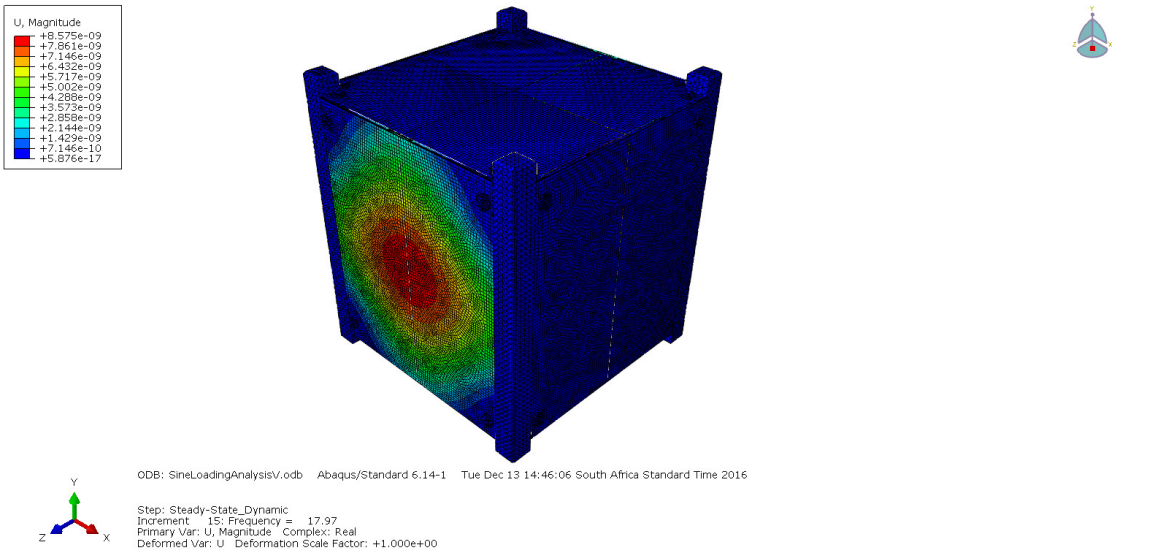

Figure 4.57: Response observed at approximately 18Hz

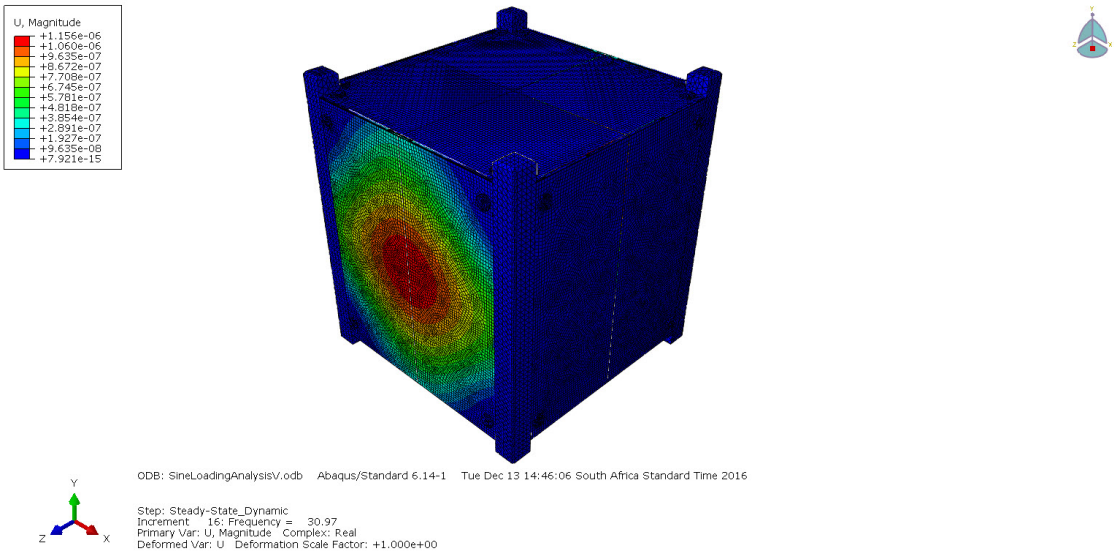

Figure 4.58: Response observed at approximately 31Hz

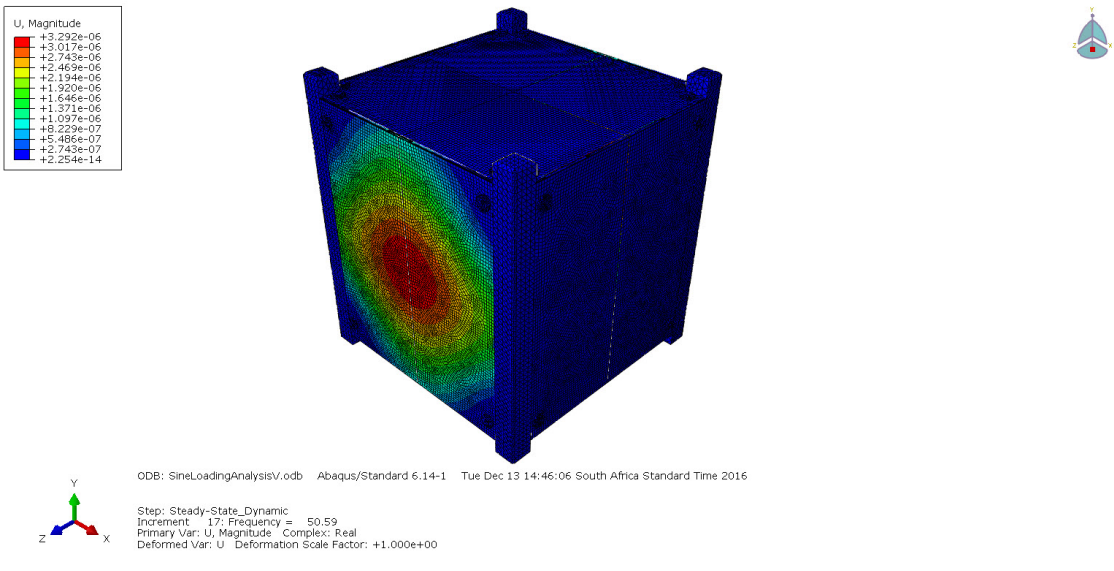

Figure 4.59: Response observed at approximately 50.6Hz

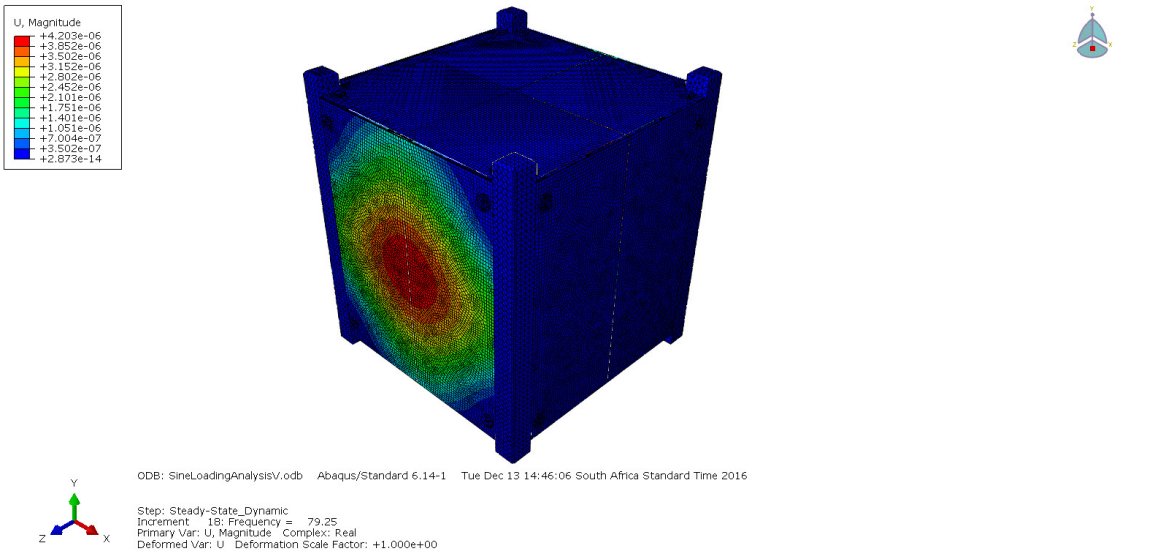

Figure 4.60: Response observed at approximately 79.25Hz

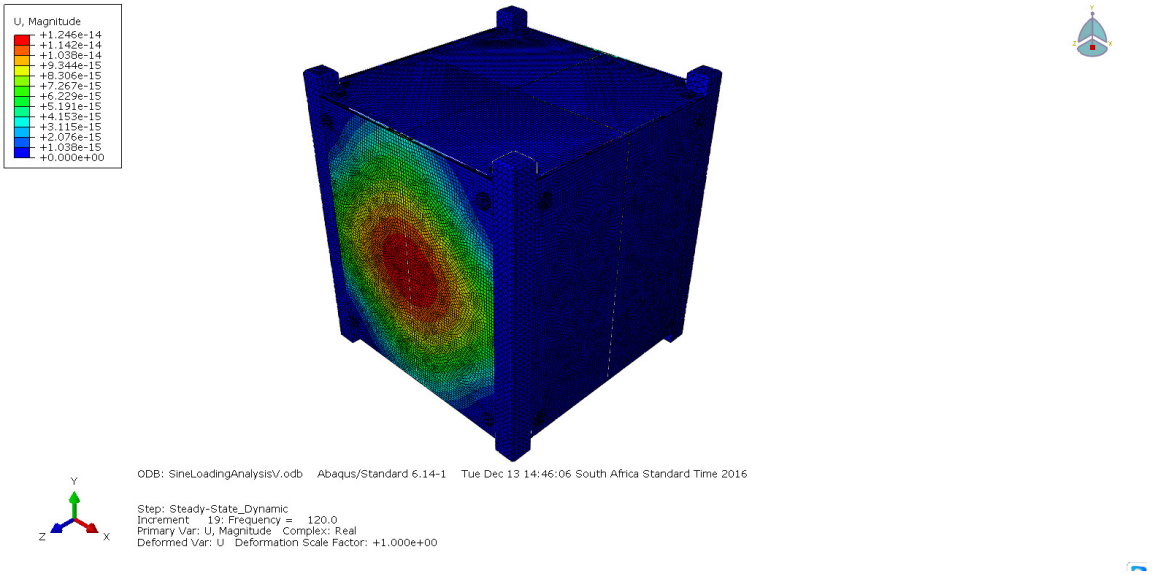

Figure 4.61: Response observed at approximately 120Hz

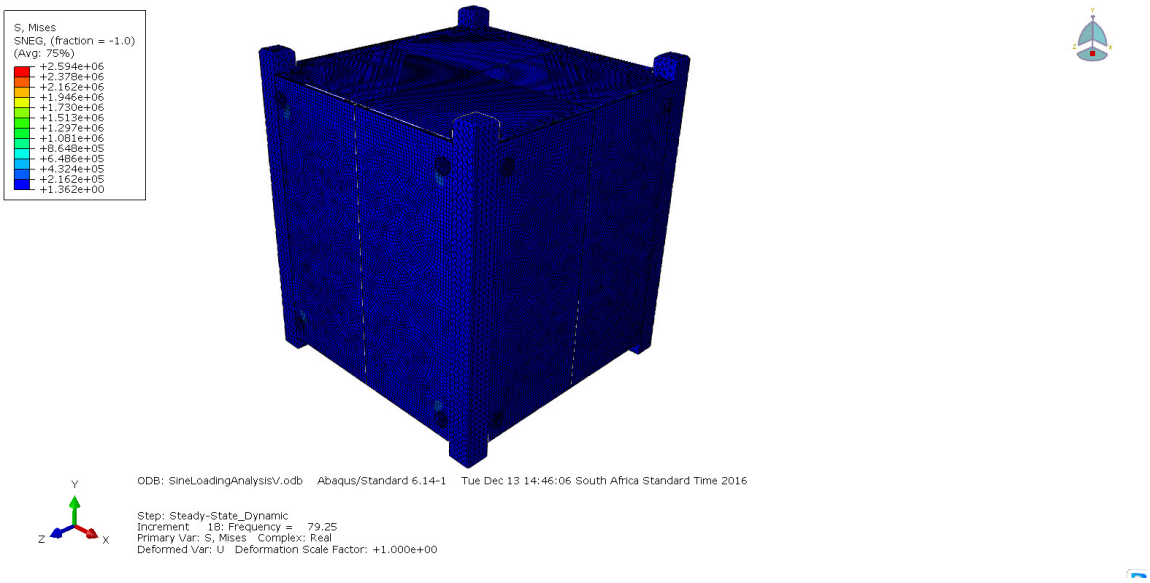

Figure 4.62: Maximum von Mises stress observed at approximately 79.25Hz

4.1.5 Cutaway Panel CubeSat Numerical Modal Data

As previously discussed in section 3.2.2.3, a concept model was created that considered a composite CubeSat with panels that included weight reduction cutouts in the panels. Once again the main data that is of interest is the deflection and maximum stress induced in the components. For this model, the sine wave vibration response was not done, as the data would not be compared to a physical model or empirical data and thus was not required.

4.1.5.1 Bolt preload conditions

The bolt torque specification is exactly the same as that of the full model CubeSat, thus the values of the stress in the bolts are exactly the same as the previous stress plot as seen in Figure 4.23. The overall deflection of the cutaway panels, however, is different due to the change of the panel profile.

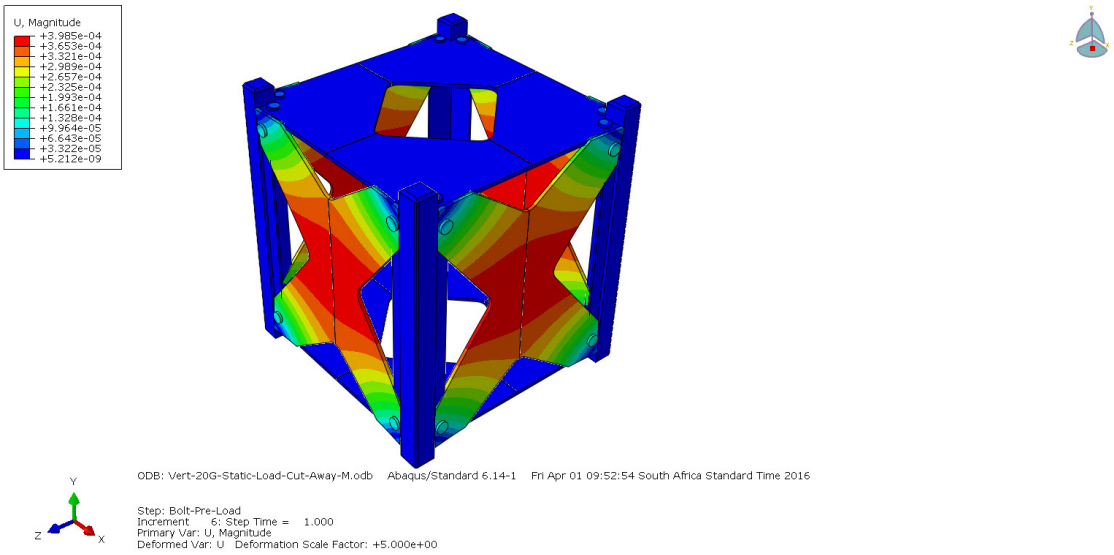

Figure 4.63: Overall CubeSat panel deflection due to the bolt loads applied.

4.1.5.2 Structural Static Load Results

4.1.5.2.1 Vertical Static Load The same test conditions were applied to the cut away concept structure model, with a 20 g vertical gravity load and the following deflection data was observed:

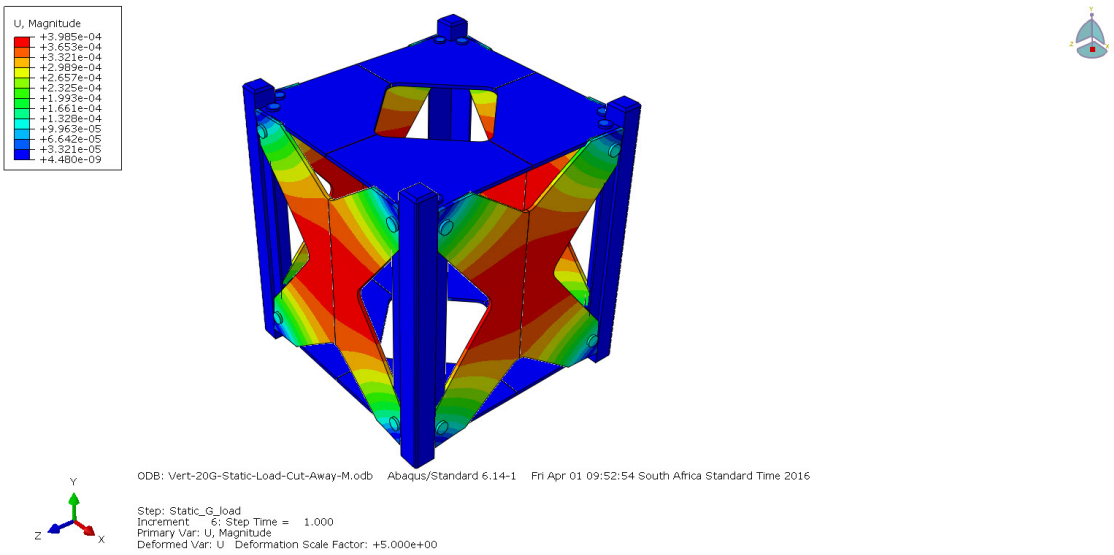

Figure 4.64: Vertical maximum overall deflection due to the applied 20 g static gravity load.

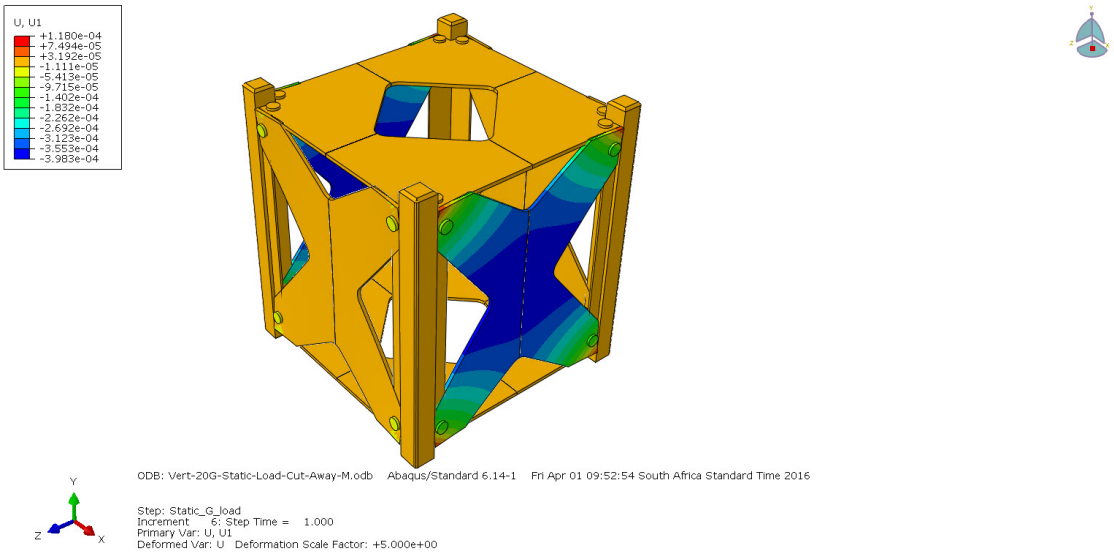

Figure 4.65: Vertical U1 deflection due to the applied 20 g static gravity load.

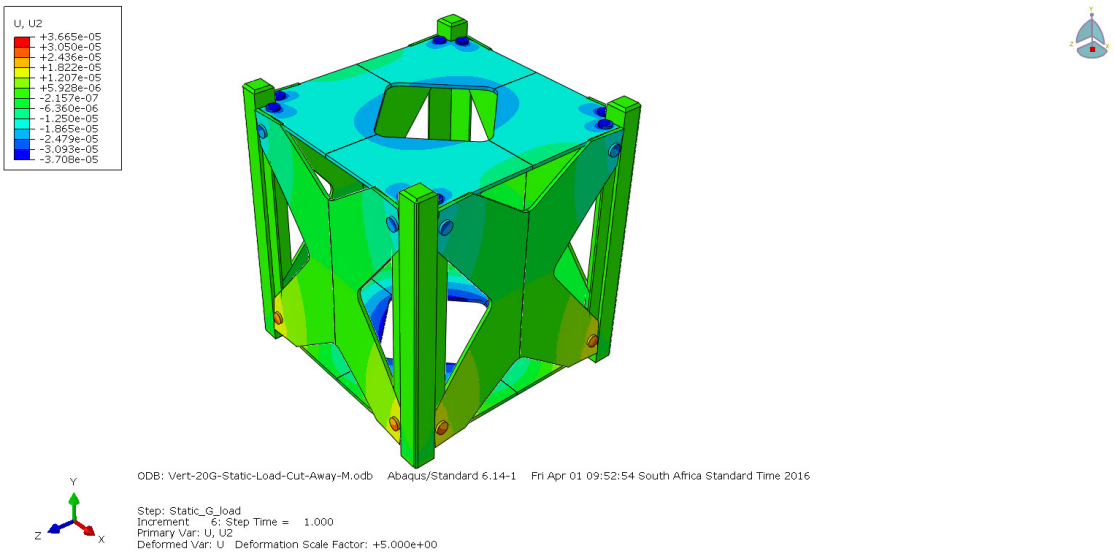

Figure 4.66: Vertical U2 deflection due to the applied 20 g static gravity load.

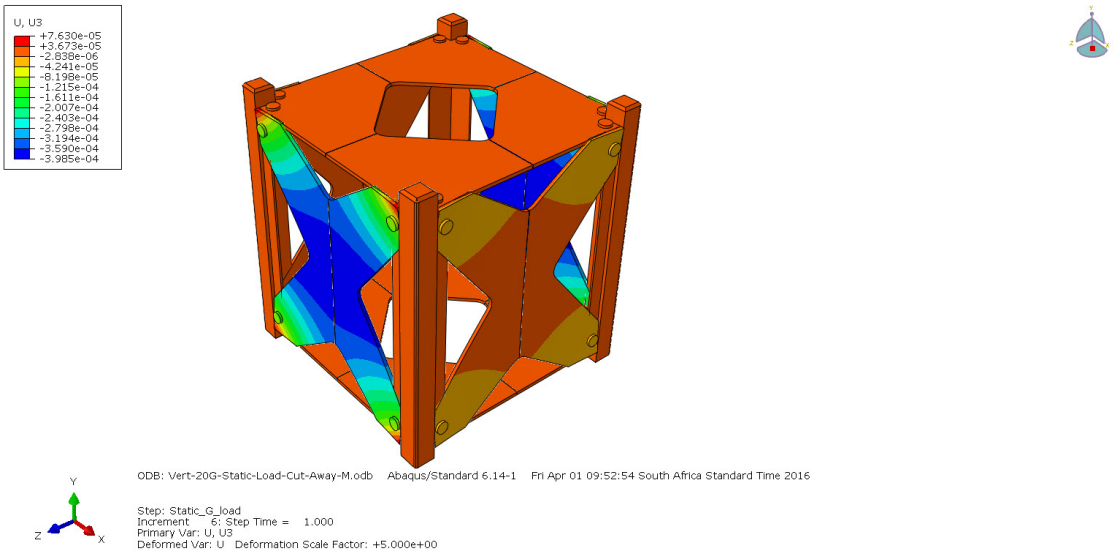

Figure 4.67: Vertical U3 deflection due to the applied 20 g static gravity load.

4.1.5.2.2 Horizontal Static Load The horizontal gravity loading on the structure was once again 10 g in a direction perpendicular to the side panel of the structure.

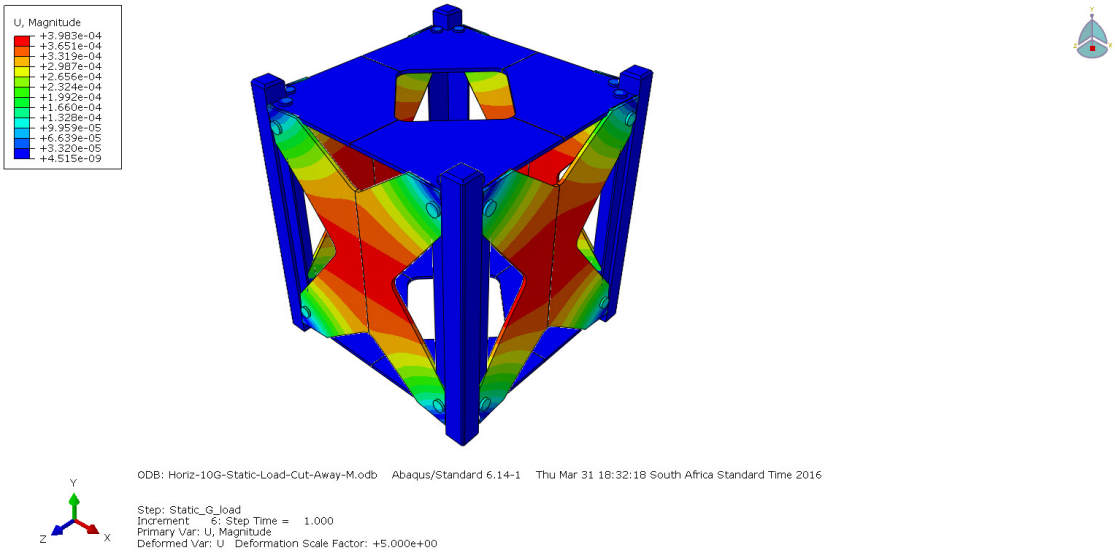

Figure 4.68: Vertical maximum overall deflection due to the applied 10 g horizontal static gravity load.

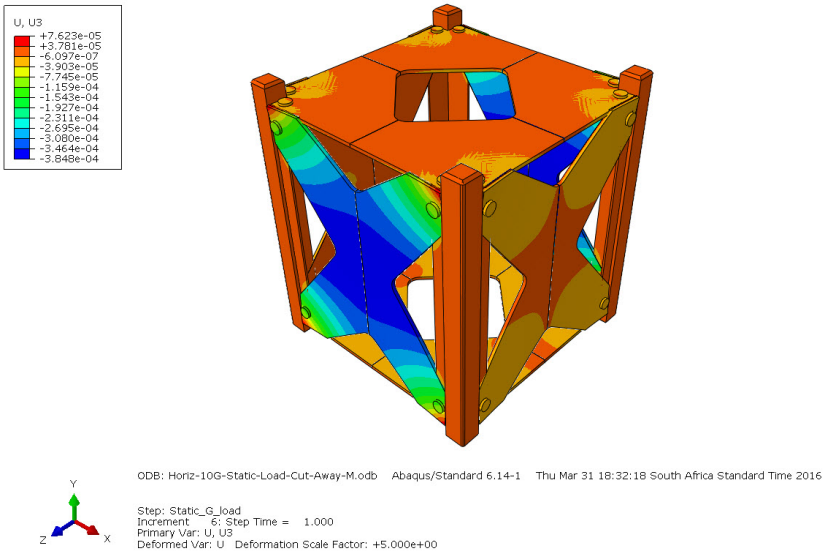

Figure 4.69: Vertical U3 deflection due to the applied 10 g horizontal static gravity load. U3 is the deflection in the same line as the applied gravity load.

4.1.5.3 Structural Natural Frequencies

The first 10 eigenvalues of the concept model are presented below:

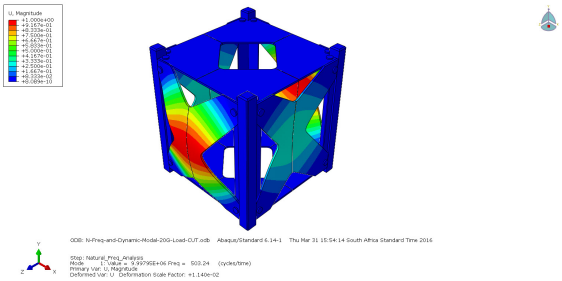

Figure 4.70: Mode 1 - 503.24Hz.

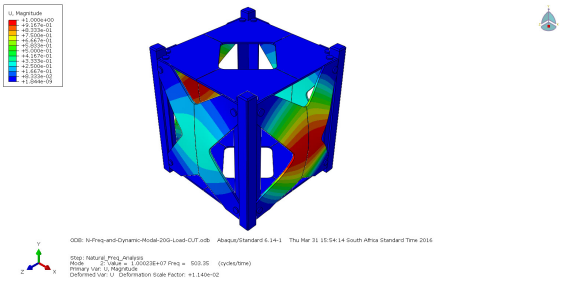

Figure 4.71: Mode 2 - 503.35Hz.

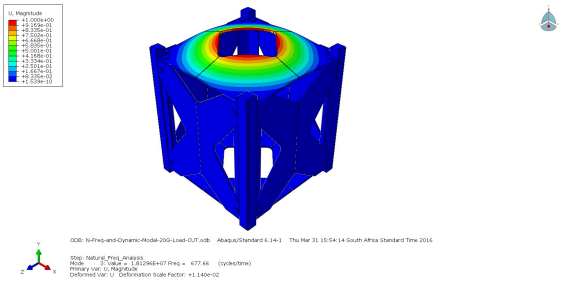

Figure 4.72: Mode 3 - 677.6Hz.

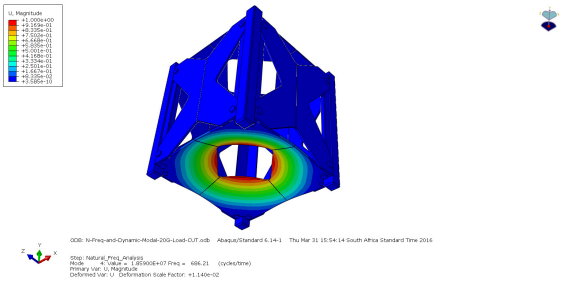

Figure 4.73: Mode 4 - 686.2Hz.

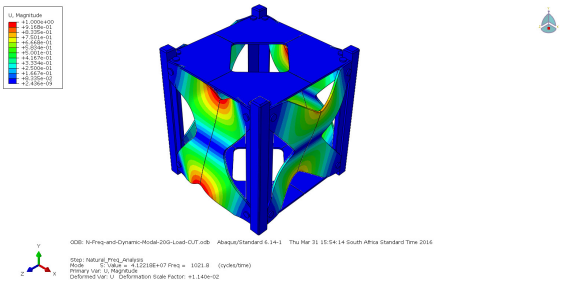

Figure 4.74: Mode 5 - 1022Hz.

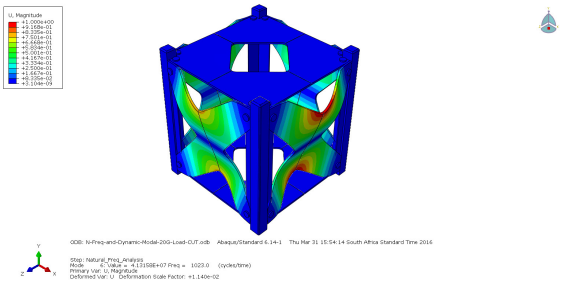

Figure 4.75: Mode 6 - 1023Hz.

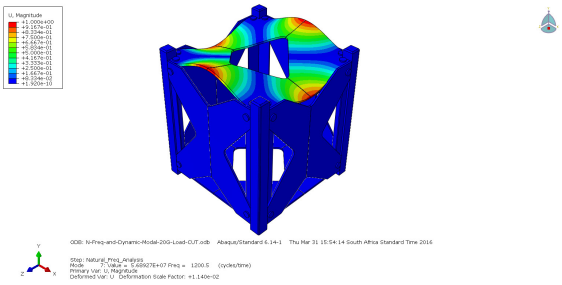

Figure 4.76: Mode 7 - 1200Hz.

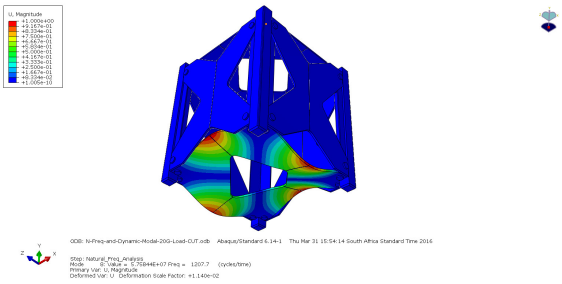

Figure 4.77: Mode 8 - 1207.7Hz.

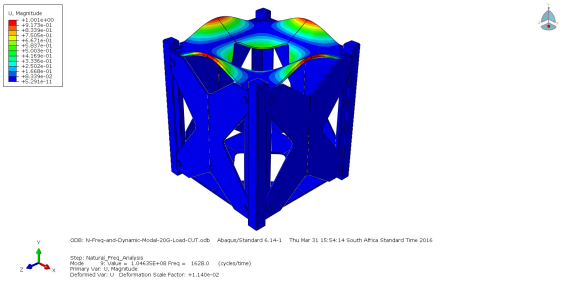

Figure 4.78: Mode 9 - 1628Hz.

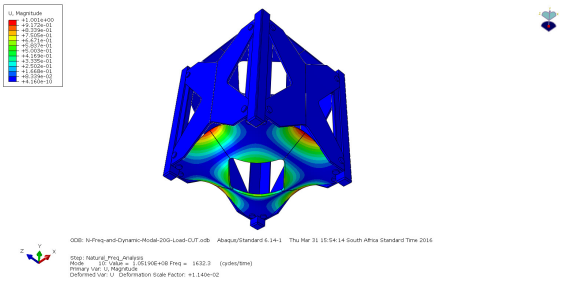

Figure 4.79: Mode 10 - 1632.3Hz.

4.1.6 2 Ply Panel Construction CubeSat Numerical Modal Data

An additional concept model was created that considered a composite CubeSat with panels that have only two carbon fibre layers to observe the effects of the reduction in thickness and load bearing materials Similar to the previous two cases, the main data that is of interest is the deflection and maximum stress induced in the components. Similarly, to the previous concept, a sine wave vibration response was not tested for in this model due to the fact that the data was not required for later processing. However, the natural frequencies and static response data of the concept is still of good comparative weighting.

4.1.6.1 Bolt preload conditions

Once again the maximum stress occurred in the bolts and is at the same torque specification as the previous two concept models. The bolt pre-loading for this concept structure produced in an ABAQUS simulation data was observed as:

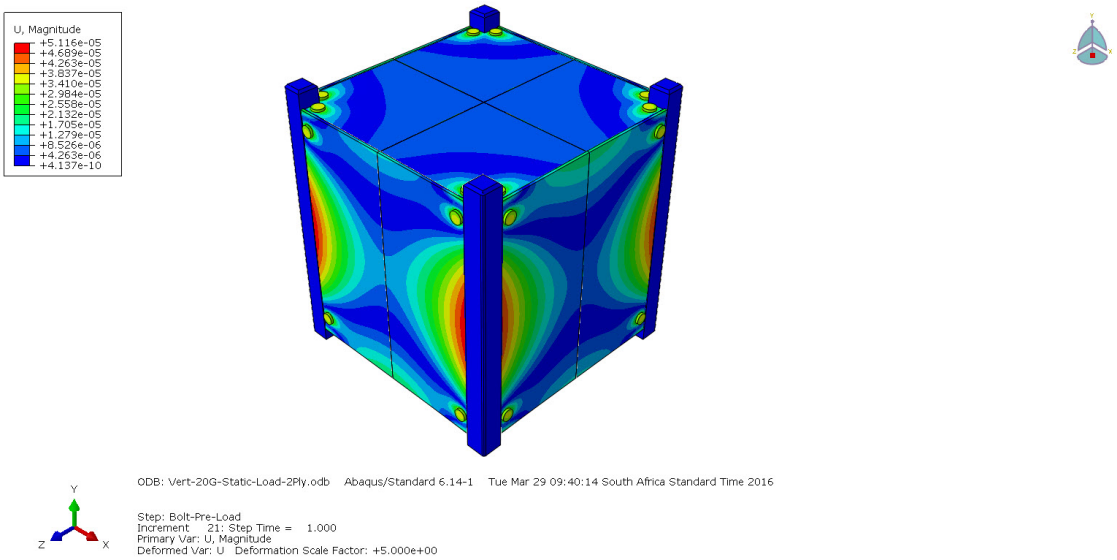

Figure 4.80: Overall CubeSat panel deflection due to the bolt loads applied.

4.1.6.2 Structural Static Load Results

4.1.6.2.1 Vertical Static Load A 20 g gravity load is once again applied in a line of action parallel to the aluminium rails as was done in the first concept model.

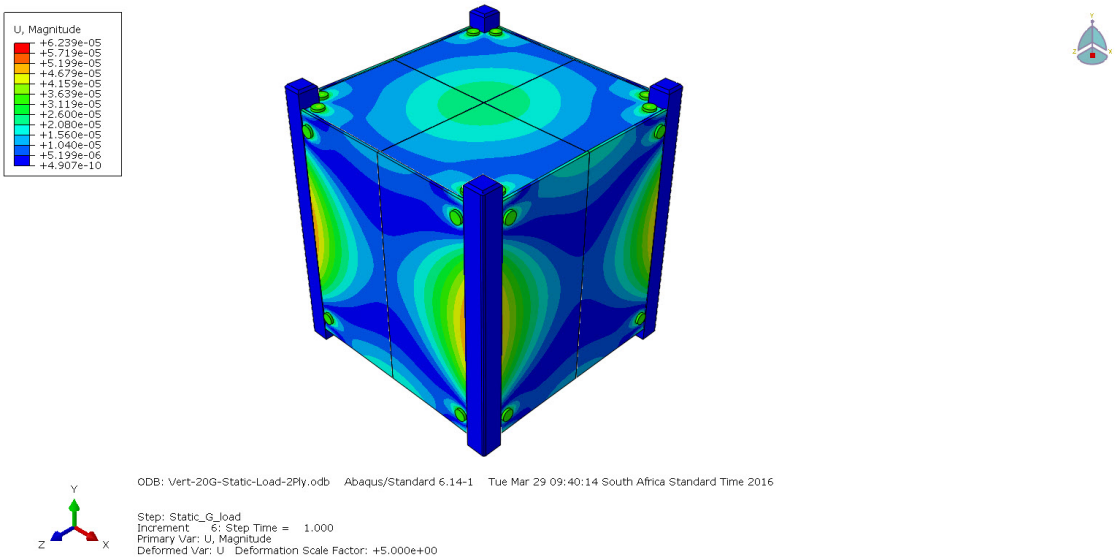

Figure 4.81: Vertical maximum overall deflection due to the applied 20 g static gravity load.

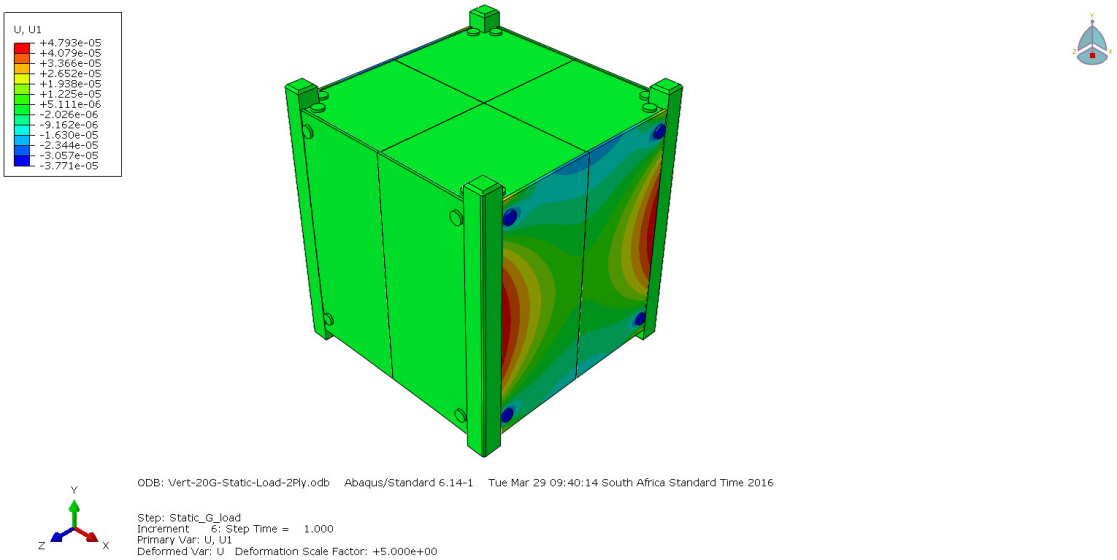

Figure 4.82: Vertical U1 deflection due to the applied 20 g static gravity load.

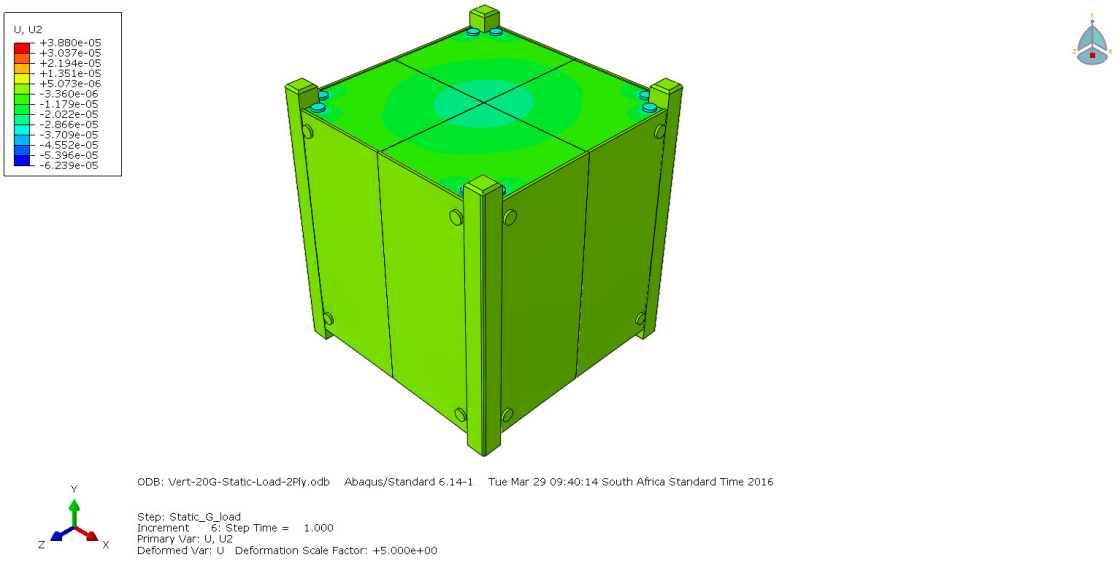

Figure 4.83: Vertical U2 deflection due to the applied 20 g static gravity load.

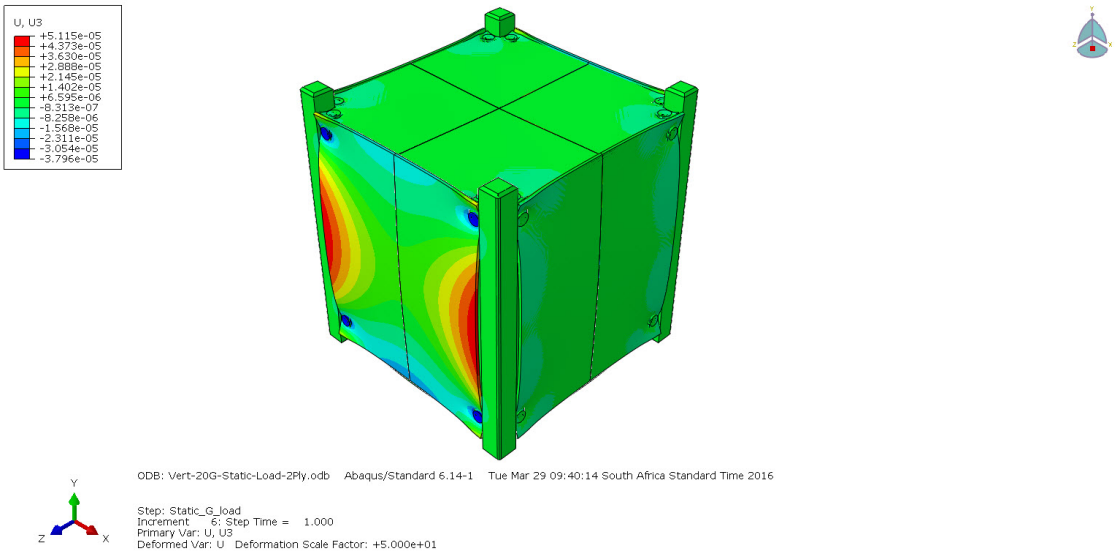

Figure 4.84: Vertical U3 deflection due to the applied 20 g static gravity load.

4.1.6.2.2 Horizontal Static Load .

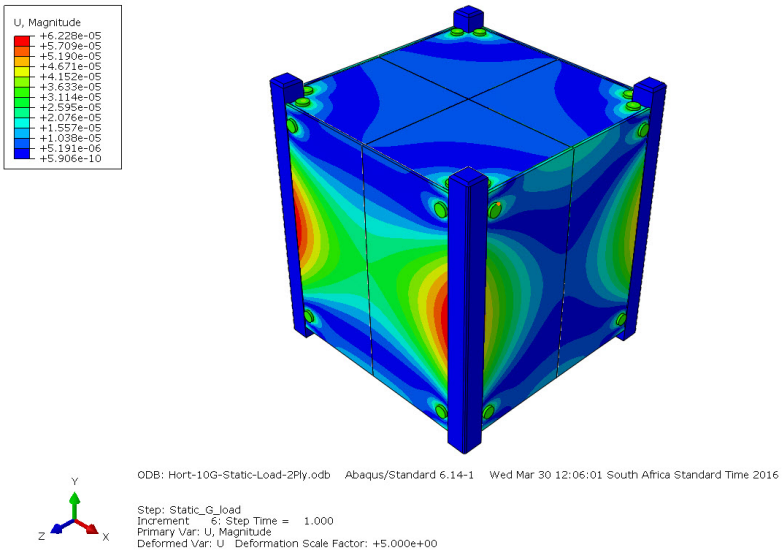

Figure 4.85: Maximum overall deflection due to the applied 10 g horizontal static gravity load.

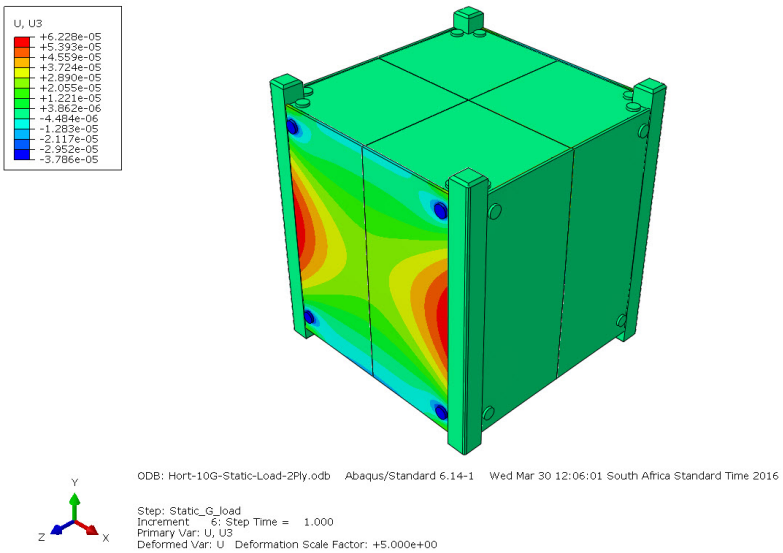

Figure 4.86: U3 deflection due to the applied 10 g horizontal static gravity load. U3 is the deflection in the same line as the applied gravity load.

4.1.6.3 Structural Natural Frequencies

The first 10 eigenvalues of the concept model are presented below:

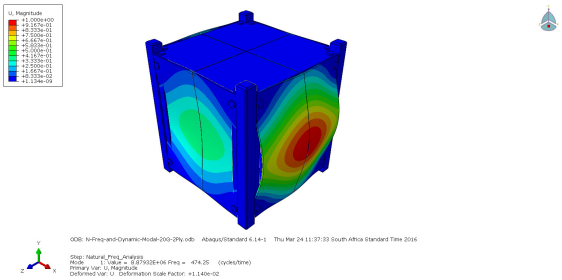

Figure 4.87: Mode 1 - 474.25Hz.

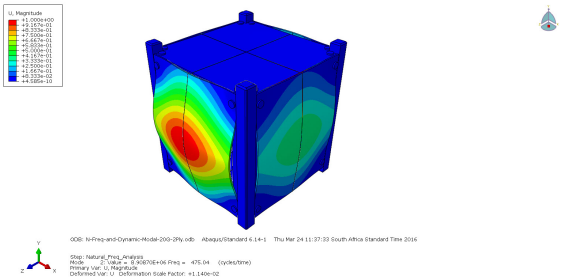

Figure 4.88: Mode 2 - 475Hz.

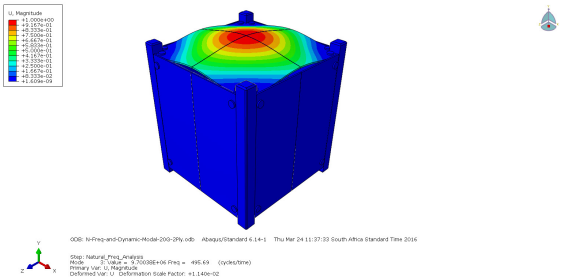

Figure 4.89: Mode 3 - 495.7Hz.

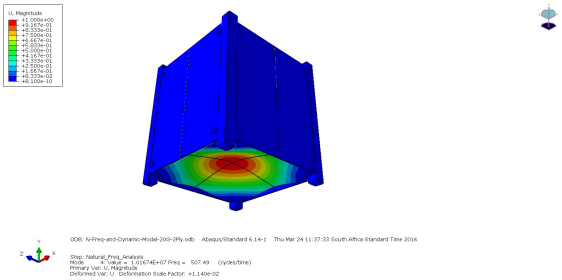

Figure 4.90: Mode 4 - 507.5Hz.

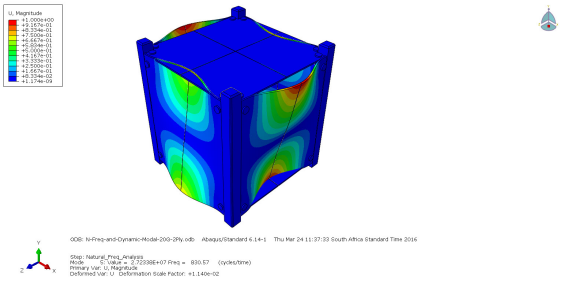

Figure 4.91: Mode 5 - 830.6Hz.

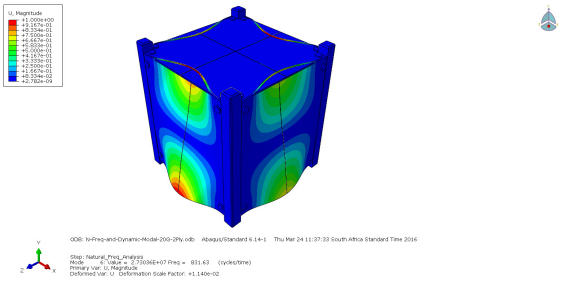

Figure 4.92: Mode 6 - 831.6Hz.

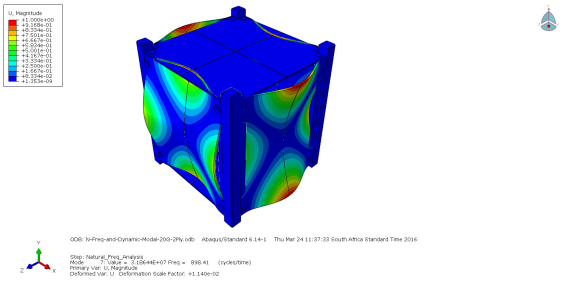

Figure 4.93: Mode 7 - 898.4Hz.

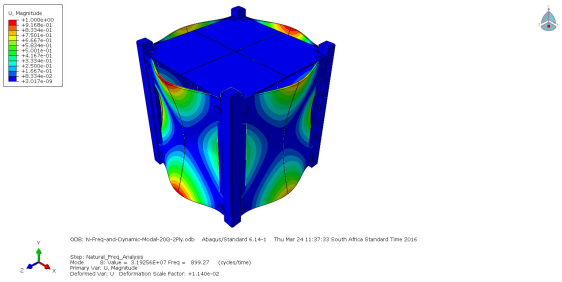

Figure 4.94: Mode 8 - 899.2Hz.

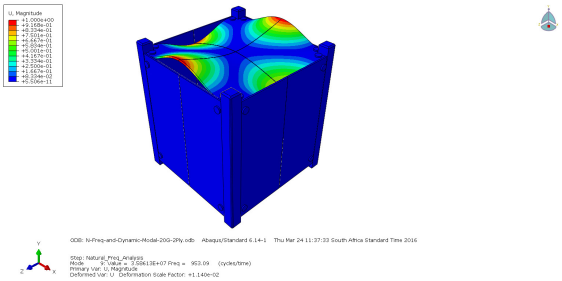

Figure 4.95: Mode 9 - 953Hz.

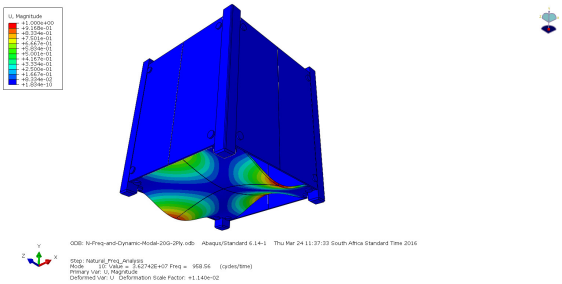

Figure 4.96: Mode 10 - 958.5Hz.

4.1.7 Material Impact Results

The impact tests that were conducted initially used a projectile velocity of 400 m/s. The intention was to run a simulation at the lower impact speed and increase it to 1 km/s and then to the final 2.5 km/s, however, the simulation only successfully ran when 400 m/s was used. Due to the extreme deformation of both the projectile and the composite material the simulation encountered a fatal error during simulation. The modelling of this impact condition is extremely complex and would require large amounts of computing power to model an accurate deformation and stress plot of the materials involved. As an indication of the stresses and deflections induced, the results of the successful 400 m/s simulation have been presented in this section. The stress wave propagation of the projectile impact is also presented. Further discussions will take place in the chapter to follow.

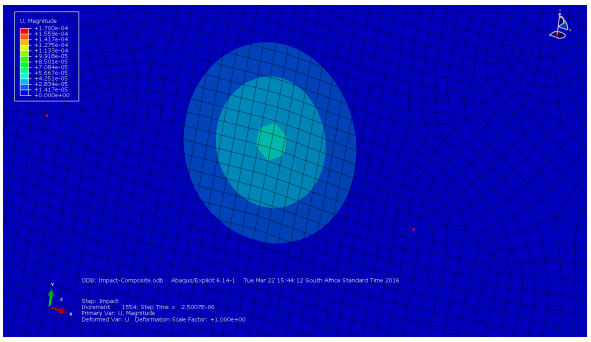

Figure 4.97: Maximum deflection of the composite panel on the opposite side surface to the impact.

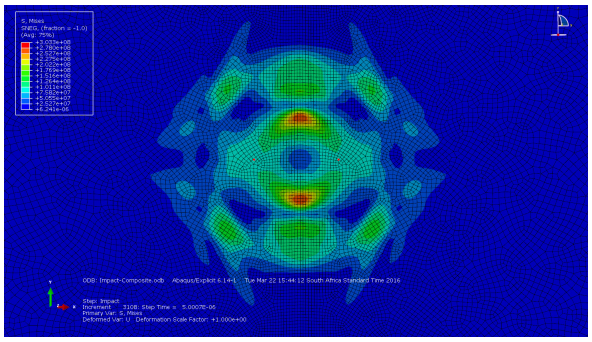

Figure 4.98: Maximum stress plot of the composite panel on the opposite side surface to the impact.

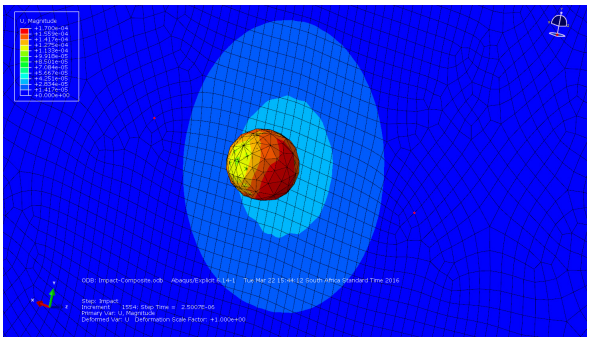

Figure 4.99: Maximum deflection of the composite panel on the impact side.

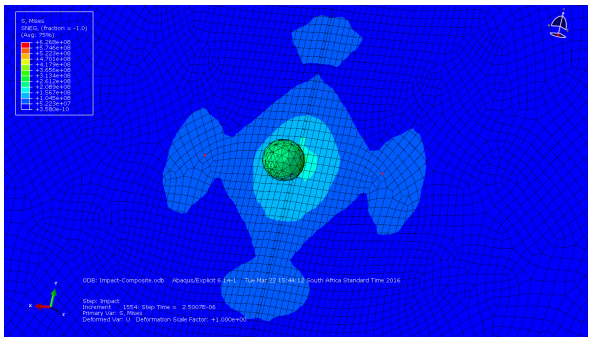

Figure 4.100: Maximum stress plot of the composite panel on the impact side.

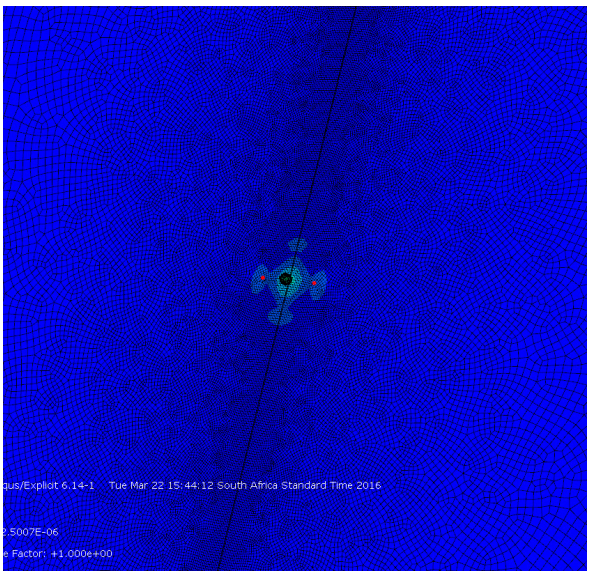

Figure 4.101: Stress wave plot 1.

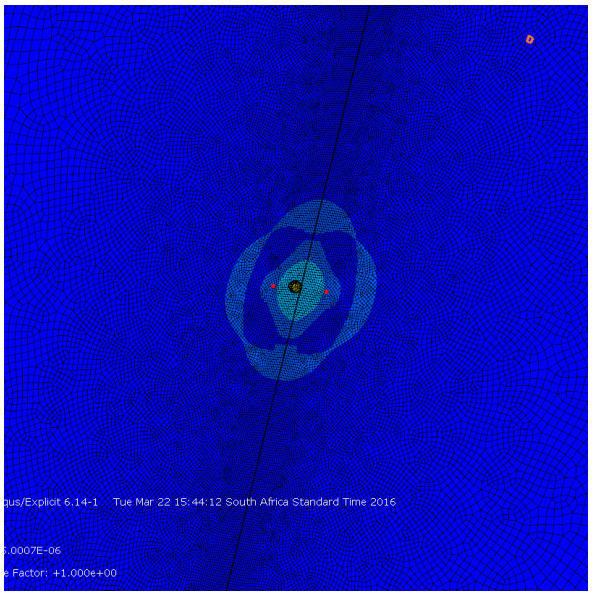

Figure 4.102: Stress wave plot 1.

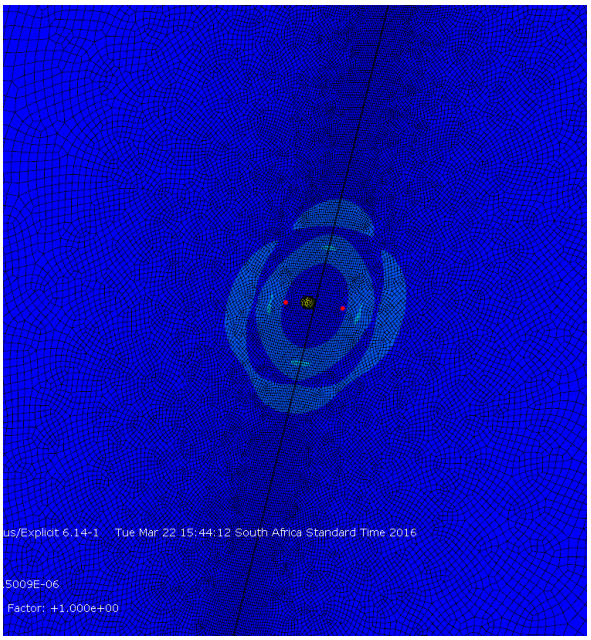

Figure 4.103: Stress wave plot 3.

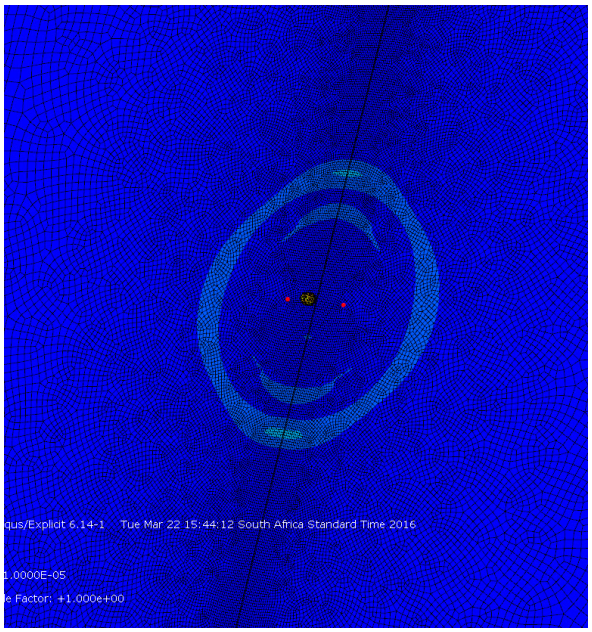

Figure 4.104: Stress wave plot 4.

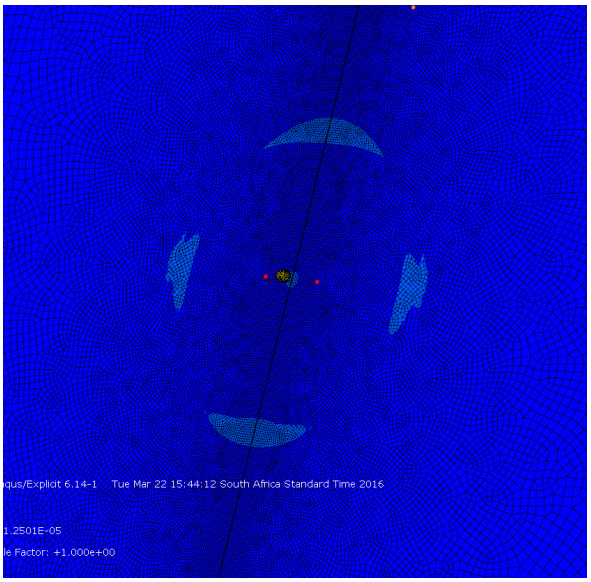

Figure 4.105: Stress wave plot 5.

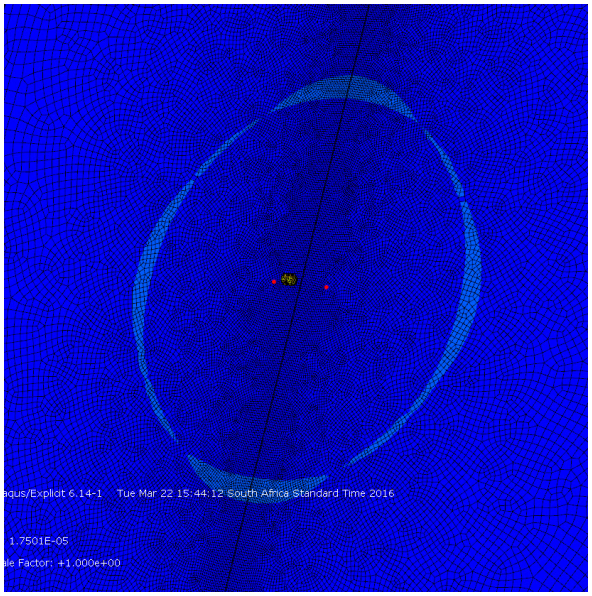

Figure 4.106: Stress wave plot 6.

4.1.8 Orbital Thermal Simulation Results

The primary purpose of space thermal simulation is to provide an indication as to what the structural surface/face temperatures are likely to be. Due to the complexity of the space environment, space thermal simulation software (NX Siemens) was used to provide approximate values for the temperature field considered. Due to the fact that the focus of this thesis is not on the thermal aspects of the structure, the consideration of the thermal effect on the structure needs to be accounted for. A single dawn dust

orbit analysis was run on the CubeSat structure, as this set-up will show the largest temperature differential that the structure could ever face. An equatorial plane orbit will induce a fluctuation of the temperature of the faces, however across a smaller temperature range. This simulation has not been run as the effects of the subsystem thermal radiation would now have a larger impact on the temperature of the structure and the sub-system specification for this satellite is at this point still unknown.
As a reference, NX Siemens provide a tutorial example based on a CubeSat simulation and the setup data from the simulation below was cross-checked with the tutorial example to ensure the correct guidelines were followed.

4.1.8.1 Full Sun exposed orbit

The full sun exposed orbit simulation comprised of the satellites' orientation being fix in attitude, this is unlikely but would be assumed to gain a worst case scenario. The orbit line is parallel to that of the earth's dawn-dusk line, to have one face fully and constantly exposed to the sun and the other face fully shadowed from the sun. Figure 4.107 provides an illustration of the orbit trajectory.

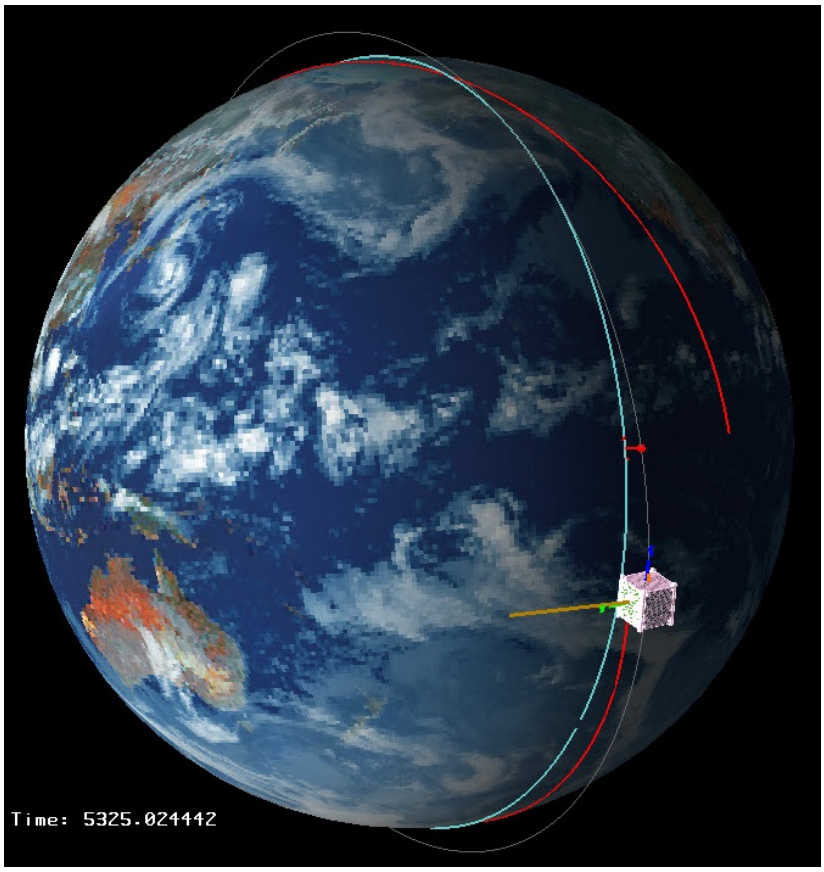

Figure 4.107: Dawn-dusk orbit trajectory of the CubeSat simulation.

The initial temperature of the structure was set to 12 degrees Celsius and the final results captured at the point the temperatures stabilised.
The final temperature field across the structure is shown in figure 4.108.

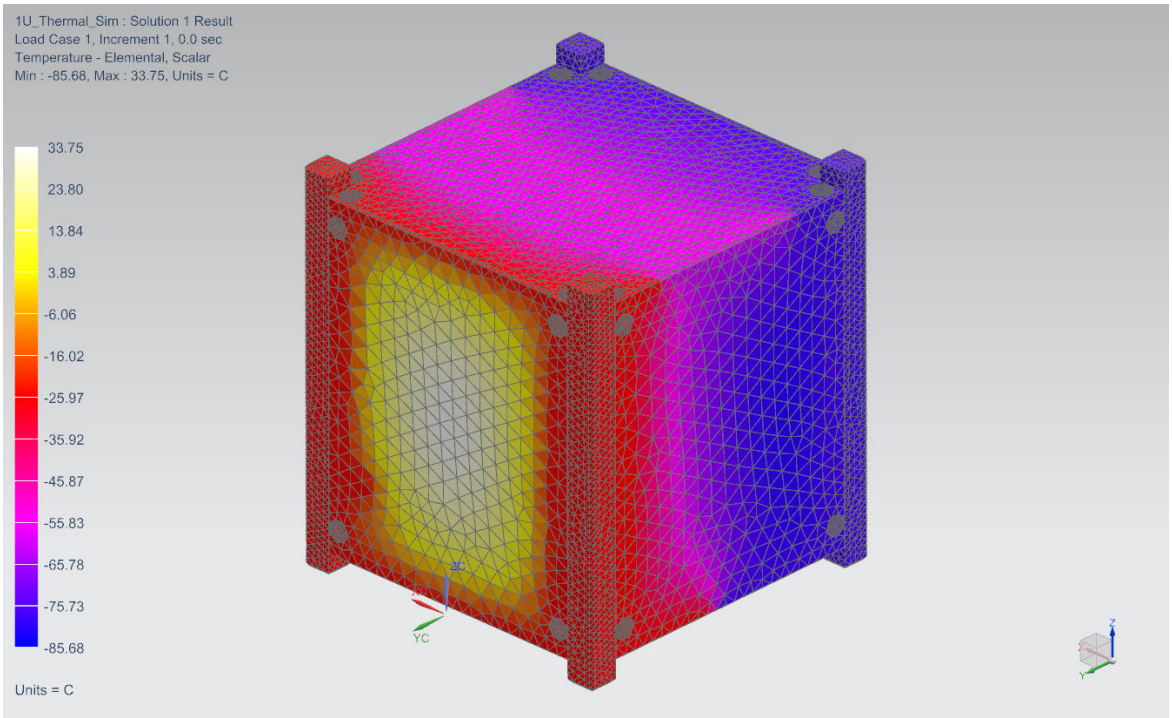

Figure 4.108: Stabilised temperature field of the CubeSat structure.

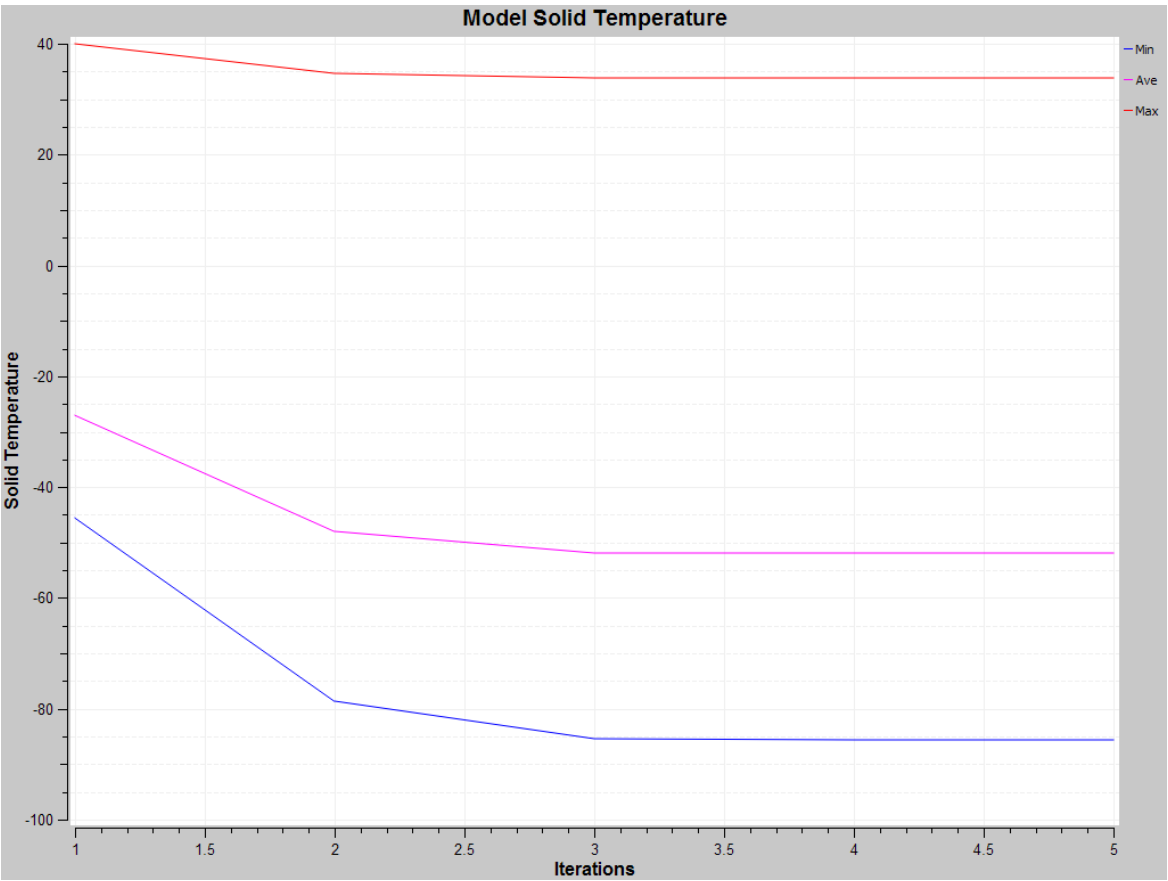

Figure 4.109: Stabilised temperature field of the CubeSat structure shown in a graph.

4.2 Empirical Data

The main collection of empirical data has been produced by the tensile and bending tests on the composite material samples. The addition of the out-gas properties of the material is also desired, however, due to the lack of funding available for the research and the limited access to out-gas testing facilities, the out-gas test was not able to be completed for this research. It must be noted that regardless of the out-gas results for this material, it would most likely not be the exact compound of material that will be used for the flight model structure. The composite reinforcement material used in the flight model would be selected from the accepted space materials listed by NASA. The material used in this research is adequate enough to prove the theoretical concepts and provide a validation of the predicted material characteristics using the theory.

4.2.1 Material Sample Testing

The physical material tests for tensile and bending will be presented in the subsections that follow. From these fundamental tests, the primary material characteristics can be determined and compared against the numerical results in a later section.

4.2.1.1 Tensile Test

The tensile tests were performed using the machine shown in figure 3.43 in the previous chapter. A total of 17 material samples were tensile tested. Table 4.1 is the raw data output produced by the tensile test machine. The dimensional parameters of the specimens are pre-programmed into the machines' software so that it can determine the modulus of elasticity. The graph in Figure 4.110 illustrates a typical good composite test profile, with an almost linear response to the applied load. All the graphs for each of the tested samples can be found in Appendix D.

	Tensile stress at Maximum Load [MPa]	Maximum Load [kN]	Tensile strain (Extension) at Break (Standard) [%]	Modulus (E-modulus) [MPa]	Area [mm^2]	Corrected gauge length at Slack correction (Automatic Young's) [mm]
1	199.579	6.985	1.3	18465	35.000	180.018
2	325.238	11.383	1.6	20154	35.000	179.989
3	303.973	10.639	1.6	20214	35.000	179.981
4	142.093	4.973	0.8	19075	35.000	179.994
5	312.496	10.937	1.7	19892	35.000	179.994
6	202.701	7.095	1.6	12848	35.000	179.974
7	260.035	9.101	1.4	19847	35.000	179.995
8	327.532	11.464	1.6	20225	35.000	179.993
9	313.487	10.972	1.5	21743	35.000	179.994
10	328.837	11.509	1.6	20533	35.000	179.997
11	255.322	8.936	1.5	18363	35.000	179.993
12	325.949	11.408	1.7	20140	35.000	179.993
13	236.046	8.262	1.2	20464	35.000	179.996
14	162.238	5.678	0.9	19672	35.000	179.992
15	317.435	11.110	1.5	21705	35.000	179.995
16	351.864	12.315	1.7	20878	35.000	179.993
17	330.121	11.554	1.6	21199	35.000	179.994
Mean	276.173	9.666	1.5	19730	35.000	179.993
Standard deviation	65.504	2.293	0.3	2011.478	0.000	0.009

Table 4.1: Raw tensile test data that was captured during testing.

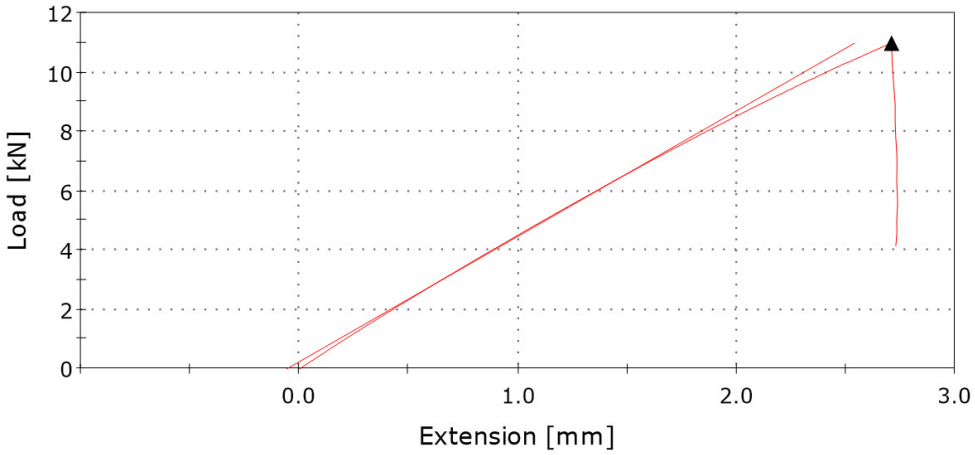

Figure 4.110: Graph (Force vs Extension) of a typical good tensile test of a specimen.

It must be noted that not all the 17 tested samples had valid results. Due to incorrect clamping of some specimens in the tensile testing machine, it was observed that some samples slipped in the gripping jaws of the machine and a few broke in the vice interfacing section. Figure 4.111 shows the test specimens after the tensile tests had been conducted.

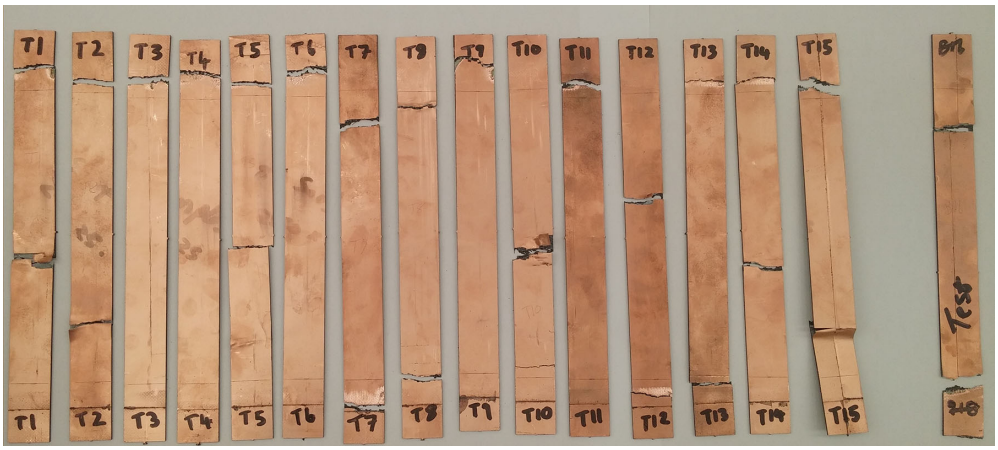

Figure 4.111: Material test specimens after tensile testing.

Due to the testing errors with some specimens, they were omitted from the final data processed for the averaged material values. The data was reprocessed in Excel and the final results of the correctly tested specimens can be seen in Table 4.2 and 4.3.

A summary of the specimens with issues are listed below. The first number indicates the raw data table number reference (Table 4.1) and the "T" is the reference to the photographed specimens in figure 4.111.

1. - Initial machine test sample
4. - (T3) Failed in Vice
6. - (T4) Failed in Vice
11. - (T9) Failed in Vice
13. - (T11) Failed in Vice

The data has been processed and the correctness of the modulus of elasticity has been checked using the fundamental stress/strain relationships and the known specimen dimensions.

Sample Number	Maximum Load [KN]	Tensile Extension [%]	Corrected Gauge length [mm]	Extension [mm]	Strain:	Maximum Tensile Stress [MPa]	Modulus of Elasticity [GPa]
1	11.383	1.6	179.989	2.88	0.016	325.229	20.327
2	10.639	1.6	179.981	2.88	0.016	303.971	18.998
3	10.937	1.7	179.994	3.06	0.017	312.486	18.382
4	9.101	1.4	179.995	2.52	0.014	260.029	18.573
5	11.464	1.6	179.993	2.88	0.016	327.543	20.471
6	10.972	1.5	179.994	2.70	0.015	313.486	20.899
7	11.509	1.6	179.997	2.88	0.016	328.829	20.552
8	11.408	1.7	179.993	3.06	0.017	325.943	19.173
9	5.678	0.9	179.992	1.62	0.009	162.229	18.025
10	11.11	1.5	179.995	2.70	0.015	317.429	21.162
11	12.315	1.7	179.993	3.06	0.017	351.857	20.697
12	11.554	1.6	179.994	2.88	0.016	330.114	20.632

Table 4.2: Processed test data of the tensile test.

Maximum Load [KN]	Tensile Extension [%]	Corrected Gauge length [mm]	Extension [mm]	Strain:	Maximum Tensile Stress [MPa]	Modulus of Elasticity [GPa]
10.673	1.533	179.993	2.760	0.015	304.929	19.824

Table 4.3: The summary of the averaged values for the range of samples tested.

4.2.1.2 Bend Test

The bend tests were conducted using the machine and jig shown in figure 2.21 and 3.44 respectively. Two batches consisting of ten samples each were tested. One batch had the copper surface of the sample on the compression side (facing upwards) and the other batch had the carbon fibre surface on the compression side (copper side down). It is expected that due to the stiffness of the carbon fibre structural layers, that the neutral axis of the shear stress through the thickness would be offset towards the carbon layers. The two batches were done to capture any effects if this was the case. Figure 4.112 and Table 4.4 show the results of the carbon fibre surface on the compression side (copper facing down in the jig). The average maximum load, average deflection at maximum load and standard deviation for the range of samples has been calculated. The flexural stress and modulus of elasticity have been calculated using equations 2.53 and 2.54 from section 2.5.7.2.

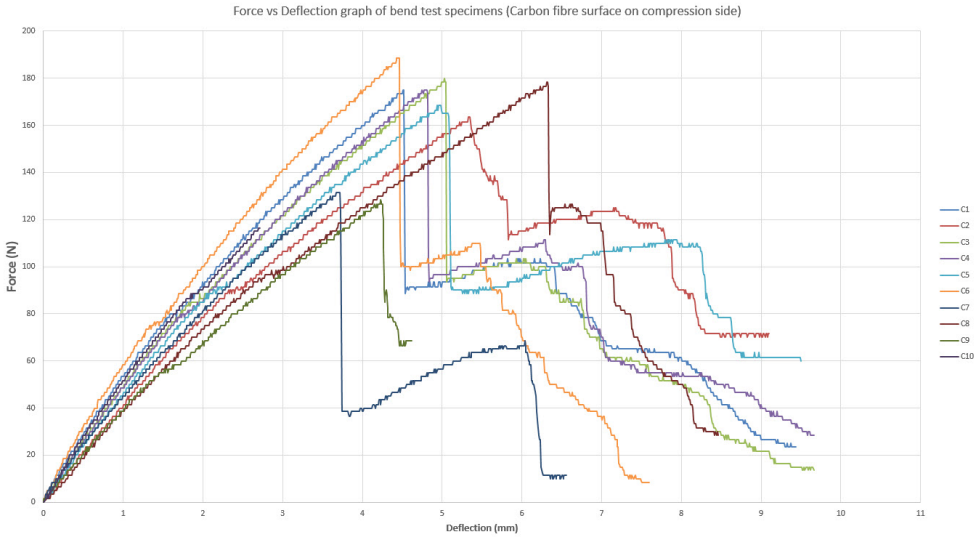

Figure 4.112: Copper facing down bend test results graph.

Max. Load Avg	175.6		Stress Flexture [MPa]	274.106414
Standard Deviation of Load	17.284		E_b [GPa]	18.483252
Standard Deviation of Load (%)	10			
Deflection Avg	4.6			
Standard Deviation of Deflection	0.6			
Standard Deviation of Deflection (%)	14			

Table 4.4: Processed Data of the bend test results batch 1.

The exact same process and calculations were done for the second batch of samples with the copper facing upwards in the jig. Figure 4.113 and Table 4.5 provides final results of the test.

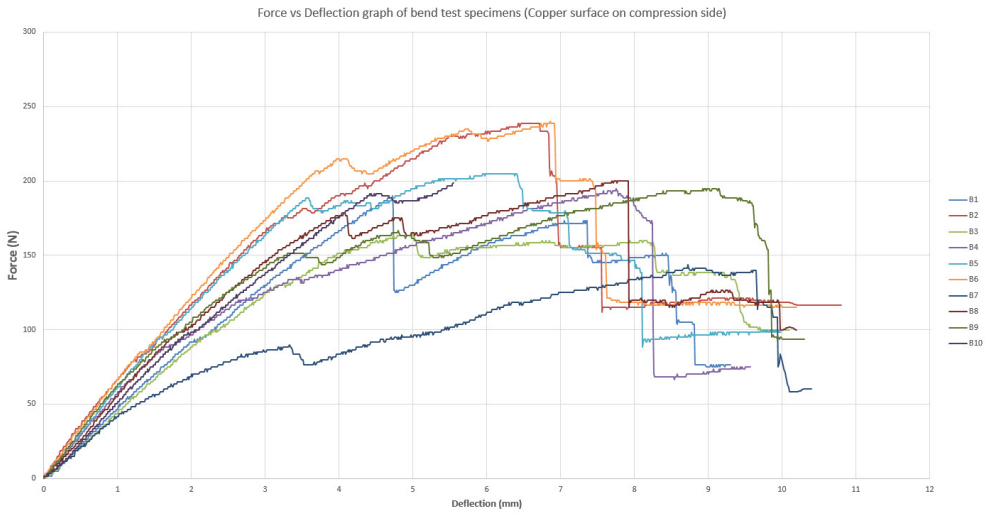

Figure 4.113: Copper facing up bend test results graph.

Max. Load Avg	204.0		***Stress Flexture [MPa]***		318.489796
Standard Deviation of Load	32.914		***E_b [GPa]***		14.5936561
Standard Deviation of Load (%)	16				
Deflection Avg	6.8				
Standard Deviation of Deflection	1.2				
Standard Deviation of Deflection (%)	18				

Table 4.5: Processed Data of the bend test results batch 2.

Appendix A.3 provides an illustration of a bend test sample positioned in the bending machine with the test jig in place.

Figure 4.114: Bend test sample in the testing machine.

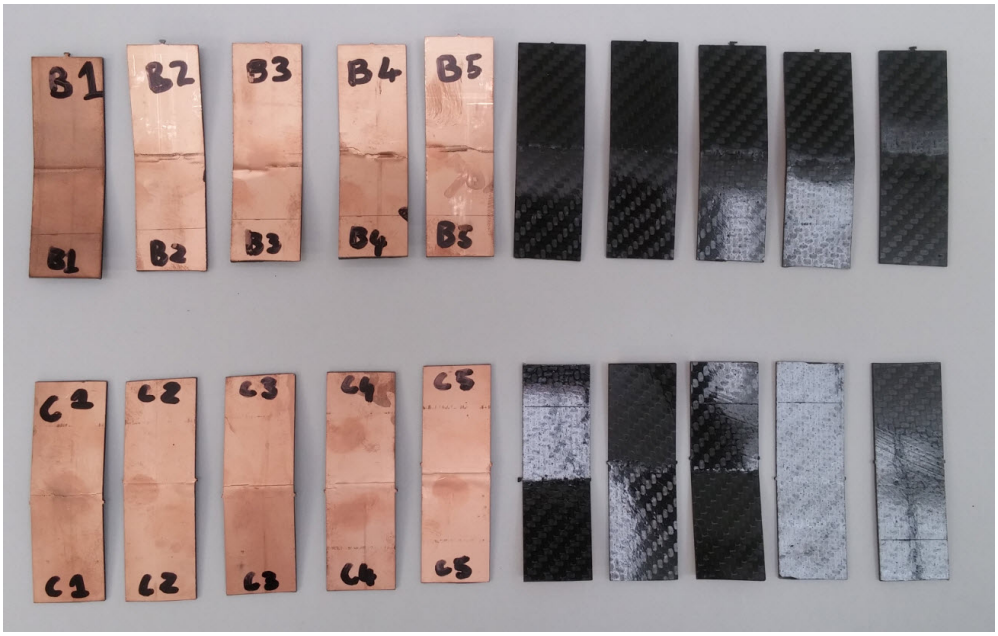

Figure 4.115: Damage to bend test samples after testing.

Observations of the damage to each sample revealed that the copper layer of the material configuration failed just before the main composite material failure. In the case where the copper layer was on the compression side of the bend test sample, the copper appeared to buckle and de-laminated from the adhesive layer and not actually break into separate pieces. In the case where the copper was on the tensile side,

the layer developed a crack at the point where the carbon fibre load layers failed. The copper appeared to undergo plastic deformation prior to the carbon fibre failure point. At no point did any of the composite samples fail and separate completely into two pieces. During inspection after failure, the samples still held together with reasonable strength when an attempt was made to separate the composite by hand. During testing, a noticeable failure in the material structure was seen by a deviation of the expected linear response during the initial loading of the specimen. Therefore, to assess the type of failure samples 9 and 10 of both sample batches were stopped at a pre-break point to assess the type of damage that had occurred. No external or visual indication of the type of failure was evident during an inspection of these samples. The discussion of these results will take place in the following chapter.

4.2.2 Modal Verification Testing

This section will present the data captured from the tests conducted using the speaker vibration jig and test method described in section 3.4.3. Two primary orientation configurations were tested on the vibration test bench, vertical orientation as seen in figure 3.52 and a horizontal direction as seen in figure 3.53. Based on the two photos referenced in the previous sentence, the speaker naturally moves in a linear pattern in a vertical axis, thus the mounting jig for the satellite has been designed so that the orientation of the satellite can be rotated through 90 degrees.

In each orientation, a control measurement was first taken by mounting the accelerometer to the centre base section of the mounting jig and running the sine wave profile through the speaker. Thereafter, the accelerometer in the same orientation (maintaining the same X and Y-axis alignment), was placed on the top surface of the satellite to measure the response of the panel.

Once both tests were run the data collected in each case for the control and the satellite response could be compared. For the Z-axis motion (primary movement direction of the speaker) the control data was subtracted from the response data, in each orientation case, to find a differential graph which would highlight the frequency zones where the satellite structure responded to the vibration. A point on each data set was matched up to synchronise the time point of each data set before finding the differential data.

The two subsections that follow present the data collected from the tests, the Z axis (speaker movement axis) control data, the measured data from the satellite panel and the differential graph from each orientation is presented. A frequency verse time graph as also been included to use as a time-based reference to the frequency sweep from 5 to 100 Hz over the 120-second test.

The accelerometer that was used for measurement was initially calibrated using a 3D printed jig that held each of the 3 accelerometer axis parallel to the gravitational line and thus allowed a know ‘g’ value to be used for calibration. For each axis a simple Arduino code was used to calculate the compensation value for that axis to ensure a reading of 1g when the unit was orientated in that axis using the jig.

4.2.2.1 Vertical jig orientation

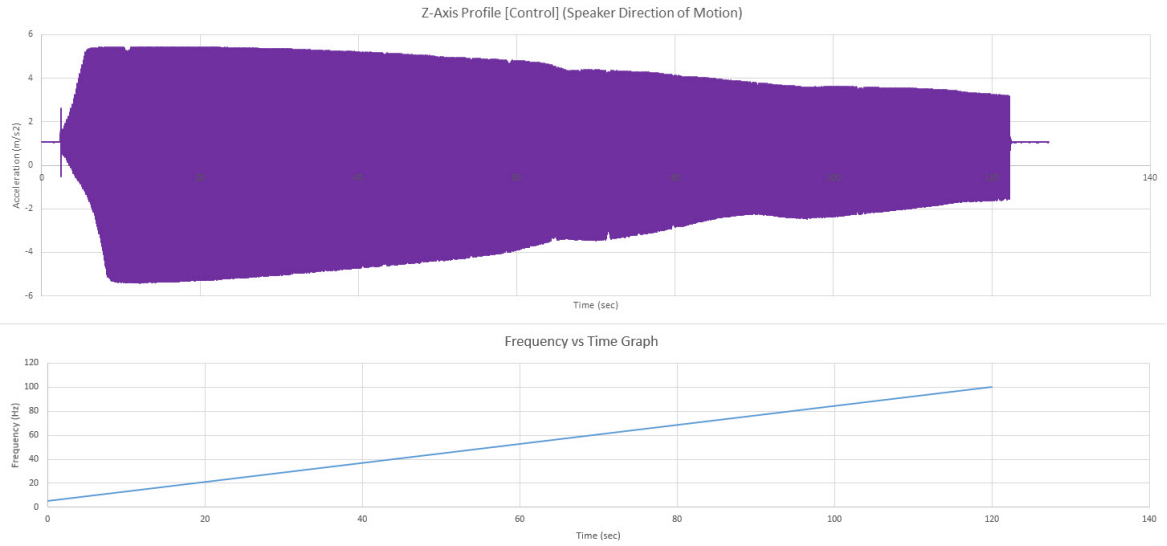

Figure 4.116: Vertical test Z axis control measurement.

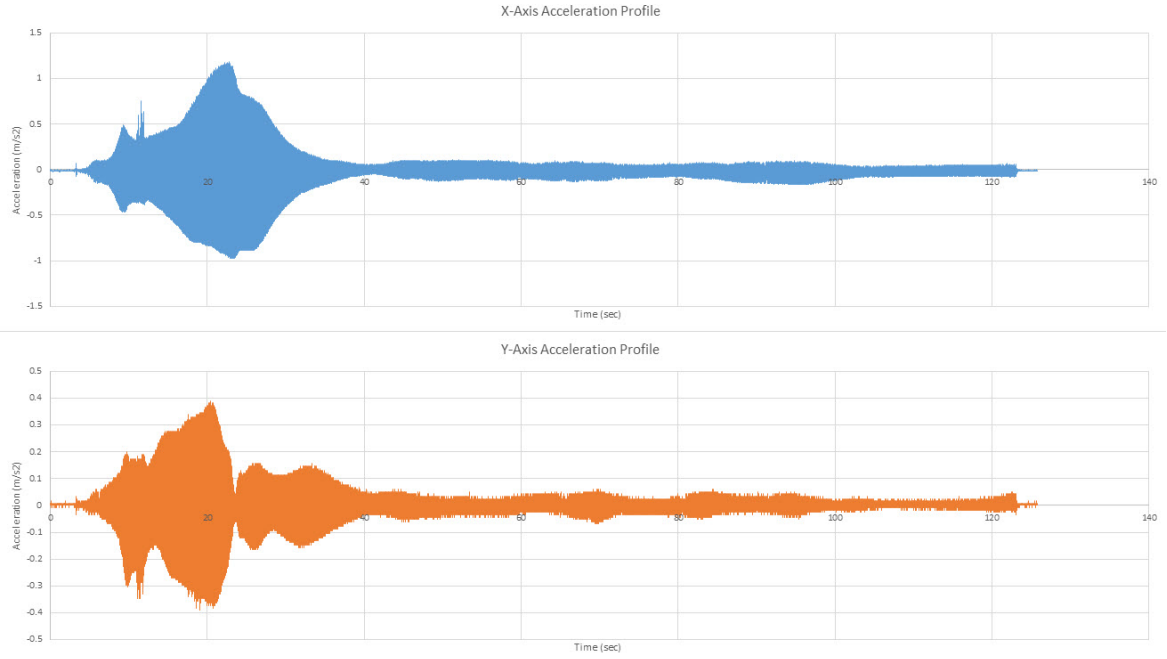

Figure 4.117: Vertical test X and Y axis measured data.

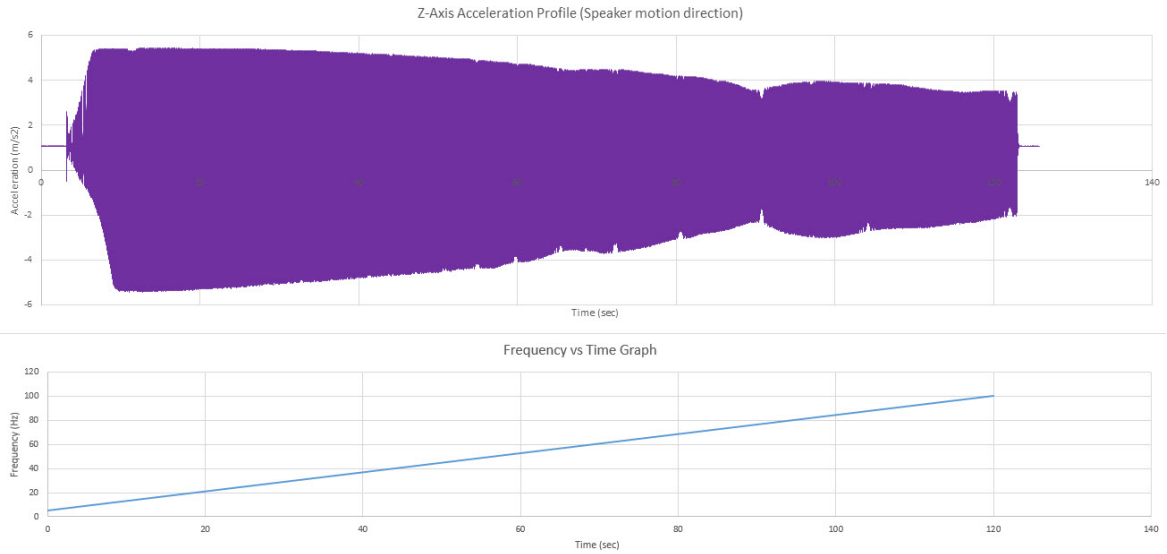

Figure 4.118: Vertical test Z axis satellite response measurement.

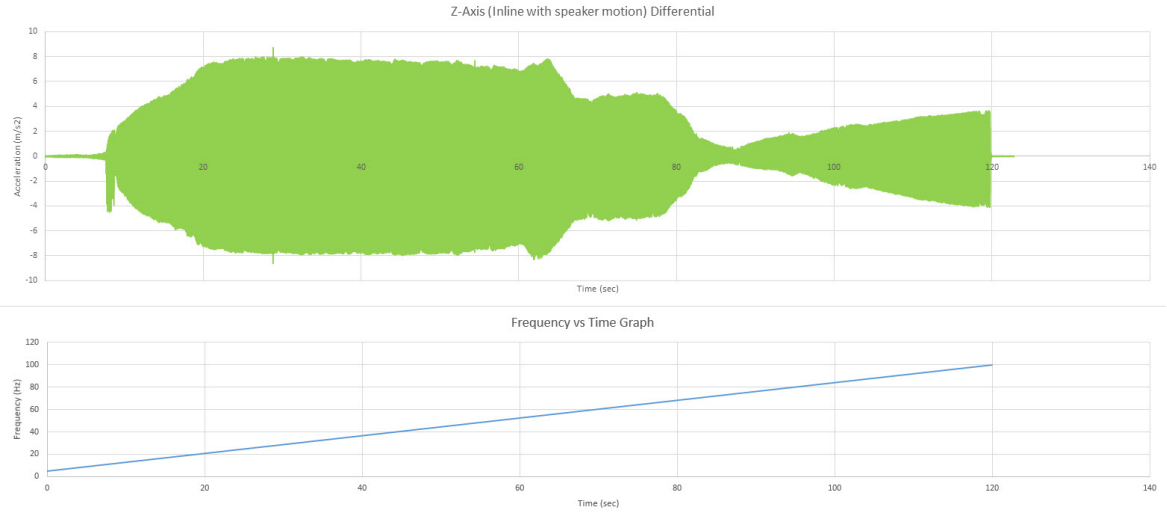

Figure 4.119: Vertical test Z axis differential graph between the control and response measurement.

4.2.2.2 Horizontal jig orientation

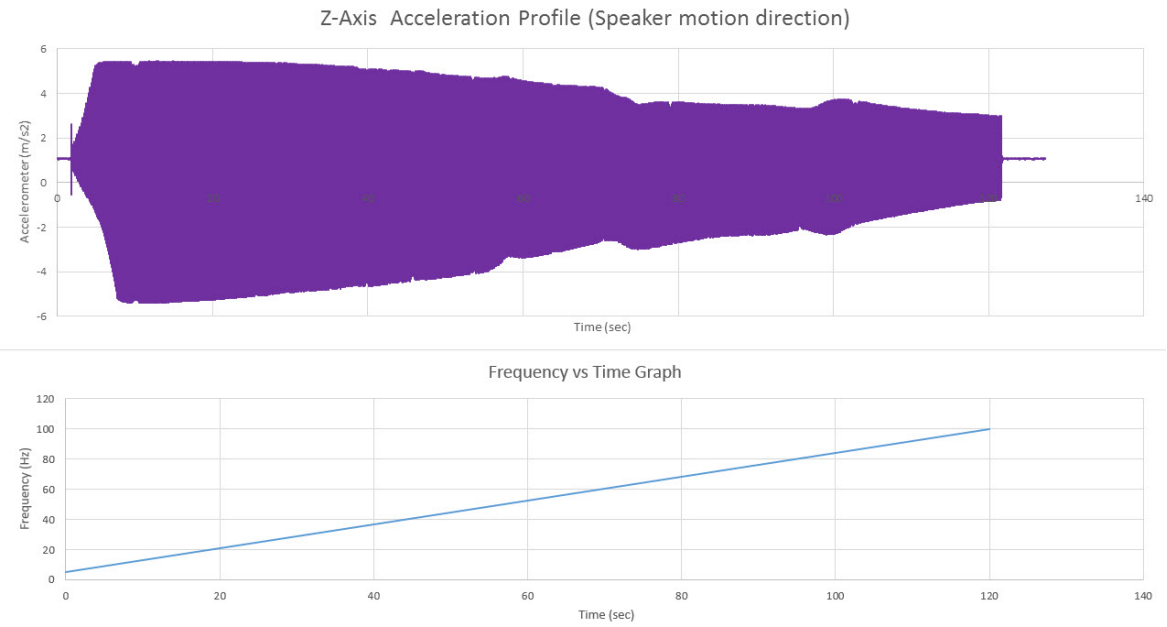

Figure 4.120: Horizontal test Z axis control measurement.

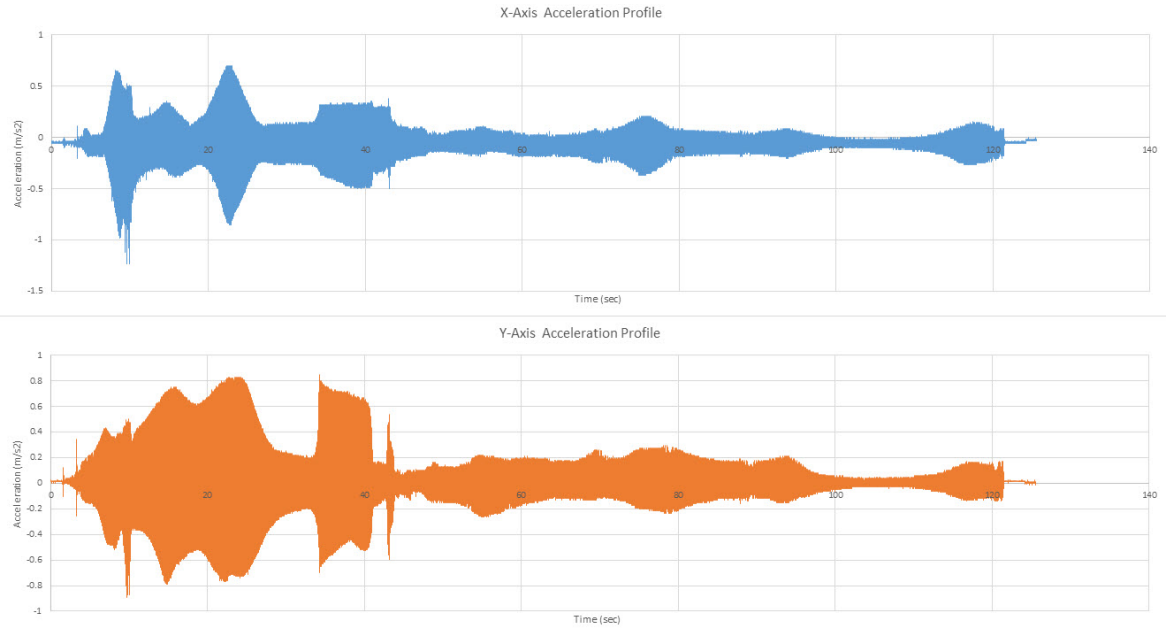

Figure 4.121: Horizontal test X and Y axis measured data.

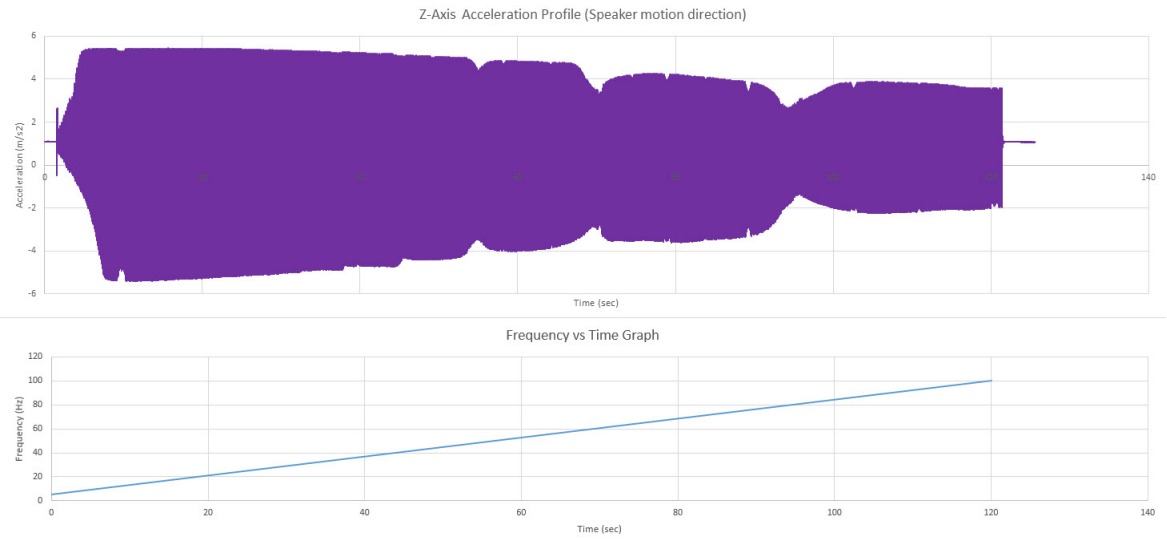

Figure 4.122: Horizontal test Z axis satellite response measurement.

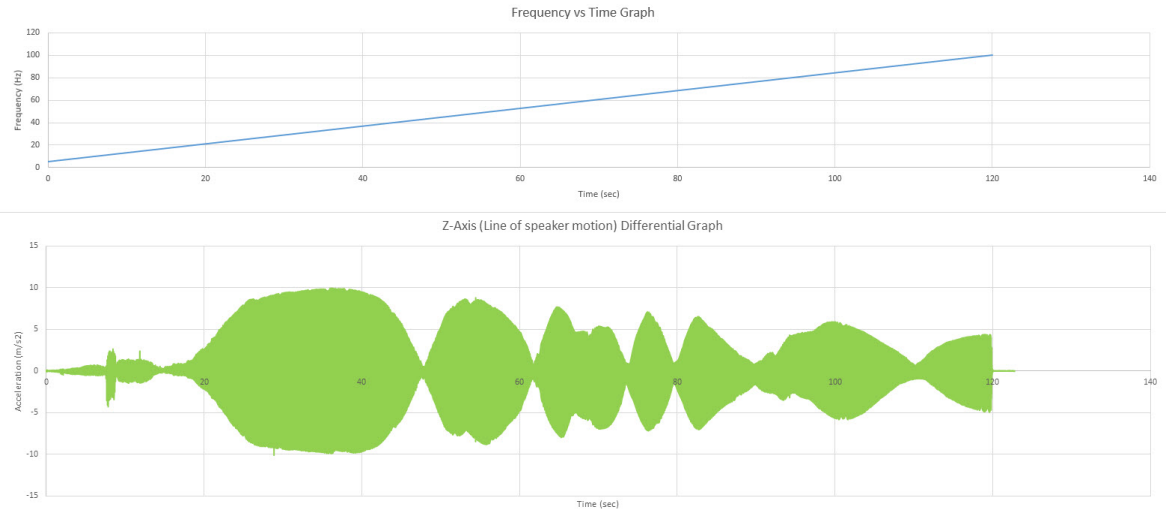

Figure 4.123: Horizontal test Z axis differential graph between the control and response measurement.

4.3 Comparison of Material Test Data

A comparison of the virtual tensile and bending test data and the empirical test data that was collected is presented in the graphs and tables below.

4.3.1 Tensile Test Data Comparison

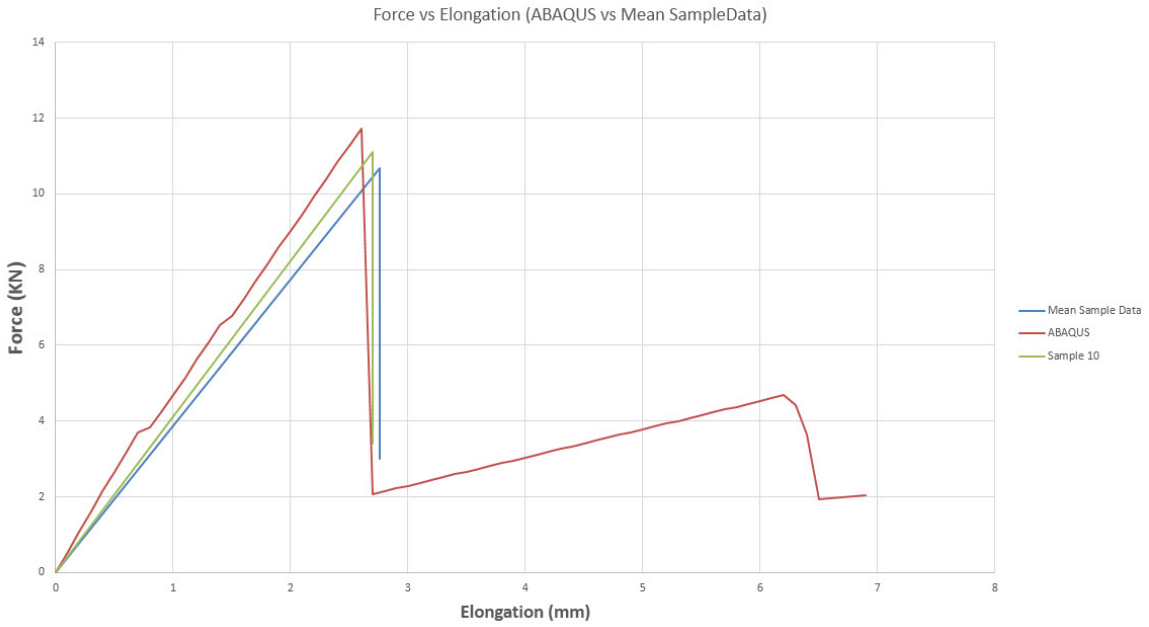

Figure 4.124: Data comparison graph of the material data, predicted from ABAQUS PFA and the actual data.

Source:	*Max. Force Tensile:*	*Elongation:*
ABAQUS PFA	11.277	2.76
Mean Sample Data	10.673	2.6
Error (%):	5.4	5.8

Table 4.6: Table summarising the data deviation and error percentage between the tensile test data.

4.3.2 Bend Test Data Comparison

4.3.2.1 Copper surface upward (on compression side of sample)

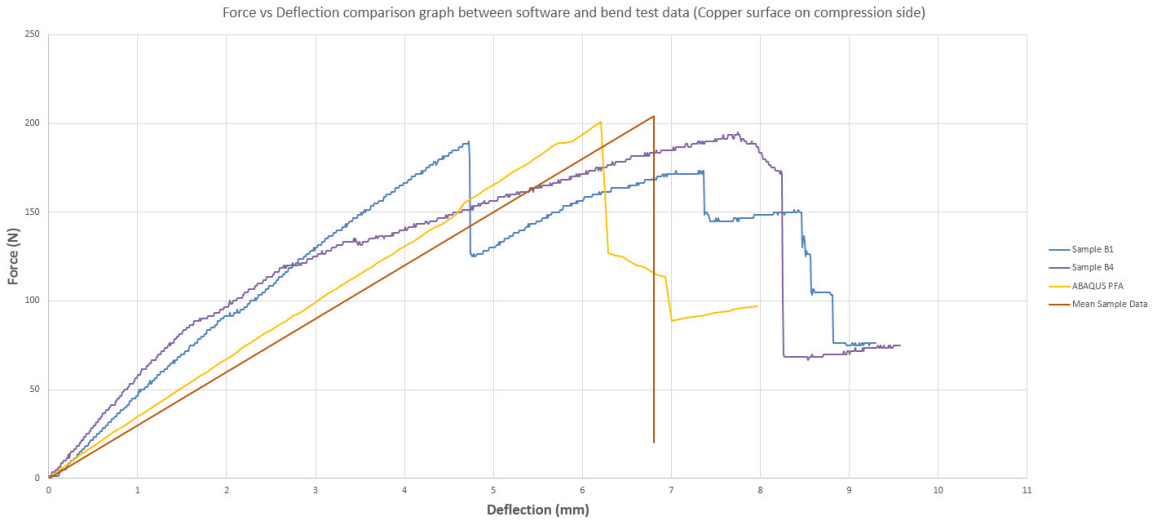

Figure 4.125: Data comparison graph of the material data, predicted from ABAQUS PFA and the actual data.

Source:	***Max. Bend Force:***	***Deflection:***
ABAQUS PFA	201	6.2
Mean Sample Data	204	6.8
Error (%):	1.5	8.8

Table 4.7: Table summarising the data deviation and error percentage between the bend test data for copper up.

4.3.2.2 Copper surface downward (on tension side of sample)

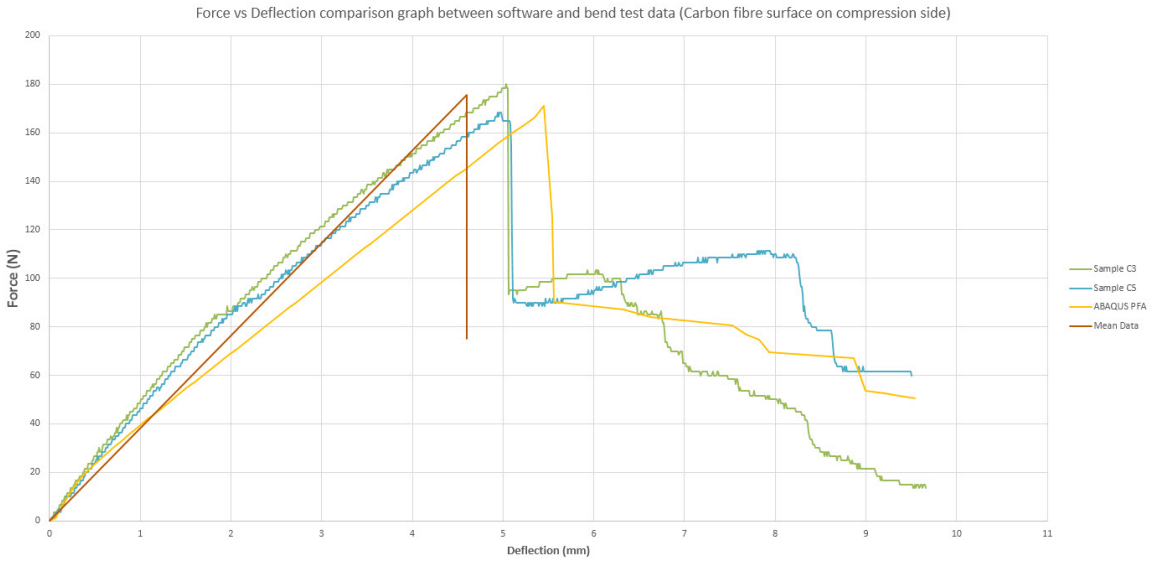

Figure 4.126: Data comparison graph of the material data, predicted from ABAQUS PFA and the actual data.

Source:	Max. Bend Force:	Deflection:
ABAQUS PFA	171.2	5.45
Mean Sample Data	175.6	4.6
Error (%):	2.5	18.5

Table 4.8: Table summarising the data deviation and error percentage between the bend test data for copper down.

4.4 Prototype CubeSat Model

The prototype (mock-up) structure was created from 3D printed representative parts for the aluminium components and multifunctional composite material layup panels produced using the infusion table available at the research lab. The panel profile dimensions were machined using a PCB milling machine and the finalisation of the countersunk holes was done by hand. The mock-up model was then assembled using countersunk M3 screws in all the hole locations. A further representation of a previously developed antenna deployment system (ADS) was also 3D printed to check the interfacing between the ADS subsystem and the structural designed. The images below show the results of the mock-up structure manufacture.

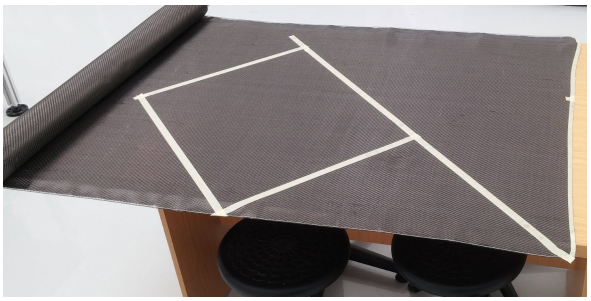

Figure 4.127: The 45 degree Section of the 2/2 Twill weave dry carbon-fibre material being prepared.

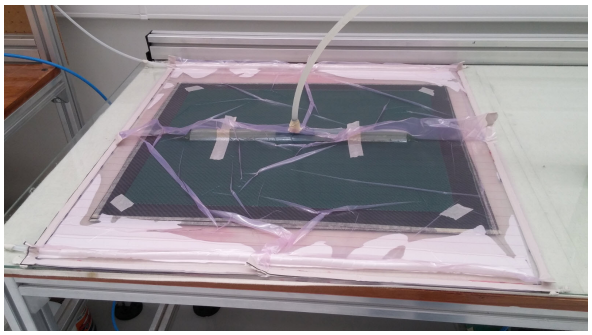

Figure 4.128: Infusion of the carbon fibre composite layers.

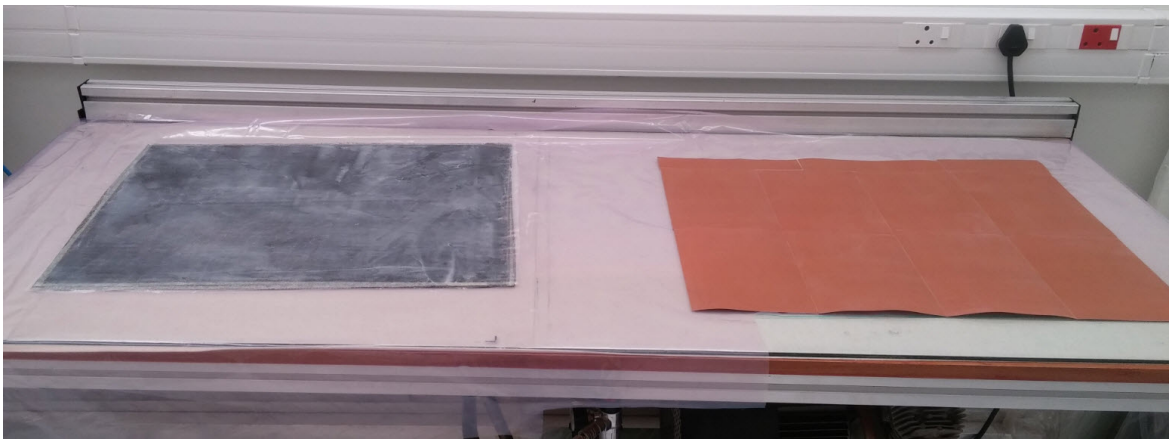

Figure 4.129: Carbon Fibre material with the adhesive layer applied and the prepared FR4 backed copper foil layer prior bonding.

After the adhesive has been applied the two layers are stacked on top of one another and a large supawood board with a vacuum bag placed over the top of the component and sealed to the table. It is important to note that the adhesive layer was levelled to approximately the thickness of the bond line control mesh to limit the inaccuracies of adhesive pooling between the layers. In previous attempts, the layer was not smoothed and the adhesive did not flow to a level bond layer, but in fact pooled in the middle of the component. A vacuum level of 80 % was achieved when pressing the two layers together.

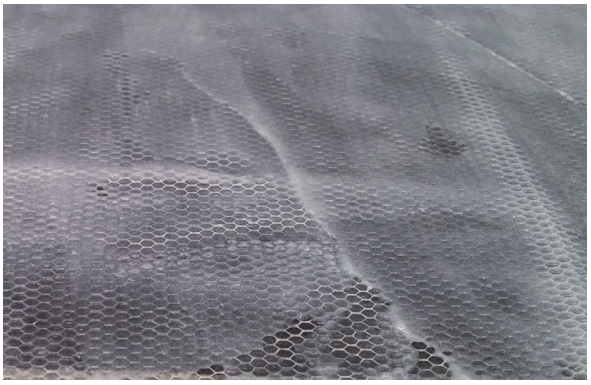

Figure 4.130: Closer view of the adhesive layer applied to the carbon fibre material with the bond-line thickness control mesh.

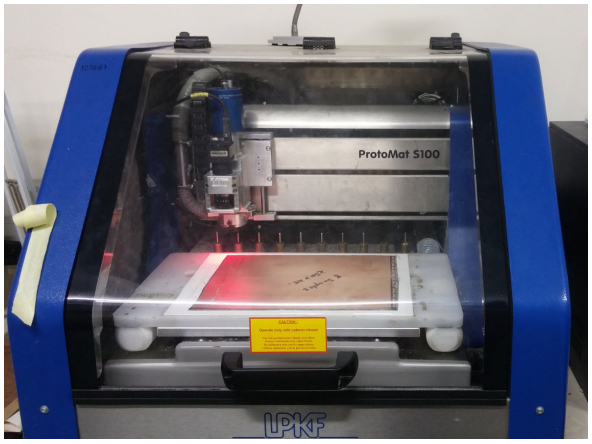

Figure 4.131: PCB machine cutting the samples and mock-up structure panel profiles.

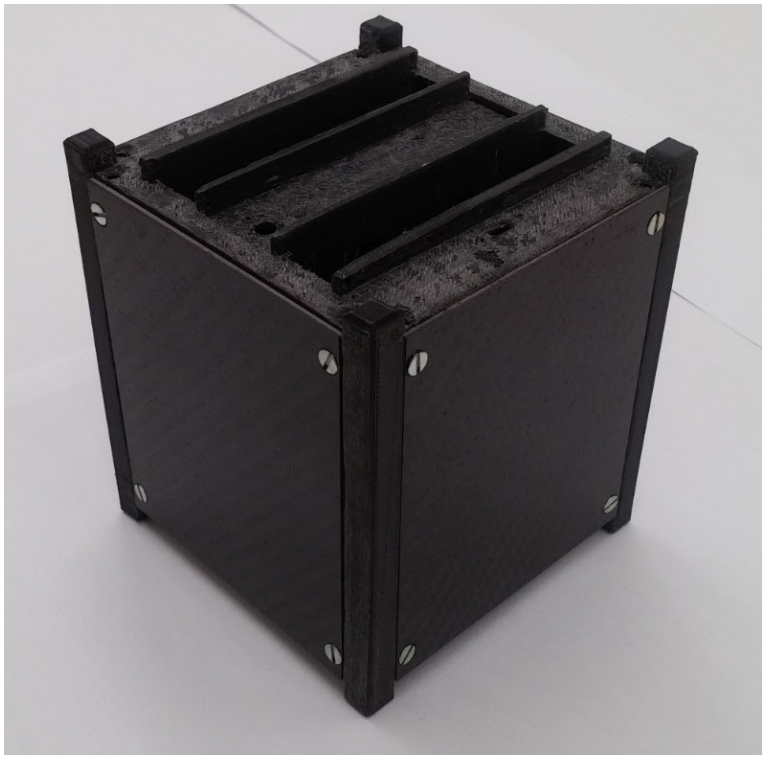

Figure 4.132: Completely assembled mock-up structure with the 3D printed ADS module in place.

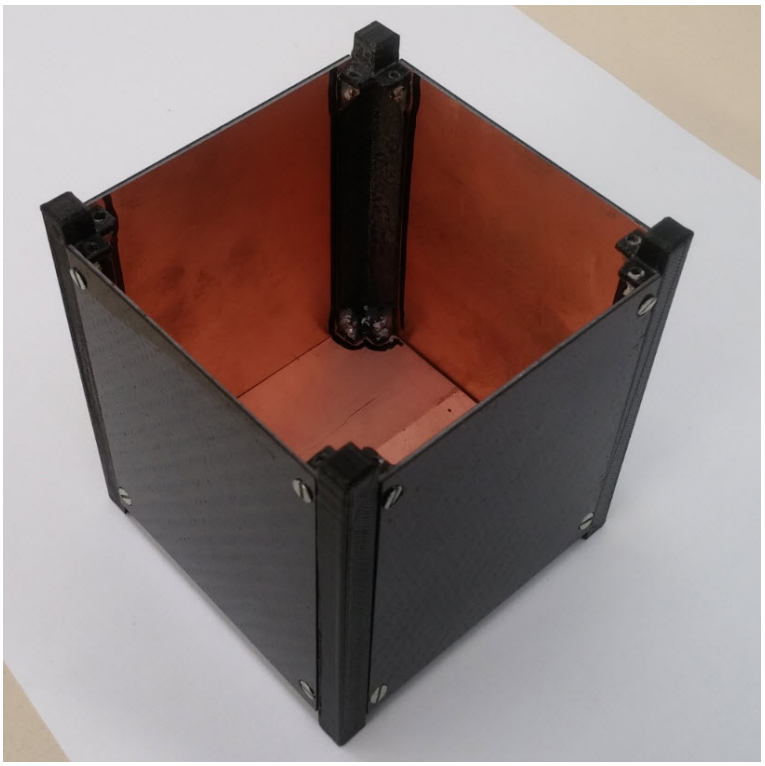

Figure 4.133: Internal copper layer of the mock-up model before PCB circuitry machining.

Figure 4.132 and 4.133 shows the completed prototype structure that had 3D printed posts to verify the form and fit all the components before the machining of the aluminium components took place.

Thereafter, the final prototype CubeSat structure was produced. A new set of carbon fibre panels was created and milled out on the PCB cutting machine. In this case, a simple surface mount LED circuit was created to demonstrate that the copper circuit function performs as a normal PCB would. Multilayer copper circuits could be integrated into the design to allow further electrical connections to take place behind the surface mount systems. A simple LED circuit was more than enough to prove the concept, as any further electrical developments would begin to leave the primary focus area of this research.

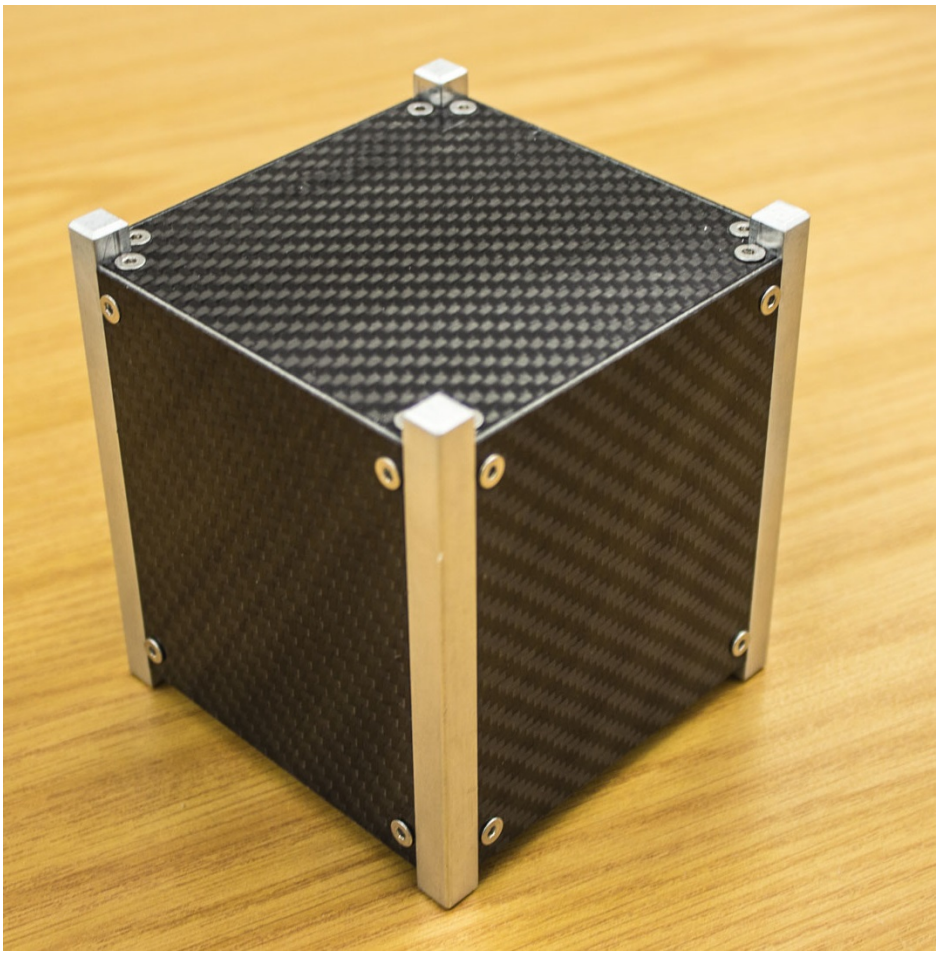

Figure 4.134: Completed CubeSat model with aluminium machined posts.

Figure 4.135 and 4.136 illustrates the completed demonstration circuitry inside the CubeSat on the copper surface that was previously blank in the 3D printed mockup model. The copper panels are all grounded through the aluminium posts and jumper wires transfer the positive power supply to each panel.

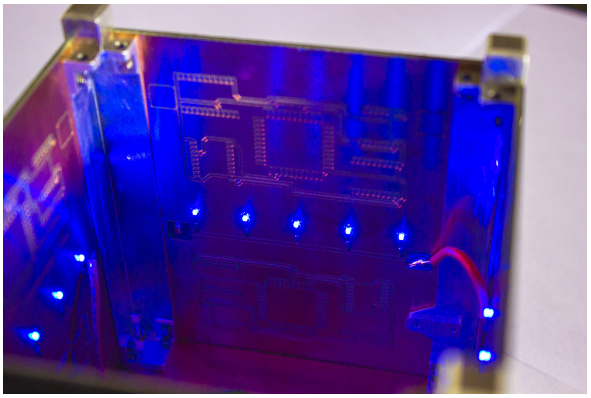

Figure 4.135: Close-up view of the machined circuitry on the internal surface of the CubeSat.

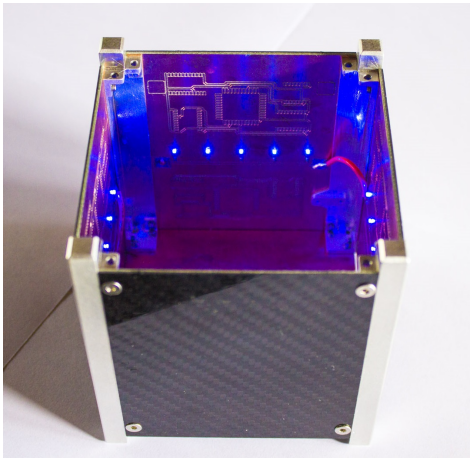

Figure 4.136: Overall view of the LED proof of concept surface mount system.

Figure 4.137 provides a comparison between the 3D printed mockup post initially used and the machined aluminium post used in the final prototype model.

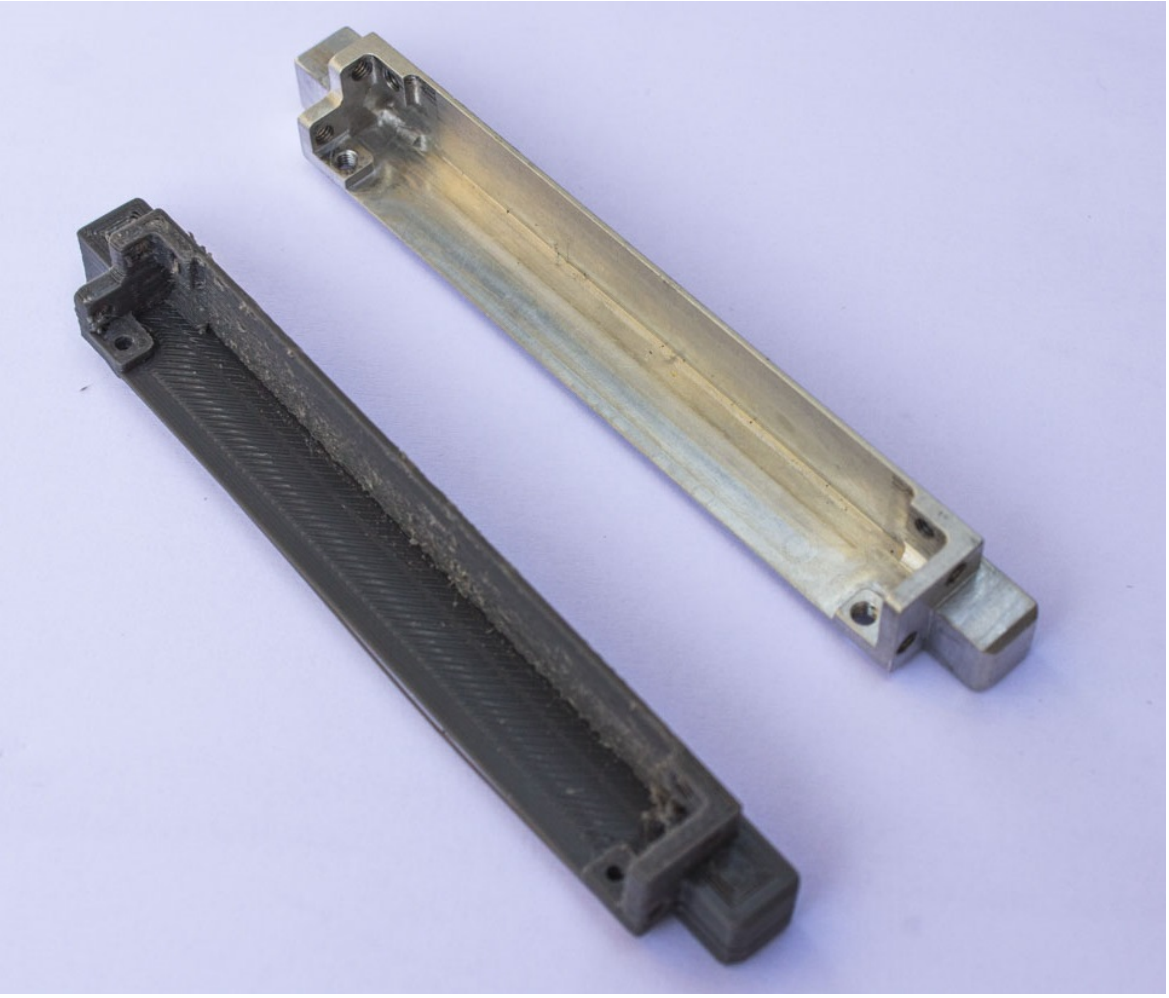

Figure 4.137: Mockup post 3D printed, made of grey PTEG plastic on the left and the final machined aluminium post on the right.

Overall the prototype CubeSat had a great surface finish on the carbon fibre, as well as good dimensional thickness accuracy of a deviation of no more than 0.2 mm across a 400 mm section of the MFC material. The material thickness on the final prototype was 1.52 mm which is 0.12 mm over the design thickness.
The machining of the outer panel profile and the circuitry on the internal surface proved to be exactly the same as a conventional PCB machining operation. It was noted that the milling bits would dull faster when cutting the carbon fibre material, however, this was expected due to the abrasive nature of the material.
There were no assembly issues or misalignments during the assembly of the prototype structure and all the components fit together as designed. Stainless steel countersunk Allen cap screws fasteners were used. A small decrease in the local strength of the material may be seen due to the machining of the fastener positions. However, considering the low material stress under loaded conditions and low stress cycles seen in operation, this reduction if strength should not be a problem but would can be checked for during physical testing as a safety precaution.

Chapter 5

Discussion and Conclusion

5.1 Discussion

The purpose of this penultimate chapter is to segment the discussion into various sections which will assist the reader to grasp the critical main points. Each of the sections below will make extensive reference to the research methodology presented in Chapter 3 and the subsequent data presented in Chapter 4. It is recommended that the previous chapters should be examined before reading of this section.
The discussions commenced with the design of the CubeSat structure and the associated influences powering the final conceptual working prototype. Each of the numerical simulations and empirical data-sets collected from the physical tests are discussed thereafter.
The manufacturing and construction of the prototype are argued to give insight into the challenges and achievements of the completed process. Finally, this chapter culminates in an inclusive and holistic supposition of this dissertation.

5.1.1 Design

The design of the multifunctional composite material CubeSat structure was challenged by various restrictive factors. The first of the two key limitations were the CubeSat standards, and secondly, to procure available budget to produce the concept prototype. In the real world environment, securing substantial funding for an experimental technology that has not yet been proven, is extremely taxing.
In the face of these limitations, three concept designs were created and presented in section 3.2.2. The original idea focused on the creation of a solid composite shell that implemented aluminium rails which could be bonded to the exterior edges of the composite shell.
Concept 1 presented rewards in terms of continuous composite and electrical connections as the side panels of the structure now became one solid shell component. The primary cause for Concept 1 not being chosen was the confined potential to fabricate the structure. The solid composite shell requires the manufacturing of specialised

moulds in order to create the single composite shell. It was extremely difficult to produce these moulds with the limited available equipment at the university.
Furthermore, a single composite shell limits the tolerance of the manufactured shell due to the uncontrollable shrinkage and warping of the composite after curing. An epoxy resin system will be used in the conceptual design that presents very low wrap and shrinkage when compared to other common resin systems, but it still exerts a role in dimensional tolerance accuracy and interfacing of components. As will be seen in all the conceptual models, the aluminium rail interface on the edges of the structure is a mandatory feature as stipulated in the CubeSat structural standards (see Section 2.2.2.2).

Structural Concept 2 (which pursued Concept 1) featured separate composite side-panels which simplified the manufacturing. These panels could be assembled on a flat-glass table and the panel profile routed out after curing was complete. Concept 2 also employed a system of interlocking panels into slots in the aluminium rails in an attempt to strengthen the entire assembled structure. The primary concerns with Concept 2 occurred in respect to the maintenance, accessibility and interchangeability of the structural components during the construction/development phase in the laboratory. The intention was to bond the panels to the aluminium rails with a high strength epoxy; however, this system poses a challenge to later disassembly or exchange/replace components of the structure after assembly.
The interchangeability of parts is important as it is highly dubious that the first iteration of the assembly would be perfect. The separate panels made machining of the circuitry on the side panels far more plausible. If there are changes made to the electrical circuitry due the development of electrical subsystems, the panels need to be exchanged without having to manufacture an entirely new satellite. It is crucial to sustain a practical design that lends itself to a lower system life-cycle budget.

Concept 3 was the final chosen design iteration due to the evolution that compensated for the various system considerations. Concept 3 now replaced the interlocking system of Concept 2 with a conventional bolting system of the panels to the aluminium rails. The higher stress point at the locations of the screws on the composite material is a drawback in this concept. Composite materials are known to be brittle and not as ductile as metals, thus the interface of the screws to the composite panel needed a smooth transition. Any protrusion from the panel surface due to the screws will interfere with outer dimensional limitations as stipulated by the CubeSat standards therefore the screws needed to be countersunk. The interchangeability, accessibility and maintainability issues highlighted in the previous concept were at this point be solved.

A large factor in the concept designs' shaping was the consideration of internal volume and weight. While Concept 3 allowed for the side panels to be near flush with the outer interface surface of the aluminium rails, the other two concepts did not. The location of the side panels in Concept 3 thus allowed for a greater internal volume increase of approximately 3 % versus those of the first two concept designs.

The lightest commercially available 1U CubeSat structure from CyldeSpace is 155 grammes, which excludes the cover panels. The manufacturers report that the conventional full model, including cover panels and solar panels, is reported to weigh

250 grammes. The cover panels would be PCB, containing both the solar panels and required connection pads.

The designed and actual MFC CubeSat weighs in at 200 grammes, again excluding the solar panels. These panels are estimated to weigh approximately 50 grammes to cover the entire surface of the CubeSat. This gives the MFC structure an overall design weight of 250 grammes.
The entire structure weighs approximately the same, but with an improved internal working volume. The increase in rigidity and stiffness of the structure when compared to the conventional structure is of huge advantage. (Section 4.1.4.3 specifies that the conventional aluminium chassis produces a maximum vertical deflection of 0.056 mm under the same conditions, where the composite structure experienced is a maximum of 0.046 mm.) Although these deflections are very small, an increase in rigidity of approximately 22% is observed. The increase in stiffness would be beneficial as it would inherently increase the natural frequencies of the structure and thus further away from the modal frequencies of the launch vehicle.

Another benefit is the combined ability for electrical engineers to include electrical circuitry and sub-systems onto the composite panels of the structure itself. This allows more available space on the internal electronic boards for larger payload systems or main electronic sub-systems. In addition, an added benefit is the secondary electromagnetic shielding that the carbon fibre material provides to the internal electronics. The carbon fibre material effectively forms a type of Faraday cage around the electronics and will additionally prevent RF interference and aid the shielding against energised solar radiation particles.

Crucially, the mass of the MFC CubeSat listed above is that of the 'worst case' configuration that uses a resin infusion manufacturing method. The recommended manufacturing method for the flight model of the CubeSat is an autoclaved prepreg, which would greatly improve the quality of the composite panels as well as reduce the mass. In a later section, it is explained that the number of plies in the composite panel can be reduced as there is sufficient room in the rigidity level, but this in turn will provide further weight reduction of the structure. The ply-layup would, however, be subjective to the system requirements of the structure, depending on whether the weight or the rigidity of the structure is more critical to the designers. Generally, there is room for designers to adapt this design to the specific mission requirements and subsequent system requirements of the structure.

The spacecraft design considerations involved the radiation effects on the composite materials, the exposure to higher level atmosphere atom oxygen particles that create the issue of oxygen erosion during Lower Earth Orbit (LEO) and the launch loads on the satellite. Once the satellite (in this case the CubeSat) is in space, there are very little physical force loads presented to the structure. The largest force loads experienced on the satellite is during the launch phase, which is discussed further in the next paragraph when the material strength properties are considered. Due to the relatively short design life of CubeSats, the radiation degradation effect on the composite material is not as highly considered as the thermal effect of the solar

radiation that the CubeSat will be exposed to. CubeSats typically have a design life of only a couple of years. As a result of the lack of propulsion on most CubeSats and the LEO pattern, de-orbiting takes place over the course of the satellites' life cycle. New regulations are also heavily restricting dormant satellites in space due to the amount of space debris present and the requirement of manufacturers to design a de-orbit phase soon after the satellite mission is complete. The thermal radiation effects are only considered to a level that provides an indication of the plausibility of the design to function in the space environment. Due to the large scope of this research, a number of tests are only executed to the level where there is an indication about the likelihood of success. In actual fact, each of these areas (for example the thermal radiation) on the structure could be treated as an independent research topic. To develop a successful concept within a reasonable time, with consideration of all the key design areas, details for each test have to be limited. The thermal radiation that the CubeSat will be exposed to is discussed in a later subsection.

The material types, characteristics and strength of the design have been considered, as this is the primary focus area of this research in the field of mechanical engineering. Firstly, the aluminium rails were made from 7075-T6 grade aluminium as it is commonly used in the aerospace industry and the T6 tempering provided a high UTS and stiffness properties, which is ideal for the relatively thick profile sections of the aluminium rails in the concept design. The majority of the material mechanics focus is on the composite material configuration. Calculations for the micro-mechanics were done using a MATLAB algorithm written based on the composite micromechanics theory presented in the theory literature review chapter.
The MATLAB program provided much faster iterative processing behind tow fibre property sizes twill weave mass per square meter configurations when selecting the twill weave type that would be used. Multiple twill weave fibre configurations were considered even though the choice was restricted to the twill weave fabric available at the varsity. The effect of using different twill weave types would primarily change the number of ply layers used in the panel construction due to the fabric thickness. The twill weave fabric available at the university provided the best trade-off between the number of layers needed, the strength and stiffness required for the prototype, the cost and availability of the material from local suppliers.

It must be noted that the dry fabric twill-weave carbon fibre would only be used for the proof of concept prototype, but the flight model itself would use twill-weave prepreg carbon fibre. The material testing discussed later considers the material in a worst-case scenario, as the prepreg would be of a higher quality. The twill-weave used in the prototype model could simply be exchanged for twill-weave prepreg of the same configuration for the flight model, and would present better mechanical properties. Thus, if the dry material shows good success rates, then the accomplishment of this material concept is highly possible.

The micromechanics theory evaluates the ply-layer properties of the carbon composite material. The data is entered into the ABAQUS FEA simulation program for further analysis in terms of the macro-mechanics behind the simulations model assembly. The ply orientation and the layer angles are programmed into ABAQUS to determine

the interlayer relations on the material and translate that to the overall assembly of the model, the aluminium rails and the other composite side panels. The stacking of the composite material also incorporates an adhesive layer and a copper foil layer to provide the electrical circuitry connections that create the secondary function of the material. Three layers of carbon fibre provide a good layup structure by allowing the top and bottom layers to be orientated with the maximum strengths in the 0 and 90-degree directions and the middle layer to be orientated at 45 degrees to provide additional strength in the offset plane. The multiple layers also increase the laminate thickness which improves the second polar moment of area and thus the rigidity of the panel as well. Since the carbon fibres are electrically conductive and provided an Electromagnetic Interference (EMI) shielding property, the material will form a type of "Faraday cage" around the internal electronic subsystems. The copper foil layer on the internal surface will provide a full ground-panel for any radio frequency components or antennas used on the satellite, if needed.

The material configuration that used only composite plys and also the consideration of panels including a core material to provide the rigidity. Due to the thickness limitations to maximise internal volume only composite ply configurations were considered to build the panel thickness.

Unfortunately, time and budget constraints did not allow for the prototype material to be out-gas tested and thus the main driver for the prepreg is required for use in the actual flight model. NASA has a database of approved composite materials for space use. Due to the unlimited possible combinations of resin and fibre systems, most of the carbon composite materials on the NASA database are limited to prepreg carbon fibre available to industries. For the flight model, one of the approved prepreg materials can be used instead of the dry material and resin matrix system used for this prototype. Should budget or facilities become available in the future to perform out-gas testing on the current CubeSat prototype material, these tests can be performed. If the material passes, from the data collected during the tests this material could very well be used on the actual flight model.

The cost of prototype production was far less than that of any commercially available structure on the CubeSat market. It has to be noted that the majority of the expenses related to CubeSat structures on the market has been attributed to flight heritage and flights into space. At the time of writing, the cost of a 3U structure used by the space research centre for their current CubeSat project was approximately R140 000. In comparison, the raw material cost of this prototype was approximately R15 000 for in-house production. The final flight model would need to use prepreg carbon fibre which would increase the cost. The cost of the composite structure would still be far lower though than a commercial structure. The lower expenditure would support motivation for the MFC structure that would be completely customisable to the specific requirements of the each CubeSat and its designated mission, in spite of the fact that the new technology lacks flight heritage.

5.1.2 Numerical Modelling Results

The next subsection aims to briefly discuss the data from each of the numerical simulations performed on the MFC structure CubeSat.

5.1.2.1 Static Load Simulations

A static load analysis design was performed on the structure to determine the response under loading. The entire launch process was taken into account before selecting the conditions that would be set for the static simulation. As discussed in section 2.5.4, the launch process can be considered quasi-static for the most part when considering the acceleration loads on the payload in the launch vehicle.

The literature review revealed that the peak acceleration loads subjected to the payloads of the launch vehicle, and the maximum peak overall load expected on the payload, is 6g to the longitudinal axis and 2g in the lateral axis. The direction of the acceleration loads are relative to the launch vehicle orientation; however, the satellite payload may not always necessarily align to the same orientation of the launch vehicle, thus the loading conditions during the simulation need to considered at this point. The orientation of the satellite would in almost every case be subjective as CubeSats are not the primary payload in the launch vehicle. Secondary payloads are positioned in the best way to 'make it fit'.

Another observation is that there is no internal mass representation in the satellite simulations. The analysis is designed to evaluate the deflection of the outer composite shell panels under the acceleration loads. The internal electronic sub-systems use a PCB stacking configuration that focuses most of the load through a short section of the aluminium corner rails of the structure. The focused load over the short length has little moment loads on the structural supports and most of the load is transferred into the CubeSat axially. The setup of the simulation uses boundary conditions to mimic the environment the satellite will be enclosed in during launch.

The simulation results prove that even with four times the expected load (20 g applied) the deflection of the composite panel and structural entities for the most part negligible. The maximum axial deflection during application of the 20 g longitudinal static load was approximately 0.06 mm which is extremely minute when considering it relatively.

The horizontal loading of the satellite (transverse to the direction of the corner rails) also yielded a maximum deflection of approximately 0.06 mm in a similar location to that of the longitudinal loading. The horizontal loading was set to 10 g, which is ten times that of the expected lateral loading; nonetheless, a large load factor was used to cover the eventuality that the satellite is positioned transverse to the orientation of the launch vehicle, but still have a load factor of two.

Although the static load deflection was insignificant and would have no real impact on the structure, the deflection characteristics of the structure can, however, be noted to

isolate any potential issues when or if a larger loading condition is encountered during the system lifecycle. In both cases, the maximum deflection occurred on the side panels of the satellite at mid-point interface near the aluminium rail. In the design, there is no fastener in this location: nevertheless, adding a fastener here may be advantageous to increase rigidity and reduce the deflection of the side panels. It is likely due to the panel shape that the deflection occurs at this point, being rectangular in shape and the bend axis across the side panel is the narrowest section of the CubeSat cover panels. The deflection profile of the top and bottom panels indicate some emergence of a membrane effect; regardless, a symmetrical deflection profile is observed as expected due to the symmetrical geometric profile of the top and bottom panels. One however, needs to bear in mind that the loading conditions are also symmetrical, but the material properties are not necessarily symmetrical in the case of composites.
The stress plots in the structural panels were not shown in the results as the bolt loads applied in the initial step of the simulation produced almost all the stress seen throughout the simulation. To keep the report manageable, the stress plot after the bolt load step was applied, and is displayed once at the beginning of the results section. After evaluation of the Von Mises stresses, the maximum stress recorded in the bolts is approximately 440 MPa, but this is result is skewed after observation of the stress plot profile. There is a marginally localised high-stress point which sees the 440 MPa stress. The high-stress anomaly is likely due to a mesh issue or node point that has not been accurately simulated. By observation of the stress plot on the bolt, it can be seen that the average stress through the bolt is approximately 250 MPa which is still well within the yield stress of the stainless steel material.

5.1.2.2 Impact Test Simulations

A brief impact analysis was performed to account for the impact of debris on the satellite. Though there is a large array of variables that need to be accounted for in such a simulation, the level of detail that this analysis involved did not need specification of the variables and consequently assumptions were made where necessary.
A dynamic analysis of a composite panel receiving a debris strike at its centre was considered. The material properties were maintained as per the previous simulation and the boundary conditions were set up to represent the panel-fastening to the structure as a whole. The specified debris material was aluminium along with a projectile velocity. A few 'low-speed' impacts were done at 400 m/s
The deformation of the debris particle itself was not an area of interest in this simulation, but rather the stress in the composite panel. At 400 m/s the panel withstood the impact, however, after observing the peak stress in the panel at the early stages of the impact, it is very likely that the panel would have suffered damage where stress cracks in the composite panel would likely appear and the panel strength would be compromised. The stress distribution across the panel is extremely good and shows an even wave of stress as it travels through the panel. Due to the insignificant loads on the structure when in space, the damage to the composite panels would have a low chance of a later fatigue failure due to the crack propagation if the panel is still intact after the debris strike.
The subsequent simulations subsequently ramped up the velocity to the likely impact speeds of 4.5 km/h when in orbit. A logical consideration from an engineering point

of view is that the panel would fail catastrophically, as the kinetic energy of a particle at this speed is enormous. As expected, the simulation failed to yield results due to large amounts of element deletion and geometry distortion. It is safe to say that an impact on the structure at this speed would destroy the satellite and no conventional or composite material design within reasonable specifications would withstand this type of impact. A debris avoidance orbit pattern would be highly recommended in any CubeSat mission before applying any type of 'armour' against debris impacts.

A large area of concern in the space community is the amount of debris building up in the space environment and the threat this poses to satellites. At this point in time it is still far more plausible to implement avoiding action against debris collisions as opposed to physical protection on-board the satellite.

5.1.2.3 Orbital Thermal Simulation

Once again, the thermal analysis was not the primary focus of this research, but it is nonetheless important to consider the thermal effects on the structure and ensure that the materials can cope with the extreme temperatures. With most composite systems, the upper temperature generally becomes the first limiting factor, as the matrix resin component cannot handle extremely high temperatures and consequently begins to degrade. Most high-grade prepreg composite material can handle temperatures of above 100 deg C, which will be the material used on the flight model of the satellite. Thus, the fact that the maximum temperature seen from the thermal simulation is about 40 deg C, this will not be an issue for the material. The minimum temperature seen in this simulation is -85 deg C, which is still within the working range of the composite material. The internal sub-systems will only produce heat and radiate that to the structure; thus it is unlikely that the sub-system components will decrease this value even further.

Once again the internal sub-systems and the thermal distribution are both not known, and therefore accurate simulations cannot be performed. The simulations that have been done, provide a good foundation to infer that the structure shows very good promise that it will, in fact, work in this environment. NASA has also been using carbon fibre composites on spacecraft for many years and the base material of this structure has space flight heritage to support it.

The orbit that has been simulated is almost impossible for the CubeSat to actually achieve and maintain; however, this orbit was selected for a worst case scenario. Fatigue of the structure has been taken into consideration as the only stress other than an impact on the structure will be due to the thermal loading as it orbits. The thermal loading will be cyclic during the orbit. One important explanation for why the fatigue has not been taken further is that the working temperature range will very likely be less than that of the simulation results. From the data and discussions with engineers of previous CubeSat temperatures, the likely working range would be between 50 deg C and -40 deg C. Due to the large difference of the thermal coefficient expansion between the aluminium and the carbon fibre composite, the side panel holes which would likely be the largest issue can be slightly slotted to allow for linear movement between

the screw and the composite panel during temperature fluctuations. This can reduce the risk of induced crack propagation in the composite material.

The design life is two years only, and this needs to be kept in mind when looking into the fatigue of the satellite structure. Two years is a very short lifespan, but under the new regulations that govern the space debris, satellites must be decommissioned after its use. The satellite will also be de-orbited until it burns up in the atmosphere.

5.1.2.4 Natural Frequency and Modal Response

The natural frequency and modal analysis performed on the satellite structure had to evaluate the type of response the structure has to the loading and vibration that it will be subjected to during the launch.
The sine vibration tests on this structure have been considered as a primary focus area, since the data can be physically verified with the available test equipment. The sine vibration test requirements only cover up to the 100Hz range as per the testing range for the European launch vehicles as listed in section 2.5.4. Because of the operation of the solid rocket boosters, the majority of the large amplitude vibrations are seen at lower frequency ranges. The higher frequency ranges are created by aerodynamic noise on the surface of the launch vehicle, are less intense in amplitude and decrease further as the air density reduces in the launch.

The first simulation that was done is the natural frequency analysis of the structure. The first 10 eigenvalues have been shown in section 4.1.4.4 for the structure that has been designed. The first mode is at 608Hz which is well above the larger vibration levels from the solid rocket boosters which range from 0 to approximately 150Hz. The remaining 9 natural modes are in very high ranges and are well above the test range of the sine vibrations.

Following the natural frequency analysis is the dynamic sine vibration response under loading of the structure. A sine vibration load ranging in amplitude of +5g to -5g was subjected to the structure for more than two minutes. To match the test criteria as close as possible, a sweep across the sine frequency bandwidth was from 5 to 120Hz.

Five main response frequencies were observed during the test and these were at 18Hz, 31Hz, 50Hz, 79Hz and 120Hz seen in section 4.1.4.5.1. In all cases, the top and bottom composite panels showed a membrane deformation effect, with the largest deflection occurring at 79Hz. The maximum deflection magnitude was approximately 0.004 mm, which is extremely small in magnitude. The horizontal response was very similar to that of the vertical test, with the frequency response ranging across 9.7, 18, 31, 50.6, 79.25 and 120Hz, seen in section 4.1.4.5.2. The maximum deflection occurred at 79.25Hz with a maximum deflection magnitude of 0.006 mm.

The amount of deformation seen in response to the applied vibration would not create any significant issues for the structure. The most likely reason for the extremely low deflection is the low density and specific mass of the composite panels and these are

able to withstand large acceleration loads with very little influence on the structural geometry. There are also no loose or flexible wires/connections exterior to the panel that would create possible electrical faults as a result of the fatiguing of the copper wires oscillating under vibration. The vibration would have a far greater impact on the integrity of the internal electronic sub-systems long before the structure will be affected.

As part of the empirical data collection and testing, a vibration analysis of a prototype MFC CubeSat structure was performed in an attempt to verify the numerical data collected from the simulation.
Both a horizontal and vertical vibration test was done on the satellite structure. A reading from the base of the jig connected to the vibration jig was recorded, as well as for the vibration on the top surface of the satellite. The two data points that were recorded could subsequently be synchronised by a constant sample rate setting by the recorder; then subtracting the vibration of the base of the jig from that of the satellite panel itself. The remaining data would be the differential between the surface of the satellite panel and that of the vibration jig and thus one can evaluate the composite panel response to the vibrations.

The vertical modal differential graph seen in figure 4.119 does not clearly show the exact positions of the response of the composite panel; however, it does show that in the 79Hz and 120Hz regions that a deflection response is observed. This denotes a correlation to the data seen in the numerical simulation model. A minuscule response is observed at approximately 15Hz which is close to the initial 18Hz mode seen in the numerical analysis data. Unfortunately, the responses between 20 and 60Hz are not as clear. Although the numerical data provides a comparatively pinpoint frequency of response, it is unlikely that this would be seen with such precision in a physical test environment. The number of contributing factors in the test are almost endless. One of the larger variables influencing the physical vibration tests is the presence of air which would create a damping effect on the vibration rig. The damping would smooth the resultant actuation of the vibration patterns on the satellite, thus reducing the clarity of the readings. Overall the test does provide an indication that the numerical simulations show agreement in particular response areas to that seen in the physical tests conducted.

Having a look at the differential graph in figure 4.123 for the horizontal orientation vibration test, the peak response areas are more clearly defined on the graph. The first frequency response highlighted by the numerical analysis was at 9.7Hz and after evaluation of the differential graph, a clear peak is seen at around 10Hz on the graph. The next frequency responses at 18 and 31Hz are not as clear and did not show distinctive peaks at these frequencies. At 50Hz on the graph, there is a clear response, with a decrease in acceleration at this zone. Between 60 and 80Hz on the graph, multiple peaks appear; however, the numerical analysis had shown the largest response to occur at 79Hz which directly correlates to a peak on the acceleration graph in figure 4.123. The responses at this point appears to taper off with a larger broader band response at approximately 100Hz on the graph.

The numerical data, for the most part, had a good correlation to the empirical data collected from the physical prototype model vibration test. The numerical model

appears to perform its exact task of providing an excellent estimation of the model response and it cannot be assumed that the numerical analysis will mimic the real world test result exactly. The number of variables at play in the actual test makes an ideal analysis virtually impossible; but the accuracy of the predictions provided by the numerical analysis appear to be within an allowable range to the actual tests data.

5.1.3 Physical material test results

Both a numerical and empirical analysis was done for the MFC material testing. The data or the numerical analysis is presented in section 4.1.1 and the empirical material test data is presented in section 4.2. The main focus of this discussion will be on the comparison between these two sets of data, for which the results are presented in section 4.3.
The material test consists of a tensile test and a 3 point bending test. The numerical analysis FEA used a PFA plug-in tool to further increase the accuracy of the failure prediction of the fibres in the laminates. The tensile comparison graph presented in figure 4.124 compares the mean physical test data curve to that of the numerical analysis, and to the closest sample failure observed in the physical material tests. Table 4.6 provides the comparison data between the FEA prediction and the average physical sample curve. A good correlation between the numerical prediction and the mean empirical sample test curve. It must also be noted that the empirical sample data is an average of an array of tests that were done, thus the deviation percentage is spread across an accumulative error between the physical test sample data. The tensile test data comparison yielded a 5.4% deviation in the tensile force on the sample and a 5.8% deviation for the elongation of the sample. The observed deviation is relatively accurate and the numerical data could, in fact, be used to form design predictions. The FEA prediction produced a slightly higher failure point, however, this is somewhat expected as the simulation assumes a perfect laminate production with no voids or misalignment of the fibres in the laminate. In reality, however, it is very difficult to create a "perfect" composite sample but to achieve a percentage error of within 6% is very good considering the manufacturing process used.

Two sets of bend tests were conducted on the samples: one for the copper skin-side up (on the compression side) and another where the copper skin was down (on the tensile side) by the three-point bending test.
Evaluating the comparison of the copper skin facing upwards as illustrated in Graph 4.125 and Table 4.7, the FEA predicted force at failure shows very good correlation to that of the mean physical sample data collected and falls within 2% of one another. Once again as expected the FEA model over-predicts the force at failure very slightly, however as previously mentioned this is due to an "ideal" laminate section assumption. The elongation, however, was a bit further off, where the physical test sample seemed to deflect more than the FEA model. The approximate 9% error is most likely due to a non-ideal laminate structure, for example, if the laminate has more percentage resin to fibre ratio than the ideal laminate ratio, it will create a more elastic laminate result. Regardless, the failure force would remain very close to the ideal level as the amount of load-bearing fibres remain unchanged.

Looking at the other bend test where the copper skin is facing downwards, presented in Graph 4.126 and Table 4.8, the resulting error is approximately twice that for both the maximum force and deflection when compared to the previous test error.
After close observation the maximum force at failure is lower than the failure force of the copper skin-upward test, which is likely due to the fact that the composite load-bearing section is now mostly under compression. As the laminate is not symmetrical, a deviation in results linked to the sample orientation was expected. The deviation matches the initial hypothesis that the laminate will not perform as well when the composite is mostly under compression. This hypothesis stems from the documented literature knowledge that composite materials perform better when subjected to tensile loads and not very well under compressive loads. The matrix material has to support more of the compressive load, as the fibres will deform and buckle under compressive loads. The performance theory would also explain the decrease in deflection before failure, as the resin matrix material is the primary component to fail and has little contribution from the fibre content.
The increase in the error between the FEA model and the physical test samples shows that composite prediction under compressive loads is in fact hard to predict accurately. The true amount that the fibre element contributes to the structural support is harder to determine and would be more sensitive to the quality of the composite. The quality of the composite under compression is heavily dependent on the resin to fibre ratio, due to the load bearing portion placed on the resin when compared to a tensile load case. In the case of a tensile load where the resin primarily hold the fibres in place and protects them, the portion of load taken up by the fibres is far greater and because the fibre weave is constructed accurately by a factory machine, the deviation in performance will be less relative to the quality of the resin infusion. The opposite is true for the compression loading of the composite material.
Keeping these theories in mind, the analysis still provides a reasonably good prediction of the performance of the laminate material, and the FEA data can be used extensively in the design discussion making process when it comes to multifunctional composite structure design.

An outgassing test of the material would have been desired to check the qualification status of the designed composite laminate. The resources, however, were not available to perform this test, but as a fail-safe alternative, the flight model laminate can use the most costly prepreg version manufactured in an autoclave of this carbon fibre construction to increase the quality of the laminate. A prepreg that has already been approved by NASA for outgassing specifications can be used to avoid this issue; however, a physical outgas test would be desired.

5.1.4 Modified design simulation results

5.1.4.1 Cutaway side panel model

A variation of the main composite CubeSat design was created in an attempt to create the lightest version of the CubeSat. One major compromise of this design is the fact that the shielding effect of the composite panel now no longer has very much of an

impact as the open holes in the side panels now allow high energy particles and radiation to directly impact the internal subsystems of the satellite. The 'cutaway' model, however, had ground for testing, as current conventional CubeSats have deployable panels when in full operation and deployed, which leaves the internal components of the satellite exposed to the space environment Thus this version of the CubeSat would be available to designers that feel they do no need the shielding properties of the composite panels.

During the analysis of this satellite the deflection due to the bolt loads, vertical and horizontal acceleration load were simulated for comparison to the original design. The natural frequencies of the structure were also evaluated.

In this configuration of the satellite, it was observed that the deflection of the panels was significantly increased when compared to the original design. The deflection due to the bolt pre-load increased from 0.05 mm to 0.4 mm, which is significant. The same is seen with the acceleration loads on the satellite where an increase form 0.04 mm to 0.4 mm was observed. Even though a large increase in the deflection of the panels was seen, the performance of the panel suggests that the structure will still meet the requirements for the CubeSat structure.

A reduction in the natural frequency from a minimum of 608Hz to 503Hz was also observed. Although the performance of the satellite has decreased, the specifications will still be within an allowable range to be used for an actual structure. The cutaway panel design still uses 3 plies of carbon fibre and only a 5 % weight saving was seen in the CAD models for the design. This is not as great as initially expected as the weight saving should be the primary area of improvement.

5.1.4.2 2 Ply composite layup model

After evaluation of the data for the original composite panel design, the large rigidity of the structure made it possible to reduce the number of ply layers in the composite material while still maintaining a strength level great enough to serve the structural function of the CubeSat. It should be noted that this does not change the original model; it is rather a simulation to observe the key effects the structure is the number of composite plies is reduced.

In section 4.1.6 the bolt pre-load effect, natural frequencies, vertical and horizontal static load simulation have been re-run on this 2 ply structure to evaluate the effects.

The deflection of the satellite panels due to the bolt pre-loads are only 0.01 mm more than the original composite structure. This is expected as the bolt pre-loads will not be as affected by a thickness change of the panel material.
The vertical and horizontal deflections, however, did see an increase in the 2 ply model as expected due to the reduction in overall rigidity of the panels. The deflection profiles are virtually identical, however, the magnitude of the deflection is 0.02 mm greater (approximately 50 % larger) than what was seen from the original construction.
The natural frequency of the structure sees a reduction from the original 608Hz to

474Hz which is approximately 22 % less.
Overall the performance of the structure still falls well within the required specifications of the CubeSat structure and a 2 ply configuration could be used. A predicted mass saving of a further 5 % is seen in the CAD model of the structure between the original and 2 ply composite structures.

5.1.5 CubeSat prototype manufacture

The composite panels were the greatest manufacturing challenge in this research. The carbon-fibre composite was created using a vacuum infusion process on a glass-table. After the composite infusion was completed, a secondary process involved the application of an adhesive layer on the carbon composite and bonding of the copper foil layer, using a vacuum pressure plate setup. The carbon composite panel had to have the excess resin material smoothed off of the peel ply surface to ensure a flat surface was obtained for the adhesive layer.
Multiple manufacturing attempts were done, as various smaller issues during manufacturing were discovered. The first issue arose during the adhesive layer application: in the first attempt the adhesive was applied by hand and was inconsistent. It was anticipated that the applied pressure via the vacuum pressure plate would level the layer and expel any excess adhesive. However, the materials deformed and the adhesive pooled in the centre of the laminate.
The solution was to use the bond line control thickness mesh (as seen in the adhesive in figure 4.130) when spreading the adhesive with a scraper across the composite laminate. The mesh would allow a level gauge to produce an even coating of adhesive before the copper layer was applied. This method seemed to work well in the final laminate production.
The second issue was that the pressure plate (a glass pane) was deforming under the vacuum pressure, thus the final attempt used a 22 mm thick piece of "supawood" above the glass pane to increase the rigidity.

The MFC panel had to be left to fully cure before the CubeSat panel profiles were milled out of the laminate sheet using a PCB milling machine. The milling process seemed to go flawlessly and posed no issues.
A set of 3D printed rails to represent the aluminium rails were created before having the actual items machined. This provided a quick and easy method of performing a form and fit verification of the components. Again no major changes needed to be done to the aluminium rail profiles.
The aluminium rail sections of the prototype were manufactured by RORA engineering, which is an extremely professional machining company that has many years experience in machining high-quality aerospace parts. The aluminium rail was machined exactly to what was specified in the design.

The new MFC CubeSat seemed to be extremely rigid once assembled and all the parts fitted perfectly together. All the edges and details of the structure turn out exactly as designed.
During the machining of the final prototype panels, the electronic circuitry was added to the internal copper surface and then the components were added. The CubeSat

underwent the vibration testing and the LED system worked perfectly without any damage once the solder joints and tracks were inspected with a microscope.

5.2 General Conclusion

Looking back at the work, the result and the discussions in this thesis, the entire concept of developing a successful working multifunctional composite structure for use on nanosatellites appears completely plausible. Considering the initial and primary objectives for this research, all the objectives were met and have been extensively covered in this study.

The first objective was to explore the current MFC technology and its implementations, and subsequently look at their application potential to nanosatellites. The literature review uncovered huge potential for this nanosatellite design, based on the success seen in the application of MFC structures in larger satellites. It has been shown that conventional structure designs can be further optimised to create greater internal volumes in the satellite and allow a single structure to perform more than one main function to the satellite system.

The technology has an extremely wide research potential well beyond the boundaries of this thesis and leaves significant room for the technology to grow and develop in the nanosatellite industry. Existing applications of MFC, regardless of where it has been applied, support the notion that this will be the future of structural design in most future spacecraft, and more specifically in smaller satellites in an attempt to maximise the overall units' functional potential. The research into the implementations of this concept structure is firmly based on proven theories and applications of this new technology and the more traditional composite design theories that are applicable.

Another primary objective was to formulate a design concept for the application to a nanosatellite, primarily focusing on CubeSats. The three key design concepts that have been covered in the discussion all have functional potential; however, the chosen concept's use of fastened composite panels allowed for modularity of the design and the ability to customise each surface of the CubeSat. This once again opens up enormous possibilities for designers to tailor the structure to mission-specific requirements; regardless, in the same way, it allows for minor design changes during the development of the satellite without affecting the complete structural design. The design of multiple panel configurations of the electrical circuitry and design updates without compromising the integration of other panels or the structure as a whole. The structure still falls within the internationally set design regulations, which are important for the future success and promotion of interest in this proposed CubeSat structure concept. The design has been kept as simple as possible, which can be an extremely challenge in itself. This mitigates the risk associated with complex system designs. By having a concept structure that works within the set regulations, with any luck, actual MFC-structured CubeSats will be built and launched in the future to provide flight heritage for the system and promote exposure of this technology in the nanosatellite industry. This could very well lead to modifications of the standards in the future to

further accommodate MFC structure designs as technology matures.

The concept design can be broken down into known design theories for composite materials, PCB design on the electrical side and overall structural design for the form and shape. The unique combination of these theories formulates the overall design process for the MFC structure, and by consideration of each sector on its own allows designers not to feel overwhelmed by a seemingly alien or novel concept idea. Current designers of spacecraft can utilise this technology without the need to relearn any new theories: they just need to combine known theories in a new way. Notably, the proposed concept structure in this research also matches or has improved the overall performance of the CubeSat structure in the respects of weight, strength, internal volume (payload volume) and functions.

Another objective was to critically evaluate the concept design with the available numerical analysis tools and physical test equipment to support the numerical analysis predictions with empirical data obtained. Numerical analysis of the concept structure applied as many FEA tools that were available at the time to construct the best picture of the structural performance when subjected to the conditions likely experienced during the system lifecycle of the satellite. Structural rigidity analyses were performed with gravitational loads, material strength tests, modal analysis (vibration loading), impact analysis and thermal considerations during orbit. In each simulation case, the structural concept performed admirably and shows promise that it will be stable during operation within its system lifecycle. Empirical analysis was applied to support the numerical analysis, notably in the sine vibration loading and the material strength test simulations. The empirical data collected from the tests indicates a good correlation among many variables in the simulation environment. The material strength testing provided results that support the use of progressive failure analysis (PFA) in FEA programs to produce more realistic failure curves for composite materials. Generally, the analysis work on the structure provides enough feedback to adjust the design for a feasible working platform. The design can naturally be optimised by performing more detailed simulations in each area; however, when considering the number of simulations for a satellite structural system and level of detail that could potentially be taken to, would be too vast for any single person to cover in one research effort within a reasonable time. Using a systems engineering approach with a holistic view of the structural design, the simulations were taken to the required level of detail to provided design data across as many key-design driving parameters as possible.

The last key object was to develop a functional prototype structure to demonstrate the manufacturing process that would be used to produce the CubeSat structure, but also to produce physical samples of the material to be used to collect empirical data. The manufacturing process developed for this multifunctional composite material was an adaptation of conventional composite manufacturing methods through infusion and combination of conventional PCB manufacturing techniques in order to produce a material that incorporates electrical circuit capabilities. The final applied manufacturing process produced excellent results after fine-tuning and adjustments trial, error and experience. The prototype CubeSat was outstanding and fully supported the feasibility of the design to be manufactured. The physical tests were fulfilled without any problems as mentioned in the previous paragraph. Input from another master's level electrical engineer was extremely optimistic about the workability of the physical

material when compared to conventional PCB material and corroborated that there was no noticeable difference from an electrical point of view during manufacturing between working with either material during the soldering and component attachment process.

Holistically, this multifunctional technology has performed superbly in its concept design and shows an eminence considerably above average for future endeavours into this technology. Relatively speaking, the research effort presented here has only scratched the surface, and the boundaries of this technology still lie far beyond what can be presented in a single master's thesis. The research has shown that the concept structure can perform its role in the space environment and has been proven as successful in all the investigated and analysed fields. When all is said and done, this application of multifunctional composite structures to nanosatellites proves itself to be extremely valid and beneficial to the field of structural design. The field of MFC is still wide open and this is only the beginning. The future of this technology will be exciting, and fascinating to track, as it grows within the space industry and beyond.

Chapter 6

Recommendations

6.1 Systems Engineering application to research

The application of systems engineering to this research is critical. During consideration of the structural subsystem of a satellite, the integration of the structure with the other satellite subsystems is essential. This will ensure that the overall satellite system operates to meet the system requirements which are based on the mission requirements.

As a future recommendation in the development of the first multifunctional composite structure to be used in a nanosatellite mission, further use of systems engineering will be required to communicate systems requirements to the various engineers working on the satellite sub-systems. Due to the fact that this research effort did not consider any specific system requirements (due to not having a defined mission specified), the designs have been left in an adaptable prototype state as more of a proof of concept. The use of systems engineering in the space industry has been around since its conception, as systems engineering's birthplace is the space industry. However, it must not be overseen that systems engineering is left aside when developing MFC structures further, as the integration of other subsystems is not more vital due to the increase in functions of the structure to the satellite system overall.

6.2 Numerical modelling recommendations

The numerical modelling applied in this research study can undoubtedly be taken to higher levels of detail. This issue was briefly mentioned in the overall conclusion of the previous chapter. Due to time restrictions and maintenance of a reasonable level of design-based simulations, advanced detailed optimisation and analysis can be investigated as an entire research paper on its own in each of the simulation fields covered during the conceptual design in this case. More significant investigation into the thermal characteristics of the structure in the space environment should also be undertaken specifically once the mission requirements have been defined and a known

operational pattern for the satellite system can be predicted.
In addition to the thermal analysis, further investigation into the electronic components can be assumed by specialist electrical engineering researchers in order to optimise the protection provided by the structure against single event upsets (SEU) created by high energy radiation particles. The radiation test can also be supplemented by physical radiation tests on prototype structures once the required test equipment becomes available.

6.3 Verification test recommendations

In future research attempts, more sophisticated tests can be instigated once the required equipment and machinery become available for physical tests on the multifunctional structure concepts. During development of an integrated MFC structure for a specific mission, the physical testing thereof will be vital to support the numerical predictions during the validation process of the systems engineering cycle. As mentioned in the previous paragraph, a priority for expanded research is the thermal and radiation testing of the material. Based on the physical data collected from the tests, various changes to optimise the design can be completed to improve the structural overall performance. Another key test (which was not available to this particular research study) is the out-gas testing of the composite materials, which will be crucial during corroboration of the structure's specifications to the satellite standards before launch will be allowed.

6.4 Design Optimisation and Future Developments of the Technology

After extensive literature reviews of other research into a similar field of work has revealed many future possibilities for multifunctional composite structures. As a few examples research into the integration of solar cells into the exterior surface of the structure can be done to enable energy harvesting capabilities for the structure as an additional function with the addition of very little mass to the structure. Furthermore, new research into extremely thin lithium-ion batteries in place of the core material of composite materials allows the composite structure to both harvest and storage of energy within the boundaries of the structure itself. These prospects are extremely exciting for future developments of this technology as advanced MFC structures could progress to a level where the structure itself is self-sustaining and can be relied on as a full support system to provide not only structural protection but also to harvest and distribute electrical power to the various sub-systems. In light of the protection to the sub-systems, further research is also undertaken in the area of thermal isolation and conduction. This transpires through the inclusion of various graphite base materials which will allow heat to be moved from one internal space within the satellite to another area that requires heating, thus making the system more energy-efficient. Other protective materials against high energy radiation particles could be included

in structures that will have missions operating in orbital regions where the radiation levels are more focused.

It can ultimately be concluded that the future possibilities for this material are virtually boundless. It can be expounded and adapted to suit the specific requirements of the satellite mission. As various developments in technology are becoming available further research can be conducted in order to refine the MFC level of technology and its application to all forms of spacecraft in the future. This will undoubtedly not be the last of multifunctional composite materials, but rather part of the initiating steps in the development of this technology.

References

Adumitroaie, A. and Barbero, E.J. Beyond plain weave fabrics i. geometrical model. *Composite Structures*, 93(5):1424 – 1432", 2011a. ISSN 0263-8223. URL http://www.sciencedirect.com/science/article/pii/S0263822310003880. [Accessed]

Adumitroaie, A. and Barbero, E.J. Beyond plain weave fabrics ii. mechanical properties. *Composite Structures*, 93(5):1449 – 1462, 2011b. ISSN 0263-8223. URL http://www.sciencedirect.com/science/article/pii/S0263822310003909. [Accessed]

Adumitroaie, A. and Barbero, E.J. Stiffness and strength prediction for plain weave textile reinforced composites. *Mechanics of Advanced Materials and Structures*, 19(1-3):169–183, 2012.

AMT-Composites. 300-450 gsm csm, 2015. URL http://www.amtcomposites.co.za/. [Accessed]

Ansar, M.,Xinwei, W., and Chouwei, Z. Modeling strategies of 3d woven composites: a review. *Composite structures*, 93(8):1947–1963, 2011.

ASTM 3039M Standard D3039. *Standard Test Method for Tensile Properties of Polymer Matrix Composite Materials*. ASTM International, West Conshohocken, PA, 2014. URL https://www.astm.org.

ASTM Standard D790. *Standard Test Methods for Flexural Properties of Unreinforced and Reinforced Plastics and Electrical Insulating Materials*. ASTM International West Conshohocken, PA, 2015. URL https://www.astm.org.

Barbero, E.J. *Introduction to Composite Materials Design, Second Edition*. Composite Materials. Taylor & Francis, 2010. ISBN 9781420079159. URL http://books.google.co.za/books?id=fZSan7b5z0IC. [Accessed]

Barbero, E.J. *Finite Element Analysis of Composite Materials using AbaqusTM*. Composite Materials. Taylor & Francis, 2013. ISBN 9781466516618. URL https://books.google.co.za/books?id=sKHT0WwTm2UC. [Accessed]

Brown, C.D. *Elements of Spacecraft Design*. AIAA education series. American Institute of Aeronautics and Astronautics, Incorporated, 2002. URL https://books.google.co.za/books?id=bvhTAAAAMAAJ. [Accessed]

Cal-Poly-SLO. *CubeSat Design Specification*. The CubeSat Program. California Polytechnic State University, Rev. 13. URL https://books.google.co.za/books?id=AND6HhsssvcC. [Accessed]

Chaphalkar, P. and Kelkar, A. D. (2001). Classical laminate theory model for twill weave fabric composites. *Composites Part A: Applied Science and Manufacturing*, 32(9):1281–1289.

Chapman, D. (2016) *High Conductivity Copper for Electrical Engineering*. European Copper Institute Publication, No. Cu0232, 2016. URL: http://copperalliance.org.uk/docs/

Clyde-Space. (2016). Cubesats structures. URL http://www.clyde-space.com/.

Coombs, C. and Holden, H.*Printed Circuits Handbook*. McGraw Hill professional. McGraw-Hill Education, 2007. ISBN 9780071510790. URL http://books.google.co.za/books?id=1Pbkeu6dZ_sC.

CubeSAT.org. Cubesat, 2015. URL http://wwdw.cubesat.org/.

Dassault-Systemes. *Analysis of Composite Materials with Abaqus*. Composite Material Simulation. 2014.

Fibre-Glast. Learning center - fundamentals of fiberglass, 2013. URL http://www.fibreglast.com/product/the-fundamentals-of-fiberglass. [Last accessed: 12 August 2013].

Fortescue,P., Swinerd,G.,and Stark,J.(2011).*Spacecraft Systems Engineering*. Wiley, ISBN 9781119978367. URL https://books.google.co.za/books?id=cCYP0rVR_IEC. [Accessed]

FUTEK-Advanced-Sensor-Technology.(2015). Bolt torque calculator. URL http://www.futek.com/boltcalc.aspx. [Accessed]

Gibson,R.F. (2010).*A review of recent research on mechanics of multifunctional composite materials and structures.* Elsevier Ltd: USA

Haland , A. (2013a) Mechanical design. URL http://nuts.cubesat.no/article/79/mechanical-design.

Haland , A. (2013b). *Development of mechanical structure for NUTS CubeSat*. Semester Report. Norwegian University of Science and Technology.

Harper, C.A. *Handbook of Plastics, Elastomers, and Composites*. HANDBOOK OF PLASTICS, ELASTOMERS & COMPOSITES. McGraw-Hill, 2002. ISBN 9780071384766. URL http://books.google.co.za/books?id=e8-FSos9PAkC.

Hashin, Z. Analysis of composite materialsa survey. *Journal of Applied Mechanics*, 50(3):481–505, 1983. URL http://appliedmechanics.asmedigitalcollection.asme.org/article.aspx?articleid=1407040.

DiP̈alma, J. , Preble, J. , Schoenoff, M. , and Motoyama, S. *(2004). Applications of Multifunctional Structures to Small Spacecraft.* SpaceWorks Inc.

Helvajian, H. and Janson, S.W. *Small Satellites: Past, Present, and Future*. Aerospace Press, 2008. ISBN 9781884989223. URL http://books.google.co.za/books?id=aJMsPAAACAAJ. [Accessed]

Hÿonny, T. K. , Park, M. , and Hsieh, K. *(2005). Fatigue fracture of embedded copper conductors in multifunctional composite structures.* Elsevier Ltd.

Ḧahn, H. T. , Maung, K. J. and Y.S. Ju. (2010). *Multifunctional integration of thin-film silicon solar cells on carbon-fiber-reinforced epoxy composites.* Elsevier Ltd.

Hopper, B.E. Vacuum infusion - the equipment and process of resin infusion, 2003. URL http://www.fibreglast.com/product/vacuum-infusion-brochure. [Last accessed: 26 October 2014].

Jang̈, Tae. S. , Oh, D. S. , Kim, J. K. , Kang, K. I. , Cha, W. Ho., and Rhee, S. Woo. (2010) *Development of multi-functional composite structures with embedded electronics for space application.* Elsevier Ltd.

ISISpace. (2016). Cubesats products. URL http://www.isispace.nl/cms/.

Ito, M. and Chou, Tsu-W. (1997). Elastic moduli and stress field of plain-weave composites under tensile loading. *Composites Science and Technology*, 57(7):787 – 800. ISSN 0266-3538. URL http://www.sciencedirect.com/science/article/pii/S0266353897000444. [Accessed]

Ito,M. and Chou,Tsu-W. (1998).An analytical and experimental study of strength and failure behavior of plain weave composites. *Journal of Composite Materials*, 32(1):2–30.

Loff , S. Cubesats overview, July 2015. URL http://www.nasa.gov/mission_pages/cubesats/overview. [Accessed]

Oberg, E., Jones, F.D., Horton, H.L., McCauley, C.J., and Ryffel, H.H.(2004).*Machinery's Handbook*. Machinery's Handbook. Industrial Press, 2004. ISBN 9780831127275. URL https://books.google. co.za/books?id=DWVsMgEACAAJ. [Accessed]

Pumpkin-Inc.(2013). Begin your cubesat mission with the cubesat kit. URL http://www.cubesatkit.com/. [Accessed]

Radius-Space. (2015). Cubesat sizes. URL http://www.radiusspace.com. [Accessed]

Rosato, D.V. and Rosato, D.V. (2004).*Reinforced Plastics Handbook*. Reinforced Plastics Handbook. Elsevier Advanced Technology. ISBN 9781856174503. URL https://books.google.co.za/books?id=AND6HhsssvcC. [Accessed]

Roylance , D. (2000). *Laminated Composite Plates*. Lecture Notes. Massachusetts Institute of Technology (MIT). URL https://ocw.mit.edu/courses/materials-science-and-engineering/3-11-mechanics-of-materials-fall-1999/modules/MIT3_11F99_laminates.pdf. [Accessed]

SuperiorEssex. (2009). *Magnet wire / winding wire engineering data handbook*. Rev1. NEMA. URL
https://www.superioressex.com/MagnetWire/Engineering_Data_Handbook.aspx. [Accessed]

Tan, P., Tong, L., and Steven,GP. (1997). Modelling for predicting the mechanical properties of textile composites a review.*Composites Part A:Applied Science and Manufacturing*, 28(11):903-922

Thomas, J. P. and Qidwai , M. A. (2004). *Mechanical design and performance of composite multifunctional materials.* Elsevier Ltd: Oxford UK

Wikimedia-Commons. (2011). File:cubesat in hand.jpg. URL http://commons.wikimedia.org/wiki/File:CubeSat_in_hand.jpg. [Accessed]

A P P E N D I C E S

Appendix A

CubeSat Physical Specifications

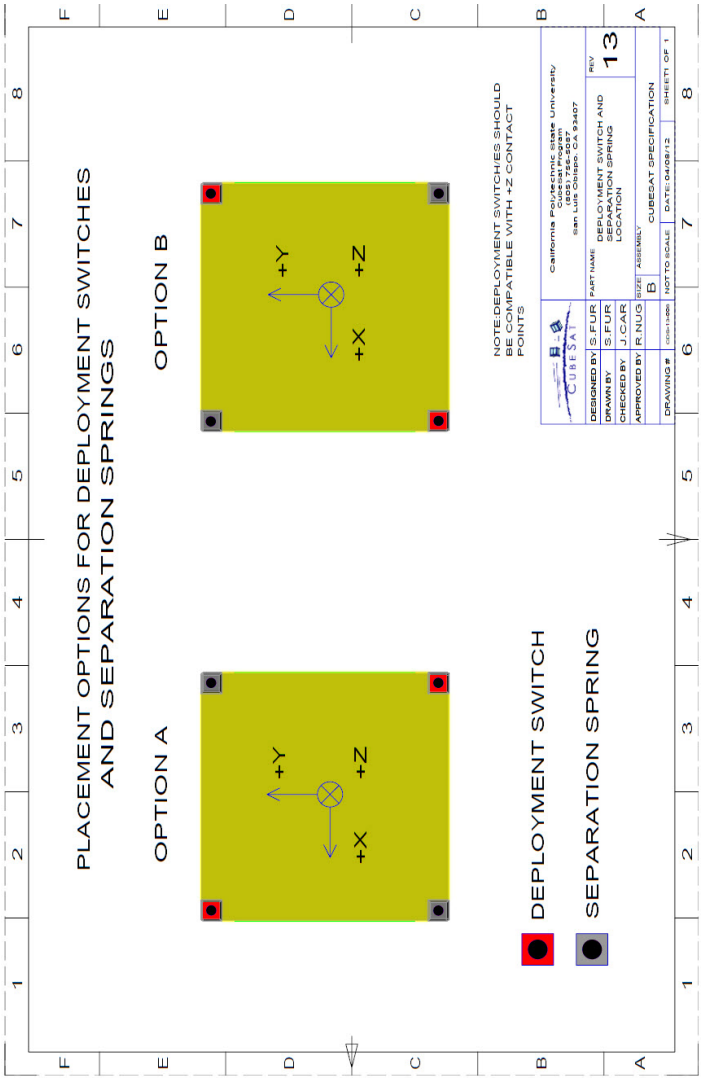

Figure A.1: Deployment Switches and Separation Spring Placement Specifications. (Cal-Poly-SLO, Rev. 13)

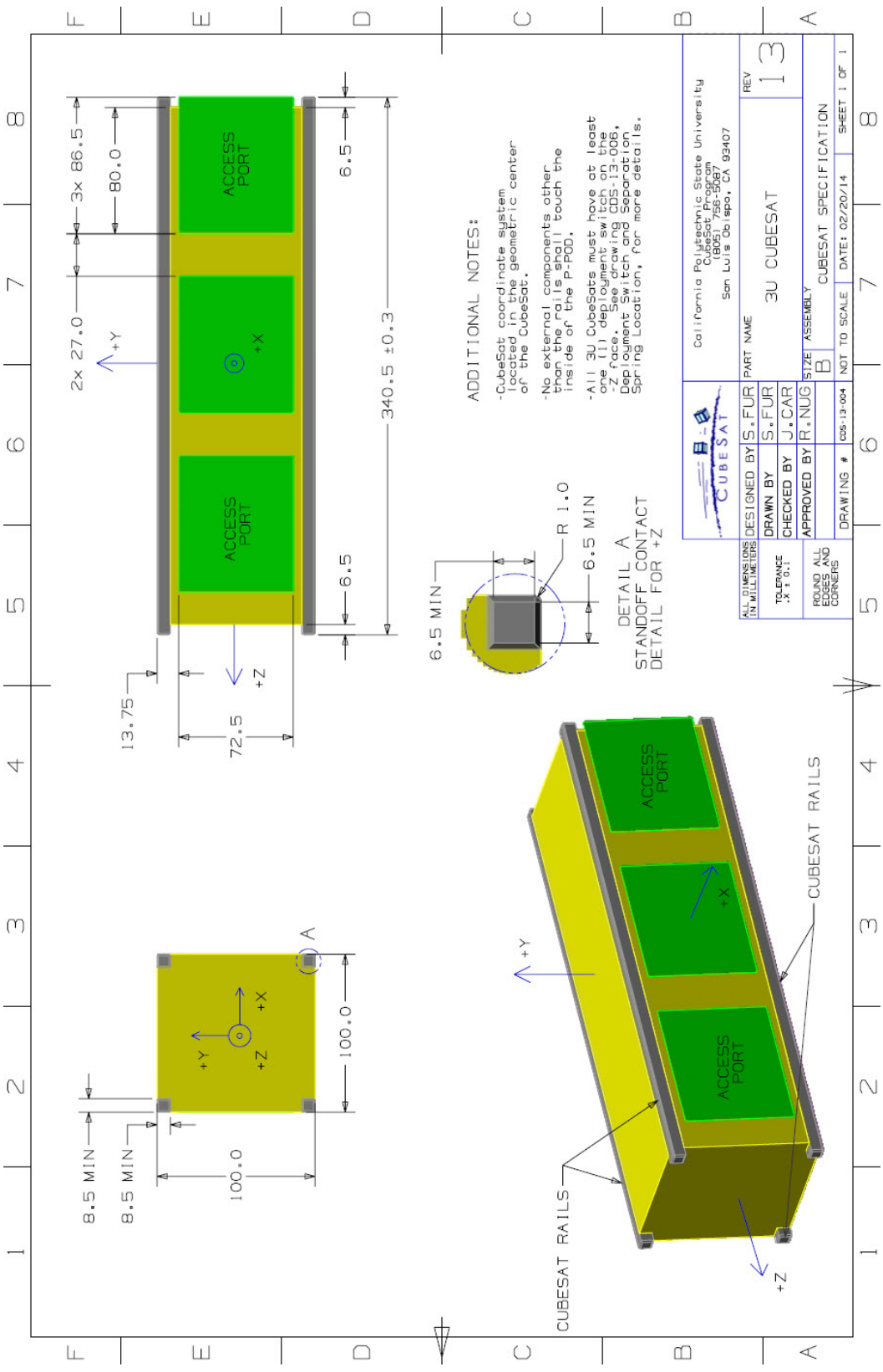

Figure A.2: 3U CubeSat Physical Dimension Specifications. (Cal-Poly-SLO, Rev. 13)

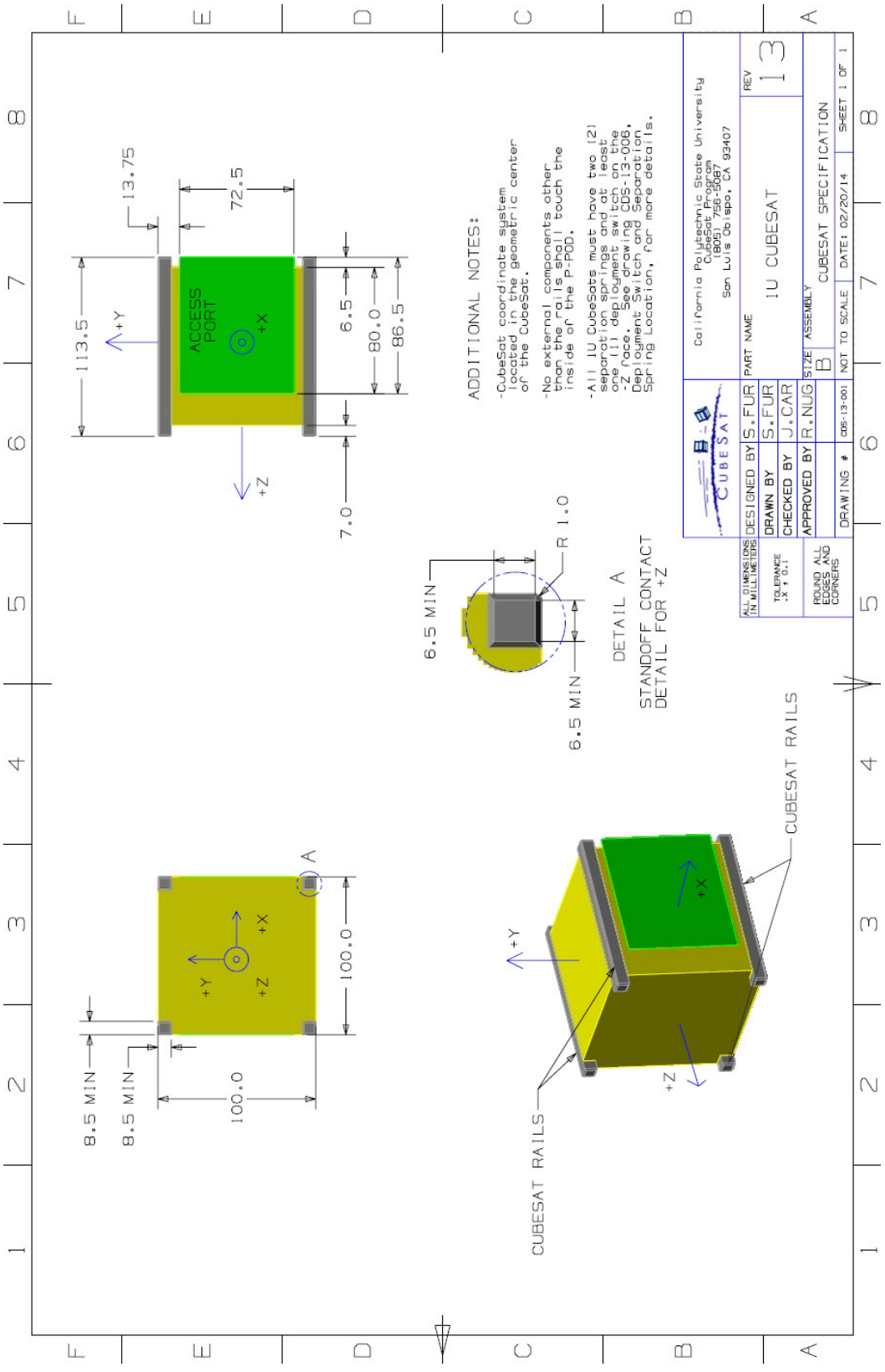

Figure A.3: 1U CubeSat Physical Dimension Specifications. (Cal-Poly-SLO, Rev. 13)

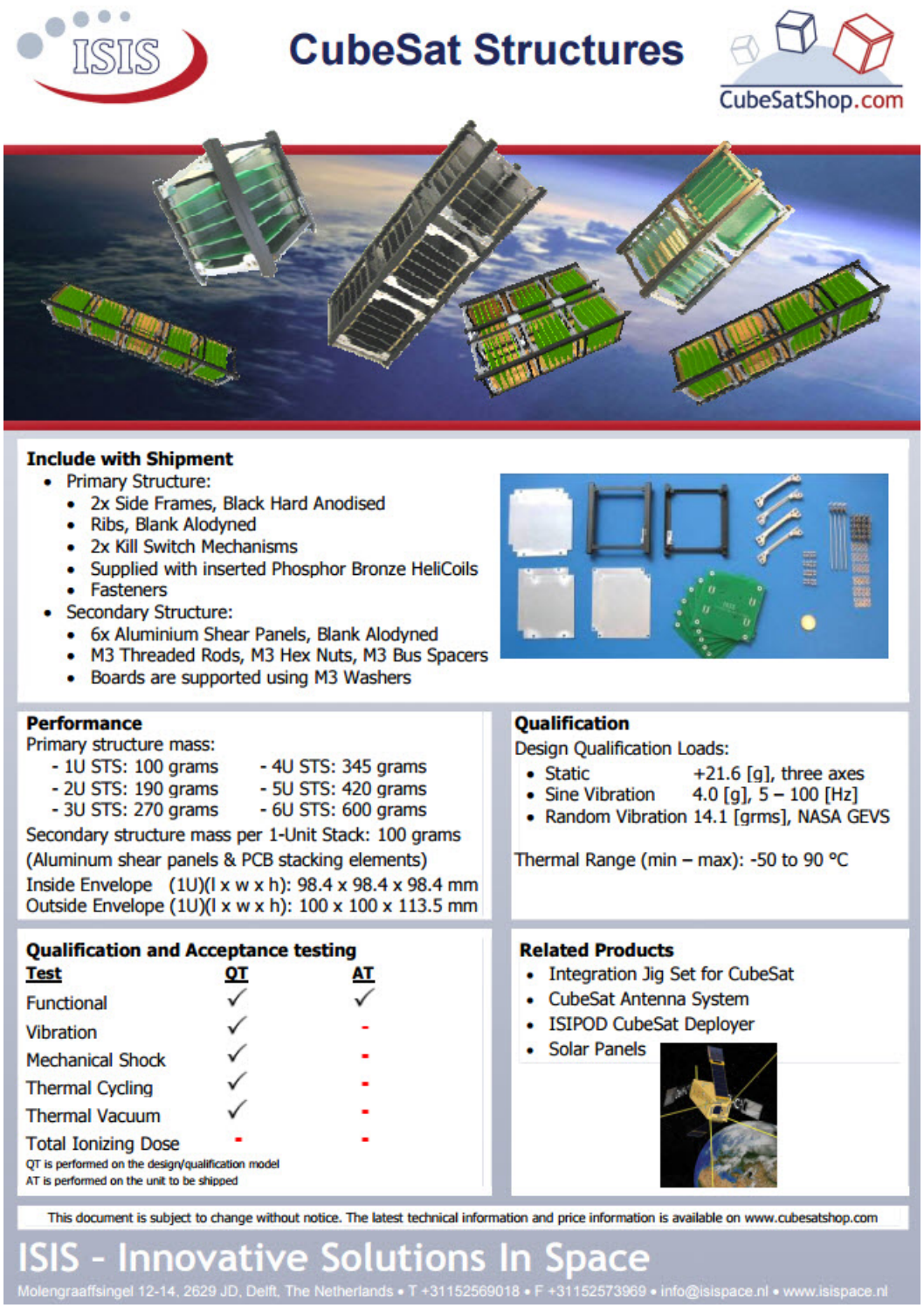

Figure A.4: ISIS Structure product performance Specifications. (ISISpace, 2016)

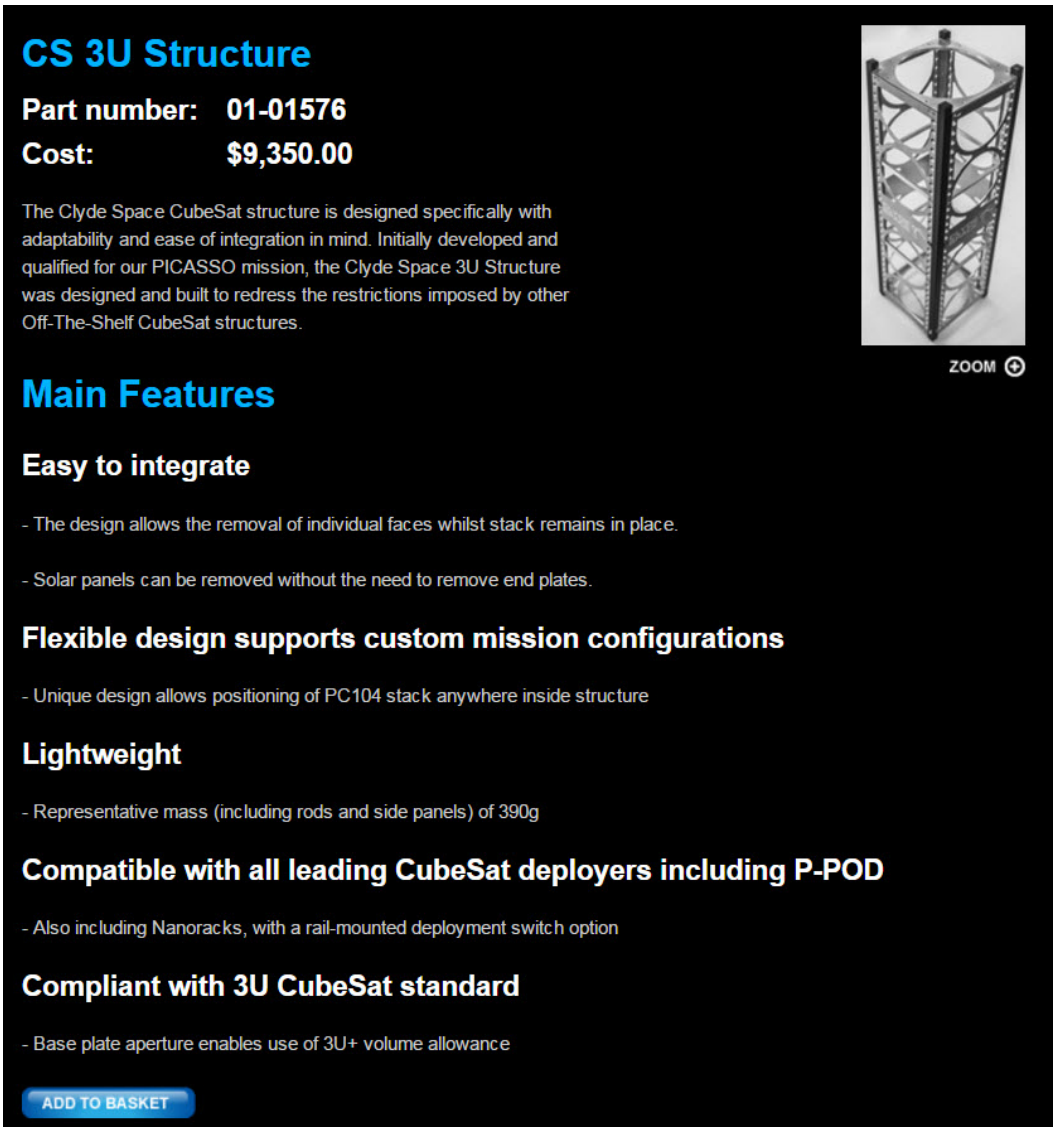

Figure A.5: Clyde Space 3U Structure Overview.
(Clyde-Space, 2016)

Appendix B

MATLAB Material Properties program

```
%Read in Material Data
%----------Carbon Fibre Properties---------------
E_f = xlsread('MaterialData.xlsx',1,'D3');
Rho_f = xlsread('MaterialData.xlsx',1,'D5');
nu_f = xlsread('MaterialData.xlsx',1,'D6');
Te_f = xlsread('MaterialData.xlsx',1,'D7');
Tc_f = xlsread('MaterialData.xlsx',1,'D8');
Er_f = xlsread('MaterialData.xlsx',1,'D9');
w = xlsread('MaterialData.xlsx',1,'D10');
CSA = xlsread('MaterialData.xlsx',1,'D11');
UTS_f = xlsread('MaterialData.xlsx',1,'D12');
Str_f = xlsread('MaterialData.xlsx',1,'D13');
tc = xlsread('MaterialData.xlsx',1,'D14');
%----------Matrix Properties [AR600]-------------
E_m = xlsread('MaterialData.xlsx',1,'N3');
Rho_m = xlsread('MaterialData.xlsx',1,'N5');
nu_m = xlsread('MaterialData.xlsx',1,'N6');
Te_m = xlsread('MaterialData.xlsx',1,'N7');
Tc_m = xlsread('MaterialData.xlsx',1,'N8');
UTS_m = xlsread('MaterialData.xlsx',1,'N9');
Str_m = xlsread('MaterialData.xlsx',1,'N10');
%-#################--Composite Material Properties-###############--

%*********************Micro-mechanics Calcs*******************
%------Fibre Volume Fraction--------
TEX=w*1000;
V_f = (TEX)./(1000*Rho_f*tc);
%-------Modulus Fibre Direction---------
E11=(E_f*V_f)+E_m*(1-V_f); %no efficency factor introduced yet
%------Modulus Transverse to Fibre Direction---------
Sc=2; %specified by book
n=((E_f ./ E_m)-1)./((E_f ./ E_m)+Sc);
E22=E_m*((1+Sc*n*V_f)./(1-n*V_f));
E33=E22;
%-------In-plane Possion's Ratio---------
v_12=(nu_f*V_f)+(nu_m*(1-V_f));
%-------In-plane Shear Modulus----------
G_f=E_f./2*(1+nu_f);
G_m=E_m./2*(1+nu_m);
S_3=0.49247-0.47603*V_f-0.02748*(V_f^2);
G_12=G_m*(1+(V_f ./ ((G_m./G_f)+S_3)));
G_13=G_12;
%--------Intralaminar Shear Modulus--------
n_4=(3-4*nu_m+(G_m./G_f))./(4*(1-V_f));
G_23=G_m*((V_f+n_4*(1-V_f))./(n_4*(1-V_f)+V_f*(G_m./G_f)));
```

Figure B.1: MATLAB code part 1.

```
%--------Transverse Possion's Ratio's---------
v_23=(((1-V_f)./nu_m)+(V_f./nu_f))^-1;
v_13=v_12;

%******************Woven Lamina Calculations**************
%------------------ "S" Matrix---------------------
v_21=v_12;
v_31=v_13;
v_32=v_23;
S11=1./E11;
S12=-v_21./E22;
S13=-v_31./E33;
S21=-v_12./E11;
S22=1./E22;
S23=-v_32./E33;
S31=-v_13./E11;
S32=-v_23./E22;
S33=1./E33;
S44=1./G_23;
S55=1./G_13;
S66=1./G_12;

S = [S11 S12 S13 0 0 0;
    S21 S22 S23 0 0 0;
    S31 S32 S33 0 0 0;
    0 0 0 S44 0 0;
    0 0 0 0 S55 0;
    0 0 0 0 0 S66];
%--------------------Transformation Matrices--------------------
theta_fdeg=xlsread('MaterialData.xlsx',1,'D16');
theta_wdeg=xlsread('MaterialData.xlsx',1,'D17');
theta_f=degtorad(theta_fdeg);
theta_w=degtorad(theta_wdeg);
s_f=sin(theta_f);
c_f=cos(theta_f);
s_w=sin(theta_w);
c_w=cos(theta_w);

T_f = [(c_f)^2 0 (s_f)^2 0 2*(c_f*s_f) 0;
      0 1 0 0 0 0;
      (s_f)^2 0 (c_f)^2 0 -2*(c_f*s_f) 0;
      0 0 0 c_f 0 -s_f;
      -(c_f*s_f) 0 (c_f*s_f) 0 (c_f)^2-(s_f)^2 0;
      0 0 0 (s_f) 0 (c_f)];
```

Figure B.2: MATLAB code part 2.

```
T_w = [0 (c_w)^2 (s_w)^2 -2*(c_w*s_w) 0 0;
      1 0 0 0 0 0;
      0 (s_w)^2 (c_w)^2 2*(c_w*s_w) 0 0;
      0 0 0 0 -c_w -s_w;
      0 (c_w*s_w) -(c_w*s_w) (c_w)^2-(s_w)^2 0 0;
      0 0 0 0 (s_w) -(c_w)];

 %---------------Transformation Compliance Matrices-----------------
T_ft=T_f.'; %transpose
T_wt=T_w.'; %transpose
Sbar_f=T_ft*S*T_f;
Sbar_w=T_wt*S*T_w;

%------------------Reduced stiffness matrix--------------------
Sbar_fr=[Sbar_f(1,1) Sbar_f(1,2) 0;
         Sbar_f(2,1) Sbar_f(2,2) 0;
         0 0 Sbar_f(6,6)];
Sbar_wr=[Sbar_w(1,1) Sbar_w(1,2) 0;
         Sbar_w(2,1) Sbar_w(2,2) 0;
         0 0 Sbar_w(6,6)];
Qbar_f=inv(Sbar_fr);
Qbar_w=inv(Sbar_wr);

%-----------------
z=xlsread('MaterialData.xlsx',1,'D18');
g_w=xlsread('MaterialData.xlsx',1,'D19');
g_f=xlsread('MaterialData.xlsx',1,'D20');
a_w=xlsread('MaterialData.xlsx',1,'D21');
a_f=xlsread('MaterialData.xlsx',1,'D22');

A11=(4/((a_f + g_f)*(a_w + g_w)))*((Qbar_f(1,1))+(Qbar_w(1,1)))*(z./2);
A12=(4/((a_f + g_f)*(a_w + g_w)))*((Qbar_f(1,2))+(Qbar_w(1,2)))*(z./2);
A21=(4/((a_f + g_f)*(a_w + g_w)))*((Qbar_f(2,1))+(Qbar_w(2,1)))*(z./2);
A22=(4/((a_f + g_f)*(a_w + g_w)))*((Qbar_f(2,2))+(Qbar_w(2,2)))*(z./2);
A66=(4/((a_f + g_f)*(a_w + g_w)))*((Qbar_f(3,3))+(Qbar_w(3,3)))*(z./2);

A=[A11 A12 0;
   A12 A22 0;
   0 0 A66];  %GPa mm (as seen on Pg 179 in Book)

%------------------Laminate Compliance Matrix--------------------
Alfa=inv(A);
```

Figure B.3: MATLAB code part 3.

```
%------------------Laminae Moduli (Woven Layer)------------------
E_x=(Alfa(1,1)*z)^-1;  %E11
E_y=(Alfa(2,2)*z)^-1;  %E22
G_xy=(Alfa(3,3)*z)^-1; %G12=G13
v_xy=-((Alfa(1,2))./(Alfa(1,1))); %v12
%G23

E_x
E_y
v_xy
G_xy
G_23
```

Figure B.4: MATLAB code part 4.

The output values correspond with the values required by ABAQUS ($E_{11}, E_{22}, \nu_{12}, G_{12}, G_{23}$).

Appendix C

Material Datasheets

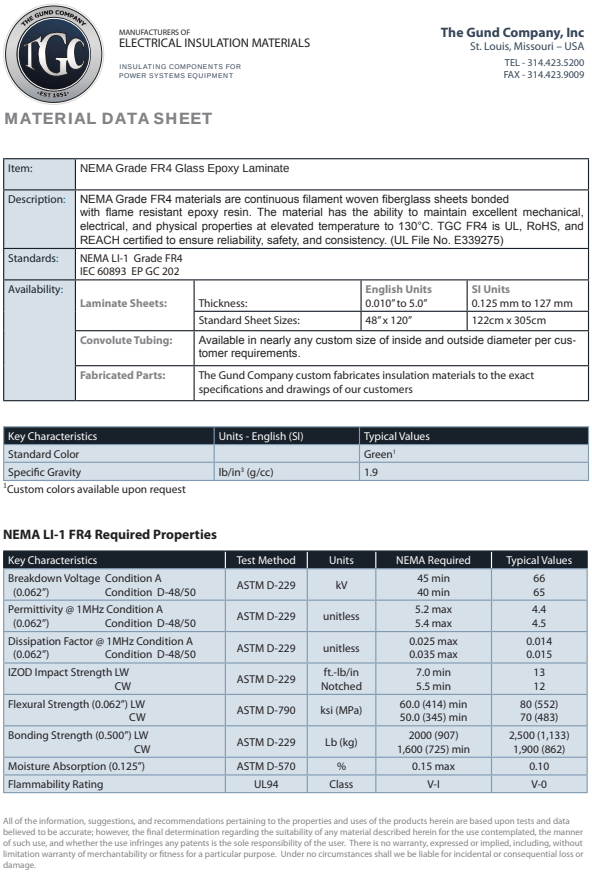

MANUFACTURERS OF
ELECTRICAL INSULATION MATERIALS

INSULATING COMPONENTS FOR
POWER SYSTEMS EQUIPMENT

The Gund Company, Inc
St. Louis, Missouri – USA
TEL - 314.423.5200
FAX - 314.423.9009

MATERIAL DATA SHEET

Item:	NEMA Grade FR4 Glass Epoxy Laminate			
Description:	NEMA Grade FR4 materials are continuous filament woven fiberglass sheets bonded with flame resistant epoxy resin. The material has the ability to maintain excellent mechanical, electrical, and physical properties at elevated temperature to 130°C. TGC FR4 is UL, RoHS, and REACH certified to ensure reliability, safety, and consistency. (UL File No. E339275)			
Standards:	NEMA LI-1 Grade FR4 IEC 60893 EP GC 202			
Availability:	**Laminate Sheets:**	Thickness:	**English Units** 0.010" to 5.0"	**SI Units** 0.125 mm to 127 mm
		Standard Sheet Sizes:	48" x 120"	122cm x 305cm
	Convolute Tubing:	Available in nearly any custom size of inside and outside diameter per customer requirements.		
	Fabricated Parts:	The Gund Company custom fabricates insulation materials to the exact specifications and drawings of our customers		

Key Characteristics	Units - English (SI)	Typical Values
Standard Color		Green[1]
Specific Gravity	lb/in^3 (g/cc)	1.9

[1]Custom colors available upon request

NEMA LI-1 FR4 Required Properties

Key Characteristics	Test Method	Units	NEMA Required	Typical Values
Breakdown Voltage Condition A (0.062") Condition D-48/50	ASTM D-229	kV	45 min 40 min	66 65
Permittivity @ 1MHz Condition A (0.062") Condition D-48/50	ASTM D-229	unitless	5.2 max 5.4 max	4.4 4.5
Dissipation Factor @ 1MHz Condition A (0.062") Condition D-48/50	ASTM D-229	unitless	0.025 max 0.035 max	0.014 0.015
IZOD Impact Strength LW CW	ASTM D-229	ft.-lb/in Notched	7.0 min 5.5 min	13 12
Flexural Strength (0.062") LW CW	ASTM D-790	ksi (MPa)	60.0 (414) min 50.0 (345) min	80 (552) 70 (483)
Bonding Strength (0.500") LW CW	ASTM D-229	Lb (kg)	2000 (907) 1,600 (725) min	2,500 (1,133) 1,900 (862)
Moisture Absorption (0.125")	ASTM D-570	%	0.15 max	0.10
Flammability Rating	UL94	Class	V-I	V-0

Figure C.1: FR4 PCB material data Page 1.

NEMA Grade FR4 Glass Epoxy Laminate

IEC 60893-3-2 EPGC 202 Required Properties

Key Characteristics	Test Method	Units	IEC Required	Typical Values
Flexural Strength	ISO 179	MPa	340 min	560
Charpy Impact Strength	--	kJ/m^2	33 min	49
Perpendicular Electric Strength (90°C in Oil, 1.5mm)	--	kV/mm	13 min	25
Parallel Breakdown Voltage (Stepped, 90°C in Oil, 3mm)	--	kV	35 min	>45
Insulation Resistance (after Water Immersion)	--	MΩ	$5(10)^4$	$>10^7$
Flammability Rating	UL94	Class	V-0	V-0
Moisture Absorption (1.5mm)	--	mg	19 max	13

Additional Engineering Properties

Key Characteristics	Test Method	Units - English (SI)	Typical Values
Tensile Strength (0.125") LW	ASTM D638	ksi (MPa)	62 (430)
Compressive Strength, Flatwise (0.500")	ASTM D695	ksi (MPa)	66 (455)
Flexural Modulus (0.062") LW CW	--	ksi (GPa)	2,900 (20) 2,600 (18)
Shear Strength (punch type, 0.062")	ASTM D732	psi (MPa)	21,500 (148)
Coefficient of Thermal Expansion	--	"/"/°C$x10^{-6}$	15
Temperature Index	--	°C	130
Glow Wire Flame Index & Ignition Temperature	IEC 60695-2-12	°C	960
Hot Wire Ignition	UL 746A	Sec	120
High Current Arc Ignition (3mm)	UL 746A	Arcs	120
Arc Resistance (0.125")	ASTM D495	Sec	140
Comparative Tracking Index (.125")	ASTM D3638*	V	230
Dielectric Strength Condition A	ASTM D149	V/mil	635
Volume Resistivity (0.062")	ASTM D257	Ω – cm	$3(10)^{15}$
High Voltage Arc Resistance	UL 746A	Sec	300
High Voltage Arc Tracking Rate	UL 746A	mm/min	0

*ASTM D3638 & IEC 112 are the same test method - IEC 60112 is slightly different,but the result is similar

Figure C.2: FR4 PCB material data Page 2.

HUNTSMAN
Enriching lives through innovation

Average lap shear strengths of typical plastic-to-plastic joints (ISO 4587)

Cured for 16 hours at 40ºC and tested at 23ºC Pretreatment - Lightly abrade and alcohol degrease.

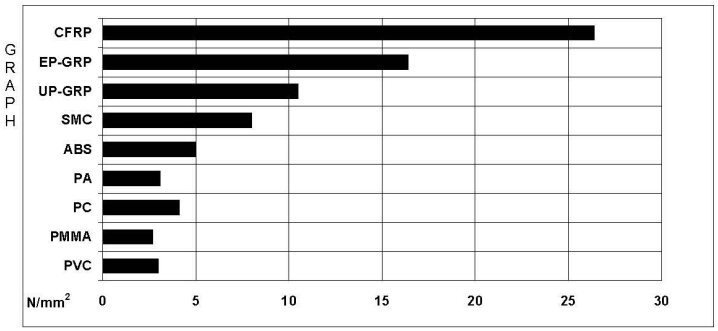

Lap shear strength versus temperature (ISO 4587) (typical average values)

Cure: 24 hours at 23ºC + 30 minutes at 80ºC (a) on GRE (b) on aluminium

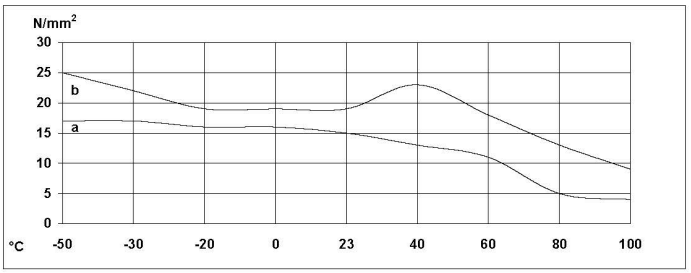

Roller peel test (ISO 4578)	Cured 16 hours/40ºC	4 N/mm
Glass transition temperature (DSC)	Cure: 16 hours at 40ºC	ca. 64ºC
	Cure 4 hours at 60°C	ca. 78ºC
Tensile strength at 23ºC (ISO 527)		20 MPa
Tensile modulus		1 Gpa
Elongation at break		5 %

March 2009 Araldite® AV 4076-1 / Hardener HV 5309-1 Page 3 of 5

Figure C.3: AV4076 Composite Epoxy Datasheet.

2.3 Physical Properties

The physical properties for the wrought material, Cu-ETP/CW004A, are shown in Table 6. These are also typical for similar coppers.

Table 6 – Properties of Cu-ETP (CW004A)

	Value	Units
Density:		
IEC standard value (1913)	8.89	g/cm³
Typical value at 20°C	8.92	g/cm³
at 1083°C (solid)	8.32	g/cm³
at 1083°C (liquid)	7.99	g/cm³
Melting Point	1083	°C
Boiling Point	2595	°C
Linear Coefficient of Thermal Expansion at:		
-253°C	0.3×10^{-6}	/K
-183°C	9.5×10^{-6}	/K
-191 to 16°C	14.1×10^{-6}	/K
25 to 100°C	16.8×10^{-6}	/K
20 to 200°C	17.3×10^{-6}	/K
20 to 300°C	17.7×10^{-6}	/K
Specific Heat (Thermal Capacity) at:		
-253°C	0.013	J/gK
-150°C	0.282	J/gK
50°C	0.361	J/gK
20°C	0.386	J/gK
100°C	0.393	J/gK
200°C	0.403	J/gK
Thermal Conductivity at:		
-253	12.98	Wcm/cm²K
-200	5.74	Wcm/cm²K
-183	4.73	Wcm/cm²K
-100	4.35	Wcm/cm²K
20	3.94	Wcm/cm²K
100	3.85	Wcm/cm²K
200	3.81	Wcm/cm²K
300	3.77	Wcm/cm²K
Electrical Conductivity (Volume) at:		
20°C (annealed)	58.0-58.9	MS/m (m/Ωmm²)
20°C (annealed)	100.0-101.5	% IACS
20°C (fully cold worked)	56.3	MS/m (m/Ωmm²)
20°C (fully cold worked)	97.0	% IACS
Electrical Resistivity (Volume) at:		
20°C (annealed)	0.017241-0.0170	
20°C (annealed)	1.724-1.70	
20°C (fully cold worked)	0.0178	
20°C (fully cold worked)	1.78	
Electrical Resistivity (Mass) at 20°C (Annealed)		
Mandatory maximum	0.15328	μΩg/m²
Temperature Coefficient of Electrical Resistance		
Annealed copper of 100% IACS (applicable from – 100°C to 200°C)	0.00393	/°C
Fully cold worked copper of 97% IACS (applicable from 0°C to 100°C)	0.00381	/°C
Modulus of Elasticity (Tension) at 20°C		
Annealed	118 000	N/mm²
Cold worked	118 000-132 000	N/mm²
Modulus of Rigidity (Torsion) at 20°C		
Annealed	44 000	N/mm²
Cold worked	44 000-49 000	N/mm²
Latent Heat of Fusion	205	J/g

HIGH CONDUCTIVITY COPPER FOR ELECTRICAL ENGINEERING | 15

Figure C.5: Copper Foil Datasheet.

ROUND, SINGLE BUILD FILM-INSULATED WIRE

Copper & Aluminum — **DIMENSIONS**

WHOLE AWG SIZE	Bare Wire Diameter						Increase in Diameter Due to Film Coating		Overall Diameter of Film-Coated Wire		WHOLE AWG SIZE
	Minimum		Nominal		Maximum		Minimum		Maximum		
	Inches	mm	Inches	mm	Inches	mm	Inches	mm	Inches	mm	
8	0.1272	3.231	0.1285	3.264	0.1294	3.297	0.0017	0.043	0.1314	3.338	8
9	0.1133	2.878	0.1144	2.906	0.1153	2.929	0.0017	0.043	0.1173	2.980	9
10	0.1009	2.563	0.1019	2.588	0.1027	2.609	0.0017	0.043	0.1047	2.660	10
11	0.0898	2.281	0.0907	2.304	0.0914	2.322	0.0017	0.043	0.0934	2.373	11
12	0.0800	2.032	0.0808	2.052	0.0814	2.069	0.0016	0.041	0.0833	2.117	12
13	0.0713	1.811	0.072	1.829	0.0726	1.843	0.0016	0.041	0.0745	1.892	13
14	0.0635	1.613	0.0641	1.628	0.0647	1.643	0.0016	0.041	0.0666	1.692	14
15	0.0565	1.435	0.0571	1.450	0.0577	1.466	0.0015	0.038	0.0594	1.509	15
16	0.0503	1.278	0.0508	1.290	0.0513	1.303	0.0014	0.036	0.0531	1.349	16
17	0.0448	1.138	0.0453	1.151	0.0458	1.163	0.0014	0.036	0.0475	1.207	17
18	0.0399	1.013	0.0403	1.024	0.0407	1.034	0.0013	0.033	0.0424	1.077	18
19	0.0355	0.902	0.0359	0.912	0.0363	0.922	0.0012	0.030	0.0379	0.963	19
20	0.0317	0.805	0.0320	0.813	0.0323	0.820	0.0012	0.030	0.0340	0.864	20
21	0.0282	0.716	0.0285	0.724	0.0288	0.732	0.0011	0.028	0.0303	0.770	21
22	0.0250	0.635	0.0253	0.643	0.0256	0.650	0.0011	0.028	0.027	0.686	22
23	0.0224	0.569	0.0226	0.574	0.0228	0.579	0.0010	0.025	0.0243	0.617	23
24	0.0199	0.505	0.0201	0.511	0.0203	0.516	0.0010	0.025	0.0217	0.551	24
25	0.0177	0.450	0.0179	0.455	0.0181	0.460	0.0009	0.023	0.0194	0.493	25
26	0.0157	0.399	0.0159	0.404	0.0161	0.409	0.0009	0.023	0.0173	0.439	26
27	0.0141	0.358	0.0142	0.361	0.0143	0.363	0.0008	0.020	0.0156	0.396	27
28	0.0125	0.318	0.0126	0.320	0.0127	0.323	0.0008	0.020	0.0140	0.356	28
29	0.0112	0.284	0.0113	0.287	0.0114	0.290	0.0007	0.018	0.0126	0.320	29
30	0.0099	0.251	0.0100	0.254	0.0101	0.257	0.0007	0.018	0.0112	0.285	30
31	0.0088	0.224	0.0089	0.226	0.0090	0.229	0.0006	0.015	0.0100	0.255	31
32	0.0079	0.201	0.008	0.203	0.0081	0.206	0.0006	0.015	0.0090	0.229	32
33	0.0070	0.178	0.0071	0.180	0.0072	0.183	0.0005	0.013	0.0081	0.205	33
34	0.0062	0.157	0.0063	0.160	0.0064	0.163	0.0005	0.013	0.0072	0.183	34
35	0.0055	0.140	0.0056	0.142	0.0057	0.145	0.0004	0.010	0.0065	0.164	35
36	0.0049	0.124	0.0050	0.127	0.0051	0.130	0.0004	0.010	0.0058	0.147	36
37	0.0044	0.112	0.0045	0.114	0.0046	0.117	0.0004	0.010	0.0052	0.132	37
38	0.0039	0.099	0.0040	0.102	0.0041	0.104	0.0003	0.008	0.0047	0.118	38
39	0.0034	0.086	0.0035	0.089	0.0036	0.091	0.0003	0.008	0.0042	0.106	39
40	0.0030	0.076	0.0031	0.079	0.0032	0.081	0.0003	0.008	0.0037	0.095	40
41	0.0027	0.069	0.0028	0.071	0.0029	0.074	0.0003	0.008	0.0033	0.085	41
42	0.0024	0.061	0.0025	0.064	0.0026	0.066	0.0002	0.005	0.0030	0.076	42
43	0.0021	0.053	0.0022	0.056	0.0023	0.058	0.0002	0.005	0.0027	0.068	43
44	0.0019	0.048	0.0020	0.051	0.0021	0.053	0.0002	0.005	0.0024	0.061	44
45	0.00169	0.0429	0.00176	0.0447	0.00183	0.0465	0.00020	0.0051	0.00220	0.0559	45
46	0.00151	0.0384	0.00157	0.0399	0.00163	0.0414	0.00020	0.0051	0.00200	0.0508	46

Figure C.4: Copper Magnetic Wire Datasheet.
(SuperiorEssex, 2009)

ALLOY 7075

DESCRIPTION

Introduced by Alcoa in 1943, alloy 7075 has been the standard workhorse 7XXX series alloy within the aerospace industry ever since. It was the first successful Al-Zn-Mg-Cu high strength alloy using the beneficial effects of the alloying addition of chromium to develop good stress-corrosion cracking resistance in sheet products. Although other 7XXX alloys have since been developed with improved specific properties, alloy 7075 remains the baseline with a good balance of properties required for aerospace applications.

Alloy 7075 is available in bare and alclad sheet and plate product forms in the annealed state as well as several tempers of the T6, T73 and T76 types.

APPLICATIONS

Alloy 7075 sheet and plate products have application throughout aircraft and aerospace structures where a combination of high strength with moderate toughness and corrosion resistance are required.

Typical applications are alclad skin sheet, structural plate components up to 4 inches in thickness and general aluminum aerospace applications.

CHEMICAL COMPOSITION LIMITS (WT. %)

Si	0.40	Zn	5.1-6.1
Fe	0.50	Ti	0.20
Cu	1.2-2.0	Others, each	0.5
Mn	0.30	Others, total	0.15
Mg	2.1-2.9	Balance, Aluminum	
Cr	0.18-0.28		

Note: Value maximum if range not shown.

MECHANICAL PROPERTIES

ALLOY 7075 All values are minimum long transverse mechanical properties except where noted.

TEMPER	THICKNESS in. (mm)	TENSILE STRENGTH ksi (MPa)	YIELD STRENGTH ksi (MPa)	ELONGATION %
O Sheet & plate	0.015-2.00 (0.38-50.80)	40 (max) (276)	21 (max) (145)	9-10
T6 Sheet	0.008-0.249 (0.203-6.32)	74-78 (510-538)	63-69 (434-476)	5-8
T651 Plate	0.250-4.000 (6.35-101.60)	78-67 (538-462)	67-54 (462-372)	9-3
T76 Sheet	0.125-0.249 (3.18-6.32)	73 (503)	62 (427)	8
T7651 Plate	0.250-1.000 (6.35-25.40)	72-71 (496-490)	61-60 (421-414)	8-6
T73 Sheet	0.040-0.249 (1.02-6.32)	67 (462)	56 (386)	8
T7351 Plate	0.250-4.000 (6.35-101.60)	69-61 (476-421)	57-48 (393-331)	7-6

Figure C.6: Aluminium 7075-T6 Page 1.

ALCLAD 7075

Two side cladding. Nominal cladding thickness is 4% on gauges under 0.062 in. (1.57 mm); 2.5% on gauges over 0.062 in. (1.57 mm). Property values for one side clad material are similar (not shown). All values are minimum long transverse mechanical properties except where noted.

TEMPER	THICKNESS in. (mm)	TENSILE STRENGTH ksi (MPa)	YIELD STRENGTH ksi (MPa)	ELONGATION %
O Sheet & plate	0.008-1.000 (0.203-6.32)	36-40 (max) (248-276)	20-21 (max) (138-145)	9-10
T6 Sheet	0.008-0.249 (0.203-6.32)	68-76 (469-524)	58-65 (400-448)	5-9
T651 Plate	0.250-4.000 (6.35-101.60)	75-67 (517-462)	65-54 (448-372)	9-3
T76 Sheet	0.125-0.249 (3.18-6.32)	68-70 (469-482)	57-59 (393-407)	8
T7651 Plate	0.250-1.000 (6.35-25.40)	69-71 (476-490)	58-60 (400-414)	8-6
T73 Sheet	0.040-0.249 (1.02-6.32)	63-66 (434-455)	51-54 (352-372)	8
T7351 Plate	0.250-1.000 (6.35-25.40)	66-69 (455-476)	54-57 (372-393)	8-7

FRACTURE TOUGHNESS

Alloy 7075 sheet and plate products offer moderately good strength/toughness relationships and are the standard of comparison for more recent 7XXX series alloy developments. Alloy 7075 sheet and plate products are not offered with guaranteed minimum fracture toughness values.

TYPICAL FRACTURE TOUGHNESS VALUES Alloy 7075 Plate

ALLOY	TEMPER	K_{Ic}:ksi√in. (MPa√m)* L-T	K_{Ic}:ksi√in. (MPa√m)* T-L
7075	T651 T7351	26 (28.6) 30 (32.0)	22 (24.2) 26 (28.6)

*Compact specimen (ASTM E399)

FATIGUE PROPERTIES

COMPARISON OF AXIAL-STRESS NOTCH-FATIGUE DATA FOR ALLOYS 7075-T73XXX 2024-T351 AND 7475-T7351 PRODUCTS

The fatigue behavior of alloy 7075 plate products is shown in the accompanying figure comparing axial-stress notch-fatigue data of 2XXX and 7XXX series alloys.

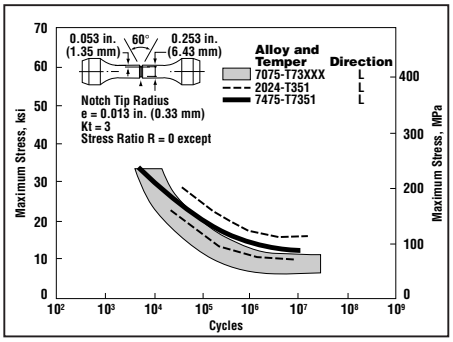

Figure C.7: Aluminium 7075-T6 Page 2.

ALLOY 7075

FATIGUE CRACK GROWTH

Fatigue crack growth rates for plate products of 7075-T6 in constant amplitude tests are compared with products of alloys 2024, 7050, and 7475.

COMPARISON OF FATIGUE CRACK GROWTH RATE DATA FOR ALLOY 7075-T651, 2024-T351 AND 7475-T651 PLATE

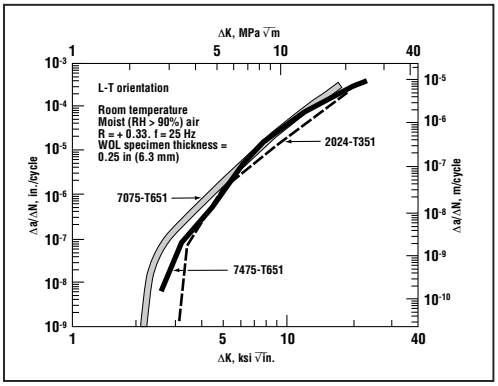

Fatigue crack growth behavior under spectrum loading is becoming increasingly important in the selection of alloys for fatigue critical aircraft structures. Various high strength aerospace alloys are compared for life prediction in flight hours using two types of fatigue spectrums; a wing root application (tension dominated), and a horizontal tail application (tension-compression).

SPECTRUM FATIGUE RANKING

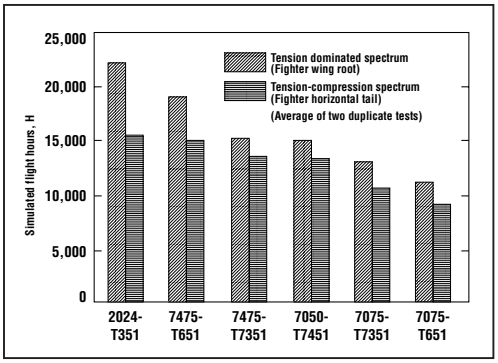

Source: U.S. Navy Contract N00019-81-C-0550/Northrop Corp.

CORROSION RESISTANCE

Alloy 7075 has been thoroughly evaluated for corrosion resistance of atmospheric weathering, stress-corrosion cracking and exfoliation in all currently available tempers. These values have been used as a standard for comparison in the development of more recent high strength aerospace alloys. Within the 7XXX series of alloys, resistance to general corrosion attack, SCC and exfoliation improves significantly in the overage tempers (T7 type) compared with peak strength tempers (T6).

Generally, the T76 type temper is considered the exfoliation resistant temper, while the T73 type temper is considered the SCC resistant temper. It should be noted that T73 is as resistant to exfoliation as T76, but at lower strength levels.

For applications where good surface appearance is required or in corrosive environments, alclad 7075 sheet and plate products are recommended.

THERMAL TREATMENT

Many heat treatments and heat treating practices are available to develop optimum strength, toughness and other desirable characteristics for proper application of alloy 7075 sheet and plate products. Refer to MIL-H-6088, *Heat Treatment of Aluminum Alloys* for additional information.

PROCUREMENT SPECIFICATIONS

PLATE		
Temper	T651	T7651
Specification	QQ-A-250/13	QQ-A-250/24
MIL-HDBK-5	Approved	
BARE SHEET		**ALCLAD SHEET**
Specification	QQ-A-250/12,24	QQ-A-250/13,25,26
MIL-HDBK-5	Approved	Approved

OTHER PRODUCT FORMS

Other product forms of alloy 7075 are extrusions, forgings, wire rod and bar, and rivets.

REFERENCES:

1. The Aluminum Association, *Standards and Data.*
2. The Aluminum Association, *Position on Fracture Toughness Requirements and Quality Control Testing T-5.*
3. MIL-H-6088, *Heat Treatment of Aluminum Alloys.*

ALCOA MILL PRODUCTS

P.O. BOX 8025 • BETTENDORF, IOWA 52722 • (800) 523-9596 • www.millproducts-alcoa.com

SPD-10-037

Figure C.8: Aluminium 7075-T6 Page 3.

Appendix D

Tensile Test Data

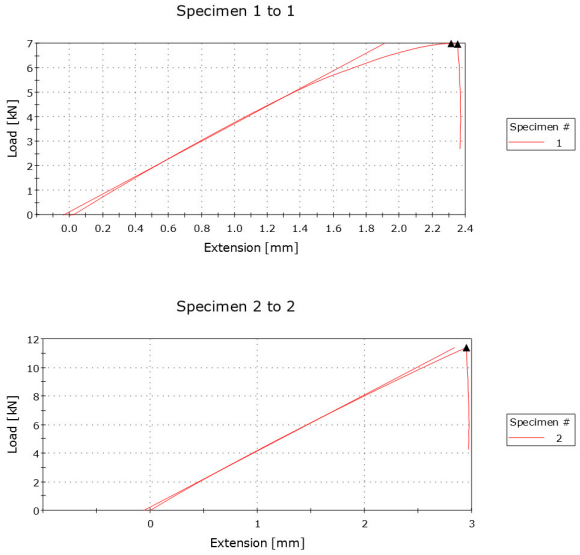

Figure D.1: Tensile Test Graphs (raw data) 1.

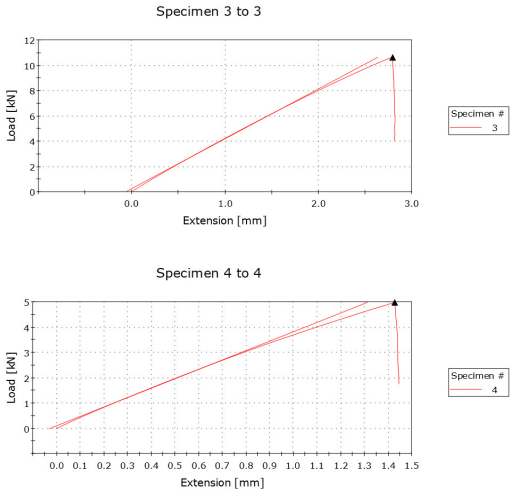

Figure D.2: Tensile Test Graphs (raw data) 2.

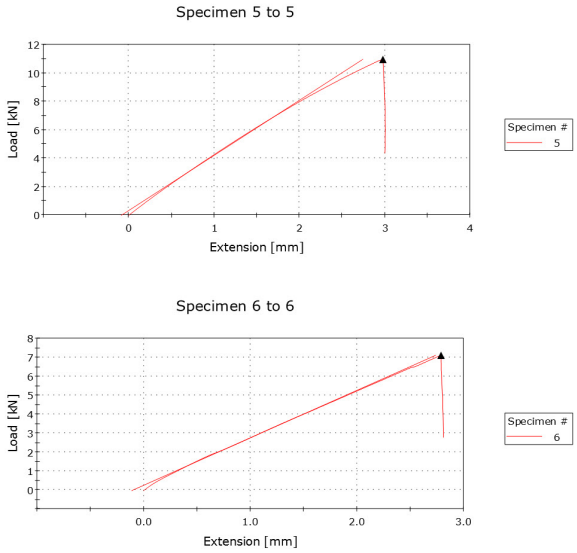

Figure D.3: Tensile Test Graphs (raw data) 3.

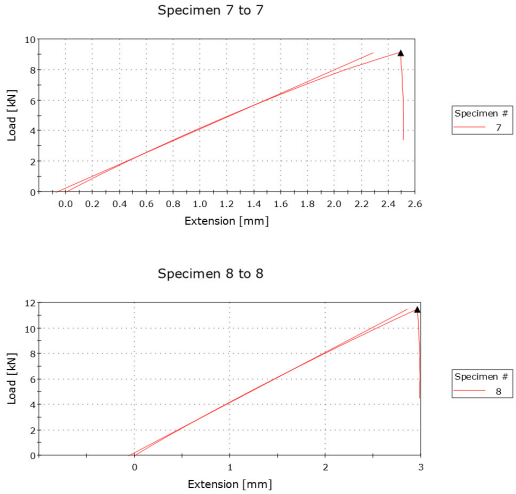

Figure D.4: Tensile Test Graphs (raw data) 4.

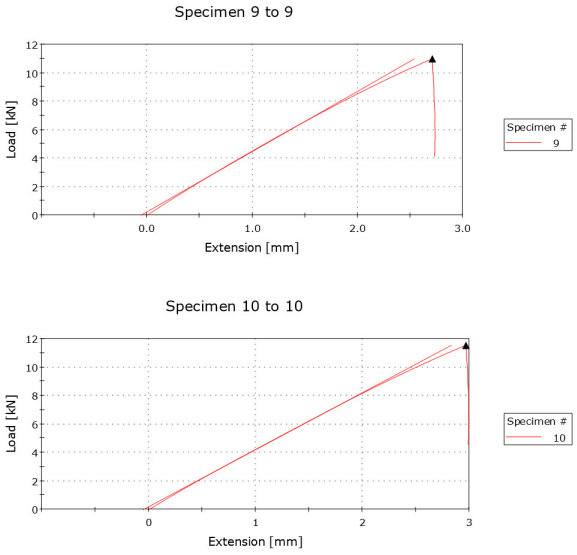

Figure D.5: Tensile Test Graphs (raw data) 5.

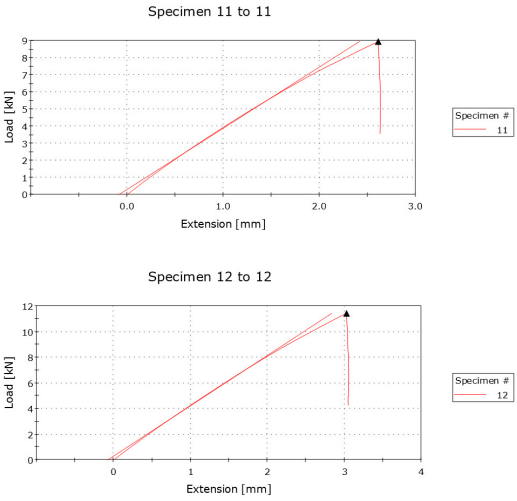

Figure D.6: Tensile Test Graphs (raw data) 6.

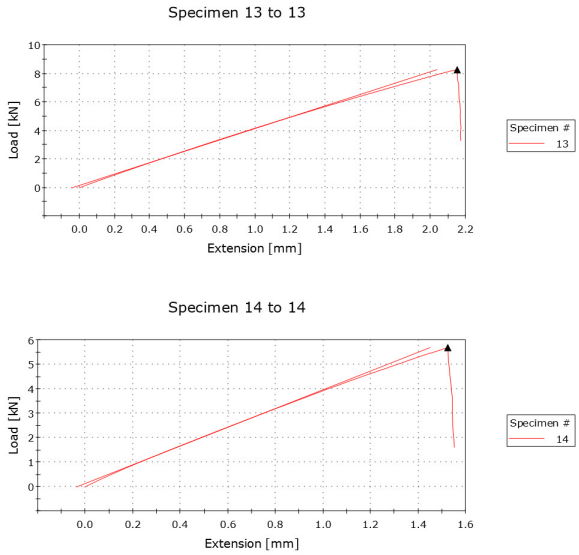

Figure D.7: Tensile Test Graphs (raw data) 7.

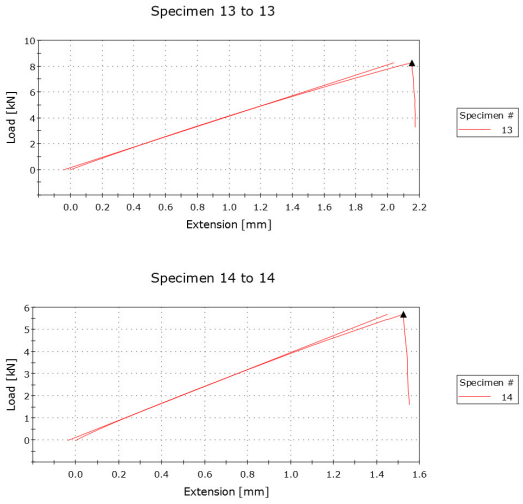

Figure D.8: Tensile Test Graphs (raw data) 8.

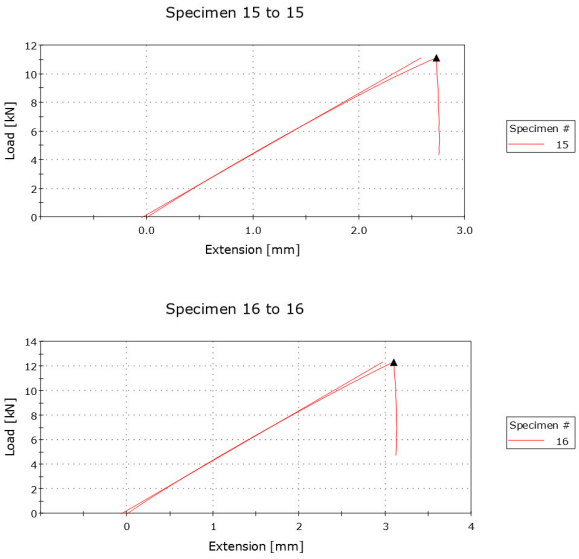

Figure D.9: Tensile Test Graphs (raw data) 9.

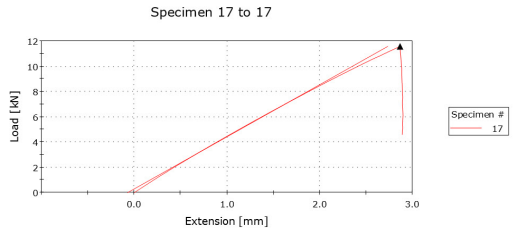

Figure D.10: Tensile Test Graphs (raw data) 10.